

Multiplexed Nanoparticle-based Immunoassays

Kathryn Alison Murray

PhD thesis submitted in partial fulfilment of the requirements of The Nottingham
Trent University for the degree of Doctor of Philosophy

This research was a collaboration with the Max Planck Institute for Biophysical
Chemistry under the FLUOROMAG consortium contract number 037465

School of Science and Technology

The Nottingham Trent University

September 2010

This work is the intellectual property of the author. You may copy up to 5% of this work for private study, or personal, non-commercial research. Any re-use of the information contained within this document should be fully referenced, quoting the author, title, university, degree level and pagination. Queries or requests for any other use, or if a more substantial copy is required, should be directed in the owner of the Intellectual Property Rights.

Abstract

Multiplexed immunoassays have been explored using the fluorescent and luminescent properties of fluorophores and nanoparticles. Epi-fluorescence microscopy, confocal laser scanning microscopy and programmable array microscopy were used to detect signals from mixtures of conventional organic fluorophores, quantum dots and silica nanoparticles doped with europium, samarium and terbium in single-welled multiplexed immunosorbent assays. Spectral unmixing was investigated using mixtures of fluorophores and cadmium selenide quantum dots. Mixtures of up to four dyes were separated quantitatively using least squares minimisation, with relative standard error ranging from 0.5 to 13 %. Silica nanoparticles doped with luminescent lanthanides were synthesised and used in a model immunoassay system for simultaneous, single-welled detection of human and mouse IgGs. The results indicated the lanthanides are well suited to multiplexed assays, mainly because of their atomic line emission bands. Analytes in a mixture could be quantified with $< 5\%$ error. The multiplexed assay developed was applied to the detection of anti-dengue IgM and IgG in mouse sera, to differentiate primary and secondary dengue infection. The assay traced the kinetics of antibody production for both IgM and IgG with an IgM/IgG ratio of 1. The fluorescence-based methods compared favourably with ELISA results ($r^2 \geq 0.8$), with results using conventional fluorophores showing the best correlation with ELISA ($r^2 > 0.98$). Differentiation of serotype specific IgGs was also explored but was complicated due to cross reactivity of the antibodies. A model to differentiate cross reactive dengue antigens was applied to the data through fitting parameters of the five parameter logistic equation to the intensity obtained for an assay. Results indicated the family of dengue antigens are too closely related to be distinguished by

the method. The model was however successful in differentiating a partially cross reactive system ($p > 0.95$).

Acknowledgements

There are some persons without whom the project could not have been completed. My supervisory team: Drs. Quentin Hanley, Selman Ali and Haida Liang, gave useful feedback and guidance. This project was funded by the EU under the FLUOROMAG consortium contract number 0374665. It was headed by Dr. Donna Arndt-Jovin of the Max Planck Institute for Biophysical Chemistry in Germany. Thanks go to her and her laboratory staff for allowing work on the PAM to proceed in her laboratory. I would also like to thank the other members of my research group: Drs. Yuan-Chen Cao and Yanzhou Zhou, Homanaz Ghafari and William Gumbs for useful discussions.

Table of Contents

Abstract.....	iii
1 Introduction.....	1
1.1 Motivation and Outline of Thesis.....	1
1.2 The immune response and immunoassays.....	3
1.3 Multiplexed methods of analysis.....	7
1.4 Probes used for fluorescence-linked immunoassays.....	8
1.5 Dengue fever.....	14
1.5.1 Molecular nature of dengue fever.....	16
1.5.2 Methods for dengue diagnosis.....	18
1.5.3 Haemagglutination Inhibition.....	18
1.5.4 Neutralisation Test.....	19
1.5.5 Complement fixation.....	20
1.5.6 ELISA.....	20
1.5.7 Nucleic acid based methods.....	21
1.6 Research Objectives.....	23
1.7 References.....	25
2 Experimental methods.....	37
2.1 Fluorescence Microscopy.....	37
2.1.1 Epifluorescence microscopy.....	40
2.1.2 Add-ons to the epi-illumination microscope.....	41
2.1.3 Confocal Microscopy.....	45
2.1.4 Programmable array microscope.....	48
2.2 Experimental Protocols.....	52
2.2.1 Synthesis and Bioconjugation of Nanoparticles.....	52
2.4 References.....	55
3 Spectral unmixing.....	58
3.1 Introduction.....	58

3.2	Theory.....	61
3.3	Materials and Methods	64
3.3.1	Reagents.....	64
3.3.2	Imaging of fluorophore and quantum dot mixtures	64
3.4	Results and Discussion	66
3.5	Discussion and Conclusions	82
3.5	References.....	84
4	Lanthanide nanoparticles: simplification of multiplexed methods of analysis	86
4.1	Introduction.....	86
4.2	Materials and Methods	92
4.2.1	Materials.....	92
4.2.2	Synthesis and characterisation of the nanoparticles.....	93
4.2.3	Synthesis of a novel ligand for Terbium	95
4.2.4	Fluorescamine	96
4.2.5	Transmission Electron Microscopy (TEM).....	96
4.2.6	Multiplexed immunoassay for human IgG and mouse IgG using NPs	97
4.3	Results and Discussion	98
4.3.1	NP characterisation	98
4.3.2	Spectral unmixing of NPs.....	112
4.3.3	Bioconjugation of Nanoparticles	114
4.4	Spectral analysis of multiplexed immunoassay	114
4.5	General discussion and conclusions.....	121
4.6	References.....	125
5	A model study: Dengue fever	129
5.1	Introduction.....	129
5.1.1	Methods and materials.....	130
5.1.2	Antigen preparation.....	131

5.1.3	Immunization and collection of sera.....	131
5.1.4	Dengue immunoassay.....	134
5.2	Results.....	138
5.2.1	Detection of IgM and IgG in a single assay well	139
5.2.2	Elisa Results	139
5.2.3	Organic Dyes Measured Confocally.....	142
5.2.4	Quantum Dots	147
5.2.5	Multiplexed Quantum Dot-based Immunoassays with PAM Readout	150
5.2.6	Lanthanide-doped Silica Nanoparticles.....	151
5.2.7	Comparison of the Four Fluorescent Immunoassays.....	153
5.3	General Discussion and Conclusions.....	165
5.4	References.....	170
6	Cross reactivity studies	172
6.1	Introduction	173
6.2	Theory.....	175
6.3	Methods and Materials	177
6.3.1	Materials.....	177
6.3.2	Assay Readout.....	177
6.3.3	Immunoassay	178
6.3.4	Data Analysis	178
6.4	Results and Discussion	179
6.5	General Discussion and Conclusions.....	185
6.6	References.....	187
7	General Discussion and Conclusions.....	188
7.1	Spectral Unmixing Of Conventional Fluorophores and Quantum Dots	188
7.2	Lanthanide-doped silica nanoparticles	190
7.3	A Model Study: Dengue Fever	191
7.4	Cross reactivity studies	192
7.5	References.....	192

Appendix 1: Linest data sets	193
Appendix 2-Calibration of the Spectrograph	195
Appendix 3-Sample of raw data from confocal results for multiplexed dengue assays	196
Appendix 4-Persistence of dengue antigen in the serum of immunised mice	199
Appendix 5- Simulations to test the robustness of the cross reactivity model	200
Appendix 6 -Publications/ Conference Proceedings	201

Table of Figures

Figure 1: Diagram of immunoglobulin G (IgG).....	4
Figure 2: Schematic of an enzyme linked immunosorbant assay (ELISA).	7
Figure 3: Basic concept of the FLISA procedure.	9
Figure 4: Global distribution of dengue virus	15
Figure 5: Schematic of flavivirus virion.....	17
Figure 6: Flavivirus structure	18
Figure 7: Jablonski diagram showing possible routes an excited fluorophore can take to return to the ground state.....	38
Figure 8: Schematic of the epi-fluorescence microscope used.....	41
Figure 9: Diagram of the optical layout of a spectrograph	43
Figure 10: The dispersion of light of two wavelengths in a prism.....	43
Figure 11: Schematic of a charged coupled device	45
Figure 12: Schematic of a confocal laser scanning microscope (CLSM).	47
Figure 13: Diagram of a version of the PAM.	49
Figure 14: Synthetic scheme for preparation of lanthanide-doped silica nanoparticles	52
Figure 15: Glutaraldehyde-mediated conjugation of two amine-reactive molecules.	54
Figure 16: Figure showing spectra of fluorescein alone ×, rhodamine B alone ■ and a mixture of the two fluorophores ♦ in buffered solution.....	66
Figure 17: Some pH-dependent structures of rhodamine B.	67
Figure 18: The pH-dependent structures of fluorescein.	68

Figure 19: Spectral unmixing of fluorescein and rhodamine B, showing spectra of the mixture (solid line), the fractional contribution of fluorescein 50 μ M (dash-dot line) and the fractional contribution of rhodamine B 20 μ M (dashed line)	70
Figure 20: Residuals plots for the quantitative unmixing of fluorescein and rhodamine B for the existing method ●, and the new method ■.....	71
Figure 21: Mixtures of fluorescein and rhodamine B in unbuffered solution.....	72
Figure 22: Mixtures of fluorescein, rhodamine B and rhodamine 101 in buffered solution..	74
Figure 23: The structure of rhodamine 101.....	75
Figure 24: Spectra of mixtures of four dyes fluorescein, rhodamine B, rhodamine 101, and eosin Y.....	76
Figure 25: The structure of eosin Y	76
Figure 26: Mixture of orange and green quantum dots indicating the dependence of orange fluorescence on green.	78
Figure 27: Diagram showing simplified organisation of two functionalised QDs in solution.	80
Figure 28: Energy diagram of luminescence in lanthanide complexes	88
Figure 29: Reaction of polycarboxylate diethylenetriaminepentaacetic acid (DTPA) with cs 124 to form a lanthanide ligand	89
Figure 30: Further modification of the lanthanide ligand to allow conjugation to other moieties.....	90
Figure 31: The synthetic method for the preparation of a new ligand for Tb.	95
Figure 32: Electron micrograph of Sm-doped silica NPs, obtained with a TEM. ...	98
Figure 33: Electron micrograph of Sm- doped silica NPs as obtained by SEM.	99
Figure 34: Luminescence spectrum of samarium-doped silica nanoparticles.	100

Figure 35: Luminescence spectrum of europium doped silica nanoparticles.....	100
Figure 36: Luminescence spectrum of silica nanoparticles doped with europium and samarium.....	101
Figure 37: ¹ HNMR spectrum of lanthanide chelate synthesised.	105
Figure 38: Predicted ¹ HNMR spectrum of lanthanide chelate.	106
Figure 39: ¹ HNMR spectrum of cs124 in DMSO-D6.	107
Figure 40: ¹ HNMR spectrum of DTPAA in DMSO-D6.....	108
Figure 41: Fluorescence spectrum of terbium-doped silica nanoparticles.	110
Figure 42: Diagram showing diffraction that occurs at a single slit of width W. ...	111
Figure 43: Luminescence spectra of mixtures of europium and samarium doped silica nanoparticles in the ratios Eu: Sm 2:3 ■, 3:7 ×, and 1:4 ♦	112
Figure 44: (a) Concentration response of human IgG on anti-human IgG, assayed with an Eu-doped SiO ₂ NP, (b) Concentration response for human IgG assayed with mouse IgG on anti-human and anti-mouse IgGs.	115
(b)Figure 45: (a) Concentration response of mouse IgG, on anti-mouse IgG, assayed with a Sm-doped SiO ₂ NP, (b) Concentration response for mouse IgG assayed with human IgG on anti-human and anti-mouse IgGs.	116
Figure 46: Format for the NP-based immunosorbant assay	134
Figure 47: ELISA response of mouse anti-dengue IgM in mice immunised with dengue antigen type 3.	139
Figure 48: ELISA response of mouse anti-dengue IgG in mice immunised with dengue antigen type 3.	140
Figure 49: ELISA response of mouse anti-dengue IgM in mice immunised with dengue antigen type 4.	140

Figure 50: ELISA response of mouse anti-dengue IgG in mice immunised with dengue antigen type 4.	141
Figure 51: Confocally measured response of mouse anti-dengue IgM in mice immunised with dengue antigen type 4.	143
Figure 52: Confocally measured response of mouse anti-dengue IgG in mice immunised with dengue antigen type 4.	144
Figure 53: Graph demonstrating the high signal to background ratio of the confocal system	146
Figure 54: Graph demonstrating the low signal to background ratio using the ELISA method.....	147
Figure 55: Anti-dengue IgG response in mice immunised with dengue antigen type 3.	148
Figure 56: Anti-dengue IgM response in mice immunised with dengue antigen type 3.	148
Figure 57: Response of mouse anti-dengue IgM and IgG in mice immunised twice with dengue antigen type 4.	151
Figure 58: Response of mouse anti-dengue IgG in mice immunised with dengue antigen type 4.	152
Figure 59: Response of mouse anti-dengue IgM in mice immunised with dengue antigen type 4.	152
Figure 60: The relationship between values of intensity obtained with CLSM readout of organic fluorophores and ELISA methods for (a) an assay for anti-dengue IgM, (b) an assay for anti-dengue IgG	155

Figure 61: The relationship between values of intensity obtained with PAM and ELISA methods for (a) an assay for anti-dengue IgM, (b) an assay for anti-dengue IgG	157
Figure 62: The relationship between values of intensity obtained with epi-illumination of QDs and ELISA methods for (a) an assay for anti-dengue IgM, (b) an assay for anti-dengue IgG	158
Figure 63: The relationship between values of intensity obtained with epi-illumination of lanthanide doped silica nanoparticles and ELISA methods for (a) an assay for anti-dengue IgM, (b) an assay for anti-dengue IgG.....	159
Figure 64: Comparison of results obtained from similar serum samples using NPs with epi-fluorescence read-out and organic dyes with CLSM read-out for (a) anti-dengue IgG and (b) IgM.....	162
Figure 65 : Comparison of results obtained from similar serum samples using QDs with PAM read-out and organic dyes with CLSM read-out for (a) anti-dengue IgG and (b) IgM	163
Figure 66: Dose response for human IgG. The line is a sigmoidal fit, modelled with 4 parameters.....	180
Figure 67: Dose response for mouse IgG. The line is a sigmoidal fit, modelled with 4 parameters.....	181
Figure 68: Dose response of anti-dengue IgG on dengue type 3 antigen. The line is a sigmoidal fit to 4 parameters.....	184

1 Introduction

1.1 Motivation and Outline of Thesis

This project developed immunoassays where multiple serum biomarkers are simultaneously detected in a single well of an assay plate using fluorescence spectroscopy. Dengue fever, which has four distinct but cross reactive forms was the virus of choice, as several biomarkers are released in response to infection by the virus. There are several immunoassay formats for detecting the presence of anti-dengue antibodies,¹⁻¹⁷ but these methods all require spatial separation of the antibodies. The serological ELISA method, though commonly used for detecting dengue antibodies, is not used to detect multiple analytes in a single well assay. Current ELISA methods are further limited by problems common to the use of enzymes: contamination of the substrate solution and the need to read the microwell shortly after completion of the enzyme/substrate reaction. The use of fluorescence-linked immunoassays gives advantages over ELISAs such as increased sensitivity, a larger dynamic range and greater stability of reagents. Fluorescence methods may also be multiplexed, thereby using lower volumes of reagents and decreasing assay time.¹⁸

The ability to spectroscopically detect multiple analytes in a single well assay is not without its challenges. These include cross reactivity of antibodies, the need for spectral unmixing, and the possibility of interaction between the fluorophores. The use of nanoparticles removes some of these challenges, as does the use of specialised fluorescence microscopy methods.

This chapter reviews the immune response and explores the history of immunoassays. The probes employed for immunoassays are listed with detailed presentation of the probes used for fluorescence-based immunoassays. Multiplexed immunoassays are mentioned with a view of presenting previous approaches to multi-analyte detection, where the current work advances the state of the art. Finally, dengue fever is presented, highlighting the need for an immunoassay that is able to accurately detect the presence of dengue antibodies.

As fluorescence microscopy methods were used for assay read out, the second chapter of the thesis introduces fluorescence and a description of the three different microscopes used: an epifluorescence, a confocal laser scanning (CLSM) and a programmable array microscope (PAM). The chapter seeks to highlight the relevant differences and relative advantages/ disadvantages among the microscopes. A review of methods for the synthesis, bioconjugation and size characterisation of nanoparticles is also contained in this chapter.

Chapter 3 describes a chemometric method for spectroscopic unmixing of conventional organic fluorophores and commercially obtained quantum dots. The algorithm used is similar to the spectral unmixing algorithm, but the standardisation method differs from previously published methods. A comparison between conventional standardisation methods and the one explored in this thesis is presented.

Chapter 4 introduces the concept of using lanthanide-doped silica nanoparticles for single well multiplexed immunosorbent assays. This work was a result of problems encountered with organic fluorophores and commercially obtained quantum dots.

The single well multiplexed assay developed in chapter 4 is applied to simultaneous detection of anti-dengue IgM and IgG in chapter 5. This chapter describes the use of conventional organic dyes, quantum dots and lanthanide-doped silica nanoparticles in the multiplexed assay. The results are compared to those obtained for multi-well ELISA detection of IgM and IgG. The relative merits of the different probes and microscopes used are discussed at length.

The final results of the thesis are presented in chapter 6, where cross reactivity between serotype specific anti-dengue IgGs is addressed. A mathematical method for distinguishing cross reactive antibodies is devised and applied first to a partially cross reactive system of human and mouse IgGs and finally to a fully cross reactive system of anti-dengue IgG types 3 and 4.

Chapter 7 presents the final discussion of the thesis. The main achievements are revisited and the possibilities of further work are listed.

1.2 The immune response and immunoassays

Immunology as a discipline came about after the observation of persons developing immunity to an infectious disease after recovery. Immunity can be defined as the state of protection from an infectious disease,¹⁹ and is derived from the Latin term *immunis*, which means exempt. A virus that elicits an immune response may be detected using immunoassays which utilise antibodies, and nucleic acid methods that detect RNA. Antibodies are glycoproteins that are involved in immune recognition and host defence systems,²⁰ and belong to the immunoglobulin class of proteins. Human immunoglobulins are heterodimers, with their basic structure consisting of four polypeptide chains that are linked by disulfide bridges. These are

two heavy chains consisting of 450 – 600 amino acid residues, and two light chains of about 220 amino acid residues. IgG is the most abundant Ig in serum and forms a Y-shaped structure (Figure 1).²⁰ It is synthesised predominantly by plasma cells after secondary exposure to antigen.

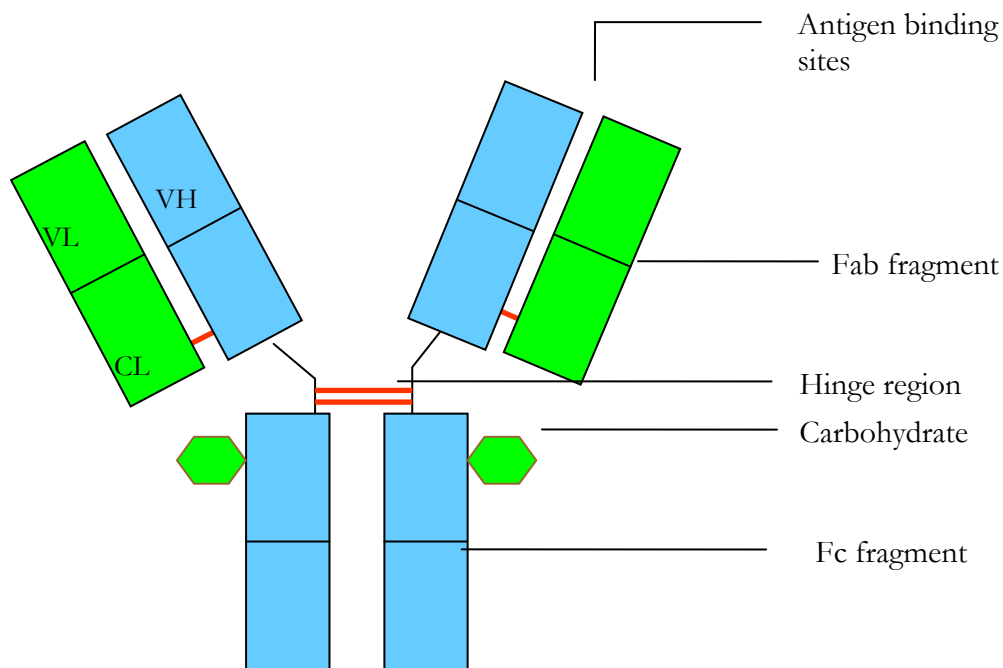


Figure 1: Diagram of immunoglobulin G (IgG), showing the blue heavy chains and the green light chains. CL represents the constant domain of the light chain, VL and VH represent the variable domains of the light and heavy chains respectively. The Fab fragment has antigen binding activity and the Fc fragment is the crystallisable region, recognised by host defence mechanisms. The antigen binding sites are the amino-terminal domains of the molecule which bind to the antigen, while the hinge region is an amino acid stretch; rich in proline and cysteine, linking the two heavy chains with disulfide bonds. The carbohydrate is an oligosaccharide.

Each heavy chain of IgG consists of one variable (V_H) and three constant domains; the light chain consists of one variable (V_L) and one constant domain. Each domain is comprised of approximately 110 amino acids, giving an IgG a total molecular

mass of approximately 150 000 Daltons. The Ig has two functionally important parts; the region of the antigen binding site (Fab) and the crystallisable region (Fc) that is recognised by host defence mechanisms. In addition to IgG there are four other antibodies: IgM, IgA, IgD and IgE. Like IgG, IgD and IgE are monomeric structures. IgM is a pentameric structure of approximately 970 kDa and IgA is dimeric with an approximate molecular mass of 385 kDa.

Antigens are molecules capable of eliciting an immune response when injected into an animal. The antigen is treated as a foreign species and its epitope binds to the paratope of its complementary antibody. Several different forces are involved in binding and the two reactants must first overcome the repulsive forces that exist between them before specific binding occurs. Initially, hydrophobic and ionic attractions exist between the epitope; the part of an antigen that is recognised by the immune system, and the paratopes; the part of the antibody that recognises the antigen. The hydrophobic paratopes interact, while oppositely charged amino acids in the epitope and paratope form what are known as salt bridges over a distance of some 100 Å. Van der Waals forces between the paratope and epitope then become involved, and as the epitope draws closer to the paratope, hydrogen bonds are formed between adjacent amino, hydroxyl and carboxyl groups at distances between 2 and 3 Å. Eventually, direct protein-protein interactions occur that strengthen the bond.²⁰ These interactions refer to localised induced fitting of the epitope and paratope to ensure shape complementarity.

Immunoassays play a prominent role in clinical science for analyses involving biological matter such as proteins, nucleic acids and hormones,²¹ and have evolved significantly since the first immunoassay for insulin, performed by Yalow and

Berson in 1959.²² The assay involved competition between unlabelled and radioactively labelled insulin for a limited amount of insulin antibody. Bound and free insulin were separated by paper chromatography and the radioactivity of the separated fractions determined using a scintillation counter. The next major advance was made in 1968 by Miles and Hales, when labelled antibodies rather than antigens were used.²³ This and the assay performed by Berson and Yalow were single-site immunometric assays,²⁰ with two-site immunometric assays first described in the 1970's.²⁴ The discovery of monoclonal antibodies by Kohler and Milstein in 1975²⁵ made available large amounts of antibodies and this made non-competitive or sandwich immunoassays more practical. While the radioactively labelled antibodies are said to be one of the most sensitive detection schemes used,²¹ they offer the disadvantages of radioisotopes, and other labels are frequently used. The more widely used of these are enzymes, used in enzyme-linked immunosorbent assays (ELISAs), a technique first reported in 1971 by two research groups working independently of each other in Sweden and the Netherlands.²⁶ ELISAs may be competitive, or may be in the sandwich format, where the sample containing the antigen is incubated on a surface that has been treated with antibody. A secondary enzyme-labelled antibody is then added and detected by a colour change after the addition of substrate (Figure 2). Indirect ELISAs are characterised by incubation of the antigen on the surface, followed by the addition of the sample containing the antibody. A secondary enzyme-labelled antibody is used for detection of antibody after addition of enzyme substrate.

A significant drawback of ELISAs is that a separate assay is required for each analyte of interest. Since it is frequently necessary or helpful to detect several biomarkers simultaneously, conventional ELISAs make the process time

consuming.²⁷ Immunoassays therefore continue to evolve and include new applications such as multiplexed methods and nanoscale levels of analysis.²⁸

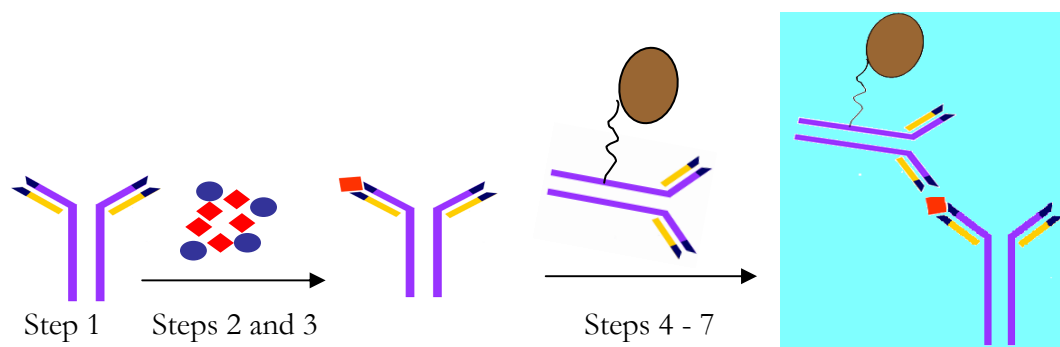


Figure 2: Schematic of an enzyme linked immunosorbant assay (ELISA). Step 1 is incubation of the primary antibody on the solid surface; steps 2 and 3 are addition of substrate followed by a wash step. Steps 4 to 7 are 4) addition of secondary antibody labelled with enzyme, 5) washing, 6) addition of colour developer, 7) addition of stop solution.

1.3 Multiplexed methods of analysis

Multiplexed methods of analysis allow simultaneous testing of several analytes in a single assay. Multianalyte technologies were developed in the early 1980s²⁹ and now include microarray and bead-based formats. At present, several multiplexed based analyses are performed using particle-based flow cytometric assays such as Luminex,³⁰ the FlowMetrix™ system³¹ and UltraPlex.²⁷ Luminex is perhaps the most well known and consists of polystyrene microbeads embedded with red and infrared fluorescent dyes. Each bead has a unique signature which is a result of differing ratios of the fluorescent dyes. The Luminex system is reported to have limits of detection and sensitivity comparable to and better than ELISA for some assays,^{18,32-41} as well as lower coefficients of variation,⁴² though some studies report no improvement.³² Imaging platforms such as Luminex are costly and not easily

accessible to most diagnostic laboratories. Other multiplexed methods are more readily adopted and include conventional microarrays,⁴³ microarrays based on electrogenerated chemiluminescent read out,⁴⁴ microfluidic immunoassay devices integrated with optically encoded beads,⁴⁵ a microfluidic-based chip, able to simultaneously measure multiple biomarkers in blood,⁴⁶ systems based on confocal read-out of quantum dots fluorescence⁴⁷ and assays using magnetic luminescent nanoparticles.⁴⁸ For these microarray-based methods, antibodies are printed onto the surface⁴⁹ and are therefore spatially separate.

Multiplexed immunoassays in a single well of an assay plate have been successfully carried out⁵⁰ using quantum dots (QDs) of different colours. The spectrum of the mixture was broken down into individual spectra using a minimisation algorithm. This is the first, and still one of the few reports where a single well fluorescent immunoassay mixture is broken down into its individual components through spectral unmixing. The result obtained was that of the fractional contribution of each QD to the composite signal from the well. Their algorithm indicates the presence or absence of an analyte, but does not predict the concentration. These assay formats, where simultaneous multiple fluorescence signals can be detected are desirable, but are difficult to implement because of the photophysical nature of fluorophores and the need for specialised equipment and unmixing algorithms.

1.4 Probes used for fluorescence-linked immunoassays

The use of fluorescent technology in immunology originally involved staining for microscopy,⁵¹ but has since been applied to immunoassay development. Fluorescence linked immunosorbant assays (FLISAs) (Figure 3) use fluorescence for

detection.⁵² While antibodies labelled with fluorophores have been used since 1941, their use then was limited to immunofixation techniques and they were only introduced as probes in immunoassays in the 1970s.⁵³ These probes provide some advantages over ELISA, although their inherent limitations can be problematic when applied to immunoassays.

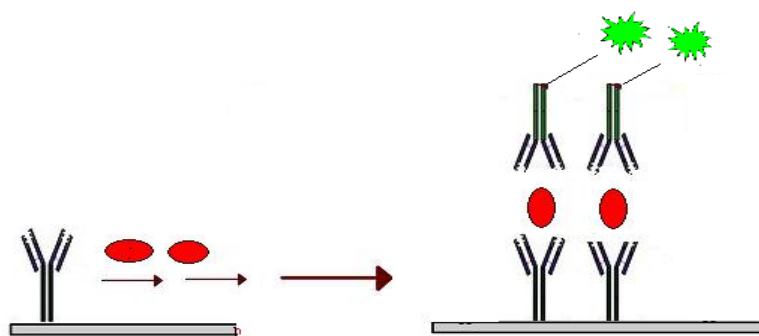


Figure 3: Basic concept of the FLISA procedure. The format is similar to ELISA, the difference being the use of fluorophore-labelled secondary antibodies.

These limitations include Rayleigh, Raman and Tyndall light scattering.⁵⁴ Rayleigh scattering is a result of interaction between excitation light and water molecules. Raman scattering is also a result of interaction between excitation light and water molecules, but the scatter peaks are shifted to longer wavelengths.⁵⁴ Tyndall scattering is reflection of excitation light off particulate matter in the sample, and like Rayleigh scattering the peaks occur at the excitation wavelength. Other limitations of fluorophores are high fluorescence background from the samples and microplate,⁵⁵ and their sensitivity to changes in their environment. In spite of this, fluorescence immunoassays have found widespread use for detection and these include their applicability to high throughput screening,^{56, 57} reduction of wash steps,⁵⁸ and the ability to multiplex.^{18, 38, 41, 59}

The applications of fluorophores to immunoassays result from the fact that they have high detection sensitivities and several measurable properties.⁶⁰ These properties include the intensity of fluorescence, the lifetime and orientation of the fluorophore, and interrelationships between these properties. Some techniques applied to immunoassays which measure these relationships are fluorescence polarisation assays^{61, 62} time-resolved immunoassays,⁶³⁻⁶⁷ and methods based on phase modulation spectroscopy.⁶⁸ As fluorescence methods are developed, instrumentation for quantifying fluorescence is also developed. Some of these developments include the programmable array microscope⁶⁹⁻⁷³ and spectral imaging systems as add-ons to a fluorescent microscope.⁷⁴

Organic fluorophores such as fluorescein and rhodamines are commonly used because of their high molar extinction coefficients ($> 90\,000\text{ M}^{-1}\text{cm}^{-1}$ at maximum excitation wavelengths) and ease of use. Indeed, these organic fluorophores have found widespread use as labels for biological macromolecules such as cells,^{75, 76} proteins and nucleic acids.⁷⁷⁻⁷⁹ This has allowed them to be used for monitoring cellular integrity and processes,⁸⁰ membrane fluidity,⁸¹ protein trafficking,⁸² signal transduction,⁸³ and enzymatic activity.⁸⁴ Organic fluorophores have also been applied to genetic mapping⁸⁵ and chromosome analysis.⁸⁶

These organic fluorophores have disadvantages. They are sensitive to pH. They have a tendency to self quench.⁷⁶ In concentrated solutions of fluorescent dyes static quenching can occur, indicated by a change in the absorption spectrum of the fluorophore. While this effect can be used to monitor processes in the cell,^{87, 88} it is

a hindrance for multiplexed measurements. Organic fluorophores have small Stokes shifts.⁸⁹ This means that the energy difference between the absorbed and emitted photon is small, and can lead to an overlap between excitation and emission wavelengths. The organic fluorophores lack photostability,⁹⁰ and this complicates measurements because of the photochemical degradation of the molecules. Finally the broad, overlapping emission bands of the organic fluorophores⁹¹ makes them generally unsuitable for multiplexed measurements.⁹² For these reasons, other fluorescent probes have been developed, which purportedly offer improvements over conventional fluorophores while still maintaining their useful characteristics. One such set of probes is quantum dots (QDs).⁹³

QDs are fluorescent nanocrystals composed of organic semiconductors. Their photophysical properties are best described through a description of semiconductors. Semiconductors are a material group which have moderately good conductivity; higher than that of insulators but lower than that of metals. Their conductivity is dependent on the temperature and chemical purity of the material, and a semiconductor is characterised as having no conductivity at absolute zero temperature.⁹⁴ As semiconductors, QDs contain electrical charge carriers and are characterised by a bandgap energy. This is the minimum energy required to excite an electron from its ground state to the first excited state.⁹⁵ The band gap energy that characterises semiconductors is formed by the energy between the conduction and valence bands of the nanocrystals. The electrons in a crystal have kinetic and potential energies, and there are areas in the crystal where all of the electron energy can be found while other areas exist where there are no electrons and no electronic energy. This energy axis of the crystal can be divided into forbidden bands; where no electrons are located, and allowed bands; that contain electrons. The forbidden

band is referred to as the conduction band, while the allowed band is the valence band. Excitation of a QD is initiated when a photon of energy greater than the band gap energy is absorbed. This results in the generation of charge carriers. Recombination of the electron and hole occurs on relaxation back to the ground state, converting the bandgap energy into a photon, and creating fluorescence.⁹⁵

QDs are typically small crystals, ranging in size from one to ten nanometers in diameter.⁹⁶ Because of their small size, the charge carriers are confined to a space smaller than they normally would in a bulk semiconductor. This is known as quantum confinement and can be manipulated by tuning the size of the QD. A smaller QD indicates greater confinement and larger band gap energy. The electron/hole pair formed is therefore of a higher energy, and fluoresces at a shorter wavelength. Similarly, a larger QD fluoresces at a longer wavelength. By carefully tuning the size of the crystals, a range of fluorescent probes can be obtained. QDs find use as biological probes⁹⁷ due to their large molar extinction coefficients; $0.5 - 5 \times 10^6 \text{ M}^{-1} \text{ cm}^{-1}$,⁹⁵ quantum efficiencies up to 85%,⁹⁵ good photostability and long lifetimes with respect to conventional organic dyes.⁹⁶ Their broad absorption bands and narrow emission bands allow them to be excited at a single wavelength, thereby making it possible to simultaneously detect multiple QD probes without the need for complex processing.⁹⁸ They have been applied extensively to multiplexed methods of analysis.^{99, 100}

Fluorescent probes are subject to non-linear behaviour and can also mix non-linearly. Non-linear processes of fluorescent probes include photobleaching and excited state reactions¹⁰¹ while within mixtures of the probes this non-linearity can be extended to photophysical interactions between the fluorophores, such as energy

transfer.¹⁰² These processes complicate spectral unmixing, as they can result in reduced fluorescence of the donor and increased fluorescence of the acceptor. Fluorescent probes also have typically broad emission bands, which could result in overlap in a hyperspectral image of a mixture. Spectral overlap needs to be separated using chemometric methods, which mainly involve the use of multivariate statistics to analyse data collected in the analytical chemistry lab.¹⁰³ Principal Components Analysis (PCA) is one of the more widely used chemometric methods, first described in 1901, and is used to determine patterns in data.¹⁰⁴ Other widely used chemometric methods include Partial Least Squares (PLS) and regression. For spectral unmixing, the chemometric methods are generally developed for the individual system of interest. This usually entails writing specific algorithms to be applied to the fluorophore system. For example, linear unmixing algorithms have been used¹⁰⁵ to spatially and spectrally separate fluorescence emission signals from fluorophores that have overlapping spectra. This was achieved through the separation of a mixture of Nile Blue and HIDC Iodide by PCA, orthogonal rotation and constrained linear least squares analysis. Similarly, multivariate curve resolution (MCR) techniques have been applied to data from a hyperspectral fluorescence imaging microarray scanner.¹⁰⁶ This method allowed quantitative measurements to be made through constrained alternating least squares analysis on an in-house developed MatLab code. Finally, maximum likelihood principal components regression has been applied to separate mixtures of acenaphthylene, naphthalene, phenanthrene. This algorithm also was a MatLab in house development.¹⁰⁷

Linearity of mixing, with clear non-overlapping signals can be obtained from probes such as silica nanoparticles doped with a fluorescent lanthanide chelated by an organic antenna.^{108, 109} Lanthanides have line-like atomic emission which is characteristic of the lanthanide of interest and this removes problems of spectral

overlap. As the silica particles are large; on average between 30 and 70 nm in diameter, and encapsulate the lanthanides within, there is little possibility of interaction between the two dyes, making the occurrence of inter-particle FRET minimal. In comparison to conventional fluorophores, fluorescent NPs have higher fluorescence intensity due to the presence of several fluorophores in a single nanoparticle. This has led to the integration of nanoprobe into bioassays, where their properties are thought to improve the features of the assays.¹¹⁰ Presently the use of these NPs does not extend beyond applications of low limits of detection, and their applicability to single-welled, multiplexed immunosorbent assays has not been clearly demonstrated. The aim is to use them in multiplexed immunoassays for dengue fever.

1.5 Dengue fever

Dengue fever is a mosquito borne *Flavivirus*, having four distinct but closely related serotypes DEN 1-4.^{1,111} It is presently one of the most important emerging tropical viral diseases in the world,¹¹² with an estimated 50 – 100 million cases yearly.¹¹³ Dengue fever produces a spectrum of diseases ranging from mild flu-like symptoms such as fever, chills and headache,¹ to dengue hemorrhagic fever (DHF) and dengue shock syndrome (DSS) which are fatal and involve plasma leakage, haemorrhage and shock.¹¹⁴ It is hypothesised that prior infection by one dengue serotype can increase the likelihood of contracting DHF on subsequent re-infection by another serotype through a process known as antibody dependent enhancement (ADE).¹¹⁵ This however, is one of several hypotheses as the exact mechanism of DHF and DSS are not well understood.

Dengue is a Spanish homonym for the Swahili term *ki dinga pepo* that was initially applied to the chikungunya viruses but came to be associated with dengue viruses.¹¹⁶ A virus believed to be dengue was first reported by the Chinese who called it water poison, in a medical encyclopaedia from the Chin dynasty, 265- 420 AD. Other early reports of the disease have also been published.¹¹⁶ The first reports of major epidemics of a virus thought to be dengue originated from Asia, Africa and North America in 1779 and 1780, but outbreaks of unusual illness thought to be dengue have been reported in the French West Indies and Panama in 1635 and 1699 respectively.¹¹⁶ The virus presently has a worldwide distribution in the tropics (Figure 4) and it is estimated that 2.5 billion persons live in dengue endemic regions. The disease presently causes more illness and death among humans than any other arbovirus.¹¹⁵

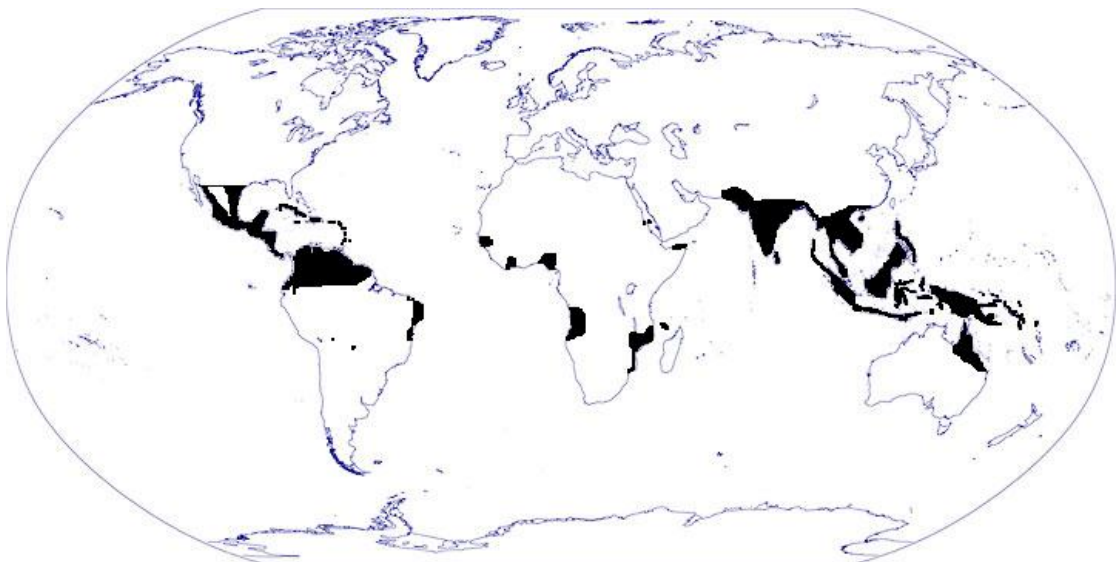


Figure 4: Global distribution of dengue virus¹¹⁵

After initial infection with one serotype of DF (primary infection), it is believed that there is lifelong immunity against a second infection with a homotypic strain.¹¹⁷ This conclusion was reached after detecting neutralising antibodies in the sera of persons that had been infected with DF some four decades previously.¹¹⁸⁻¹²⁰ A person may be infected by a second serotype however, resulting in a secondary infection. Primary and secondary DF infections may be differentiated since their kinetics of antibody production are different.¹²¹ A person infected with dengue fever has an initial rise in IgM antibodies, generally between days 4 and 7 of the illness, with a peak around 2 weeks, after which the IgM antibody concentration decreases to undetectable levels.¹²¹ IgG antibodies show a contrasting pattern to IgM, as only low levels of anti-dengue IgG are detected initially, thus meaning that IgM antibody levels greatly exceed those of IgG.¹²² Secondary dengue infection causes a prompt immune response known as an anamnestic response, which leads to IgG being the primary antibody to be produced. High IgG levels of antibody are detected early and rise quickly, while the concentration of IgM is low and rises only modestly.¹²² Generally, a primary infection is characterised by a low IgG to IgM ratio while the reverse holds for a secondary infection.

1.5.1 Molecular nature of dengue fever

Electron microscopy has shown the dengue virus to be comprised of an electron dense core surrounded by a lipid bilayer (Figure 5).¹²³

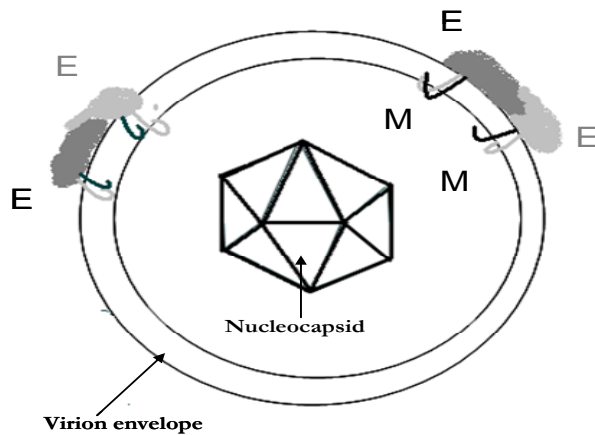


Figure 5: Schematic of flavivirus virion. E: envelope protein; M: membrane associated protein. ¹²⁴

The virion contains three structural proteins, seven non-structural proteins and a single strand of RNA genome of 10 700 nucleotides. The three structural proteins are the core protein (C) which is 100 amino acids, the membrane protein (M), 75 amino acids, and the envelope (E) which is 495 amino acids in size (Figure 6). The envelope protein (E) is implicated in host cell binding and haemagglutination, ¹²⁵ and this is the protein against which primary antibody responses are displayed. ¹²⁶ The non-structural proteins are NS1, NS2a, NS2b, NS3, NS4a, NS4b and NS5. Antibodies are formed against NS1 on infection with the virus. NS3 has protease and helicase activity. NS5 is the viral RNA-dependent RNA polymerase while the other four non-structural proteins are small and thought to be involved in membrane localisation of NS3 and NS5 through protein-protein interactions. This structure is typical of the *Flaviviridae* family of viruses of which Japanese encephalitis and tick-borne encephalitis are also members. As a result, these viruses have common group epitopes on the envelope protein allowing for cross reactivity during serologic testing. ¹¹⁵

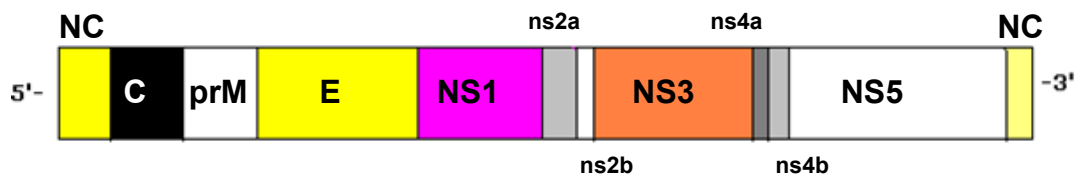


Figure 6: Flavivirus structure, showing C, the core protein; prM, the membrane protein; E, the envelope protein; and NS 1 – 5, the non-structural proteins.¹²⁴

1.5.2 Methods for dengue diagnosis

There are two basic methods for diagnosing DF. These are detection of the virus and detection of antibodies to the virus, known as serology. Virus detection traditionally refers to isolating the virus from a laboratory culture, but now includes detection of viral RNA in the sera or tissues, and detection of specific antigens.¹²⁷

Isolation of dengue virus from culture is the definitive test for the virus, but its use is limited due to some disadvantages which include the time consuming nature of the test. The test involves incubation of the patient's diluted serum sample on the mosquito-derived cell culture. This is left for a week at 28°C, after which the cell culture is screened for the presence of the virus using fluorescently stained serotype specific antigens.⁹² The common serologic tests used for diagnosis of dengue fever are hemagglutination inhibition (HI), complement fixation (CF), neutralisation test (NT), and ELISAs for IgG and IgM. These methods will now be described to indicate accepted protocols for the detection of anti-dengue IgG antibodies.

1.5.3 Haemagglutination Inhibition

Haemagglutination inhibition (HI) was the first serological assay finding general use in clinical laboratories, and remains the gold standard for the newer serological tests.²⁰ This method involves the agglutination of antigen-coated red blood cells and

is based on the premise that virus particles have a membrane protein known as hemagglutinin on their envelope which binds to sialic acid receptors that are located on the cells. The HI test is sensitive and reproducible, and is able to differentiate between primary and secondary infection. It has three main disadvantages however, which prevent its widespread application. The first of these is the need to pre-treat the sample to remove non-specific inhibitors of hemagglutination, followed by a step where the serum sample is absorbed with type O human red blood cells to remove non-specific agglutinins. The second main disadvantage is the need for paired serum samples. Both acute and convalescent serum samples are required as the change in HI titer between the convalescent and acute samples determines whether infection is primary or secondary. Finally, there are problems with cross reactivity, which make it difficult to distinguish between dengue and other *Flaviviruses*, as well as among the different serotypes of dengue.⁹²

1.5.4 Neutralisation Test

The plaque reduction neutralisation test (PRNT) is the serological method of choice for dengue serotyping.¹²⁸ The PRNT was first described in the 1950s and was adapted for dengue in 1967.¹²⁹ This test is very time consuming¹³⁰ and few laboratories use it in their research.¹²⁸ For the test, the serum specimen being examined is first diluted then mixed with a standardised amount of virus. The mixture is then plated onto virus susceptible cells and overlaid with a semi-solid restrictive medium. If a virus initiates an infection, a localised area of infection known as a plaque is produced. Plaques are counted and the amount present is compared to the starting concentration of the virus to determine the reduction of

viral activity. In spite of its labour intensive nature, this test remains the gold standard for serotyping and any tests developed need to be compared with it.

1.5.5 Complement fixation

Complement is a set of serum proteins that are able to react with antibody-antigen complexes. When the reaction occurs on the surface of a cell, the cell is destroyed through the formation of transmembrane structures. The complement fixation test¹³¹⁻¹³³ uses sheep red blood cells (SRBC), anti SRBC antibody, complement, the antibody against the desired antigen (or antigen for the desired antibody) and the serum sample. If the antigen or antibody is present in the serum sample, the SRBC is not destroyed. If the antigen or antibody of interest is not present, complement destroys the anti-SRBC and SRBC complex.

1.5.6 ELISA

ELISA (Figure 2) is presently the most frequently used technique for dengue serological studies¹²⁸ and several formats have been designed for detecting dengue virus antibodies. These include IgM/IgG capture ELISA in separate wells of an assay plate.^{10, 134} Since 1984, dengue fever has been diagnosed through the detection of serum anti-dengue IgM using dengue IgM antibody capture ELISA (MAC-ELISA), using a mixture of all four dengue antigens. Positive and borderline samples were subsequently evaluated using hemagglutination inhibition (HI) testing and after 1992, IgG-ELISA.¹³⁵ HI testing suffers from several disadvantages as mentioned previously, and while MAC-ELISA is widely used, it is not the best method for early diagnosis of the virus. Additionally, neither method allows for serotyping.

1.5.7 Nucleic acid based methods

Isolation of the virus by cell culture and reverse transcriptase polymerase chain reaction (RT-PCR) are recommended for early detection of the virus.¹²⁷ Since virus isolation by cell culture can take more than seven days before a result is obtained,¹³⁶ RT-PCR methods of diagnosis have been developed.¹³⁷⁻¹⁴² An advantage of using PCR methods is the ability to multiplex.^{137, 141, 143} Routinely, serotyping is carried out using a two step approach of RT-PCR followed by nested PCR. This procedure is costly and time consuming, and a one-step, single-tube method has been developed,¹⁴⁴ as well as a 1-step single-tube duplex RT-PCR.¹⁴⁵

PCR affords a sensitive, specific, multiplexed method of detection, but it is still too costly for extensive application,^{8, 146} particularly in areas where dengue is endemic. As a result, novel detection systems which incorporate high sensitivity with short operation time and easy processing are required. These include biosensors,¹⁴⁷ microfluidic devices integrated with fluorescence cross correlation spectroscopy (FCCS),¹⁴⁸ a magnetophoretic fluorescence sensor⁷ and serological test kits,^{4, 15-16, 149-150} which have varied sensitivities.

Generally, nucleic acid methods of diagnosis are able to detect lower levels of the virus than the cheaper serological methods. These methods can be applied to multiplexed measurement of the different forms of the virus, unlike serological methods. Table 1 summarises the relative limits of detection of the two methods, showing the relative detection limits for the two methods. The concentration unit 1 pfu mL⁻¹ refers to a single virus particle in a millilitre of solution. Since a virus

particle weighs 22 M Da (0.8 fg), ¹²³ this indicates a limit of detection of 0.8 fg mL⁻¹, which is substantially lower than those obtained through serology.

Biomarker	Method	LOD
E protein ¹⁵¹	QCM	1.727 µg mL ⁻¹
NS-1 ¹⁵¹	QCM	0.740 µg mL ⁻¹
NS-1 (DEN-1) ¹⁵²	QCM	1 ng mL ⁻¹
NS-1 (DEN-2) ¹⁵²	QCM	4 ng mL ⁻¹
NS-1 (DEN-2) ¹⁵³	ELISA	4 ng mL ⁻¹
Viral DNA	NASBA ¹⁵⁴	1 pfumL ⁻¹
	NASBA ¹⁵⁵	1pfu mL ⁻¹
	RT-PCR ⁹²	1 pfu mL ⁻¹

Table 1: Limits of detection for some methods of dengue diagnosis

1.6 Research Objectives

On the basis of existing knowledge, the following objectives were set for this present study. First, to use chemometrics to quantitatively separate mixtures of conventional organic dyes and quantum dots. A simple spectral unmixing algorithm was applied for quantitative analysis of fluorescence mixtures. Organic dyes were used in immunoassays to establish the possibility of detecting multiple targets in a single well of an assay plate, thereby creating novel multiplexed immunoassays for dengue antibodies.

The next part of the study concentrated on the development of a simplified approach to spectral unmixing using silica nanoparticles doped with chelated lanthanides. Similarly, limits of detection of these NPs were determined and their behaviour in mixtures established. The overarching goal was a multiplexed immunoassay using these NP probes to detect multiple viral targets.

The multiplexed methods designed in the first and second parts of the study were applied to serum samples obtained from mice immunised with dengue antigens, to test the hypothesis that multiple forms of a virus can be detected in a single well of an assay plate by separation of fluorescent signals. A variety of methods were used to prove this hypothesis: epi-fluorescence microscopy, confocal laser scanning microscopy and programmable array microscopy. All assays were compared to conventional multi-well ELISAs.

Finally, as viruses of the same family may have similar antigenic sites on the antibodies, cross reactivity of one virus with another can occur during the diagnostic

process. Model studies involving human and mouse IgGs were used to establish the applicability of a statistical method already in existence for pesticides, to differentiate between cross reactive Flavivirus antibodies. The applicability of this method to dengue fever was explored through the use of simulated and real data.

1.7 References

- (1) Abhyankar, A. V.; Dash, P. K.; Saxena, P.; Bhargava, R.; Parida, M. M.; Jana, A. M.; Sahni, A. K.; Rao, P. V. L. Comparison of a dipstick dot-ELISA with commercial assays for anti-dengue virus IgM antibodies. *Viral Immunol.* **2006**, *19*, 630-636.
- (2) A-Nuegoonpipat, A.; Panthuyosri, N.; Anantapreecha, S.; Chanamaa, S.; Sa-Ngasang, A.; Sawanpanyalert, P.; Kurane, I. Cross-reactive IgM responses in patients with dengue or Japanese encephalitis. *J. Clin. Virol.* **2008**, *42*, 75-77.
- (3) Atias, D.; Liebes, Y.; Chalifa-Caspi, V.; Bremand, L.; Lobel, L.; Marks, R. S.; Dussart, P. Chemiluminescent optical fiber immunosensor for the detection of IgM antibody to dengue virus in humans. *Sens. Actuator B-Chem.* **2009**, *140*, 206-215.
- (4) Bessoff, K.; Delorey, M.; Sun, W.; Hunsperger, E. Comparison of two commercially available dengue virus (DENV) NS1 capture enzyme-linked immunosorbent assays using a single clinical sample for diagnosis of acute DENV infection. *Clin. Vaccine Immunol.* **2008**, *15*, 1513-1518.
- (5) Blacksell, S. D.; Bell, D.; Kelley, J.; Mammen, M. P., Jr.; Gibbons, R. V.; Jarman, R. G.; Vaughn, D. W.; Jenjaroen, K.; Nisalak, A.; Thongpaseuth, S.; Vongsouvath, M.; Davong, V.; Phouminh, P.; Phetsouvanh, R.; Day, N. P. J.; Newton, P. N. Prospective study to determine accuracy of rapid serological assays for diagnosis of acute dengue virus infection in Laos. *Clin. Vaccine Immunol.* **2007**, *14*, 1458-1464.
- (6) Blacksell, S. D.; Mammen Jr., M. P.; Thongpaseuth, S.; Gibbons, R. V.; Jarman, R. G.; Jenjaroen, K.; Nisalak, A.; Phetsouvanh, R.; Newton, P. N.; Day, N. P. J. Evaluation of the Panbio dengue virus nonstructural 1 antigen detection and immunoglobulin M antibody enzyme-linked immunosorbent assays for the diagnosis of acute dengue infections in Laos. *Diagnostic Microbiology and Infectious Disease*, **2008**, *60*, 43-49.
- (7) Chang, W.; Shang, H.; Perera, R. M.; Lok, S.; Sedlak, D.; Kuhn, R. J.; Lee, G. U. Rapid detection of dengue virus in serum using magnetic separation and fluorescence detection. *Analyst* **2008**, *133*, 233-240.
- (8) Chen, S.; Chuang, Y.; Lu, Y.; Lin, H.; Yang, Y.; Lin, C. A method of layer-by-layer gold nanoparticle hybridization in a quartz crystal microbalance DNA sensing system used to detect dengue virus. *Nanotechnology* **2009**, *20*, 215501.
- (9) Cohen, A. L.; Dowell, S. F.; Nisalak, A.; Mammen, M. P., Jr.; Petkanchanapong, W.; Fisk, T. L. Rapid diagnostic tests for dengue and leptospirosis: antibody detection is insensitive at presentation. *Trop. Med. Int. Health* **2007**, *12*, 47-51.
- (10) Dittmar, D.; Cleary, T. J.; Castro, A. Immunoglobulin G-Specific and Immunoglobulin M-Specific Enzyme-Linked Immunosorbent Assay for Detection of Dengue Antibodies. *J. Clin. Microbiol.* **1979**, *9*, 498-502.

- (11) Dos Santos, F. B.; Nogueira, R. M. R.; Lima, M. R. Q.; De Simone, T. S.; Schatzmayr, H. G.; Lemes, E. A. B.; Harris, E.; Miagostovich, M. P. Recombinant polypeptide antigen-based immunoglobulin G enzyme-linked immunosorbent assay for serodiagnosis of dengue. *Clin. Vaccine Immunol.* **2007**, *14*, 641-643.
- (12) Houghton-Trivino, N.; Montana, D.; Castellanos, J. Dengue-yellow fever sera cross-reactivity; challenges for diagnosis. *Rev Salud Publica (Bogota)* **2008**, *10*, 299-307.
- (13) Falconar, A. K. I.; de Plata, E.; Romero-Vivas, C. M. E. Altered enzyme-linked immunosorbent assay immunoglobulin M (IgM). *Clin. Vaccine Immunol.* **2006**, *13*, 1044-1051.
- (14) Kuno, G.; Gomez, I.; Gubler, D. J. An Elisa Procedure for the Diagnosis of Dengue Infections. *J. Virol. Methods* **1991**, *33*, 101-113.
- (15) Rivetz, B.; Siman-Tov, D.; Ambal, E.; Jaramillo, A.; Ben-Zvi, A.; Tartakovsky, B.; Fish, F. New dengue antibody assay with unique differential detection of IgG and IgM antibodies. *Clin. Biochem.* **2009**, *42*, 180-184.
- (16) Sekaran, S. D.; Lan, E. C.; Subramaniam, G. Comparison of five serological diagnostic assays for the detection of IgM and IgG antibodies to dengue virus. *Afr. J. Microbiol. Res.* **2008**, *2*, 141-147.
- (17) Ueda Fick de Souza, Vanda Akiko; Tateno, A. F.; Oliveira, R. R.; Domingues, R. B.; Araujo, E. S.; Kuster, G. W.; Pannuti, C. S. Sensitivity and specificity of three ELISA-based assays for discriminating primary from secondary acute dengue virus infection. *J. Clin. Virol.* **2007**, *39*, 230-233.
- (18) Biagini, R. E.; Sammons, D. L.; Smith, J. P.; MacKenzie, B. A.; Striley, C. A. F.; Semenova, V.; Steward-Clark, E.; Stamey, K.; Freeman, A. E.; Quinn, C. P.; Snawder, J. E. Comparison of a multiplexed fluorescent covalent microsphere immunoassay and an enzyme-linked immunosorbent assay for measurement of human immunoglobulin G antibodies to anthrax toxins. *Clin. Diagn. Lab. Immunol.* **2004**, *11*, 50-55.
- (19) Kubly, J., Ed.; In *Immunology*; Goldsby, R. A., Kindt, T. J. and Osborne, B. A., Eds.; W. H. Freeman & Co Ltd: 2000; .
- (20) Wild, D., Ed.; In *The Immunoassay Handbook*; Macmillan Direct Ltd.: Hants, UK, 1994; .
- (21) Wu, A. H. B. A selected history and future of immunoassay development and applications in clinical chemistry. *Clin. Chim. Acta* **2006**, *369*, 119-124.
- (22) Berson, S. A.; Yalow, R. S. General principles of radioimmunoassay (Reprinted from Clinica Chimica Acta, vol 22, pg 51-69, 1968). *Clin. Chim. Acta* **2006**, *369*, 125-143.
- (23) Miles, L. E.; Hales, C. N. Labelled antibodies and immunological assay systems. *Nature* **1968**, *219*, 186-189.
- (24) Readhead, C.; Addison, G. M.; Hales, C. N.; Lehmann, H. Immunoradiometric and 2-Site Assay of Human Follicle-Stimulating Hormone. *J. Endocrinol.* **1973**, *59*, 313-323.

- (25) Kohler, G.; Milstein, C. Continuous cultures of fused cells secreting antibody of predefined specificity (Reprinted from Nature, vol 256, 1975). *J. Immunol.* **2005**, *174*, 2453-2455.
- (26) Lequin, R. M. Enzyme Immunoassay (EIA)/Enzyme-Linked Immunosorbent Assay (ELISA). *Clin. Chem.* **2005**, *51*, 2415-2418.
- (27) Pang, S.; Smith, J.; Onley, D.; Reeve, J.; Walker, M.; Foy, C. A comparability study of the emerging protein array platforms with established ELISA procedures. *J. Immunol. Methods* **2005**, *302*, 1-12.
- (28) Magliulo, M.; Roda, B.; Zattoni, A.; Michelini, E.; Luciani, M.; Lelli, R.; Reschiglian, P.; Roda, A. An innovative, flow-assisted, noncompetitive chemiluminescent immunoassay for the detection of pathogenic bacteria. *Clin. Chem.* **2006**, *52*, 2151-2155.
- (29) Price, C. P.; Newman, D. J., Eds.; In *Principles and Practice of Immunoassay*; Macmillan: London, 1997; .
- (30) Vignali, D. A. A. Multiplexed particle-based flow cytometric assays. *J. Immunol. Methods* **2000**, *243*, 243-255.
- (31) Fulton, R. J.; McDade, R. L.; Smith, P. L.; Kienker, L. J.; Kettman, J. R. In *Advanced multiplexed analysis with the FlowMetrix(TM) system*; Clinical Chemistry; 29th Annual Oak Ridge Conference; AMER ASSOC CLINICAL CHEMISTRY: WASHINGTON; 2101 L STREET NW, SUITE 202, WASHINGTON, DC 20037-1526, 1997; Vol. 43, pp 1749-1756.
- (32) Liu, M. Y.; Xydakis, A. M.; Hoogeveen, R. C.; Jones, P. H.; Smith, E. O. B.; Nelson, K. W.; Ballantyne, C. M. Multiplexed analysis of biomarkers related to obesity and the metabolic syndrome in human plasma, using the luminex-100 system. *Clin. Chem.* **2005**, *51*, 1102-1109.
- (33) Clavijo, A.; Hole, K.; Li, M. Y.; Collignon, B. Simultaneous detection of antibodies to foot-and-mouth disease non-structural proteins 3ABC, 3D, 3A and 3B by a multiplexed Luminex assay to differentiate infected from vaccinated cattle. *Vaccine* **2006**, *24*, 1693-1704.
- (34) Heijmans-Antonissen, C.; Wesseldijk, F.; Munnikes, R. J. M.; Huygen, F. J. P. M.; van der Meijden, P.; Hop, W. C. J.; Hooijkaas, H.; Zijlstra, F. J. Multiplex bead array assay for detection of 25 soluble cytokines in blister fluid of patients with complex regional pain syndrome type 1. *Mediators Inflamm.* **2006**, 28398.
- (35) van Gageldonk, P. G. M.; van Schaijk, F. G.; van der Klis, F. R.; Berbers, G. A. M. Development and validation of a multiplex immunoassay for the simultaneous determination of serum antibodies to Bordetella pertussis, diphtheria and tetanus. *J. Immunol. Methods* **2008**, *335*, 79-89.
- (36) Gu, A.; Mo, H.; Xie, Y.; Peng, R.; Bei, J.; Peng, J.; Li, M.; Chen, L.; Feng, Q.; Jia, W.; Zeng, Y. Evaluation of a Multianalyte Profiling Assay and an Enzyme-Linked Immunosorbent Assay for Serological Examination of Epstein-Barr Virus-Specific Antibody Responses in Diagnosis of Nasopharyngeal Carcinoma. *Clin. Vaccine Immunol.* **2008**, *15*, 1684-1688.

- (37) Djoba Siawaya, J. F.; Roberts, T.; Babb, C.; Black, G.; Golakai, H. J.; Stanley, K.; Bapela, N. B.; Hoal, E.; Parida, S.; van Helden, P.; Walzl, G. An evaluation of commercial fluorescent bead-based luminex cytokine assays. *PLoS One* **2008**, *3*, e2535.
- (38) Wagner, B.; Freer, H. Development of a bead-based multiplex assay for simultaneous quantification of cytokines in horses. *Vet. Immunol. Immunopathol.* **2009**, *127*, 242-248.
- (39) Goldman, E. R.; Liu, J. L.; Bernstein, R. D.; Swain, M. D.; Mitchell, S. Q.; Anderson, G. P. Ricin Detection Using Phage Displayed Single Domain Antibodies. *Sensors* **2009**, *9*, 542-555.
- (40) Sharma, R. K.; Rogojina, A. T.; Chalam, K. V. Multiplex immunoassay analysis of biomarkers in clinically accessible quantities of human aqueous humor. *Mol. Vis.* **2009**, *15*, 60-69.
- (41) Watson, D. S.; Reddy, S. M.; Brahmakshatriya, V.; Lupiani, B. A multiplexed immunoassay for detection of antibodies against avian influenza virus. *J. Immunol. Methods* **2009**, *340*, 123-131.
- (42) Rao, R. S.; Visuri, S. R.; McBride, M. T.; Albala, J. S.; Matthews, D. L.; Coleman, M. A. Comparison of multiplexed techniques for detection of bacterial and viral proteins. *J. Proteome Res.* **2004**, *3*, 736-742.
- (43) Hartmann, M.; Schrenk, M.; Dottinger, A.; Nagel, S.; Roeraade, J.; Joos, T. O.; Templin, M. F. Expanding assay dynamics: A combined competitive and direct assay system for the quantification of proteins in multiplexed Immunoassays. *Clin. Chem.* **2008**, *54*, 956-963.
- (44) Deiss, F.; LaFratta, C. N.; Symer, M.; Blicharz, T. M.; Sojic, N.; Walt, D. R. Multiplexed Sandwich Immunoassays Using Electrochemiluminescence Imaging Resolved at the Single Bead Level. *J. Am. Chem. Soc.* **2009**, *131*, 6088-+.
- (45) Diercks, A. H.; Ozinsky, A.; Hansen, C. L.; Spotts, J. M.; Rodriguez, D. J.; Aderem, A. A microfluidic device for multiplexed protein detection in nanoliter volumes. *Anal. Biochem.* **2009**, *386*, 30-35.
- (46) Qin, L.; Vermesh, O.; Shi, Q.; Heath, J. R. Self-powered microfluidic chips for multiplexed protein assays from whole blood. *Lab Chip* **2009**, *9*, 2016-2020.
- (47) Nichkova, M.; Dosev, D.; Davies, A. E.; Gee, S. J.; Kennedy, I. M.; Hammock, B. D. Quantum dots as reporters in multiplexed immunoassays for biomarkers of exposure to agrochemicals. *Anal. Lett.* **2007**, *40*, 1423-1433.
- (48) Nichkova, M.; Dosev, D.; Gee, S. J.; Hammock, B. D.; Kennedy, I. M. Multiplexed immunoassays for proteins using magnetic luminescent nanoparticles for internal calibration. *Anal. Biochem.* **2007**, *369*, 34-40.
- (49) Lian, W.; Wu, D.; Lim, D. V.; Jin, S. Sensitive detection of multiplex toxins using antibody microarray. *Anal. Biochem.* **2010**, *401*, 271-279.
- (50) Goldman, E. R.; Clapp, A. R.; Anderson, G. P.; Uyeda, H. T.; Mauro, J. M.; Medintz, I. L.; Mattoussi, H. Multiplexed toxin analysis using four colors of quantum dot fluororeagents. *Anal. Chem.* **2004**, *76*, 684-688.

- (51) Marts, R. O. Fluorescence microscopy for measuring fibril angles in pine tracheids. *Stain Technol.* **1955**, *30*, 243-248.
- (52) Matsukuma, E.; Kato, Z.; Omoya, K.; Hashimoto, K.; Li, A.; Yamamoto, Y.; Ohnishi, H.; Hiranuma, H.; Komine, H.; Kondo, N. Development of fluorescence-linked immunosorbent assay for high throughput screening of interferon-gamma. *Allergol. Int.* **2006**, *55*, 49-54.
- (53) Price, C. P.; Newman, D. J., Eds.; In *Principles and practice of immunoassay*; Macmillan: Stockton, London, 1997; .
- (54) Zepp, R. G.; Sheldon, W. M.; Moran, M. A. Dissolved organic fluorophores in southeastern US coastal waters: correction method for eliminating Rayleigh and Raman scattering peaks in excitation-emission matrices. *Mar. Chem.* **2004**, *89*, 15-36.
- (55) Richards, C. I.; Hsiang, J.; Senapati, D.; Patel, S.; Yu, J.; Vosch, T.; Dickson, R. M. Optically Modulated Fluorophores for Selective Fluorescence Signal Recovery. *J. Am. Chem. Soc.* **2009**, *131*, 4619-4621.
- (56) Vicennati, P.; Bense, N.; Wagner, A.; Creminon, C.; Taran, F. Sandwich immunoassay as a high-throughput screening method for cross-coupling reactions. *Angew. Chem. -Int. Edit.* **2005**, *44*, 6863-6866.
- (57) Taipa, M. A. Immunoassays: Biological tools for high throughput screening and characterisation of combinatorial libraries. *Comb. Chem. High Throughput Screen.* **2008**, *11*, 325-335.
- (58) Ghafari, H.; Zhou, Y.; Ali, S.; Hanley, Q. S. Confocal detection of planar homogeneous and heterogeneous immunosorbent assays. *J. Biomed. Opt.* **2009**, *14*, 064022.
- (59) Wilson, R.; Spiller, D. G.; Prior, I. A.; Bhatt, R.; Hutchinson, A. Magnetic microspheres encoded with photoluminescent quantum dots for multiplexed detection. *J. Mater. Chem.* **2007**, *17*, 4400-4406.
- (60) Geddes, C. D.; Lakowicz, J. R., Eds.; In *Advanced concepts in spectroscopy: Small molecule sensing*; Geddes, C. D., Lakowicz, J. R., Eds.; Topics in fluorescence spectroscopy; Springer Science + Business Media, Inc.: New York, USA, 2005; Vol. 9, pp 327-2.
- (61) McGiven, J. A.; Tucker, J. D.; Perrett, L. L.; Stack, J. A.; Brew, S. D.; MacMillan, A. P. Validation of FPA and cELISA for the detection of antibodies to Brucella abortus in cattle sera and comparison to SAT, CFT, and iELISA. *J. Immunol. Methods* **2003**, *278*, 171-178.
- (62) Cooreman, S.; Cuypers, E.; De Doncker, M.; Van Hee, P.; Uyttenbroeck, W.; Neels, H. Comparison of three immunoassays and one GC-MS method for the determination of valproic acid. *Immuno-anal. Biol. spec.* **2008**, *23*, 240-244.
- (63) Bacigalupo, M. A.; Meroni, G.; Secundo, F.; Scalera, C.; Quici, S. Antibodies conjugated with new highly luminescent Eu³⁺ and Tb³⁺ chelates as markers for time resolved immunoassays. Application to simultaneous determination of clenbuterol and free cortisol in horse urine. *Talanta* **2009**, *80*, 954-958.

- (64) Chen, Y.; Lu, Z. H. Dye sensitized luminescent europium nanoparticles and its time-resolved fluorometric assay for DNA. *Anal. Chim. Acta* **2007**, *587*, 180-186.
- (65) Harma, H.; Keranen, A. M.; Lovgren, T. Synthesis and characterization of europium(III) nanoparticles for time-resolved fluoroimmunoassay of prostate-specific antigen. *Nanotechnology* **2007**, *18*, 075604.
- (66) Harma, H.; Soukka, T.; Lovgren, T. Europium nanoparticles and time-resolved fluorescence for ultrasensitive detection of prostate-specific antigen. *Clin. Chem.* **2001**, *47*, 561-568.
- (67) Yuan, J. L.; Wang, G. L. Lanthanide-based luminescence probes and time-resolved luminescence bioassays. *Trac-Trends Anal. Chem.* **2006**, *25*, 490-500.
- (68) Lakowicz, J. R.; Maliwal, B.; Ozinskas, A.; Thompson, R. B. Fluorescence Lifetime Energy-Transfer Immunoassay Quantified by Phase-Modulation Fluorometry. *Sens. Actuator B-Chem.* **1993**, *12*, 65-70.
- (69) Hanley, Q. S.; Verveer, P. J.; Jovin, T. M. Optical sectioning fluorescence spectroscopy in a programmable array microscope. *Appl. Spectrosc.* **1998**, *52*, 783-789.
- (70) Hanley, Q. S.; Verveer, P. J.; Jovin, T. M. Spectral imaging in a programmable array microscope by hadamard transform fluorescence spectroscopy. *Appl. Spectrosc.* **1999**, *53*, 1-10.
- (71) Hanley, Q. S.; Verveer, P. J.; Gemkow, M. J.; Arndt-Jovin, D.; Jovin, T. M. An optical sectioning programmable array microscope implemented with a digital micromirror device. *J. Microsc. -Oxf.* **1999**, *196*, 317-331.
- (72) Hanley, Q. S.; Jovin, T. M. Highly multiplexed optically sectioned spectroscopic imaging in a programmable array microscope. *Appl. Spectrosc.* **2001**, *55*, 1115-1123.
- (73) Hagen, G. M.; Caarls, W.; Thomas, M.; Hill, A.; Lidke, K. A.; Rieger, B.; Fritsch, C.; van Geest, B.; Jovin, T. M.; Arndt-Jovin, D. J. In *In Biological applications of an LCoS-based programmable array microscope (PAM)* - art. no. 64410S; Farkas, D., Leif, R. and Nicolau, D. V., Eds.; Imaging, Manipulation, and Analysis of Biomolecules, Cells, and Tissues V; PROCEEDINGS OF THE SOCIETY OF PHOTO-OPTICAL INSTRUMENTATION ENGINEERS (SPIE); Conference on Imaging, Manipulation, and Analysis of Biomolecules, Cells, and Tissues V; SPIE-INT SOC OPTICAL ENGINEERING: BELLINGHAM; 1000 20TH ST, PO BOX 10, BELLINGHAM, WA 98227-0010 USA, 2007; Vol. 6441, pp S4410-S4410.
- (74) Zhou, Y.; Dickenson, J. M.; Hanley, Q. S. Imaging lifetime and anisotropy spectra in the frequency domain. *J. Microsc. -Oxf.* **2009**, *234*, 80-88.
- (75) Elson, E. L.; Schlessinger, J.; Koppel, D. E.; Axelrod, D.; Webb, W. W. Measurement of lateral transport on cell surfaces. *Prog. Clin. Biol. Res.* **1976**, *9*, 137-147.

- (76) Hamann, S.; Kiilgaard, J. F.; Litman, T.; Alvarez-Leefmans, F. J.; Winther, B. R.; Zeuthen, T. Measurement of cell volume changes by fluorescence self-quenching. *J. Fluoresc.* **2002**, *12*, 139-145.
- (77) Ferrari, B. C.; Bergquist, P. L. Quantum dots as alternatives to organic fluorophores for Cryptosporidium detection using conventional flow cytometry and specific monoclonal antibodies: Lessons learned. *Cytom. Part A* **2007**, *71A*, 265-271.
- (78) Hayden, M. J.; Nguyen, T. M.; Waterman, A.; Chalmers, K. J. Multiplex-ready PCR: A new method for multiplexed SSR and SNP genotyping. *BMC Genomics* **2008**, *9*, 80.
- (79) Lin, S.; Chang, G.; Lin, C. Novel wave length-resolved fluorescence detection for a high-throughput capillary electrophoresis system under a diascopic configuration. *J. Chromatogr. A* **2008**, *1192*, 198-201.
- (80) Uhler, S. A.; Cai, D. W.; Man, Y. F.; Figge, C.; Walter, N. G. RNA degradation in cell extracts: Real-time monitoring by fluorescence resonance energy transfer. *J. Am. Chem. Soc.* **2003**, *125*, 14230-14231.
- (81) Nipper, M. E.; Majd, S.; Mayer, M.; Lee, J. C. -; Theodorakis, E. A.; Haidekker, M. A. Characterization of changes in the viscosity of lipid membranes with the molecular rotor FCVJ. *Biochim. Biophys. Acta-Biomembr.* **2008**, *1778*, 1148-1153.
- (82) Vinnakota, K. C.; Mitchell, D. A.; Deschenes, R. J.; Wakatsuki, T.; Beard, D. A. Analysis of the diffusion of Ras2 in *Saccharomyces cerevisiae* using fluorescence recovery after photobleaching. *Phys. Biol.* **2010**, *7*, 026011.
- (83) Suresh, M.; Das, A. New coumarin-based sensor molecule for magnesium and calcium ions. *Tetrahedron Lett.* **2009**, *50*, 5808-5812.
- (84) Lee, W.; Lee, Y.; Lee, J.; Davis, L. M.; Deininger, P.; Soper, S. A. Cross-Talk-Free Dual-Color Fluorescence Cross-Correlation Spectroscopy for the Study of Enzyme Activity. *Anal. Chem.* **2010**, *82*, 1401-1410.
- (85) Shalon, D.; Smith, S. J.; Brown, P. O. A DNA microarray system for analyzing complex DNA samples using two-color fluorescent probe hybridization. *Genome Res.* **1996**, *6*, 639-645.
- (86) Debnath, M.; Prasad, G. B. K. S.; Bisen, P. S. In *In Situ Hybridization*; SPRINGER: 233 SPRING STREET, NEW YORK, NY 10013, UNITED STATES, 2010; pp 153-169.
- (87) Zhuang, X. W.; Ha, T.; Kim, H. D.; Centner, T.; Labeit, S.; Chu, S. Fluorescence quenching: A tool for single-molecule protein-folding study. *Proc. Natl. Acad. Sci. U. S. A.* **2000**, *97*, 14241-14244.
- (88) Chen, Y. D.; Blumenthal, R. On the use of Self-Quenching Fluorophores in the Study of Membrane-Fusion Kinetics - the Effect of Slow Probe Redistribution. *Biophys. Chem.* **1989**, *34*, 283-292.
- (89) Divya, O.; Mishra, A. K. Understanding the concept of concentration-dependent red-shift in synchronous fluorescence spectra: Prediction of λ_{max} (SFS) and optimization of $\Delta\lambda$ for synchronous fluorescence scan. *Anal. Chim. Acta* **2008**, *630*, 47-56.

- (90) Hilderbrand, S. A.; Shao, F.; Salthouse, C.; Mahmood, U.; Weissleder, R. Upconverting luminescent nanomaterials: application to in vivo bioimaging. *Chem. Commun.* **2009**, 4188-4190.
- (91) Kho, K. W.; Stoddart, P. R.; Harris, M.; Mazzolini, A. P. Confocal fluorescence polarization microscopy for linear unmixing of spectrally similar labels. *Micron* **2009**, *40*, 212-217.
- (92) Kao, C.; King, C.; Chao, D.; Wu, H.; Chang, G. J. Laboratory diagnosis of dengue virus infection: current and future perspectives in clinical diagnosis and public health. *J. Microbiol. Immunol. Infect.* **2005**, *38*, 5-16.
- (93) Abrams, B.; Dubrovsky, T. Quantum dots in flow cytometry. *Methods Mol. Biol.* **2007**, *374*, 185-203.
- (94) Enderlein, R.; Horing, N., Eds.; In *Fundamentals of Semiconductor Physics and Devices*; World Scientific Publishing Company: Singapore, 1997; .
- (95) Chan, W., Ed.; In *Bio-applications of Nanoparticles*; Landes Bioscience: Austin, Texas, 2007; .
- (96) Pinaud, F.; Michalet, X.; Bentolila, L. A.; Tsay, J. M.; Doose, S.; Li, J. J.; Iyer, G.; Weiss, S. Advances in fluorescence imaging with quantum dot bio-probes. *Biomaterials* **2006**, *27*, 1679-1687.
- (97) Biju, V.; Itoh, T.; Anas, A.; Sujith, A.; Ishikawa, M. Semiconductor quantum dots and metal nanoparticles: syntheses, optical properties, and biological applications. *Anal. Bioanal. Chem.* **2008**, *391*, 2469-2495.
- (98) Medintz, I. L.; Uyeda, H. T.; Goldman, E. R.; Mattoussi, H. Quantum dot bioconjugates for imaging, labelling and sensing. *Nat. Mater.* **2005**, *4*, 435-446.
- (99) Hu, M.; Yan, J.; He, Y.; Lu, H.; Weng, L.; Song, S.; Fan, C.; Wang, L. Ultrasensitive, Multiplexed Detection of Cancer Biomarkers Directly in Serum by Using a Quantum Dot-Based Microfluidic Protein Chip. *ACS Nano* **2010**, *4*, 488-494.
- (100) Karlin-Neumann, G.; Sedova, M.; Falkowski, M.; Wang, Z.; Lin, S.; Jain, M. Application of quantum dots to multicolor microarray experiments: four-color genotyping. *Methods Mol. Biol.* **2007**, *374*, 239-251.
- (101) Volkmer, A.; Hatrick, D. A.; Birch, D. J. S. Time-resolved nonlinear fluorescence spectroscopy using femtosecond multiphoton excitation and single-photon timing detection. *Meas Sci Technol* **1997**, *8*, 1339-1349.
- (102) Lakowicz, J. R. In *Principles of Fluorescence Spectroscopy*; Springer: New York, 2006; .
- (103) Brereton, R. In *Applied Chemometrics for Scientists*; John Wiley & Sons, Ltd: West Sussex, England, 2007; , pp 1.
- (104) Brereton, R. In *Chemometrics Data Analysis for the Laboratory and Chemical Plant*; John Wiley & Sons, Ltd: West Sussex, England, 2003; , pp 485.
- (105) Keenan, M. R.; Timlin, J. A.; Van Benthem, M. H.; Haaland, D. M. Algorithms for constrained linear unmixing with application to the

- hyperspectral analysis of fluorophore mixtures. *Imaging Spectrometry VIII* **2002**, 4816, 193-202.
- (106) Haaland, D. M.; Timlin, J. A.; Sinclair, M. B.; Van Benthem, M. H.; Martinez, M. J.; Aragon, A. D.; Werner-Washburne, M. Multivariate curve resolution for hyperspectral image analysis: Applications to microarray technology. *Spectral Imaging: Instrumentation, Applications, and Analysis II* **2003**, 4959, 55-66.
 - (107) Schreyer, S. K.; Bidinosti, M.; Wentzell, P. D. Application of maximum likelihood principal components regression to fluorescence emission spectra. *Appl. Spectrosc.* **2002**, 56, 789-796.
 - (108) Tan, M. Q.; Wang, G. L.; Hai, X. D.; Ye, Z. Q.; Yuan, J. L. Development of functionalized fluorescent europium nanoparticles for biolabeling and time-resolved fluorometric applications. *J. Mater. Chem.* **2004**, 14, 2896-2901.
 - (109) Ye, Z. Q.; Tan, M. Q.; Wang, G. L.; Yuan, J. L. Novel fluorescent europium chelate-doped silica nanoparticles: preparation, characterization and time-resolved fluorometric application. *J. Mater. Chem.* **2004**, 14, 851-856.
 - (110) Gomez-Hens, A.; Fernandez-Romero, J. M.; Aguilar-Caballeros, M. P. Nanostructures as analytical tools in bioassays. *Trac-Trends Anal. Chem.* **2008**, 27, 394-406.
 - (111) Xu, H.; Di, B.; Pan, Y.; Qiu, L.; Wang, Y.; Hao, W.; He, L.; Yuen, K.; Che, X. Serotype 1-specific monoclonal antibody-based antigen capture immunoassay for detection of circulating nonstructural protein NS1: Implications for early diagnosis and serotyping of dengue virus infections. *J. Clin. Microbiol.* **2006**, 44, 2872-2878.
 - (112) Mackenzie, J. S.; Gubler, D. J.; Petersen, L. R. Emerging flaviviruses: the spread and resurgence of Japanese encephalitis, West Nile and dengue viruses. *Nat. Med.* **2004**, 10, S98-S109.
 - (113) Guzman, M. G.; Kouri, G. Dengue and dengue hemorrhagic fever in the Americas: lessons and challenges. *J. Clin. Virol.* **2003**, 27, 1-13.
 - (114) Martin, N. C.; Pardo, J.; Simmons, M.; Tjaden, J. A.; Widjaja, S.; Marovich, M. A.; Sun, W.; Porter, K. R.; Burgess, T. H. An immunocytometric assay based on dengue infection via DC-SIGN permits rapid measurement of anti-dengue neutralizing antibodies. *J. Virol. Methods* **2006**, 134, 74-85.
 - (115) Gubler, D. J. Dengue and dengue hemorrhagic fever. *Clin. Microbiol. Rev.* **1998**, 11, 480-+.
 - (116) Halstead, S. B., Ed.; In *Dengue*; Pasvol, G., Hoffman, S., Eds.; Tropical Medicine: Science and Practice; Imperial College Press: London, UK, 2008; Vol. 5, pp 485-13.
 - (117) Sabin, A. B. Research on dengue during World War II. *Am. J. Trop. Med. Hyg.* **1952**, 1, 30-50.
 - (118) Halstead, S. B. Etiologies of Experimental Dengues of Siler and Simmons. *Am. J. Trop. Med. Hyg.* **1974**, 23, 974-982.

- (119) Papaevangelou, G.; Halstead, S. B. Infections with 2 Dengue Viruses in Greece in 20th-Century - did Dengue Hemorrhagic-Fever Occur in 1928 Epidemic. *J. Trop. Med. Hyg.* **1977**, *80*, 46-51.
- (120) Okuno, Y.; Fukunaga, T.; Tadano, M.; Fukai, K.; Ikeda, T.; Sekii, K.; Ariyoshi, H. Serological Studies on Volunteers Inoculated Experimentally with a Dengue Virus-Strain in 1943. *Biken J.* **1983**, *26*, 161-163.
- (121) Innis, B. L.; Nisalak, A.; Nimmannitya, S.; Kusalerdchariya, S.; Chongswasdi, V.; Suntayakorn, S.; Puttisri, P.; Hoke, C. H. An Enzyme-Linked Immunosorbent-Assay to Characterize Dengue Infections Where Dengue and Japanese Encephalitis Co-Circulate. *Am. J. Trop. Med. Hyg.* **1989**, *40*, 418-427.
- (122) Vaughn, D. W.; Whitehead, S. S.; Durbin, A. P. In *Dengue*; Barrett, A., Stanberry, L., Eds.; Vaccines: For biodefense and emerging and neglected diseases; Elsevier Inc.: London, UK, 2009; pp 287-324.
- (123) Kuhn, R. J.; Zhang, W.; Rossmann, M. G.; Pletnev, S. V.; Corver, J.; Lenches, E.; Jones, C. T.; Mukhopadhyay, S.; Chipman, P. R.; Strauss, E. G.; Baker, T. S.; Strauss, J. H. Structure of dengue virus: Implications for flavivirus organization, maturation, and fusion. *Cell* **2002**, *108*, 717-725.
- (124) Petersen, L. R.; Rochrig, J. T. Emerging Infectious Diseases. <http://www.cdc.gov/ncidod/eid/vol7no4/petersenG2.htm> (accessed 03/10, 2009).
- (125) Ocegueda, Leopoldo F., III; Patiris, P. J.; Chiles, R. E.; Busch, M. P.; Tobler, L. H.; Hanson, C. V. Short report: Flavivirus serology by Western blot analysis. *Am. J. Trop. Med. Hyg.* **2007**, *77*, 159-163.
- (126) Chiou, S.; Crill, W. D.; Chen, L.; Chang, G. J. Enzyme-linked Immunosorbent assays using novel Japanese encephalitis virus antigen improve the accuracy of clinical diagnosis of flavivirus infections. *Clin. Vaccine Immunol.* **2008**, *15*, 825-835.
- (127) World Health Organisation In *Laboratory diagnosis*; World Health Organisation, Ed.; Dengue haemorrhagic fever: diagnosis, treatment, prevention and control; World Health Organisation: Geneva, Switzerland, 1997; pp 34-47.
- (128) Guzman, M. G.; Kouri, G. Dengue diagnosis, advances and challenges. *Int. J. Infect. Dis.* **2004**, *8*, 69-80.
- (129) Russell, P.; Nisalak, N. Dengue virus identification by the plaque reduction neutralization test. *J. Immunol* **1967**, *99*, 291-296.
- (130) Jirakanjanakit, N.; Sanohsomneing, T.; Yoksan, S.; Bhamarapravati, N. The micro-focus reduction neutralization test for determining dengue and Japanese encephalitis neutralizing antibodies in volunteers vaccinated against dengue. *Trans. R. Soc. Trop. Med. Hyg.* **1997**, *91*, 614-617.
- (131) Scott, R. M.; Russell, P. K. Complement-Fixation Blocking Activity of Anti-Dengue IgM Antibody. *J. Immunol.* **1972**, *109*, 875-&.
- (132) Tesh, R. B. Method for the Isolation and Identification of Dengue Viruses, using Mosquito Cell-Cultures. *Am. J. Trop. Med. Hyg.* **1979**, *28*, 1053-1059.

- (133) Bondre, V. P.; Sapkal, G. N.; Yergolkar, P. N.; Fulmali, P. V.; Sankararaman, V.; Ayachit, V. M.; Mishra, A. C.; Gore, M. M. Genetic characterization of Bagaza virus (BAGV) isolated in India and evidence of anti-BAGV antibodies in sera collected from encephalitis patients. *J. Gen. Virol.* **2009**, *90*, 2644-2649.
- (134) Kuno, G.; Gomez, I.; Gubler, D. J. An Elisa Procedure for the Diagnosis of Dengue Infections. *J. Virol. Methods* **1991**, *33*, 101-113.
- (135) Rigau-Perez, J. G.; Gubler, D. J.; Vorndam, A. V.; Clark, G. G. Dengue surveillance: United States, 1986-1992. *Morb. Mortal. Weekly Rep.* **1994**, *43*, 7-19.
- (136) Poersch, C. D.; Pavoni, D. P.; Queiroz, M. H.; de Borba, L.; Goldenberg, S.; dos Santos, C. N. D.; Krieger, M. A. Dengue virus infections: comparison of methods for diagnosing the acute disease. *J. Clin. Virol.* **2005**, *32*, 272-277.
- (137) Chinnawirotpisan, P.; Mammen, M. P., Jr.; Nisalak, A.; Thaisomboonsuk, B.; Narupiti, S.; Thirawuth, V.; Putnak, R.; Zhang, C. Detection of concurrent infection with multiple dengue virus serotypes in Thai children by ELISA and nested RT-PCR assay. *Arch. Virol.* **2008**, *153*, 2225-2232.
- (138) Godoy dos Santos, H. W.; Ramos Silva Poloni, T. R.; Souza, K. P.; Menjon Muller, V. D.; Tremeschin, F.; Nali, L. C.; Fantinatti, L. R.; Amarilla, A. A.; Alfonso Castro, H. L.; Nunes, M. R.; Casseb, S. M.; Vasconcelos, P. F.; Badra, S. J.; Moraes Figueiredo, L. T.; Aquino, V. H. A simple one-step real-time RT-PCR for diagnosis of dengue virus infection. *J. Med. Virol.* **2008**, *80*, 1426-1433.
- (139) Houg, H. S. H.; Chen, R. C. M.; Vaughn, D. W.; Kanesa-athan, N. Development of a fluorogenic RT-PCR system for quantitative identification of dengue virus serotypes 1-4 using conserved and serotype-specific 3' noncoding sequences. *J. Virol. Methods* **2001**, *95*, 19-32.
- (140) Lo, C. L. H.; Yip, S. P.; Cheng, P. K. C.; To, T. S. S.; Lim, W. W. L.; Leung, P. H. M. One-step rapid reverse transcription-PCR assay for detecting and typing dengue viruses with GC tail and induced fluorescence resonance energy transfer techniques for melting temperature and color multiplexing. *Clin. Chem.* **2007**, *53*, 594-599.
- (141) Seah, C. L. K.; Chow, V. T. K.; Tan, H. C.; Chan, Y. C. Rapid, Single-Step Rtpcr Typing of Dengue Viruses using 5 Ns3 Gene Primers. *J. Virol. Methods* **1995**, *51*, 193-200.
- (142) Gurukumar, K. R.; Priyadarshini, D.; Patil, J. A.; Bhagat, A.; Singh, A.; Shah, P. S.; Cecilia, D. Development of real time PCR for detection and quantitation of Dengue Viruses. *Virol. J.* **2009**, *6*, 10.
- (143) Das, S.; Pingle, M. R.; Munoz-Jordan, J.; Rundell, M. S.; Rondini, S.; Granger, K.; Chang, G. - J.; Kelly, E.; Spier, E. G.; Larone, D.; Spitzer, E.; Barany, F.; Golightly, L. M. Detection and serotyping of dengue virus in serum samples by multiplex reverse transcriptase PCR-ligase detection reaction assay. *J. Clin. Microbiol.* **2008**, *46*, 3276-3284.
- (144) Saxena, P.; Dash, P. K.; Santhosh, S. R.; Shrivastava, A.; Parida, M.; Rao, P. V. L. Development and evaluation of one step single tube multiplex RT-PCR for rapid detection and typing of dengue viruses. *Virol. J.* **2008**, *5*, 20.

- (145) Dash, P. K.; Parida, M.; Santhosh, S. R.; Saxena, P.; Srivastava, A.; Neeraja, M.; Lakshmi, V.; Rao, P. V. L. In *In Development and evaluation of a 1-step duplex reverse transcription polymerase chain reaction for differential diagnosis of chikungunya and dengue infection*; Diagnostic Microbiology and Infectious Disease; International Conference on Emerging and Reemerging Viral Diseases of Tropic and Sub-Tropic; ELSEVIER SCIENCE INC: NEW YORK; 360 PARK AVE SOUTH, NEW YORK, NY 10010-1710 USA, 2008; Vol. 62, pp 52-57.
- (146) Chen, L. H.; Wilson, M. E. Transmission of dengue virus without a mosquito vector: Nosocomial mucocutaneous transmission and other routes of transmission. *Clin. Infect. Dis.* **2004**, *39*, E56-E60.
- (147) Teles, F. R. R.; Prazeres, D. M. F.; Lirna-Filho, J. L. Trends in dengue diagnosis. *Rev. Med. Virol.* **2005**, *15*, 287-302.
- (148) Zhang, Y.; Bahns, J. T.; Jin, Q.; Divan, R.; Chen, L. Toward the detection of single virus particle in serum. *Anal. Biochem.* **2006**, *356*, 161-170.
- (149) Zainah, S.; Wahab, A. H. A.; Mariam, M.; Fauziah, M. K.; Khairul, A. H.; Roslina, I.; Sairulakhma, A.; Kadimon, S. S.; Jais, M. S. M.; Chua, K. B. Performance of a commercial rapid dengue NS1 antigen immunochromatography test with reference to dengue NS1 antigen-capture ELISA. *J. Virol. Methods* **2009**, *155*, 157-160.
- (150) Shrivastva, A.; Tripathi, N. K.; Parida, M.; Dash, P. K.; Jana, A. M.; Lakshmana, R. P., V. Comparison of a dipstick enzyme-linked immunosorbent assay with commercial assays for detection of Japanese encephalitis virus-specific IgM antibodies. *J. Postgrad. Med.* **2008**, *54*, 181-185.
- (151) Wu, T. Z.; Su, C. C.; Chen, L. K.; Yang, H. H.; Tai, D. F.; Peng, K. C. Piezoelectric immunochip for the detection of dengue fever in viremia phase. *Biosens. Bioelectron.* **2005**, *21*, 689-695.
- (152) Tai, D.; Lin, C.; Wu, T.; Huang, J.; Shu, P. Artificial receptors in serologic tests for the early diagnosis of dengue virus infection. *Clin. Chem.* **2006**, *52*, 1486-1491.
- (153) Young, P. R.; Hilditch, P. A.; Bletchly, C.; Halloran, W. An antigen capture enzyme-linked immunosorbent assay reveals high levels of the dengue virus protein NS1 in the sera of infected patients. *J. Clin. Microbiol.* **2000**, *38*, 1053-1057.
- (154) Usawattanakul, W.; Jittmittraphap, A.; Endy, T. R.; Nisalak, A.; Tapchaisri, P.; Looareesuwan, S. Rapid detection of dengue viral RNA by nucleic acid sequence based amplification (NASBA). *J. Clin. Virol.* **2003**, *28*, S67-S67.
- (155) Wu, S. J. L.; Lee, E. M.; Putvatana, R.; Shurtleff, R. N.; Porter, K. R.; Suharyono, W.; Watts, D. M.; King, C. C.; Murphy, G. S.; Hayes, C. G.; Romano, J. W. Detection of dengue viral RNA using a nucleic acid sequence-based amplification assay. *J. Clin. Microbiol.* **2001**, *39*, 2794-2798.

2 Experimental methods

In this chapter, we explore the various instruments used throughout the research period, followed by protocols developed or adapted. As the main instrumentation used was the fluorescence microscope, a great deal of detail is placed on fluorescence, with the salient features of the three microscopes used described. General references are given at the end of the chapter.

2.1 Fluorescence Microscopy

Fluorescence microscopy was discovered by a German microscopist Köhler in 1904,¹ and has found several biological applications.²⁻⁶ The basic principles of optical microscopy apply to fluorescence microscopy, the main difference being the use of specialised light sources and filters for detection of fluorescence.

Fluorescence is one form of luminescence, which may be defined as the emission of light from an electronically excited state of a substance.⁷ Fluorescence occurs from a singlet excited state, where the electron in the excited orbital has an opposing spin to the electron in the ground state orbital. As a result, the return of the electron to the ground state is spin allowed and occurs quickly, on the order of nanoseconds. Phosphorescence, another form of luminescence, occurs when light is emitted from a triplet excited state; the electron in the excited orbital has the same spin as the one in the ground state orbital. Return to the ground state is spin forbidden and takes a significantly longer time. The Jablonski diagram (Figure 7) shows the number of possible routes whereby a specimen excited by a light source can return to the ground state, emitting either fluorescence or phosphorescence.

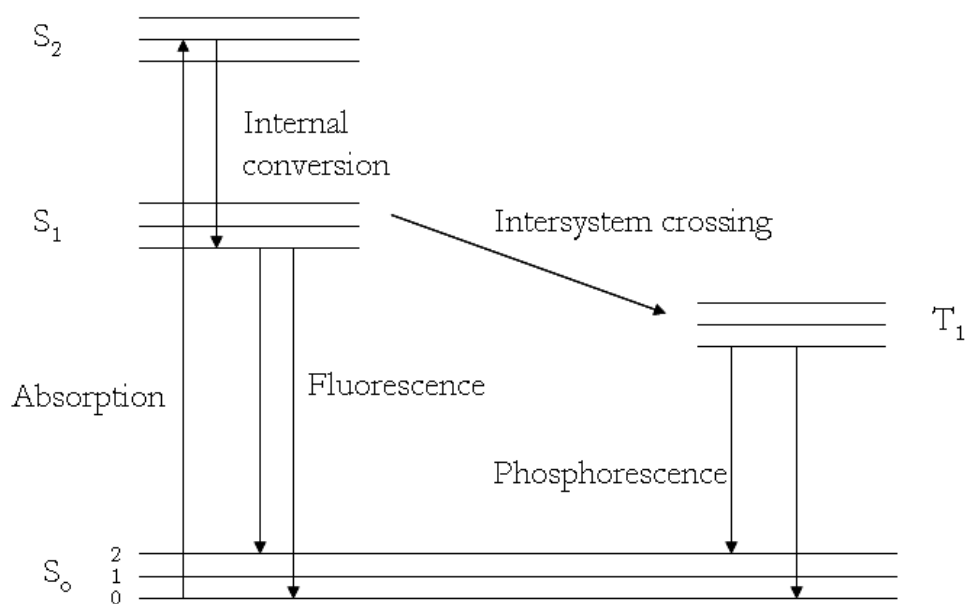


Figure 7: Jablonski diagram showing possible routes an excited fluorophore can take to return to the ground state⁷

Fluorescence intensity is directly related to the intensity of the excitation light and is proportional to the number of absorbing molecules in the sample. This may be explained theoretically. When light of intensity I_o is directed through a fluorescent sample, the sample absorbs some of the incident radiation, and light not absorbed is transmitted by the substance. The transmitted light may be called I and the light absorbed by the sample can be represented by $(I_o - I)$. The intensity of fluorescence, which occurs as a result of absorbance of I_o , is given by Equation 2-1.⁸

$$F = Q(I_o - I) \quad \text{Equation 2-1}$$

where F is fluorescence intensity, I_o is the light intensity before absorption, I is the light intensity after absorption and Q is the quantum efficiency. The absorbance A , according to Lambert's law is given in Equation 2-2.⁸

$$A = -\log\left(\frac{I}{I_o}\right) \rightarrow I = I_o e^{-A} \quad \text{Equation 2-2}$$

It therefore follows that ⁸

$$F = Q(I_o - I_o e^{-A}) \rightarrow F = QI_o(1 - e^{-A}) \quad \text{Equation 2-3}$$

As A approaches zero, e^{-A} approaches one and F approaches zero; when A approaches ∞ , e^{-A} approaches 0 and $F=QI_o$. When A is very small, $1-e^{-A}$ approaches A and $F=AQI_o$. If A is replaced by ϵc , where ϵ is a constant and c is concentration of the sample, then for low concentrations $F = \epsilon c QI_o$. This means that fluorescence is directly proportional to the concentration. For high concentrations, $F=QI_o$, which is independent of concentration.⁸ The range over which fluorescence intensity is proportional to concentration has been determined experimentally through a calibration curve of the relationship between relative fluorescence and absorbance. It was found that two phenomena lead to reduced fluorescence intensity at high absorbance values. These are the inner filter effect; also known as excitation absorbance, and reabsorption. The inner filter effect may be defined as the reduction of excitation intensity in the layers of a fluorescing object further from the light source, owing to absorption by the fluorophore.⁸ This phenomenon occurs when fluorescing molecules are not all equally well situated to collect the excitation light, resulting in the layer closest to the light source receiving more light than layers further from the source. I_o is then greater than I and fluorescence intensity is reduced. Reabsorption occurs for some fluorophores because of the overlap of absorption and emission spectra. In this instance, fluorescence can be reabsorbed by surrounding fluorophores, leading to a reduction in fluorescence yield.

2.1.1 Epifluorescence microscopy

The term epifluorescence microscopy refers to a system where the excitation and emission light pass through the same objective.⁷ This format is advantageous as most of the excitation is moved away from the detector. Figure 8 shows a schematic of the epi-illumination microscope used for this project. This is an Olympus IX71 inverted microscope, with a mercury lamp for excitation. The light from the excitation source passes through an excitation filter, also called a primary filter, which serves to provide light over a narrow band of wavelengths. This light is able to excite the specimen. On return to ground state, the specimen emits light which is passed through an emission or barrier filter. This filter typically has a low transmission at the wavelengths of excitation, but high at the wavelengths of emission. The dichroic beam splitter, also known as the dichroic mirror is positioned below the objective and serves to separate emitted light from unabsorbed excitation light. This is accomplished through an interference coating, which reflects light below a specified wavelength into the objective, and transmits light above this, allowing it to reach the eyepiece and detector. The filters used throughout the project consisted of band pass excitation filters, long pass emission filters and dichroic mirrors. The samples were generally contained in 96 and 384-welled glass bottomed plates with thickness of 170 μm . These were mounted on an automated stage (Merzhäuser, Wetzlar, Germany) powered by a USB port.

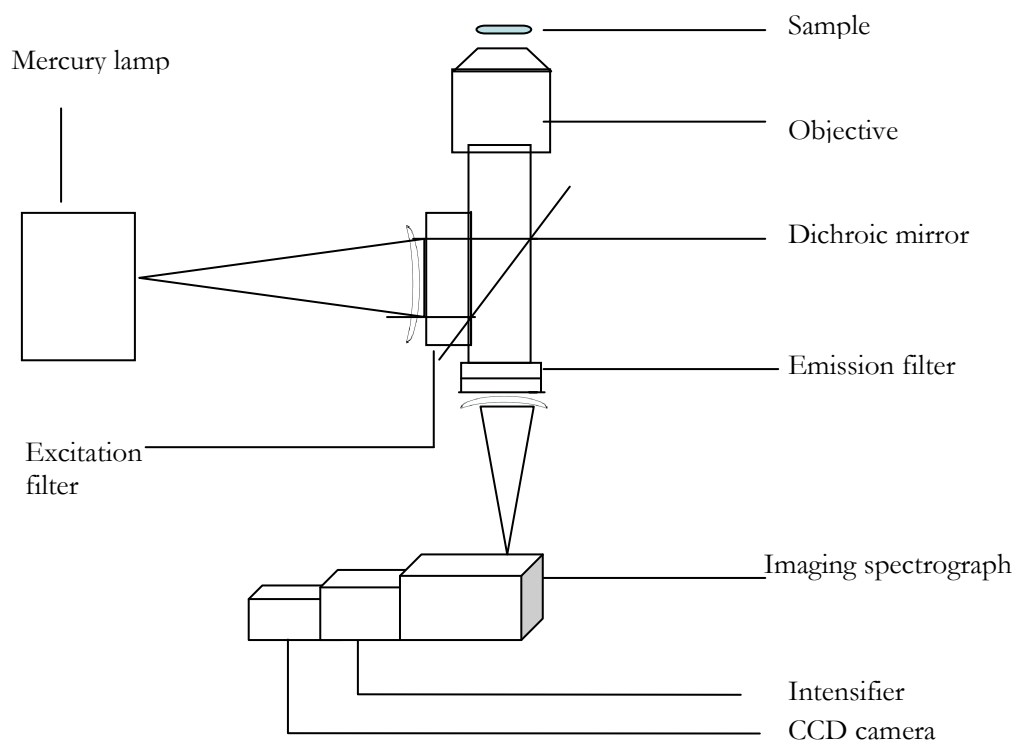


Figure 8: Schematic of the epi-fluorescence microscope used

2.1.2 Add-ons to the epi-illumination microscope

The add-ons to the epi-fluorescence microscope used were a spectrograph (PARISS; LightForm Inc., Hillsborough, NJ), intensifier (II118MD; Lambert Instruments, Leutengewolde, The Netherlands) and CCD camera (PCO.1600; PCO Computer Optics GmbH, Kilheim, Germany), all shown in Figure 8. While the intensifier is a useful add-on for doing lifetime measurements, its applications were beyond the scope of this project and will not be discussed.

A spectrograph allows the transformation of spectral information into an image, thereby providing a graphical means of monitoring the behaviour of fluorophores. The process of transformation is referred to as spectral imaging, although the terms hyperspectral imaging and multispectral imaging are also used.

The optical layout of a spectrograph is shown in Figure 9.⁹ This structure applies to both diffraction grating and prism spectrographs; only prism spectrographs will be mentioned here and schematic of a prism is shown in Figure 10. Light passes through a prism and is refracted by the angle β , which is dependent on the prism angle ϵ , the angle of incidence α , and the refractive index of the prism n . The relationship between these when the light is refracted parallel to the base of the prism is given by:¹⁰

$$\frac{\sin(\beta + \epsilon)}{2} = n \sin\left(\frac{\epsilon}{2}\right) \quad \text{Equation 2-4}$$

The change in refraction with respect to the change in refractive index is then given by:¹⁰

$$\frac{d\beta}{dn} = \frac{2 \sin\left(\frac{\epsilon}{2}\right)}{\cos[(\beta + \epsilon)/2]} = \frac{2 \sin\left(\frac{\epsilon}{2}\right)}{\sqrt{1 - n^2 \sin^2(\epsilon/2)}} \quad \text{Equation 2-5}$$

The difference in refractive angle $d\beta$ for a difference in wavelength $d\lambda$ is the angular dispersion:¹⁰

$$\frac{d\beta}{d\lambda} = \frac{2 \sin\left(\frac{\epsilon}{2}\right)}{\sqrt{1 - n^2 \sin^2(\epsilon/2)}} \frac{dn}{d\lambda} \quad \text{Equation 2-6}$$

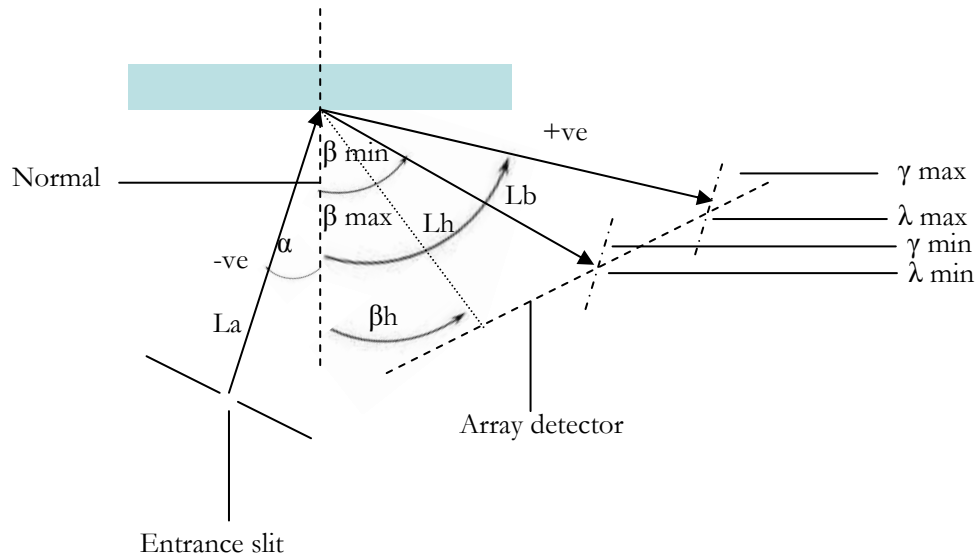


Figure 9: Diagram of the optical layout of a spectrograph, where α , angle of incidence; β , angle of refraction (min) at shortest wavelength (max) at longest wavelength; λ wavelength; γ , the inclination of a ray L_b to focal plane at a specific wavelength; L_a , distance from the entrance slit to the first active optic (such as a collimating mirror); L_b , distance from final optic to the detector; L_h , perpendicular distance from the first optic to the focal plane; β_h , angle from the normal to L_h ; normal, the reference line perpendicular to the optics; γ , inclination of a ray L_b to the focal plane at a specific wavelength.⁹

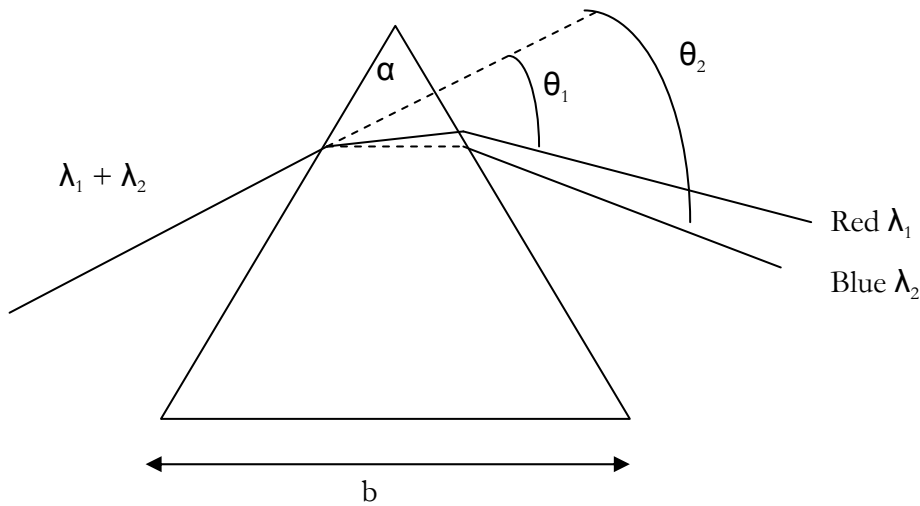


Figure 10: The dispersion of light of two wavelengths in a prism. The prism has an apex α , and baselength b . Two rays having wavelength λ_1 and λ_2 are refracted upon entering and exiting the prism according to Snell's law. As expected, blue light is more highly refracted than red light.¹¹

Equation 2-6 indicates that the angular dispersion is dependent on the angle of the prism,⁸ The linear dispersion, which defines the spread of the spectrum across the focal distance, is the product of the angular dispersion and the focal length of the optics used:¹⁰

$$\frac{dx}{d\lambda} = f \frac{d\beta}{d\lambda} \quad \text{Equation 2-7}$$

The spectrograph used in this research was designed for use in the wavelength range 360 – 920 nm and optimised for use with a digital CCD as detector. It had a slit width of 25 µm, a slit height of 5 mm and a spatial resolution of 0.6 µm. Unlike other prism-based spectrographs, this system was adapted to allow high aberration correction. Spectral imaging allowed mixtures of fluorophores with distinct spectral profiles to be separated without further processing. When dyes have a large spectral overlap, the spectrum of the mixture is a linear combination of the individual components as long as the fluorophores mix linearly. If a fluorescence spectrum of the individual components is obtained, the observed mixture can be resolved into its components through spectral unmixing which is facilitated by the spectrograph.

A charge coupled device (CCD) camera converts optical brightness into electrical signals, using CCDs. A CCD is a type of detector that stores its charge as a two-dimensional array. The design consists of layers of semiconductor silicon capped with a layer of silica. A pattern of conducting Si electrodes is placed on the surface of the silica (Figure 11). The surface is further broken down into pixels; a positive potential is applied to two-thirds of the pixels while the final third has a less positive potential applied, thereby creating a potential well. Construction involves a p-doped region sitting on an n-doped substrate, thereby creating a p-n junction. The p-

doped region absorbs light and an electron is liberated. The hole formed moves to the n-doped substrate and the electrons accumulate in the potential wells. The electrons stored in the pixels are transferred to the data processing device by sequentially changing the voltage at each of their three parts. This charge transfer is efficient and is more efficient than a photomultiplier tube.¹² The CCD camera used had a resolution of 1600×1200 (horizontal by vertical) and a pixel size of $7.4 \times 7.4 \mu\text{m}^2$.

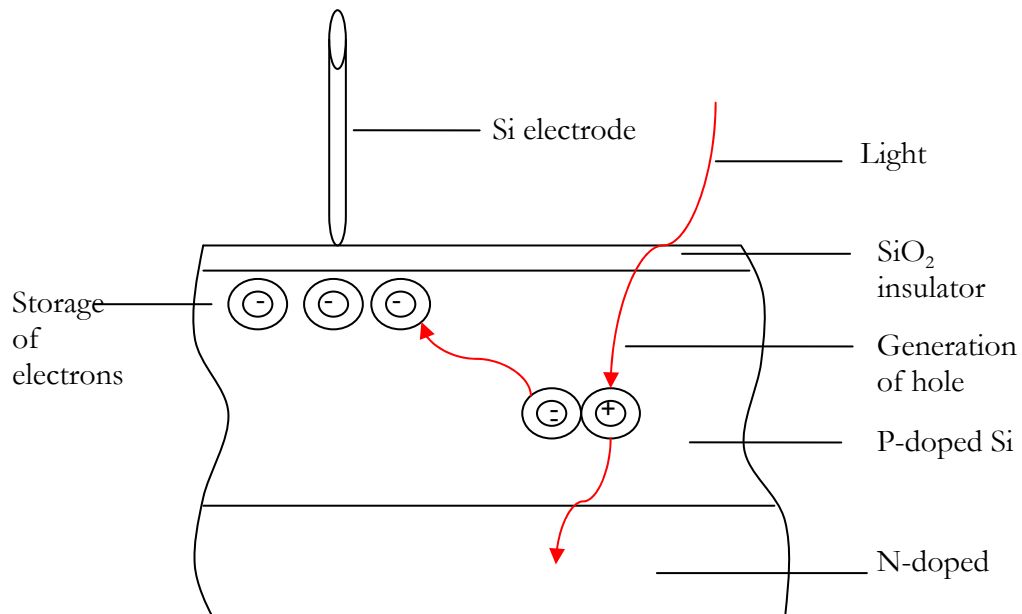


Figure 11: Schematic of a charged coupled device¹²

2.1.3 Confocal Microscopy

The set up of the fluorescence microscope described in Figure 8 suffers from the issue of out-of-focus fluorescence due to the blurring of the image as a result of the light emitted being spread out in a cone. The confocal microscope blocks out-of-focus fluorescence through the use of pinholes, in a process known as optical sectioning. Each point of a confocal image represents the sum of in-focus information from the focal plane. The confocal microscope was first invented by

Marvin Minsky in 1955 and has since become an important tool for imaging biological samples. The original system consisted of two pinholes and two objective lenses but confocal systems used today consist of a single objective with pinholes. Figure 12 is a schematic of a confocal laser scanning microscope (CLSM). The light source is a laser, the detector is a photomultiplier tube and a computer controls the scanning mirrors. A single point is focussed onto the specimen by a dichroic beam splitter and two mirrors. Each mirror twists on its axis and deflects the laser beam. One mirror scans light in one direction across the specimen and the second scans at right angles to the first. The light from the specimen is detected by the photomultiplier tube and the computer builds an image from the photomultiplier tube's output.

The objective plays an important role in the general theory of confocal microscopy. It focuses the excitation light onto a spot of the specimen, collects the fluorescence from the specimen and images it onto the detection pinhole. Even in a system without aberrations, the spot focused onto the detector is smeared by diffraction. This spread is described by the point spread function, which characterises the imaging properties of the system. The point spread function is a diverging spherical wavefront that extends 4π steradians (sr). The objective transforms this point to a converging spherical wavefront which is clipped according to the aperture of the objective. Clipping leads to the smearing of the point source, which forms the three dimensional point spread function. In an ideal aberration free lens the point spread function is determined by the wavelength of the light, the numerical aperture of the lens and diffraction. The lateral coordinate is given by:¹³

$$v = r \frac{2\pi}{\lambda_m} \sin \alpha = r \frac{2\pi}{\lambda} NA \quad \text{Equation 2-8}$$

where r is the radial coordinate relative to the optical axis, $\lambda_m = \lambda/n$ is the wavelength of the optical field having refractive index n , α is the semi-aperture angle of focussing and $NA = n \sin \alpha$ is the numerical aperture.

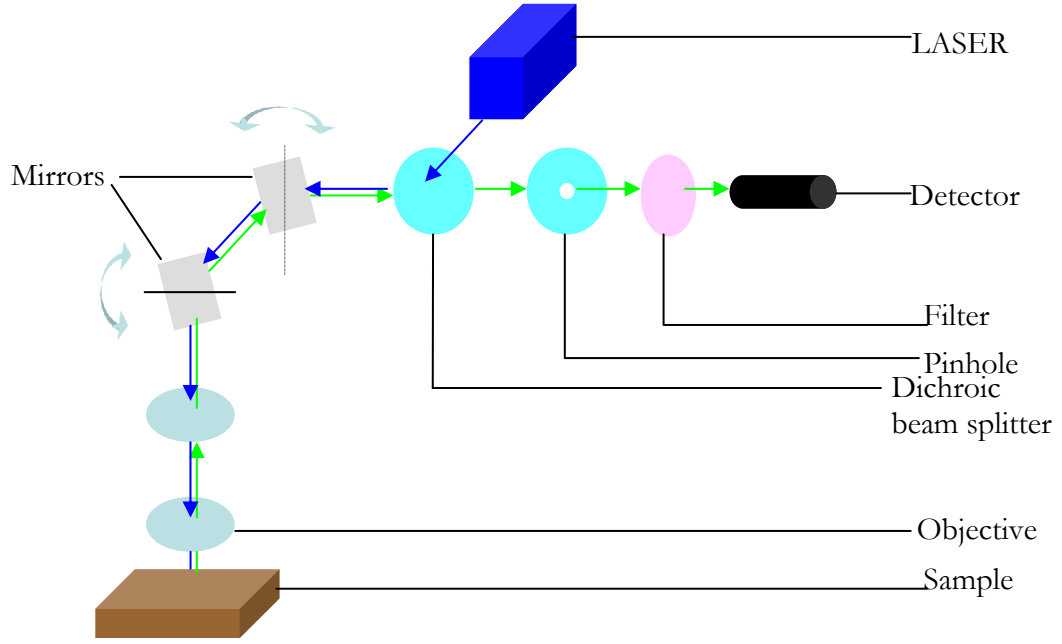


Figure 12: Schematic of a confocal laser scanning microscope (CLSM).¹⁴

The axial coordinate is defined by:¹³

$$u = z \frac{2\pi}{\lambda_m} \sin^2 \alpha = z \frac{2\pi}{\lambda} \frac{NA^2}{n} \quad \text{Equation 2-9}$$

where z is a distance relative to the focal point.

The intensity along the optical axis is then given by:¹³

$$I(u, o) \propto \left(\frac{\sin(u/4)}{u/4} \right)^2 \quad \text{Equation 2-10}$$

The third dimension of the point spread function is the volume, which can be calculated by the diffraction theory. In the lateral plane this results in a circular Airy pattern, and in the axial plane the result is significant elongation that is larger than the lateral pattern by a factor of $\sim 3.3/\sin(\alpha)$.

The image in the epi-fluorescence microscope is a result of the point spread function being shift-invariant: its shape remains constant for every point within the field of view. This results in the cone-shaped spread of light. The image of the confocal microscope is the product of its excitation and emission point spread functions, and this reduces the width of the function. This is approximated to be cylindrical.

In this project, the optical sectioning capabilities of the confocal were used to obtain the maximum intensity on the surface of the assay by taking images along the vertical axis, 10 μm below and above the surface of the glass.

2.1.4 Programmable array microscope

The programmable array microscope (PAM) is an optical sectioning microscope for spectroscopic characterisation of biological materials based on programmable spatial light modulators (SLMs) (Figure 13). The confocal microscope is limited by the fact that it illuminates one spot at a time. The widefield microscope images faster than the confocal and is more light efficient, but it cannot perform optical sectioning.

The PAM allows both fast efficient imaging with optical sectioning and has excitation and emission efficiencies superior to those of the CLSM, by modulating the SLMs to create two images. The difference gives the true confocal image. The first PAM for fluorescence was described in 1998 by Quentin Hanley, Peter Verveer and Thomas Jovin¹⁵ and had a digital micromirror device (DMD) as its SLM.

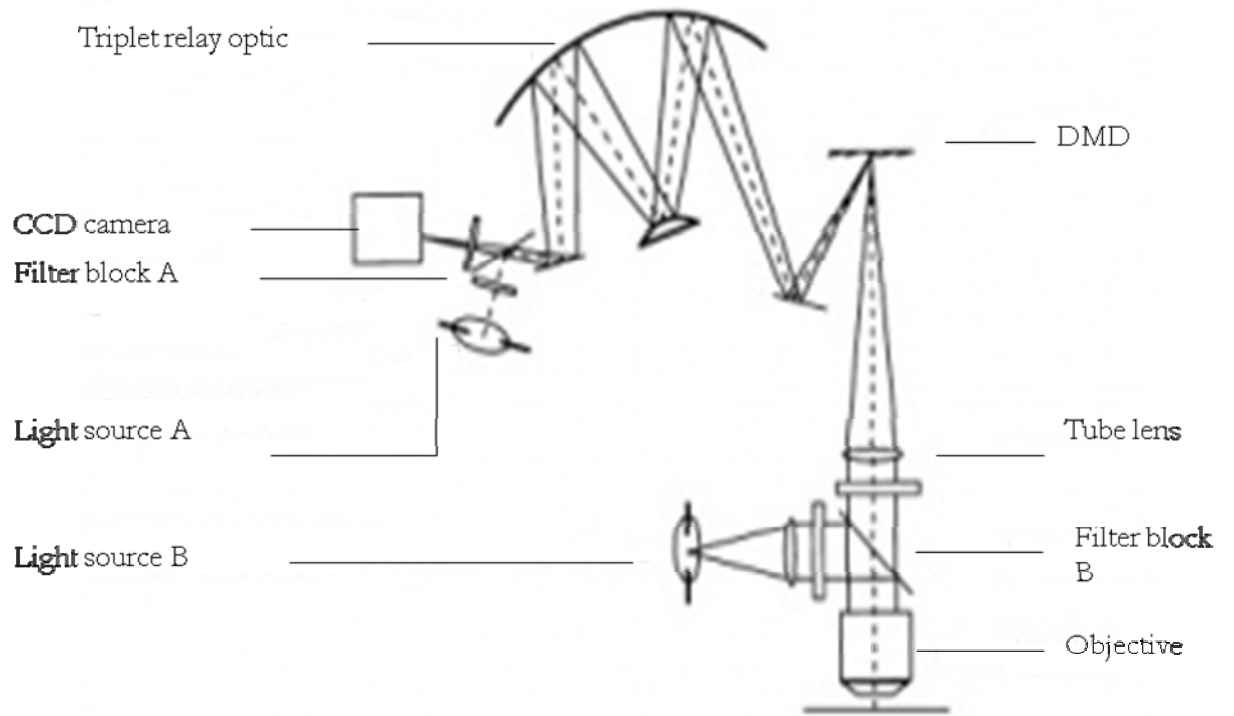


Figure 13: Diagram of a version of the PAM. The DMD directs light to and from the microscope's object plane when illuminated using light source and filter block A. This microscope can be used in standard epi-illumination mode using light source and filter block B. The triplet relay system is positioned such that the CCD camera and focal plane are both normal to the DMD¹⁶

The DMD consisted of an array of square mirrors, each of which can be tilted $\pm 10^\circ$ to the normal. The DMD may be switched to the “on” position to reflect light to the object at conjugate positions to the focal plane forming the conjugate image I_c , or to the “off” position where it reflects light that originates from non-focal planes and other ‘out-of-focus’ fluorescence, forming a non-conjugate image, I_{nc} . The sum

of I_c and I_{nc} is a conventional wide field image. The conjugate and non-conjugate images were reflected to two different 2-D cameras.

The confocal image is created by changing the modulation of the SLM, which has continuous coordinates of $S_i(x_d, y_d)$. In the on position this value is 1, in the off position it is 0. An object O having coordinates (x_o, y_o, z_o) is scanned over z_s , and is illuminated by the following intensity, which integrates the contributions from all sources of excitation (Equation 2-11).¹⁷

$$I_i(x_o, y_o, z_o) = \iint_{-\infty}^{+\infty} S_i(M_u, M_v) H_{ex}(x_o - u, y_o - v, z_o) du dv \quad \text{Equation 2-11}$$

Here M is the magnification of the objective and H_{ex} is the excitation point spread function of the objective.

The SLM is modulated N times, and the conjugate image formed is the sum of all the modulations, and the contribution from all points in the object. This is given by Equation 2-12.¹⁷

$$I_c(x_d, y_d, z_s) = \frac{T}{N} \sum_{i=0}^{N-1} S_i(x_d, y_d) \iiint_{-\infty}^{+\infty} H_{em}\left(\frac{x_d}{M} - u, \frac{y_d}{M} - v, w\right) I_i(u, v, w) O(u, v, w - z_s) du dv dw \quad \text{Equation 2-12}$$

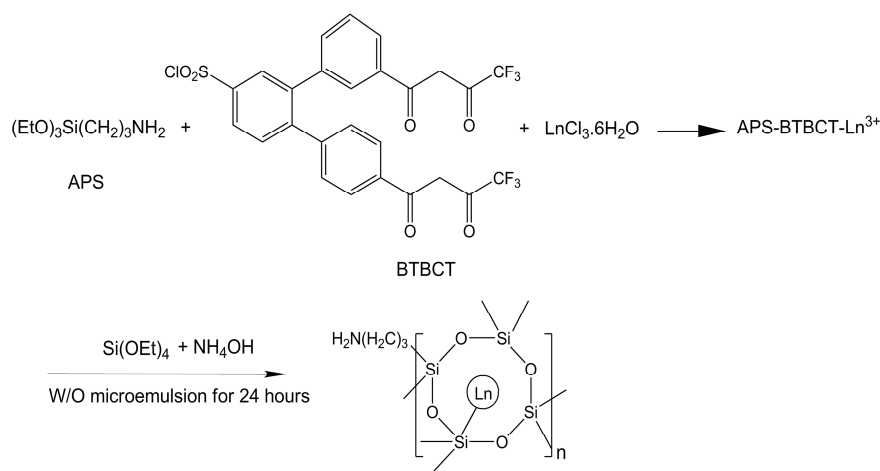
In Equation 2-12, H_{em} is the emission point spread function and T is the total integration time. The non conjugate image Inc is calculated by replacing $S_i(x_d, y_d)$ with $1 - S_i(x_d, y_d)$.

The PAM used for this research featured a ferroelectric liquid-crystal-on-silicon (LCoS; SXG-R2D, Forth, Dimension Displays, Dumfermline, Scotland) SLM instead of the DMD. The conjugate and non-conjugate images are acquired simultaneously with a single CCD camera, and a final image is formed by subtraction of the non-conjugate from the conjugate image. Before formation of the final image, the conjugate and non-conjugate images are registered through a step size optimisation of the parameters translation, rotation and magnification. A background image is subtracted from the pair of registered images, the non-conjugate image is transformed to overlap the conjugate image and is then subtracted to obtain the final image. The transformation and subtraction have a computation time less than the lowest possible integration time of ~ 16 ms, making this instrument a real-time device.

2.2 Experimental Protocols

This section illustrates protocols used for synthesis and bioconjugation of nanoparticles.

2.2.1 Synthesis and Bioconjugation of Nanoparticles



W/O microemulsion consists of Triton X-100, n-octanol, cyclohexane and water

Figure 14: Synthetic scheme for preparation of lanthanide-doped silica nanoparticles¹⁸

Silica nanoparticles doped with lanthanide chelates were synthesised (Figure 14) using a water in oil (W/O) microemulsion copolymerisation method. The chelate 4,4'-bis(4,4,4-trifluoro-1,3-dioxobutyl)-o-terphenyl-4'-sulfonyl chloride (BTBCT) was mixed in a 2:1 mole ratio with the lanthanide Eu and Sm. To this was added (3-aminopropyl) triethoxysilane (APS) (2.6 μL) and cyclohexane (0.08 mL) and the resulting mixture was sonicated for 15 minutes on a Cavitator Ultrasonic Cleaner (Mettler Electronics Corp). After sonication, the solution was added to a microemulsion consisting of Triton X 100 (1.11 mL), cyclohexane (4.66 mL), n-

octanol (1.06 mL), and water (0.28 mL) and stirred for 30 minutes at room temperature. Tetraethyl orthosilicate (TEOS) (0.05 mL) was then added and the copolymerisation was commenced after the addition of concentrated ammonia (0.05 mL). The reaction was left to proceed at room temperature for 24 hours after which time acetone was added and the mixture was centrifuged at 4000 rpm for 30 minutes. The white nanoparticles isolated were washed several times with ethanol and then PBS to remove unreacted materials.

This work conjugated antibodies with amine functionalised SiO₂ NPs. Several different conjugation procedures were attempted: 1-ethyl-3-(3-dimethylaminopropyl)carbodiimide hydrochloride (EDC) and N-Hydroxysulfosuccinimide (sulfo-NHS) assisted coupling of the amine groups on the NPs to the carboxyl groups on the proteins and the avidin/biotin interaction. Avidin was conjugated to the amine groups on the NPs and the amine groups on the proteins using glutaraldehyde chemistry. Linking the NPs to the sulfhydryl groups of the Fab fragments of proteins was also explored.

Glutaraldehyde mediated conjugation

Glutaraldehyde may be used to link primary amines (Figure 15). BSA was used to create a flexible bridge between the NPs and the avidin, thereby reducing steric hindrance with the rigid surface of the assay plate and the NP.

Protocol¹⁸

1 mg lanthanide doped silica NPs was added to 3 mg BSA, and 0.3 mL 1 % glutaraldehyde in 1.2 mL PBS. This mixture was stirred at room temperature for 22

hours, after which 1 mg sodium borohydride was added for a further 2 hours. The mixture was centrifuged at 10 000 rpm for 10 minutes, washed with PBS, and the pellet was redissolved in PBS with 0.4 mg avidin and a further 0.3 mL 1% glutaraldehyde. This was stirred at room temperature for 22 hours followed by reduction with 1 mg sodium borohydride. The resulting conjugate was centrifuged at 10 000 rpm for 10 minutes and washed several times with PBS. Proof of conjugation of the nanoparticles to the avidin was evidenced with a luminescence signal when bound to a biotinylated antibody.

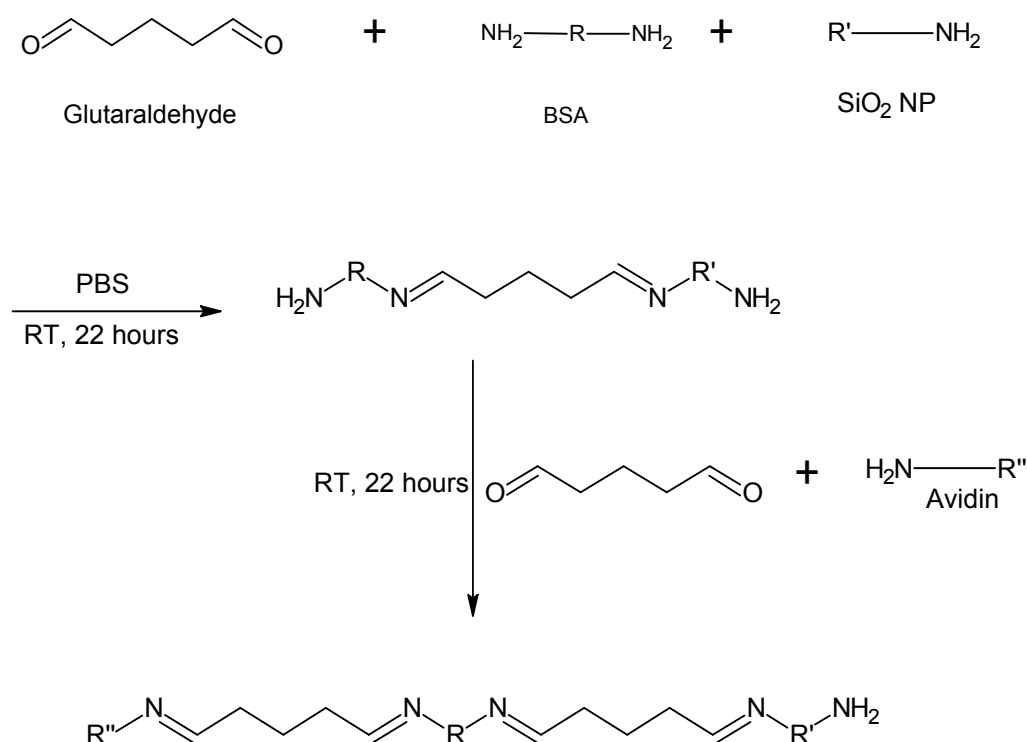


Figure 15: Glutaraldehyde-mediated conjugation of two amine-reactive molecules.

2.4 References

- (1) Rost, F. W. In *Fluorescence microscopy*; Cambridge University Press: Cambridge, UK, 1995; Vol. II.
- (2) Berg, R. H. J. *Microsc. -Oxf.* **2004**, *214*, 174-181.
- (3) Hagen, G. M.; Caarls, W.; Thomas, M.; Hill, A.; Lidke, K. A.; Rieger, B.; Fritsch, C.; van Geest, B.; Jovin, T. M.; Arndt-Jovin, D. J. In *In Biological applications of an LCoS-based programmable array microscope (PAM) - art. no. 64410S*; Farkas, D., Leif, R. and Nicolau, D. V., Eds.; Imaging, Manipulation, and Analysis of Biomolecules, Cells, and Tissues V; PROCEEDINGS OF THE SOCIETY OF PHOTO-OPTICAL INSTRUMENTATION ENGINEERS (SPIE); Conference on Imaging, Manipulation, and Analysis of Biomolecules, Cells, and Tissues V; SPIE-INT SOC OPTICAL ENGINEERING: BELLINGHAM; 1000 20TH ST, PO BOX 10, BELLINGHAM, WA 98227-0010 USA, 2007; Vol. 6441, pp S4410-S4410.
- (4) Thaler, C.; Vogel, S. S. *Cytom. Part A* **2006**, *69A*, 904-911.
- (5) Zimmermann, T.; Rietdorf, J.; Pepperkok, R. *FEBS Lett.* **2003**, *546*, 87-92.
- (6) Dinant, C.; van Royen, M. E.; Vermeulen, W.; Houtsmuller, A. B. J. *Microsc. -Oxf.* **2008**, *231*, 97-104.
- (7) Lakowicz, J. R. In *Principles of Fluorescence Spectroscopy*; Springer: New York, 2006; .
- (8) Phloem, J. S.; Tanke, H. J. In *Introduction to fluorescence microscopy*; Oxford University Press: Oxford, UK, 1987; .
- (9) Lerner, J. M. *Cytom. Part A* **2006**, *69A*, 712-734.
- (10) Demtroder, W. In *Laser Spectroscopy: Basic Concepts and Instrumentation*; Springer-Verlag: Heidelberg, Germany, 2003; , pp 987-109.
- (11) Ingle, J. D.; Crouch, S. R. In *Spectrochemical Analysis*; Prentice-Hall Inc.: New Jersey, USA, 1988; , pp 590.
- (12) Harris, D. C. In *Quantitative Chemical Analysis*; W.H. Freeman and Company: New York, USA, 2003; , pp 475-476.
- (13) Muller, M. In *Introduction to Confocal Fluorescence Microscopy*; SPIE-The International Society for Optical Engineering: Washington, USA, 2006; , pp 119-1-11.
- (14) Kaminski, C. F. Z. *Phys. Chemie-Int. J. Res. Phys. Chem. Chem. Phys.* **2005**, *219*, 747-774.
- (15) Hanley, Q. S.; Verveer, P. J.; Jovin, T. M. *Appl. Spectrosc.* **1998**, *52*, 783-789.
- (16) Hanley, Q. S.; Verveer, P. J.; Gemkow, M. J.; Arndt-Jovin, D.; Jovin, T. M. J. *Microsc. -Oxf.* **1999**, *196*, 317-331.
- (17) Verveer, P. J.; Hanley, Q. S.; Verbeek, P. W.; Van Vliet, L. J.; Jovin, T. M. J. *Microsc. -Oxf.* **1998**, *189*, 192-198.

- (18) Tan, M. Q.; Wang, G. L.; Hai, X. D.; Ye, Z. Q.; Yuan, J. L. *J. Mater. Chem.* **2004**, *14*, 2896-2901.

- General references for spectrographs

- (1) Haraguchi, T.; Shimi, T.; Koujin, T.; Hashiguchi, N.; Hiraoka, Y. *Genes Cells* **2002**, *7*, 881-887.
- (2) Elder, A. D.; Frank, J. H.; Swartling, J.; Dai, X.; Kaminski, C. F. *J. Microsc. -Oxf.* **2006**, *224*, 166-180.
- (3) Lerner, J. M. *Cytom. Part A* **2006**, *69A*, 712-734.
- (4) Demtroder, W. In *Laser Spectroscopy: Basic Concepts and Instrumentation*; Springer-Verlag: Heidelberg, Germany, 2003, pp 987-109.

General references for confocal microscopy

- (1) Kho, K. W.; Stoddart, P. R.; Harris, M.; Mazzolini, A. P. *Micron* **2009**, *40*, 212-217.
- (2) Muller, M. In *Introduction to Confocal Fluorescence Microscopy*; SPIE-The International Society for Optical Engineering: Washington, USA, 2006, pp 1-11.
- (3) Zucker, R. M.; Rigby, P.; Clements, I.; Salmon, W.; Chua, M. *Cytom. Part A* **2007**, *71A*, 174-189.
- (4) Corle, T. R.; Kino, G. S. In *Confocal scanning optical microscopy and related imaging systems*; Academic Press, Inc.: California, USA, 1996.
- (5) Paddock, S. W., Ed.; In *Confocal Microscopy: Methods and Protocols*; Methods in Molecular Biology; Humana Press Inc.: New Jersey, USA, 1999; Vol. 122, pp 446.

General references for PAM

- (1) Hanley, Q. S.; Verveer, P. J.; Jovin, T. M. In *Imaging and Spectroscopy with Programmable Array Microscopes*; Denton, B. M., Ed.; Further Developments in Scientific Optical Imaging; The Royal Society of Chemistry: Cambridge, UK, 2000; pp 164-175.
- (2) Fulwyler, M.; Hanley, Q. S.; Schnetter, C.; Young, I. T.; Jares-Erijman, E. A.; Arndt-Jovin, D.; Jovin, T. M. *Cytom. Part A* **2005**, *67A*, 68-75.
- (3) Hanley, Q. S.; Jovin, T. M. *Appl. Spectrosc.* **2001**, *55*, 1115-1123.
- (4) Hanley, Q. S.; Verveer, P. J.; Gemkow, M. J.; Arndt-Jovin, D.; Jovin, T. M. *J. Microsc. -Oxf.* **1999**, *196*, 317-331.
- (5) Hanley, Q. S.; Verveer, P. J.; Jovin, T. M. *Appl. Spectrosc.* **1999**, *53*, 1-10.
- (6) Hanley, Q. S.; Verveer, P. J.; Jovin, T. M. *Appl. Spectrosc.* **1998**, *52*, 783-789.
- (7) Verveer, P. J.; Hanley, Q. S.; Verbeek, P. W.; Van Vliet, L. J.; Jovin, T. M. *J. Microsc. -Oxf.* **1998**, *189*, 192-198.

General references for synthesis of nanoparticles and bioconjugate strategies

- (1) Tan, M. Q.; Wang, G. L.; Hai, X. D.; Ye, Z. Q.; Yuan, J. L. *J. Mater. Chem.* **2004**, *14*, 2896-2901.
- (2) Ye, Z. Q.; Tan, M. Q.; Wang, G. L.; Yuan, J. L. *J. Mater. Chem.* **2004**, *14*, 851-856.
- (3) Hermanson, G. T. In *Bioconjugate Techniques*; Elsevier: UK, 1996.

3 Spectral unmixing

The first part of the study looked at methods for separating mixtures of organic fluorophores and quantum dots. This chapter focuses on the application of an algorithm for linear spectral unmixing through a study of dyes in mixtures.

3.1 Introduction

Multi-fluorophore analysis requires specialised excitation and emission detection schemes,¹ and allows visualisation of many parts of the same sample simultaneously.² There are extensive reports of the principle, with some of the earlier work being in the area of fluorescence *in situ* hybridisation. The ability to label seven targets with just three fluorescent dyes through a combinatorial labelling scheme was demonstrated³ using haptenized DNA probes. Fluorescence microscopy was used and results were determined based on fluorescence intensity ratios. Different filter blocks were required for viewing fluorescein isothiocyanate (FITC) and tetramethyl rhodamine isothiocyanate (TRITC), and the authors mention the usefulness of a single filter set for the two. Later, all 24 chromosomes could be labelled and imaged through a band pass filter⁴ and eventually spectral karyotyping (SKY) was developed.⁵ SKY is a technique based on spectroscopy and imaging, where fluorescence microscopy, CCD-imaging and Fourier spectroscopy are all used to determine the image spectrum. For imaging, a custom designed triple band pass filter which could simultaneously excite Spectrum Green, Cy3, Texas Red, Cy5 and Cy5.5 was used. These dyes are excited in the blue, yellow, and red regions of the spectrum. Colour separation was achieved through the observation of the

Euclidian distance between a normalised spectrum and the normalised reference spectra.

Techniques such as SKY are unsuitable for quantitative analysis of samples which may have co-localized fluorophores,² as chromosomes have spatially isolated signatures. For co-localised probes the technique of linear unmixing is most suitable. Linear unmixing assumes that the emission spectrum of the mixture is a linear combination of the individual fluorophore spectra, weighted by their relative abundance.⁶ The relative abundance of each fluorophore is available as a spectral profile, and this profile is used to assemble a matrix of fluorophore specific weighting factors. The specific weighting factors are then used to give the contribution of each fluorophore. The same can be done for excitation profiles when a sample is excited with multiple wavelengths and collected with a single channel.⁷

Linear unmixing algorithms have been used to separate fluorescence emission signals from fluorophores that have overlapping spectra.^{8,9,10} The algorithms used assume that there is a linear relationship between concentration and the signal being measured.¹¹ Spectral interferences that are unaccounted for,¹² factors that result in curvature of the concentration-response function, changes to the position and width of response bands¹³ all make the application of classical curve resolution methods difficult.

Garini *et al.* discussed the principles and applications of spectral unmixing of microscopic images.¹⁴ The spectrum of the individual fluorophore is first taken and the total intensity at each wavelength is the sum of each component of the mixture.

The linear decomposition algorithm finds the concentration of each dye such that the sum of the individual spectra gives the spectrum of the mixture: ¹⁴

$$I_{\lambda} = \sum_i C_i I_i(\lambda) \quad \text{Equation 3-1}$$

where I_{λ} is the spectrum of the fluorophore mixture, the concentration of each fluorophore is given by C_i , and I_i refers to the intensities of the individual fluorophores. This expression can also be expressed in matrix form. The algorithm requires that spectra of individual fluorophores are imaged initially, under the same experimental conditions as the mixtures are imaged. There is a further requirement for the fluorophores to be linearly independent of each other. This means that energy transfer and charge transfer processes that occur in a mixture cannot be analysed using the typical linear decomposition methods.

Methods and applications of linear spectral unmixing have been described for spatially separated and co-localised fluorophores. Depending on their proximity, co-localised fluorophores can undergo reactions due to pH effects,¹⁵ quenching,¹⁶ ion pairing and energy transfer.¹⁷ In analyses, if samples of variable pH are used this will limit accurate separation of components of the mixture. At constant pH, ion pairing may occur, also reducing the ability to accurately separate the fluorophores. At high concentration, inner filter effects and quenching occur, also making typical linear unmixing methods unsuitable.

Here co-localised samples of fluorescein, rhodamine B, rhodamine 101 and eosin Y were unmixed. CdSe ZnS-capped carboxylate functionalised quantum dots were also mixed and attempts were made to decompose the spectra into individual

components. Unmixing was initially done using the method described for linear decomposition as described previously.¹⁴ The method was then modified to account for the processes such as ion pairing that can occur between fluorophores in a mixture.

3.2 Theory

Linear regression models consist of paired data sets (x_i, Y_i) , representing a fixed value (x) and a value for the response variable Y . Y is dependent on the value of x and the amount of random error present. The mathematical model for single component linear regression having a simple analytical solution is:¹⁸

$$Y_i = \beta_0 + \beta_1 x_i + \varepsilon \quad \text{Equation 3-2}$$

where β_0 is the intercept, β_1 is the coefficient of x_1 and therefore defines the contribution to the value of Y by x_1 and ε is the error in the measurement. The values of β_0 and β_1 need to be found such that there is a minimum sum of squares of the deviations from the line through a set of x and Y data.

The spectrum of the individual fluorophores can be described as $I_i(\lambda)$, where i is 1, 2, 3,..., N , and refers to the index of the fluorophore being evaluated with N being the total number of fluorophores. $I(\lambda)$ is a vector with dimensions M , which is the number of wavelength points being evaluated. The concentration of each fluorophore is C_p , and the equation of the entire spectrum measured spectrum is shown in Equation 3-1. The concentration of a fluorophore is obtained by finding the inverse of $I_i(\lambda)$ and multiplying by $I(\lambda)$.

When multiple fluorophores are imaged together, the use of a spectral imager allows simple separation of the mixture into its individual components. In a complex sample, this is not the case as processes can occur among fluorophores that serve to change their profiles. If the pH of the solution is not controlled, spectroscopic changes can occur when pH sensitive dyes are mixed: absorption and emission profiles can change. These changes also occur in unbuffered solutions of the individual dyes, but in mixed solutions there is the possibility that the change in structure could lead to spectral overlap. Examples of this have been documented,¹⁹ Other processes include chemical interactions; such as hydrogen bonding between dyes, ion changes²⁰ and isomerism,²¹ both of which could have a similar effect on the mixture solution as pH. With this in mind, a different approach was taken, where reference spectra comprised of mixtures of the fluorophores at different concentrations were collected. The slope and intercept of these spectra were used to simulate a curve of what was assumed to be present in the measured curve. Least squares optimisation was used to predict the concentration of the dye in the mixture through a linear model involving a dependent variable (fluorescence intensity) Y_j , which is a function of i independent variables x_1, x_2, \dots, x_i (concentration). The functional relationship between the two is given by the equation of a straight line:¹⁸

$$Y_j = \beta_{0j} + \beta_1 x_1 + \beta_2 x_2 + \dots + \beta_i x_i \quad \text{Equation 3-3}$$

where β_0 refers to the intercept and $\beta_1, \beta_2, \dots, \beta_i$ are the concentration coefficients as obtained by a least squares fit of a set of standards. Linear combinations of the mixture spectra were calculated using $\beta_1, \beta_2, \dots, \beta_i$ and β_0 , and the sum of squared differences between the measured and calculated spectra were minimised using least squares optimisation software. The least squares principle chooses values of x_1, x_2, \dots, x_i such that the sum of squared residuals (SS) is minimized:²²

$$SS = \sum_{i=1}^n (Y_i - \hat{Y}_i)^2$$

Equation 3-4

This value is minimised by adjusting the concentration of fluorophores present.

3.3 Materials and Methods

3.3.1 Reagents

Fluorescein (Acros Organics, lot no. A0222026), rhodamine B (Acros Organics, lot no. A0081279) rhodamine 101 (Fluka, lot no. 1246518) and eosin Y (Sigma Aldrich, lot no. 20696DJ) were used in the study of dye mixtures. The CdSe ZnS-capped carboxylate functionalised quantum dots (Evident Technologies) selected were Adirondack Green (Lot no. AWN0512C, λ_{ex} 497nm, λ_{em} 515 nm), Hops Yellow (Lot no. AWN30J2C, λ_{ex} 537, λ_{em} 560 nm) and Fort Orange (Lot no. KFN0612C2, λ_{ex} 581nm, λ_{em} 594 nm), designated green, yellow and orange respectively. Solutions containing fluorescein were made in 5 mM NaOH pH 9.2 (Sigma Aldrich lot no. 14122HD). The standards were made using mixtures of varying concentrations of the dyes assumed to be in the ‘unknown’ sample.

3.3.2 Imaging of fluorophore and quantum dot mixtures

Standards and samples were imaged using an add-on to an inverted microscope (Figure 8) (IX71; Olympus UK Ltd, Southall, UK). Images were collected using an image intensifier (II118MD; Lambert Instruments, Leutingewolde, The Netherlands) attached to a CCD camera (PCO.1600; PCO Computer Optics GmbH, Kelheim, Germany). The intensified camera system was attached to an imaging spectrograph (PARISS; Lightform Inc., Hillsborough, NJ) and then to the bottom port of the microscope. The microscope was illuminated using a mercury burner (Olympus USH-103OL; Olympus UK Ltd, Southall, UK). When imaging QDs, the light was passed through a UV filter cube consisting of a 330 – 385 nm band pass excitation filter, 400 nm dichroic mirror and 420 nm long pass emission filter (U-MWU2;

Olympus UK Ltd, Southall, UK). For fluorescent dyes, a filter cube consisting of a 450 DF55 nm excitation filter, dichroic mirror of 485 nm and 500 nm long pass emission filter (XF77-2; Omega Optical Inc., Brattleboro VT) was used.

Data analysis

The LINEST function in Microsoft excel was used to obtain β_{0j} and β_j for the standard calibration curve. Using intensity readings for known samples at selected wavelengths, a matrix of concentration and intensity as a function of wavelength was constructed. Regression using the LINEST function for multiple components was carried out: the syntax for this operation is LINEST(known_y's,known_x's,const,stat). Known y's were the measured intensity readings and known x's were the concentrations of the standards within the mixture. The constant value was set at TRUE, which allowed the model to calculate the intercept for the regression line. The statistic value was also set at TRUE, allowing the model to calculate the standard error in the coefficients, the regression coefficient and other statistical information (which were not used). A spreadsheet showing the results of this regression is shown in Appendix 1 (page 193). The values obtained for β_{0j} and β_j were then used in Equation 3-3 to simulate a curve for the 'unknown' mixture. The sum of squared differences between the simulated and measured curves was calculated and minimised by adjusting the concentration of the fluorophores present. The mixture of dyes was modelled as a mixture of known mixtures and the minimum number of components chosen was two.

3.4 Results and Discussion

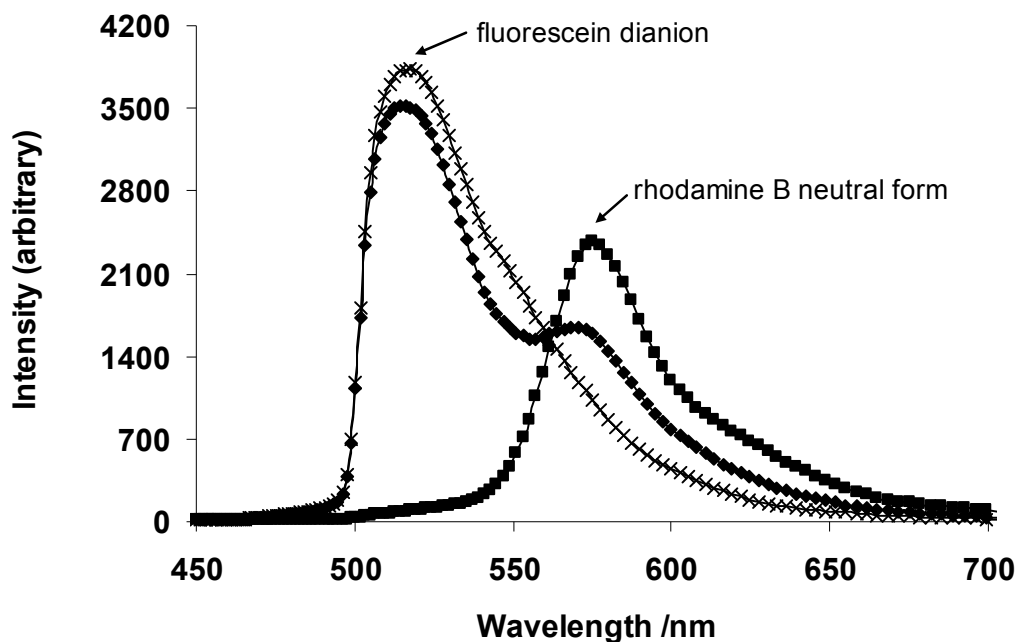


Figure 16: Figure showing spectra of fluorescein alone ×, rhodamine B alone ■ and a mixture of the two fluorophores ♦ in buffered solution.

Figure 16 shows spectra of fluorescein, rhodamine B and a mixture of the two dyes. Fluorescein has maximum excitation and emission wavelengths at 490 and 515 - 520 nm respectively, while rhodamine B has maxima at 543 and 575 nm for excitation and emission respectively. Both dyes were excited with a 470 DF 35 band pass filter, with emission collected by a 515 nm long pass excitation filter. Both dyes are pH sensitive, having varied pH dependant forms. Their multiplicity of structures is a result of the xanthene and benzoic acid groups, which have several ionisation states.²³ Figure 17 shows some of the possible structures of rhodamine B. In solution, the dye can exist as a cation or in neutral form. The neutral form can exist as an equilibrium mixture of the coloured, fluorescent zwitterion and the colourless

lactone.²⁴ The lactone can also dimerize, and the nitrogen atoms can be protonated. These relationships in solution are important for correct interpretation of mixtures containing rhodamine B.

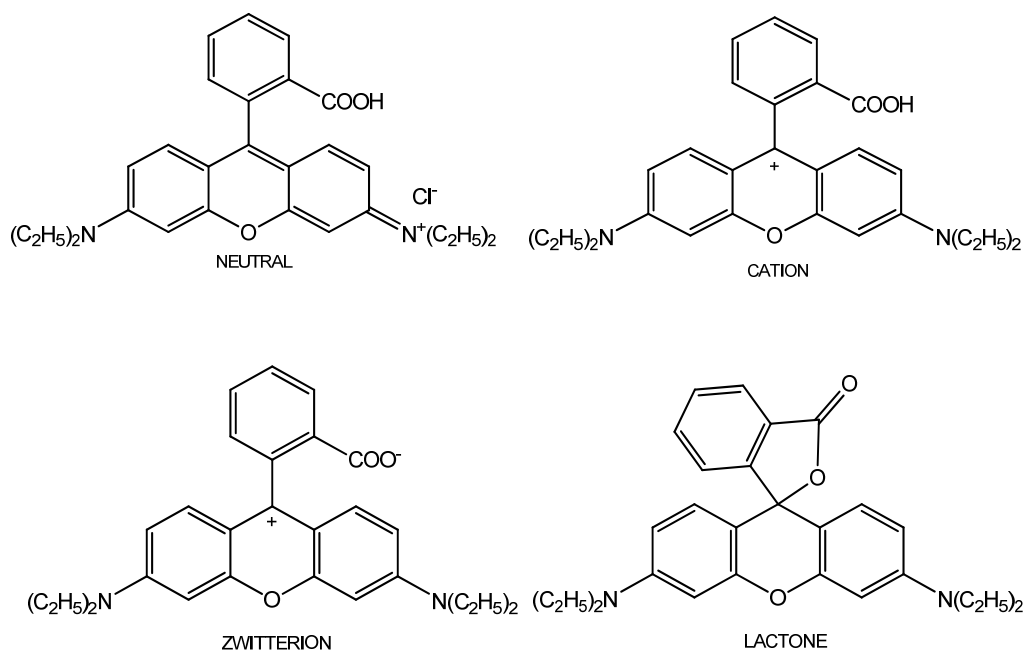


Figure 17: Some pH-dependent structures of rhodamine B. The neutral forms are present at pH 13 to 4, the cation is formed between pH 3 and 1.²⁶

Seven forms of fluorescein are shown in Figure 18. As seen, fluorescein has multiple pH dependent forms including the yellow cation and zwitterion, the red quinone, the colourless lactone, and the green anions and dianion. In basic solution ($pH > 8$), the predominant species is the dianion.

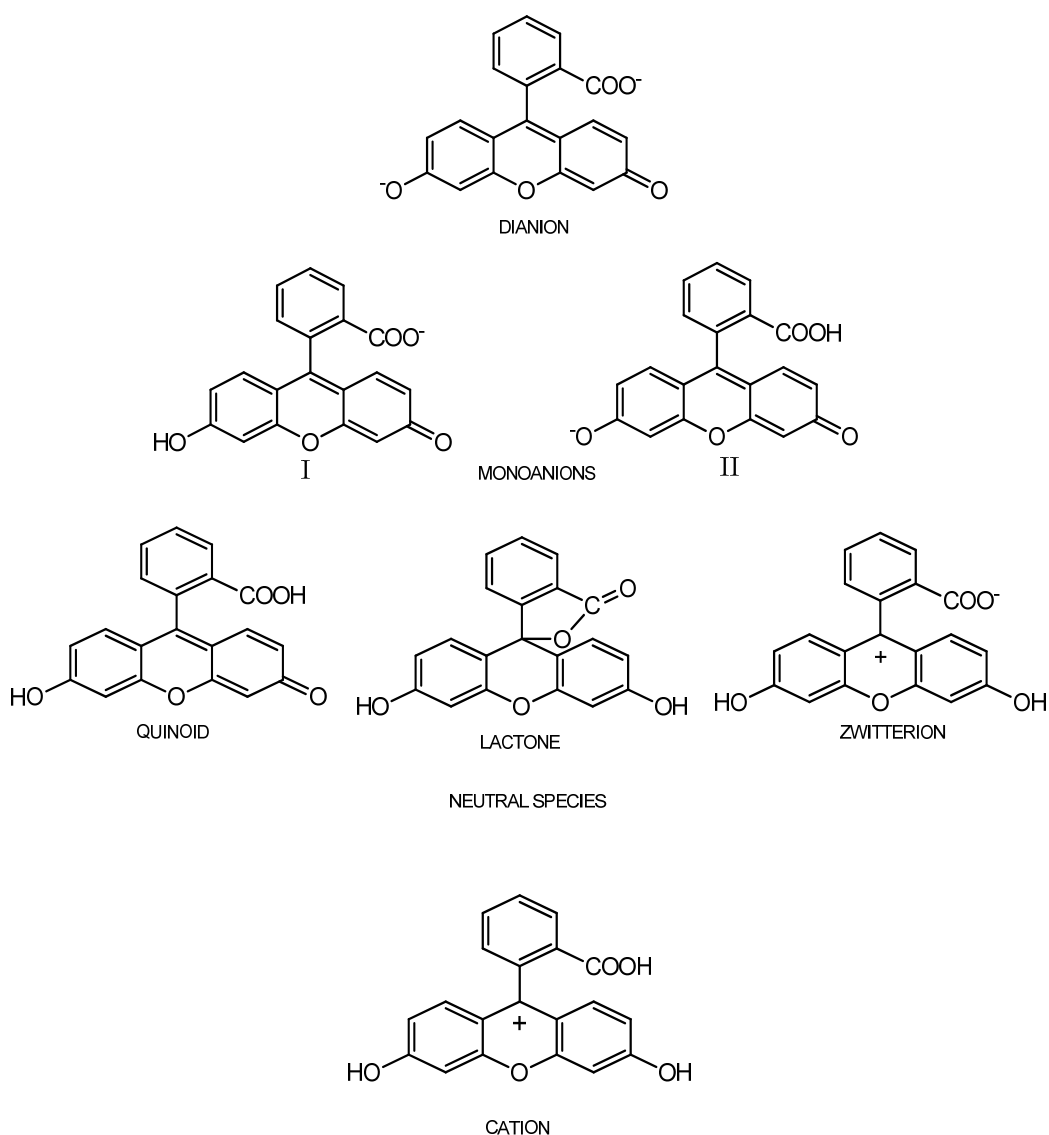


Figure 18: The pH-dependent structures of fluorescein. The cationic and neutral forms have pK_a 3.1 to 3.4 and 6.3 respectively, with the pK_a of lactonization 2.4.²³ The formation of the dianion from the anion has a pK_a of 6.3 to 6.8²⁵

Chemometric separation was performed on mixtures of fluorescein and rhodamine B. Table 3 presents the separation after a mixture of dyes were used as the standards to compute Y_p , while Table 2 shows separation using individual standards with Equation 3-1. The unmixed spectra are shown in Figure 19.

It is readily apparent when Tables 2 and 3 are compared, that the method of separation using mixtures of standards gave a better approximation to the actual

concentration of the dyes than the method where individual fluorophores were used to unmix the data.

[Actual]/mM	[Predicted]/mM	[Actual]/mM	[Predicted]/mM
RB	RB	F	F
0.020	$0.039 \pm 7.38\text{E-}04$	4.000	$0.032 \pm 9.76\text{E-}05$
0.030	$0.049 \pm 7.43\text{E-}04$	0.040	$0.022 \pm 9.82\text{E-}05$
0.010	$0.013 \pm 2.23\text{E-}04$	0.020	$0.014 \pm 2.95\text{E-}05$
0.001	$0.001 \pm 4.07\text{E-}05$	0.010	$0.009 \pm 5.39\text{E-}06$

Table 2: Relationship between actual and predicted concentrations for fluorescein and rhodamine B in a mixture of the two dyes, obtained using existing method

[Actual]/mM	[Predicted]/mM	[Actual]/mM	[Predicted]/mM
RB	RB	F	F
0.020	$0.021 \pm 1.60\text{E-}04$	0.050	$0.050 \pm 5.71\text{E-}05$
0.030	$0.030 \pm 2.55\text{E-}04$	0.040	$0.040 \pm 9.12\text{E-}05$
0.010	$0.007 \pm 5.22\text{E-}04$	0.020	$0.022 \pm 1.86\text{E-}04$
0.001	$0.001 \pm 4.53\text{E-}04$	0.010	$0.012 \pm 1.62\text{E-}04$

Table 3: Relationship between actual and predicted concentrations for fluorescein and rhodamine B in a mixture of the two dyes, obtained using new separation technique. The error in the prediction is calculated using Solver.

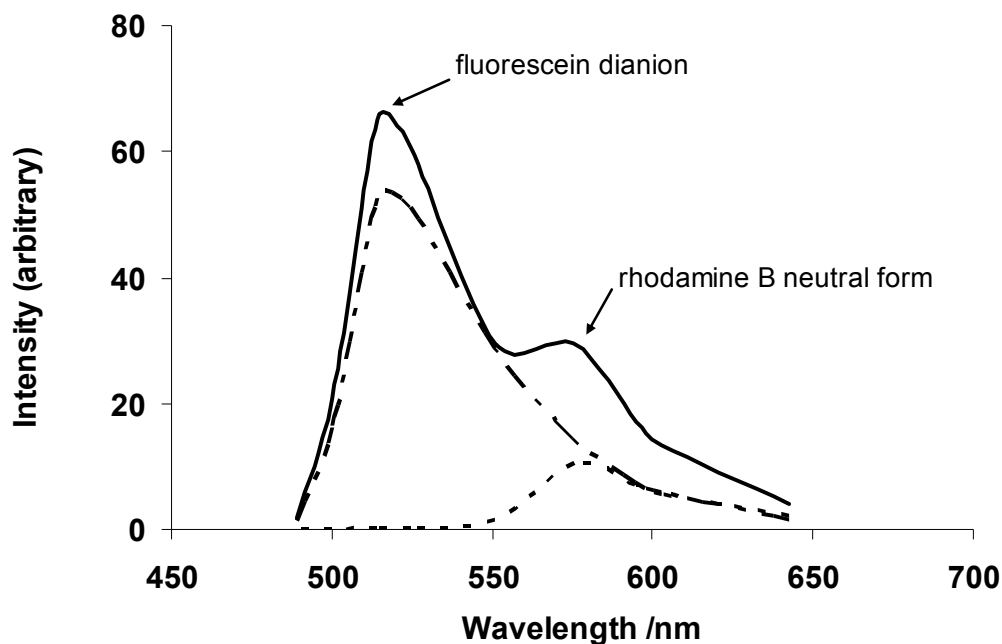


Figure 19: Spectral unmixing of fluorescein and rhodamine B, showing spectra of the mixture (solid line), the fractional contribution of fluorescein 50 μ M (dash-dot line) and the fractional contribution of rhodamine B 20 μ M (dashed line)

Mixtures were unmixed using both individual standards and mixtures of standards, and the fractional contribution of each component to the mixture is demonstrated in Figure 19. For fluorescein, the RSD with the existing method (individual standards) was 14%, while that for the new method (mixtures of standards) was 0.5%. With rhodamine B, the RSD was 11% and 8% for the existing and new methods respectively. The residuals plots further highlight the improvement of the new method over the old (Figure 20).

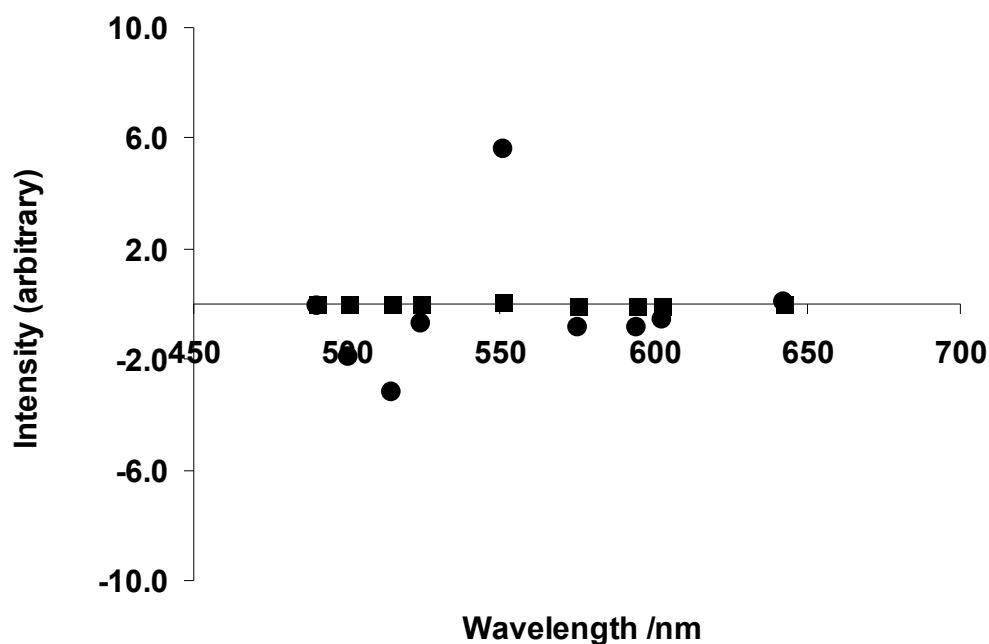


Figure 20: Residuals plots for the quantitative unmixing of fluorescein and rhodamine B for the existing method ●, and the new method ■

The residual plots (Figure 20) highlight the relative success of the unmixing models, with the previous method showing greater deviations near to the excitation maxima of the fluorophores. This method is unable to account for the behaviour of the dyes such as subtle wavelength shifts and energy transfer effects in a mixture. Figure 20 shows an underprediction of the amount of fluorescein present, and an overprediction for the amount of rhodamine B. Creating standards that are already mixed provided a model that has taken into account ion changes, chemical interactions of the dyes and photophysical behaviours which would not be seen in a spectrum of an individual fluorophore. It has been previously stated that the use of mixed fluorophores as standards is not recommended,² as they give an untrue representation of the individual fluorophore components. The results shown (Tables 2 and 3; Figure 20) indicate that the use of mixed fluorophores is beneficial.

The experiment presented in Figure 16 is performed at pH 9.2. The species present are the fluorescein dianion ²³ (Figure 18) and the zwitterion of rhodamine B ²⁶ (Figure 17). At this pH, significant interaction between rhodamine B and the carboxyl groups on fluorescein is unlikely.

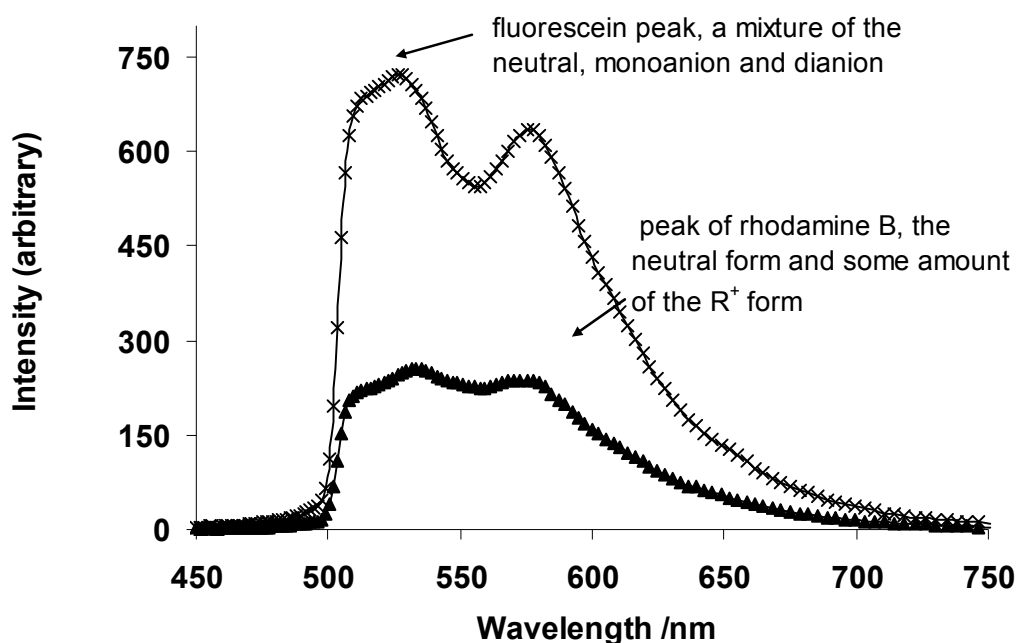


Figure 21: Mixtures of fluorescein and rhodamine B in unbuffered solution. The solid line represents a mixture of 22 μM rhodamine B with 50 μM fluorescein, \times is 11 μM rhodamine B with 2 μM fluorescein.

In unbuffered solutions, other species of the two fluorophores would be present. Subtle changes in pH can affect the position of the emission maxima and solutions need to be pH controlled. The effect of pH can be tested with a mixture of fluorescein and rhodamine B measured in deionised water as the solvent (Figure 21). The stock solution of fluorescein was also prepared in unbuffered solution.

Figure 21 shows a difference in the shape of the fluorescein peak. It is significantly broader (compared to Figure 16), and there appear to be two species there, at 515 and 526 nm. For this experiment it is recognised as a broadened fluorescein peak, however in a mixture of unknown dyes, this could be misinterpreted as two species with similar emission maxima. The broad peak is easily explained by the photophysical behaviour of fluorescein. In unbuffered solutions it is possible to obtain a mixture of different forms of fluorescein. In this experiment, unfortunately the pH of the solution was not recorded, but the water used for making the solutions had a pH between 5 and 6, indicating the presence of the quinoid, lactone, zwitterion, monoanion and dianion forms each of which has a different emission maximum.²³ Another effect of unbuffered solutions of fluorescein is reduced fluorescence of the dye. The dianion gives the most intense emission²⁷ and this predominates at $\text{pH} > 8$. Solutions of fluorescein with $\text{pH} < 8$ contain the lactone, which is colourless and has limited absorption. The presence of the lactone lends itself to reduced fluorescence in solution. For rhodamine B, the acidic solution means that the main species are the neutral and some amounts of the protonated forms of the dye. In acidic solution, the carboxyl group of the zwitterion becomes protonated and increasing acidity leads to successive protonation of the nitrogen groups. The species known as R^{++} (occurring at $\text{pH} 3 - 1$) consists of a protonated carboxyl and N group and has an orange colour. The species known as R^{+++} (formed at $\text{pH} < 1$) is formed on protonation of the second N, and is yellow. The forms all have different excitation maxima. Additionally, the reactions occurring at acid pH: dimerization and ion pairing, lead to a departure from Beer Lambert's law and the system is no longer linear. This explains why linear unmixing; even with mixtures of standards, was not effective for quantitative separation of the mixture: the RSD between calculated and actual concentrations of fluorescein was 65 %, and

that for rhodamine B was 174 % when a mixture of unbuffered dyes was prepared. These results highlight the need for careful control of pH when doing quantitative analyses of fluorescent mixtures.

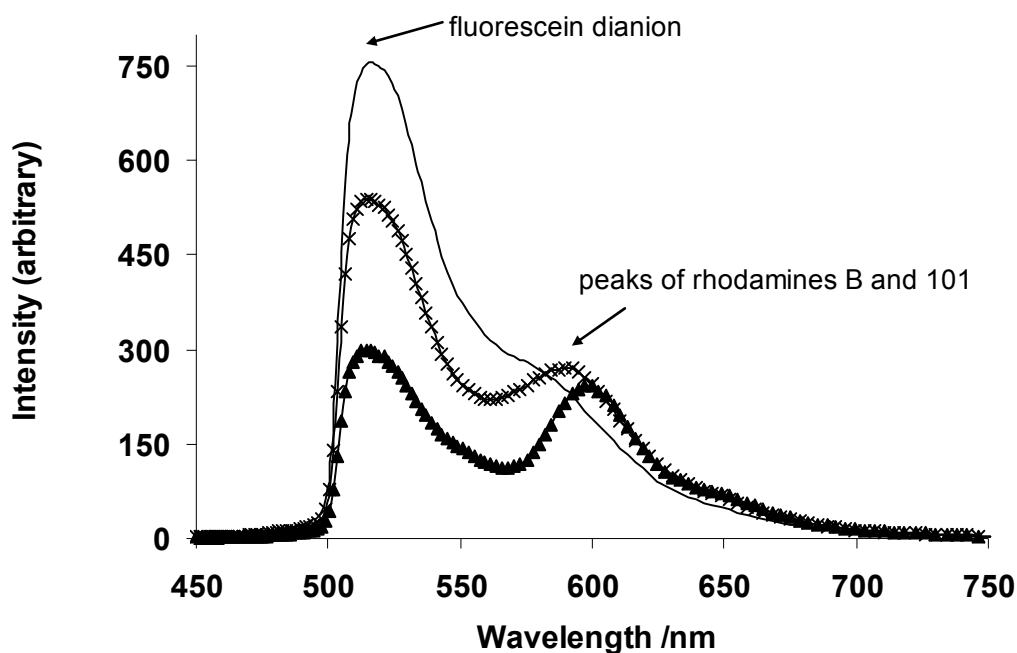


Figure 22: Mixtures of fluorescein, rhodamine B and rhodamine 101 in buffered solution. The solid line represents a mixture of 48 μM fluorescein, 10 μM rhodamine B and 50 μM rhodamine 101, \times represents a mixture of 38 μM fluorescein with 20 μM rhodamine B and 10 μM rhodamine 101, and \blacktriangle is a mixture of 19 μM fluorescein, 5 μM rhodamine B and 20 μM rhodamine 101.

An attempt was made to determine how many fluorophores can be accurately separated using the new method. Figure 22 shows the spectra of the mixtures with 3 dyes. The third dye is rhodamine 101, having excitation and emission maxima at 560 and 589 nm respectively. Figure 23 shows the structure of rhodamine 101. Unlike the other xanthenes dyes, it is largely insensitive to its environment because the amine groups are all tertiary.²⁸ The spectra do not show distinct peaks for rhodamine 101 and rhodamine B; there is the appearance of a broad band that is

characteristic of neither rhodamine B nor rhodamine 101. However, the shift of emission was accounted for in the standard solutions, and this should allow the mixture to be separated. This mixture of 3 dyes however, was not easily separated. The RSD between the predicted and actual concentrations was 65 % and 34 % respectively for rhodamine B and rhodamine 101. The model appeared to have some difficulty distinguishing the two fluorophores from each other. The RSD for fluorescein was 13 %, higher than previously obtained in the mixture of fluorescein and rhodamine B.

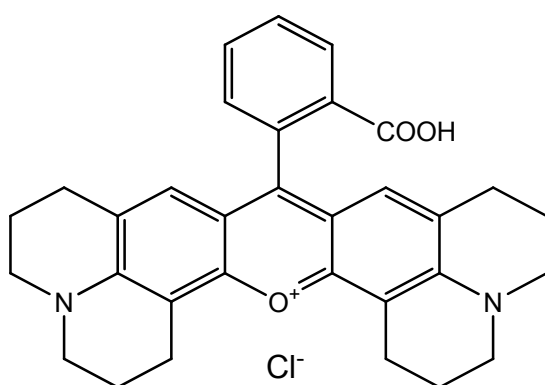


Figure 23: The structure of rhodamine 101

The inability to separate the 3 dyes appeared to be a result of the high concentration of the dye mixture: the addition of rhodamine 101 increased the absorbance of the mixture, creating a non-linear absorbance of light. To test this hypothesis, the effect of high concentrations of dyes in the mixture on the ability to separate the spectra was investigated. The experiment with the mixture of 3 dyes was repeated with the solutions diluted by a factor of 10. The RSD between the predicted and actual concentrations was 2% for fluorescein, 9% for rhodamine B and 7% for rhodamine 101. This indicated that the higher concentration of dyes was indeed the cause for the poor performance of the unmixing procedure. To further

prove that low concentrations of multiple dyes can be unmixed using the method, a fourth dye was added to the mixture (Figure 24).

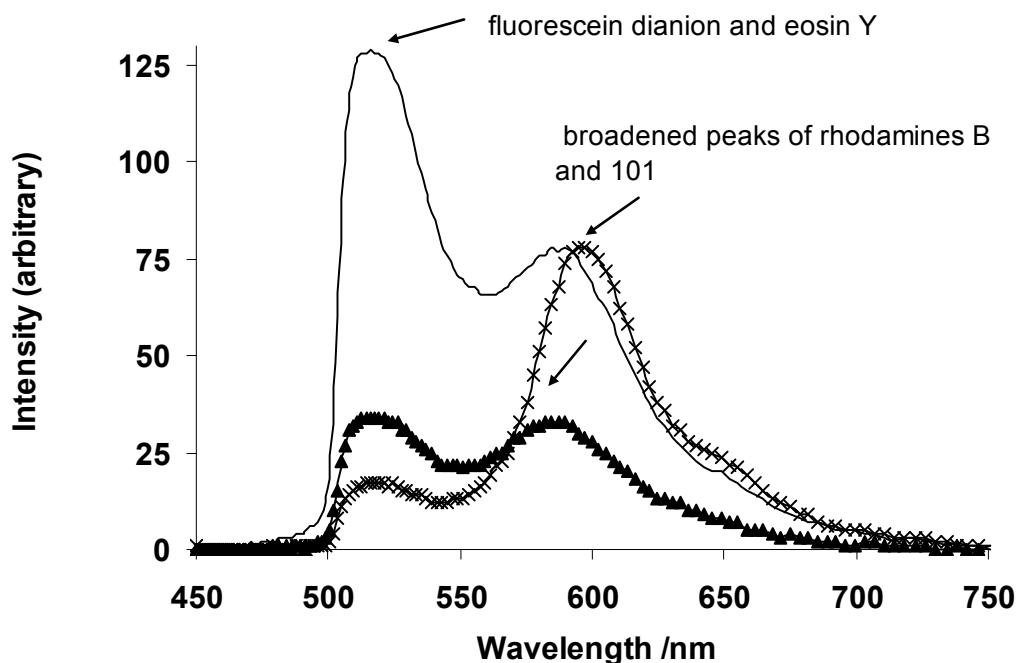


Figure 24: Spectra of mixtures of four dyes fluorescein, rhodamine B, rhodamine 101, and eosin Y. The solid line is the spectrum of a mixture containing 2 μM fluorescein, 5 μM rhodamine B, 2 μM rhodamine 101 and 3 μM eosin Y, \times is a mixture containing 1 μM fluorescein, 6 μM rhodamine B, 8 μM rhodamine 101 and 2 μM eosin Y, \blacktriangle is a mixture containing 8 μM fluorescein, 8 μM rhodamine B, 4 μM rhodamine 101 and 1.3 μM eosin Y.

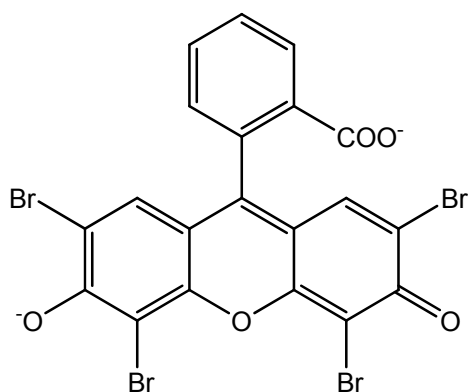


Figure 25: The structure of eosin Y

The fourth dye added was eosin Y (Figure 25), a tetra-bromo derivative of fluorescein, having excitation and emission maxima at 490 and 525 nm respectively.

There is a broad band between 515 and 525 nm. In spite of the proximity of the emission maxima of these two dyes (fluorescein and eosin Y, 7 nm), the model was able to distinguish between them, and the RSDs between the predicted and actual concentrations were 3%, 2%, 13% and 7% for fluorescein, rhodamine B, rhodamine 101 and eosin Y respectively. This indicates that despite the addition of a fourth species to the mixture, spectral unmixing can be successfully carried out. It would appear incongruous that four dyes were separated with greater success than three dyes. These results prove the hypothesis that high concentrations of dyes do not mix linearly and cannot be separated using linear least squares unmixing. These experiments highlight yet another restriction when using conventional fluorophores: the dyes are linear over only a narrow concentration range and concentrations need to be made such that the absorbance is less than 0.1 absorbance units. Departure from linearity reduces the ability to accurately identify and quantify the dyes present in a mixture.

This section presented an analysis of quantitative spectral unmixing of fluorophores, with a new method of calibrating multi-fluorophore systems. Separation of fluorescent dyes is normally hampered by effects of pH, photophysical interactions, and differences in maximum excitation and emission wavelengths of the dyes in a mixture, to name a few. By creating standards that take all effects into consideration, the process of unmixing spectra is tractable. Through a series of experiments, it has been established that it is possible to control the experiment such that the mixture can be easily separated. These controls include control of pH, ensuring that concentrations are low, and selecting dyes that have well spaced emission maxima. Other probes that can remove the need for these controls and simplify multiplexed analyses were therefore investigated.

The focus was changed to QDs, to determine if their widely publicised improvement over conventional organic dyes is realised when applied to spectral unmixing. Figure 26 shows the spectra of a mixture of the QDs for separation. This is a mixture of green and orange QDs, but the peak for green (515 nm) is not visible. The orange QD was kept constant at approximately 10 nM, while that of the green QD was incrementally decreased. Figure 26 shows that the intensity of the orange QD decreased with decreasing green concentration. These two QDs could not be separated using the same method as the organic dyes, and no other method was attempted.

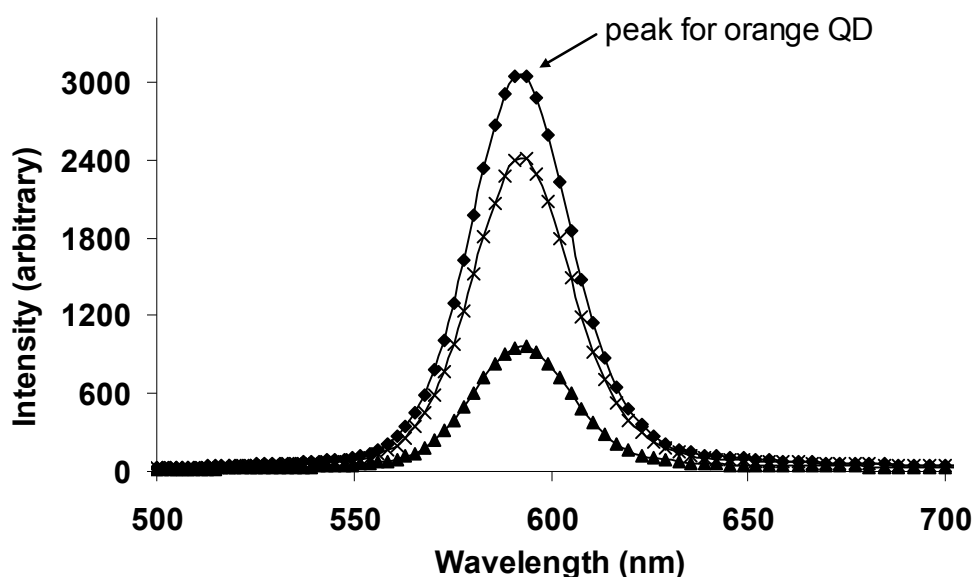


Figure 26: Mixture of orange and green quantum dots indicating the dependence of orange fluorescence on green. In this mixture, the orange concentration is kept constant and the green concentration is decreased from ■ 9 nM to x 3 nM to ▲ 0.8 nM.

The inability to separate is related to the non-linearity of mixing with the QDs, brought about through what is believed to be Förster (or Fluorescence) resonance energy transfer (FRET). This is a photophysical phenomenon where the intensity

emitted by the donor is decreased, while that of the acceptor is increased. The occurrence of FRET is dependent on the distance between the acceptor and donor, the spectral overlap between the donor emission and acceptor absorption spectra, and the relative orientation of the transition dipoles for the donor and acceptor. The observance of FRET occurring between the quantum dots is a phenomenon which isn't expected to occur in solution, based on the relative sizes and the proximity of one QD to another. There has been a report of FRET occurring due to long-range resonance transfer between two different sizes of QDs in gelatin.²⁹ The gelatin ensured close proximity of the QDs, the donor emission spectrum overlapped with the acceptor absorption spectrum and FRET was permitted through a dipole-dipole interaction. In another report, FRET was evidenced between QDs of two different sizes in a single droplet of water.³⁰ This was attributed to a decrease in the distance between the donor and acceptor species, allowing FRET to occur through dipole-dipole interactions. FRET between QDs has been demonstrated in closely spaced systems,³¹ such as would occur in a solid.³² In our experiment, the reactions occurred in solution, and some other mechanism must be taking place to allow energy transfer. The following is proposed: there was an interaction between the carboxylate functionalisations of the QDs which could possibly be a hydrogen bond. This hypothetical bond has a distance of 261 pm,³³ based on the length of the hydrogen bond between dimerized carboxylic acids. If this is the case, then, the aggregate formation due to the functionalisation allows for energy transfer to occur over the distance between the sensitizer (green QD) and the acceptor (orange QD), in spite of the low concentrations QDs; less than 10 nM. This proposed mechanism is shown in Figure 27. This is one of the possible explanations of why the intensity of the orange QD increases as the concentration of the green QD is increased.

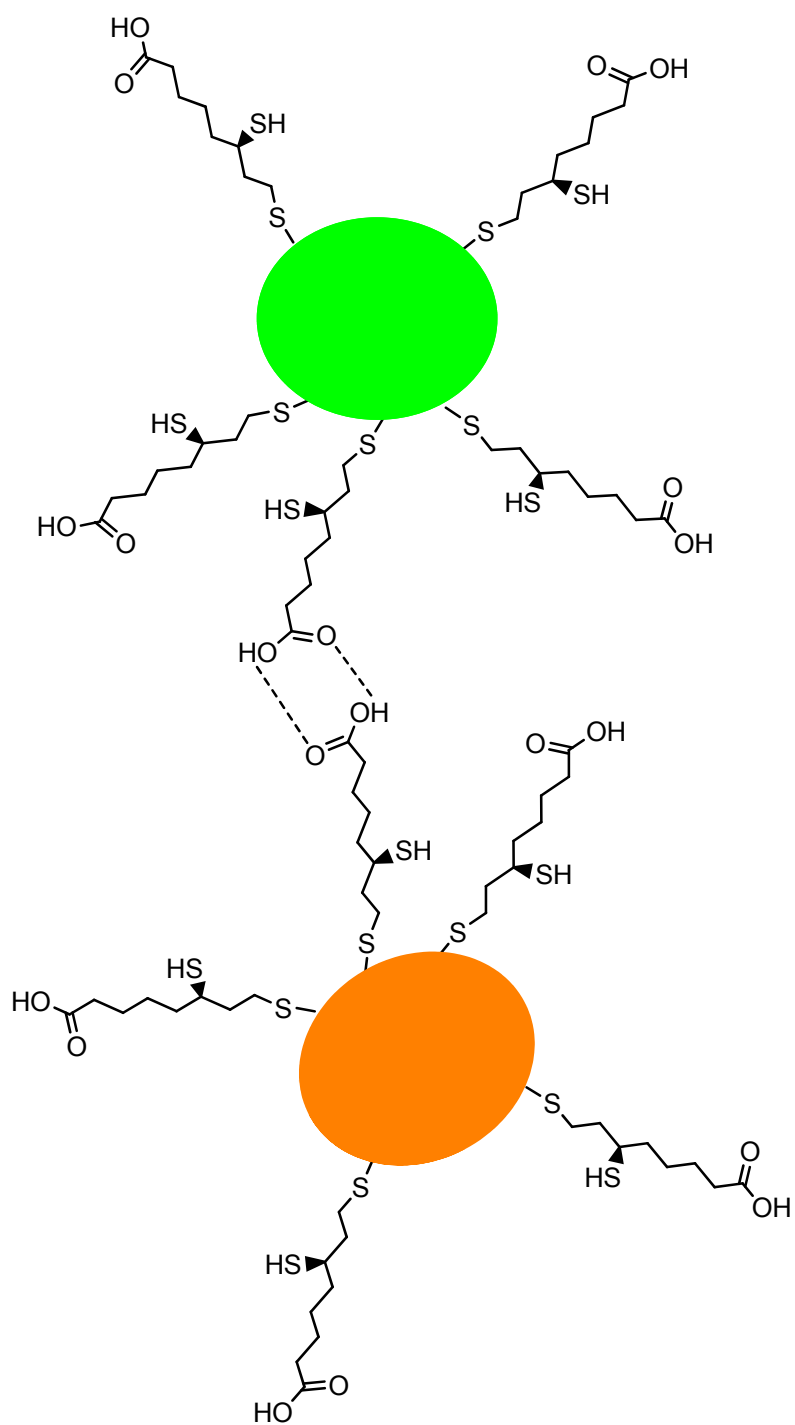


Figure 27: Diagram showing simplified organisation of two functionalised QDs in solution. The diagram shows ZnS capping with dihydrolipoic acid functionalisation.³⁴ There is hydrogen bonding between the carboxylate groups

The hypothesis that FRET is occurring between aggregated QDs needs to be explored in greater detail. The energy transfer efficiency between the orange and green QDs can be calculated using intensity data, as shown in Equation 3-5.³⁵

$$E = 1 - \frac{I_{DA}}{I_D} \quad \text{Equation 3-5}$$

Where E is the energy transfer efficiency, and I_{DA} and I_D are the intensities of the donor (green) QD in the presence and absence of the acceptor (orange) respectively. This value of energy transfer efficiency can be used to determine the distance between the donor and acceptor, using Equation 3-6.³⁵

$$R = R_0 \left(\frac{1}{E} - 1 \right)^{1/6} \quad \text{Equation 3-6}$$

As fluorescence imaging lifetime (FLIM) measurements were not obtained for the QD system, it is not possible to state whether all the quenching is related to FRET. However, provided that no other interactions altered the emission intensities, an energy transfer efficiency of 0.257 is obtained from intensity data. This gives the distance between the donor and acceptor as $1.19 R_0$. As R_0 is in the range of 20 to 60 Å,³⁶ this indicates that the distance between the centres of the emission and adsorption dipoles is probably on the order of the size of the QDs. This means that the separation between them is minimal, possibly corresponding to the 261 pm length of the hypothetical hydrogen bonds. It must be noted however, that Equation 3-5 only provides an average FRET efficiency value, and therefore cannot define a definite distance in solution.³⁶ In our case, this equation is not the best

method for determination of the distance between donor-acceptor pairs. The present situation requires different expressions derived through experiments where the rate of energy transfer is averaged over the distribution of the FRET pairs.

3.5 Discussion and Conclusions

The chapter presented a new method for calibrating a system containing a mixture of fluorophores, such that the dyes' spectra could be quantitatively unmixed. The principle of spectral unmixing assumes that the intensity at a single pixel is a result of the sum of the individual components in the mixture. Experiments performed show this to be somewhat misleading, as fluorophores do not always mix in this manner. Reactions in the mixture can create new species which do not absorb or emit in the same manner as individual fluorophores. When this occurs, using individual standards is of little utility. This has been demonstrated through a series of experiments, illustrating the need for the new method. When a mixture of two dyes was quantitatively unmixed using existing methods, the results did not always correspond well with actual concentrations (Tables 2 and 3, Figure 20).

The need for pH and concentration control has also been highlighted. It was shown that when these controls are in place, up to four dyes (and possibly more) could be unmixed with low RSD between the calculated and actual concentrations. Without controls in place, the method is of little utility.

Linear least squares minimisation was proven to be an effective method for spectral unmixing of fluorophores. However, the intrinsic properties of fluorescent dyes allow for non linear mixing.³⁷ Processes such as excited state reactions, which are

exhibited by the coumarins, also allow for non linear mixing.³⁸ Another is the pH dependence of some fluorophores such as fluorescein, rhodamine B and eosin Y. Each form has a different emission maximum, thereby leading the model to assume that another species is present. In the case of QDs, their nonlinearity was a result of energy transfer between the molecules in the mixture. While the size of the quantum dot may not allow for overlap of the molecules, the carboxylate functionalisation in solution caused dimerisation of carboxylic acids, thereby bringing the QDs closer together. QDs satisfy all criteria of broad excitation and narrow emission bands, resistance to photobleaching and longer lifetimes than organic fluorophores, but there is still the need for probes that do not interact when colocalised. This caused attention to be turned to silica nanoparticles doped with lanthanides. The silica encapsulates the lanthanide thereby preventing photobleaching and the particles can be made large enough to prevent interparticle FRET. Even if small particles are used and aggregation occurs, the large Stokes shift of the lanthanides prevent them being FRET pairs with each other, while allowing FRET pairing with QDs in other applications. The use of these probes will be discussed in the following chapter.

3.5 References

- (1) Goldman, E. R.; Clapp, A. R.; Anderson, G. P.; Uyeda, H. T.; Mauro, J. M.; Medintz, I. L.; Mattoussi, H. *Anal. Chem.* **2004**, *76*, 684-688.
- (2) Zimmermann, T. *Microscopy Techniques* **2005**, *95*, 245-265.
- (3) Nederlof, P. M.; Vanderfluer, S.; Wiegant, J.; Raap, A. K.; Tanke, H. J.; Ploem, J. S.; Vanderploeg, M. *Cytometry* **1990**, *11*, 126-131.
- (4) Speicher, M. R.; Ballard, S. G.; Ward, D. C. *Nat. Genet.* **1996**, *12*, 368-375.
- (5) Schrock, E.; duManoir, S.; Veldman, T.; Schoell, B.; Wienberg, J.; Ferguson-Smith, M. A.; Ning, Y.; Ledbetter, D. H.; BarAm, I.; Soenksen, D.; Garini, Y.; Ried, T. *Science* **1996**, *273*, 494-497.
- (6) Thaler, C.; Vogel, S. S. *Cytom. Part A* **2006**, *69A*, 904-911.
- (7) Zimmermann, T.; Rietdorf, J.; Pepperkok, R. *FEBS Lett.* **2003**, *546*, 87-92.
- (8) Keenan, M. R.; Timlin, J. A.; Van Benthem, M. H.; Haaland, D. M. *Imaging Spectrometry Viii* **2002**, *4816*, 193-202.
- (9) Haaland, D. M.; Timlin, J. A.; Sinclair, M. B.; Van Benthem, M. H.; Martinez, M. J.; Aragon, A. D.; Werner-Washburne, M. *Spectral Imaging: Instrumentation, Applications, and Analysis Ii* **2003**, *4959*, 55-66.
- (10) Timlin, J. A.; Haaland, D. M.; Sinclair, M. B.; Aragon, A. D.; Martinez, M. J.; Werner-Washburne, M. *BMC Genomics* **2005**, *6*, 72.
- (11) Haaland, D. M.; Easterling, R. G.; Vopicka, D. A. *Appl. Spectrosc.* **1985**, *39*, 73-83.
- (12) Wilson, B. E.; Kowalski, B. R. *Anal. Chem.* **1989**, *61*, 2277-2284.
- (13) Gemperline, P. J.; Long, J. R.; Gregoriou, V. G. *Anal. Chem.* **1991**, *63*, 2313-2323.
- (14) Garini, Y.; Young, I. T.; McNamara, G. *Cytom. Part A* **2006**, *69A*, 735-747.
- (15) Li, C.; Henry, E.; Mani, N. K.; Tang, J.; Brochon, J.; Deprez, E.; Xie, J. *Eur. J. Org. Chem.* **2010**, 2395-2405.
- (16) Metivier, R.; Badre, S.; Meallet-Renault, R.; Yu, P.; Pansu, R. B.; Nakatani, K. *J. Phys. Chem. C* **2009**, *113*, 11916-11926.
- (17) Sasaki, H.; White, S. H. *Biophys. J.* **2009**, *96*, 4631-4641.
- (18) J. O. Rawlings, S. G. Pantula and D. A. Dickey In *Applied Regression Analysis: A Research Tool*; Springer-Verlag: New York, 1998; .
- (19) Takahashi, Y.; Maeda, A.; Kojima, K.; Uchida, K. *Jpn. J. Appl. Phys. Part 2 - Lett.* **2000**, *39*, L218-L220.
- (20) Sarkar, A.; Ali, M.; Baker, G. A.; Tetin, S. Y.; Ruan, Q.; Pandey, S. *J Phys Chem B* **2009**, *113*, 3088-3098.

- (21) Elbaraka, M.; Deumie, M.; Viallet, P.; Lampidis, T. J. *J. Photochem. Photobiol. A-Chem.* **1991**, *62*, 195-216.
- (22) Scheaffer, R. L.; McClave, J. T. In *Probability and Statistics for Engineers*; Wadsworth Publishing Company: Belmont, California 94002, 1995; .
- (23) Klonis, N.; Sawyer, W. H. *Journal of Fluorescence* **1996**, *6*, 147-157.
- (24) Mchedlov-Petrosyan, N. O.; Vodolazkaya, N. A.; Doroshenko, A. O. *J. Fluoresc.* **2003**, *13*, 235-248.
- (25) Lavis, L. D.; Rutkoski, T. J.; Raines, R. T. *Anal. Chem.* **2007**, *79*, 6775-6782.
- (26) Ramette, R. W.; Sandell, E. B. *J. Am. Chem. Soc.* **1956**, *78*, 4872-4878.
- (27) Sjöback, R.; Nygren, J.; Kubista, M. *Spectrochimica Acta Part A: Molecular and Biomolecular Spectroscopy* **1995**, *51*, L7-L21.
- (28) Zakharenko, O. K.; Trusova, V. M.; Gorbenko, G. P. *Journal of Biological Physics and Chemistry* **2008**, *8*, 43-48.
- (29) Xu, L.; Xu, J.; Li, W.; Zhao, W.; Sun, P.; Ma, Z.; Huang, X.; Chen, K. *J. Mater. Sci.* **2007**, *42*, 9696-9699.
- (30) Xu, L.; Xu, J.; Ma, Z.; Li, W.; Huang, X.; Chen, K. *Appl. Phys. Lett.* **2006**, *89*, 033121.
- (31) Parascandolo, G.; Savona, V. *Superlattices Microstruct.* **2007**, *41*, 337-340.
- (32) Kagan, C. R.; Murray, C. B.; Bawendi, M. G. *Phys. Rev. B* **1996**, *54*, 8633-8643.
- (33) Fuller, W. **1959**, *63*, 1717.
- (34) Schmid, G. In *Nanoparticles: From Theory to Application*; Wiley-VCH: Weinheim, 2010; , pp 458-459.
- (35) Murray, K.; Cao, C. Y.; Ali, A.; Hanley, Q. *Analyst* **2010**, *135*, 2132-2138.
- (36) Lakowicz, J. R. In *Principles of Fluorescence Spectroscopy*; Springer: New York, 2006; .
- (37) Takahashi, Y.; Maeda, A.; Kojima, K.; Uchida, K. *J Lumin* **2000**, *87-9*, 767-769.
- (38) Morlet-Savary, F.; Ley, C.; Jacques, P.; Fouassier, J. P. *J Phys Chem A* **2001**, *105*, 11026-11033.

-

4 Lanthanide nanoparticles: simplification of multiplexed methods of analysis

The unfavourable characteristics of organic fluorophores and quantum dots in multiplexed experiments prompted the search for probes that mix linearly, are bright, have narrow emission bands, have large Stokes' shifts and can be excited simultaneously. Silica nanoparticles doped with lanthanides have all these properties and were selected for application to multiplexed analyses. Nanoparticles doped with chelated Eu and Tb have been used previously and extensively characterised, but their application to single well multiplexed immunosorbent assays had not been described. It was not the intention of this work to further characterise the particles, and this is therefore not presented. What this work set out to achieve was to create additional particles; doped with Sm and a mixture of Eu and Sm, create a ligand suitable for chelating Tb while binding it to the wall of silica, and to use these probes in immunoassays. Presented here is an introduction to the lanthanides, their spectral properties and their previous uses in immunosorbent assays. Then, nanoparticles containing chelated lanthanides are synthesised, the two probes were mixed in varied ratios and the spectra of the mixtures were separated using a simple unmixing algorithm. Finally, the probes are applied to a single well multiplexed assay, where human and mouse IgGs were simultaneously detected in a model study.¹

4.1 Introduction

The fluorescence of some lanthanides, particularly europium (Eu), terbium (Tb), samarium (Sm) and dysprosium (Dy) can be enhanced when chelated by organic

ligands.² Lanthanide chelates have unique properties, making them suitable as labels in various applications such as bioassays, high throughput assays, screening studies and in time resolved spectroscopy. Their use enhances the signal to noise ratio.³ The unique properties include their line-like emission spectra, long fluorescence lifetimes, no self quenching, high quantum yield of fluorescence, good solubility and large Stokes shifts.⁴ Line-like emission spectra and large Stokes shift eliminate background fluorescence in time resolved immunofluorometric applications (TRIFAs), and long lifetimes allow better separation between the signal and noise.⁵ These characteristics are a result of the Laporte forbidden $f - f$ transitions of shielded inner shell electrons.⁶ The 4f electrons of the lanthanide trivalent ions are shielded by the outer 5s and 5p electrons. As a result, the ions retain atomic properties even after complexation. Direct excitation of these shielded electrons results in weak emission, but the use of a suitable ligand leads to sensitised emission, where the ligand is excited followed by an intersystem crossing (ISC) from the ligand's singlet state to the triplet state. This is followed by energy transfer to the low lying emissive state of the excited lanthanide ion⁷ (Figure 28). Energy transfer can also occur from the singlet state, but generally occurs from the triplet state. This is because ISC from the triplet state is enhanced by the paramagnetic lanthanide ions which lie closer to the triplet state. Energy transfer from the singlet state is slower and cannot compete with fluorescence and ISC.^{8,9} Figure 28 illustrates the absorption of light by a chromophore, leading to promotion to the first excited state (S_1). There is then intersystem crossing to the triplet state (T_1) of the chromophore followed by energy transfer to the excited state of the lanthanide ($^{2S+1}L'_J$). The metal centre then becomes deactivated and returns to the ground state. When radiative deactivation occurs light is emitted in the form of luminescence.¹⁰

Direct excitation of the lanthanides is inefficient due to narrow intrinsic absorption bands ($< 2 \text{ nm}$), and low molar absorptivity ($< 1 \text{ M}^{-1}\text{cm}^{-1}$).¹¹ The ligand must contain a sensitising chromophore with energy higher than that of the lanthanide's excited state such that excitation is efficient and irreversible. This is known as the antenna effect. The ligand also protects the lanthanide luminescence from being quenched by molecules such as water which has high-energy vibrations. Quenching of the fluorescence by O-H vibrations of lanthanides having a short gap between the lowest excited state energy level and the highest ground state level tends to occur.¹² This leads to nonradiative deactivation of the lanthanide metal centre.¹⁰

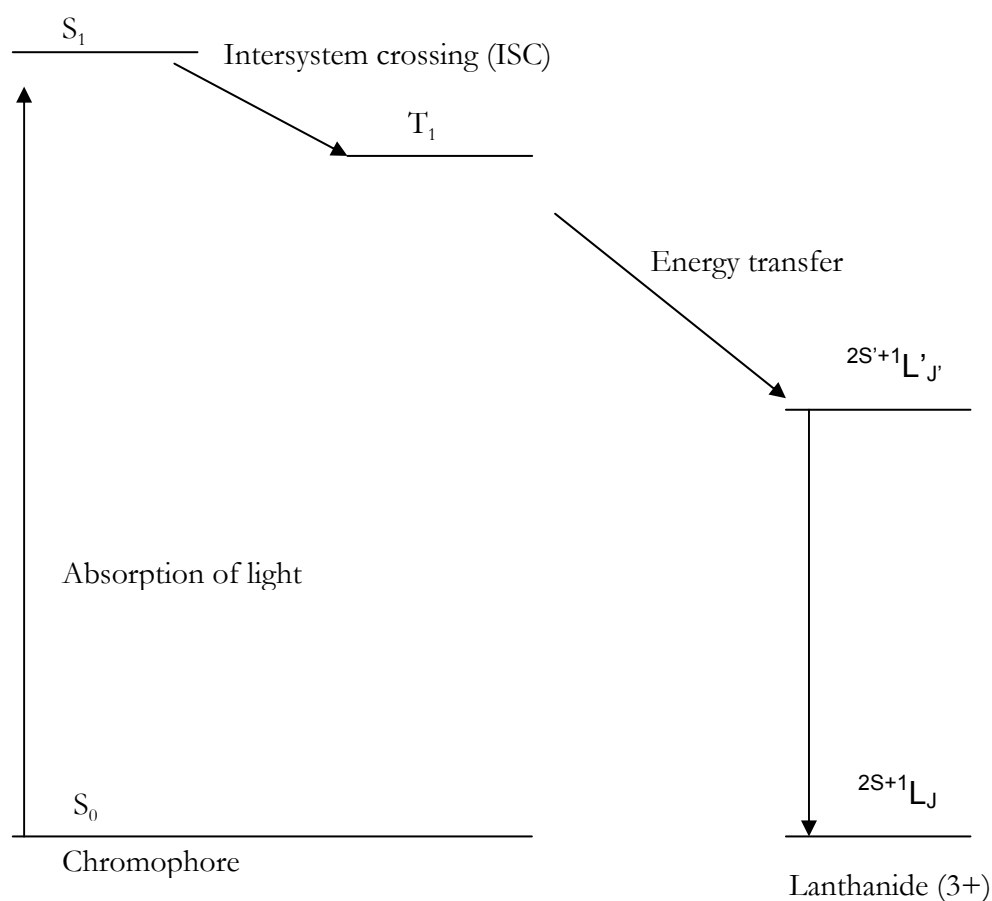


Figure 28: Energy diagram of luminescence in lanthanide complexes

The majority of studies involving the use of lanthanides as biomarkers use ligands such as β -diketones, aromatic amine derivatives such as pyridine, bipyridine, terpyridine and phenanthroline, and macrocycles.¹³ A commonly used lanthanide ligand is the polycarboxylate diethylenetriaminepentaacetic acid (DTPA), which when covalently attached to an antenna, allows luminescence of the lanthanides.

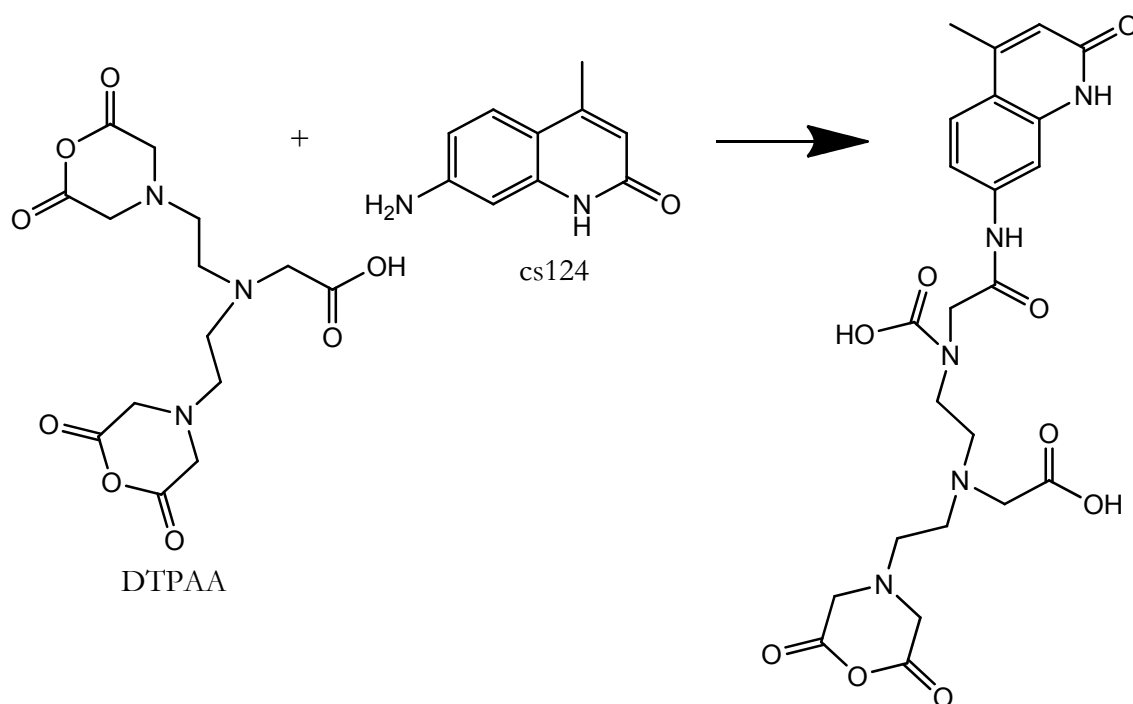


Figure 29: Reaction of polycarboxylate diethylenetriaminepentaacetic acid (DTPA) with cs 124 to form a lanthanide ligand

7-amino-4-methyl-2(1H)-quinolinone; also known as carbostyryl 124 or cs 124, acting as the antenna (Figure 29) has reportedly sensitised both europium and terbium.⁴ The dianhydride form of DTPA can be conjugated to amine-containing molecules, or can be further modified to prevent nucleophilic acyl substitution reactions which occur readily with the non-specific dianhydride. These modifications include conversion to the isothiocyanate form for reaction with

amines, and conversion to the maleimide, bromoacetamide and pyridyldithio forms for reaction with thiols (Figure 30).¹⁴

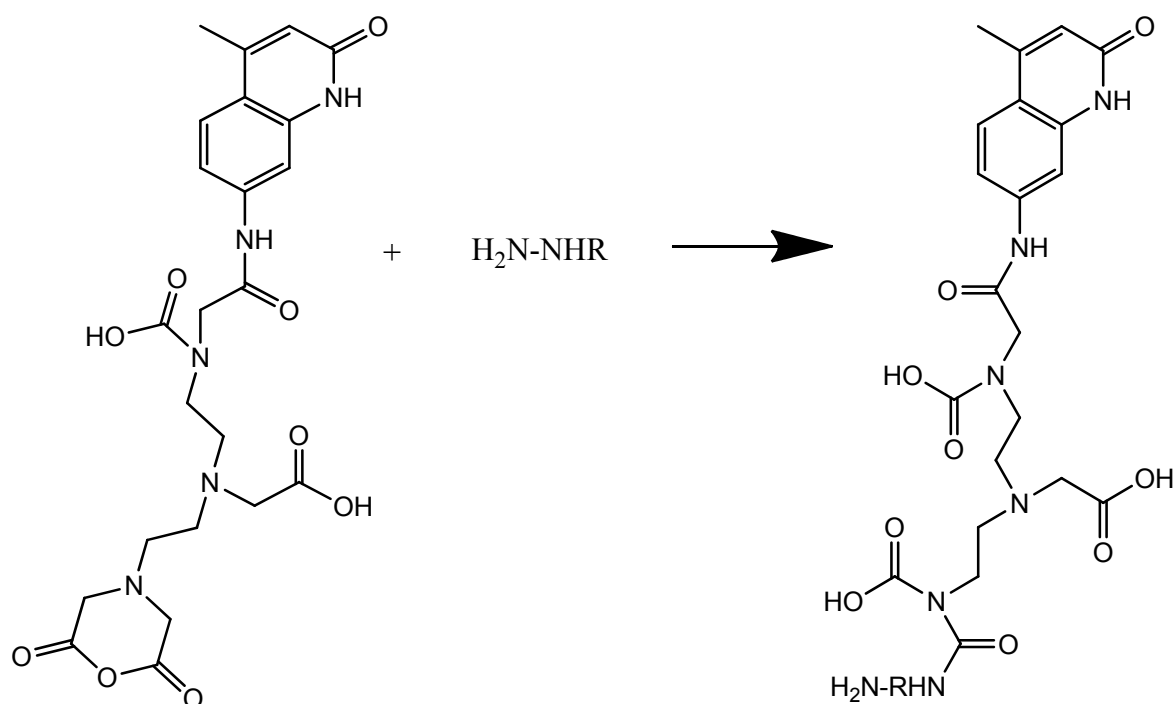


Figure 30: Further modification of the lanthanide ligand to allow conjugation to other moieties. R refers to any amine or thiol reactive group.

Lanthanide fluorescence may be further enhanced by compounds that protect the complex from solvent interference. Enhancement may also be brought about through cofluorescence, a process whereby the fluorescence of the lanthanide is increased through the use of another non luminescent lanthanide such as Gd^{3+} .¹⁵

Nanoparticles (NPs) that contain thousands of lanthanide chelates have been developed for use in time resolved immunoassays.¹⁶ Earlier reports explored the use of polystyrene beads doped with a europium complex for detection of prostate specific antigen (PSA).¹⁶ The use of polystyrene NPs doped with terbium, europium, samarium and dysprosium complexes have also been reported as potential labels for multiplexed immunoassays, after their use in the detection of PSA.¹⁷ The chelates

are not covalently bound to the NP wall and dye leakage has been known to occur, causing a decrease in the NP signal.¹⁸ Additionally, polystyrene NPs are hydrophobic and agglomerate in aqueous solution, presenting problems during surface modification and bio-labelling applications.¹⁹ These factors prompted the synthesis of silica NPs containing first Eu complexes¹⁹⁻²¹ as an alternative, due to silica's hydrophilicity and ease of surface modification. Other reports noted the synthesis of lanthanide complexes on the surface of the silica.²²⁻²⁴ Incorporating the complexes into the silica particles allows for particles with more than one optical encoding to be synthesised,²⁴ making multiplexed measurements possible.

Since the initial studies on luminescent lanthanide doped silica NPs, some reports have been made of dye-doped NPs containing more than one optical encoding. Liu *et al.* synthesised such particles through the hybridisation of silica particles doped with FITC and a terbium complex. The complex was made on the surface of the doped silica particles. The novel particles exhibited both the fluorescent properties of FITC and terbium.²⁴ There are few reports of multi-fluorescent dye doped SiO₂ NPs. In one report, the silica was doped with controlled ratios of Eu and Tb chelated by 2,9-bis[N,N-bis(carboxymethyl)aminomethyl]-1,10-phenanthroline and used in a time resolved immunofluorimetric assay (TrIFA) for human hepatitis B surface antigen.⁵ In the other, the particles are 210 nm silica spheres containing Eu and Sm chelated by 4,4,4-trifluoro-1-(2-thienyl)-1,3-butanedione.²⁵ The study examined energy transfer within the system.

The properties of lanthanide complexes and lanthanide-doped SiO₂ NPs allow them to be used extensively in Tr-FIAs, and while their usefulness in two-colour detection imaging applications have been alluded to,²⁶ no known studies have

separated the NPs using spectral unmixing, and little research has been carried out in creating more than one optically encoded NP. The present work examines the use of lanthanides as probes for simplifying spectral unmixing and reports the separation of mixtures of fluorescent probes for multiplexed measurements. The novelty of the work lies in the use of silica NPs doped with lanthanides as replacements for conventional fluorescent dyes and QDs in spectral unmixing, the synthesis of an NP containing Eu and Sm in the same silica matrix which has not been previously demonstrated for particles < 100 nm, and the synthesis of a ligand that is able to chelate all three lanthanides. Spectral unmixing of the NPs will be compared to unmixing spectra of fluorescent dyes and QDs. The utility of the NPs is further demonstrated in a novel single-welled multiplexed immunoassay using commercially obtained mouse and human IgGs.

4.2 Materials and Methods

4.2.1 Materials

The reagents for the synthesis of SiO₂-doped nanoparticles: EuCl₃·6H₂O and SmCl₃·6H₂O (both 99.99 %), the chelate 4,4''-bis(4,4,4-trifluoro-1,3-dioxobutyl)-o-terphenyl-4'-sulfonyl chloride (BTBCT) (≥ 95 %, Lot no. 1156533), 3-aminopropyl triethoxysilane (APS) (99%, Lot no. 10330CH-417), cyclohexane (99.5 %, Lot no. S42405-257), Triton® X-100 (Lot no. S42329-367), n-octanol (99 %, Lot no. 01706DE) and tetraethyl orthosilicate (TEOS) (≥ 99 %, Lot no. 1332815) were all obtained from Sigma Aldrich UK (Sigma-Aldrich, Dorset UK). 4-phenylspiro-[furan-2(3H),1-phthalan]-3,3'-dione (fluorescamine) (98%, Lot no. 80129) was also obtained from Sigma-Aldrich. Deionised water (Milli-Q purification system; Millipore UK Ltd.) was used to prepare all solutions. All reagents for the

multiplexed immunoassay were also obtained from Sigma Aldrich. These were goat anti-mouse IgG (whole molecule) (Lot no. M8642), mouse IgG (Lot no. I5381), goat anti-mouse IgG (Fab specific)-Biotin (Lot no. B0529), human IgG (Lot no. I4506), goat anti-human IgG (whole molecule) (Lot no. I1886), technical grade casein from bovine milk (Lot no. C7078) and carbonate-bicarbonate buffer capsules (Lot no. C3041). Biotinylated anti-human IgG was prepared in-house.

4.2.2 Synthesis and characterisation of the nanoparticles

The method for preparing the nanoparticles is outlined in Chapter 2. After the 24 hour synthesis, acetone was added and the mixture was centrifuged (as outlined previously). The particles obtained upon centrifugation were then suspended in approximately 15 mL ethanol and transferred into 2 mL eppendorf tubes (1.5 mL/tube). The tubes were centrifuged (10 000 g, 30 minutes), the supernatant was discarded, a further 1.5 mL of ethanol were added followed by further centrifugation. This process was repeated for a total of 7 washes; first with ethanol (4 times) and then with water (3 times). After the final wash with water the particles were stored in PBS (pH 7.4). These wash steps served to remove all unreacted chemicals, thereby ensuring that luminescence of the doped silica particles was a result of the chelated lanthanides bound to the wall of silica only, and not unbound reagents in solution. The speed and time of centrifugation further served as an indicator of the stability of the particles made. The ligand BTBCT is unable to excite Tb^{3+} , and another ligand had to be synthesised. This needed to have a group that could be bound to the silica wall, thereby preventing leakage of the chelated lanthanide. The group chosen was (3-aminopropyl)triethoxysilane (APS), and the procedure is outlined below (Figure 31).

7-Amino-4-methyl-2-hydroxyquinoline, known as carbostyryl 124 (cs124) (10 mg, 0.0574 mmol) was dissolved in DMF (200 μ L). This was added dropwise with stirring to the dianhydride of diethylenetriaminepentaacetic acid (DTPAA) (100 mg, 0.287 mmol) and triethylamine (40 μ L) in a solution of DMF (4.7 mL). After stirring at room temperature for 1 hour, APS (10.4 mg, 47 μ mol) was added and stirring was continued for a further hour. The reaction was quenched by the addition of water (5 mL) and the chelate formed, DTPA-cs124-APS was recrystallised from chloroform and the pale yellow crystals formed were dried and stored at 2 – 8°C for reaction with the lanthanides. This structure of the chelate was difficult to prove, as the presence of water and DMF, after days of drying by high vacuum and rotary evaporator pumps, was still evident in the NMR spectra. This made it difficult to integrate the peaks successfully. It was possible however, to compare the chelate NMR data with computer generated NMR data, and these will be discussed. The specific ^1H NMR shifts looked for were those for carboxylic acids (indicating that the anhydride rings had opened), and the amide bonds formed when cs 124 and APS bind to DTPAA. As structural evidence was not definitive, the success of the synthetic procedure had to be based on the spectroscopy of a silica nanoparticle doped with Tb chelated by the ligand synthesised. The only structure which could provide such a particle would be the product of the reaction that is shown in Figure 31.

4.2.3 Synthesis of a novel ligand for Terbium

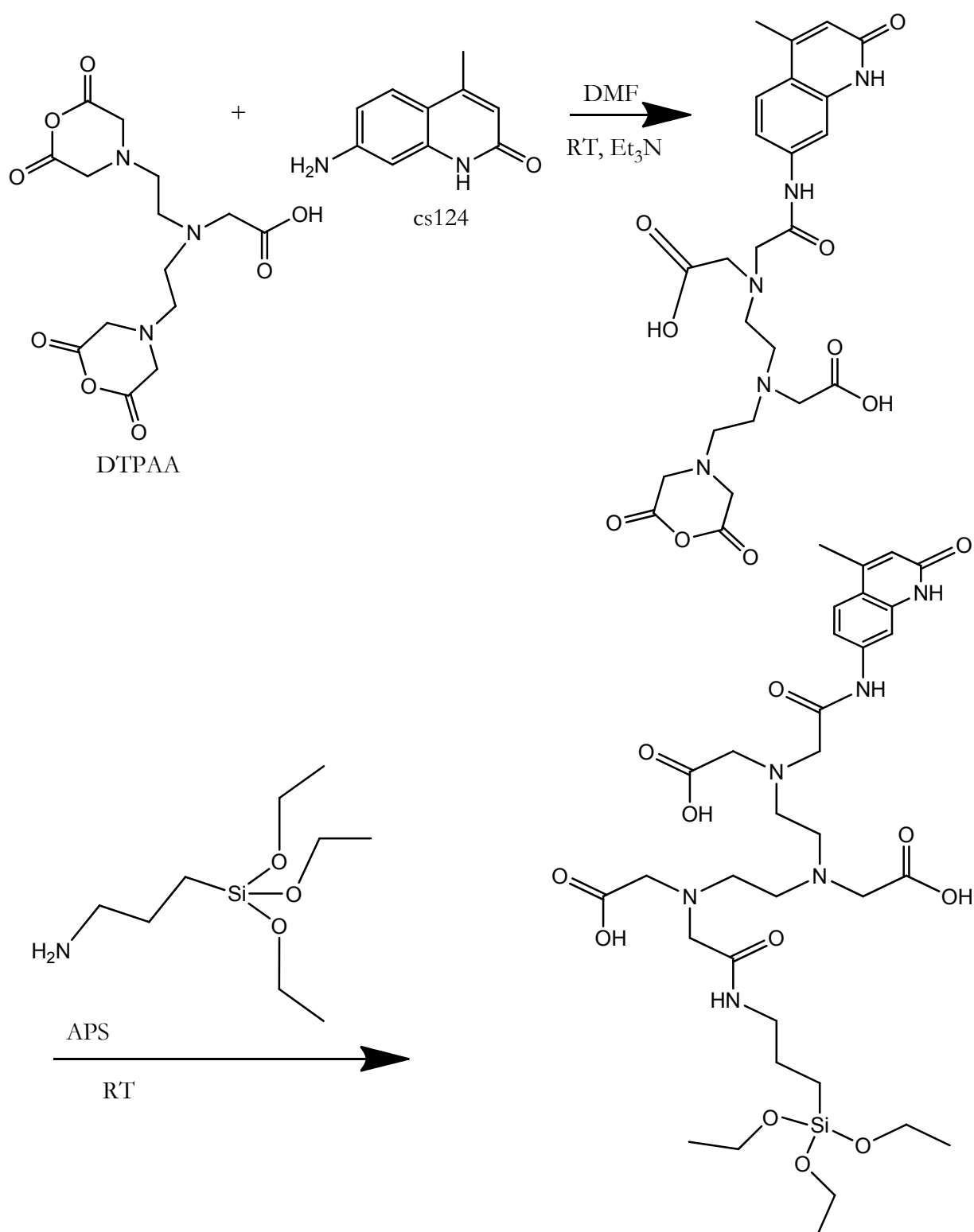


Figure 31: The synthetic method for the preparation of a new ligand for Tb.

4.2.4 Fluorescamine

4-phenylspiro[furan-2(3)l'-phthalan]-3,3-dione, (fluorescamine), was used to determine the presence of amine groups on the surface of the nanoparticles. This reagent is itself non-fluorescent, but reacts only with primary amines to form highly fluorescent pyrrolinones.²⁷ Any excess reagent is also non-fluorescent, thereby making fluorescamine suitable for the detection of primary amines in basic pH (pH > 7).²⁸

A stock solution of 1.5 mg (0.011 M) fluorescamine in 0.5 mL dimethyl sulfoxide (DMSO) was made immediately before use. 5 μ L of the solution were added to a tube containing 15 μ L PBS (0.003 M fluorescamine) and a further 5 μ L were added to a tube containing 15 μ L of NPs (0.1 M) in PBS. The mixtures were vortexed and left at room temperature for 15 minutes, after which the tubes were centrifuged and the pellet washed with PBS. This was to ensure that any colour change would be a result only of amines on the particles. The presence of primary amines was denoted by blue-green fluorescence following illumination with a UV light source, 254/306 nm excitation, 0.12A @ 220 V, 50 Hz (Mineralight® Lamp, Ultraviolet Products, Inc., San Gabriel, California, USA.). All analyses were performed in triplicate.

4.2.5 Transmission Electron Microscopy (TEM)

A transmission electron microscope (TEM) was used to determine the sizes of the nanoparticles made. The TEM used was a JEM-2010 JEOL (Jeol UK Ltd., Herts, UK), accelerating voltage 200 keV, tungsten filament, electron beam current 10 μ A. Images were recorded using a Gatan SC1000 ORIUS CCD camera (Model 832) with an image size of 4008 x 2672 pixels. The nominal resolution of the instrument is ~ 0.2 nm,²⁹ and this is dependant on the wavelength of electrons. The resolution

is reduced through spherical and chromatic aberrations, while increasing the accelerating voltage improves resolution.³⁰ The magnification used was x 200 000 and contrast at this resolution was achieved with the use of an objective aperture. This provided scattering contrast by absorbing electrons that were scattered at an angle greater than the semi-aperture angle.³¹ For this contrast mechanism, dark areas of the resulting micrograph represent electron dense areas, as these produce the greatest amount of scatter.

4.2.6 Multiplexed immunoassay for human IgG and mouse IgG using NPs

Multiplexed immunoassays were performed by first immobilising a mixture of anti-mouse IgG and anti-human IgG ($50\text{ }\mu\text{g mL}^{-1}$) in carbonate/bicarbonate buffer (pH 9.65, 0.05 M) on the surface of a 384-well glass bottom plate (Porsvair; Flowgen, Nottingham, UK). The plate was left to shake at room temperature overnight followed by blocking with a solution of 1% casein for 2 hours. After washing with PBS, a mixture of human IgG and mouse IgG was added and incubated at room temperature for 2 hours. After washing excess antigen from the wells, the biotinylated anti-mouse IgG and antihuman IgG antibodies; which had been incubated with the avidin linked NPs for 4 hours, were added to the wells in a 1:1 volume ratio. The plate was incubated overnight at room temperature with shaking. A final wash was performed and the plate imaged using the inverted fluorescence microscope.

4.3 Results and Discussion

4.3.1 NP characterisation

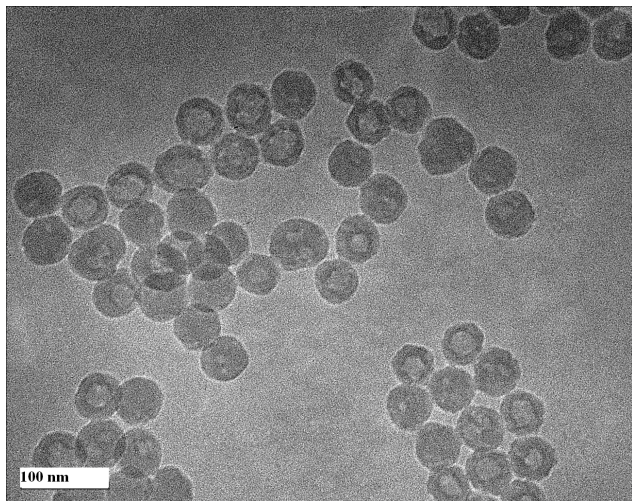


Figure 32: Electron micrograph of Sm-doped silica NPs, obtained with a TEM. Mag $\times 200\,000$. Particles were obtained after spinning at high speed.

Figure 32 shows an electron micrograph of silica NPs doped with lanthanides obtained using a TEM. The image shows spherical, uniform particles having diameter of 40 ± 10 nm (40 NPs measured). No elemental analysis was performed on the particles, however, when looking at Figure 32, the particles show a dark ring around the inside of the particles. According to the theory of transmission electron microscopy, the darker region represents the presence of a more electron dense material. This region suggests that the chelated lanthanide is present and bonded to the inner wall of the silica NP. This is in keeping with previously published observations.²⁰

Figure 32 further indicates that there is very little aggregation. It was observed that when the particles are first centrifuged, a high speed (10 000 rpm was the speed chosen) prevents aggregation. This was determined after initial micrographs of the

NPs showed aggregation when spun at a low speed (5000 rpm) (Figure 33). When figures 32 and 33 are compared, the two most easily comparable observations are size and the presence/absence of aggregates. As the particles obtained after spinning at low speeds are bigger (90 ± 10 nm) and more aggregated, the decision was made to switch to the highest speed of the centrifuge available thereby allowing smaller particles to be collected. Unfortunately a comparison could not be made from a single micrograph as the TEM was not in operation when Figure 33 was obtained, and the sizes obtained in Figure 32 were not easily visualised with the SEM.

The nanoparticles were imaged using a fluorescence microscope. Their spectra are shown in Figures 34 through 36 and 41. Assignment of the main peaks for each spectrum is shown on the figures, and an explanation for the width of the emission peaks follows the figures.

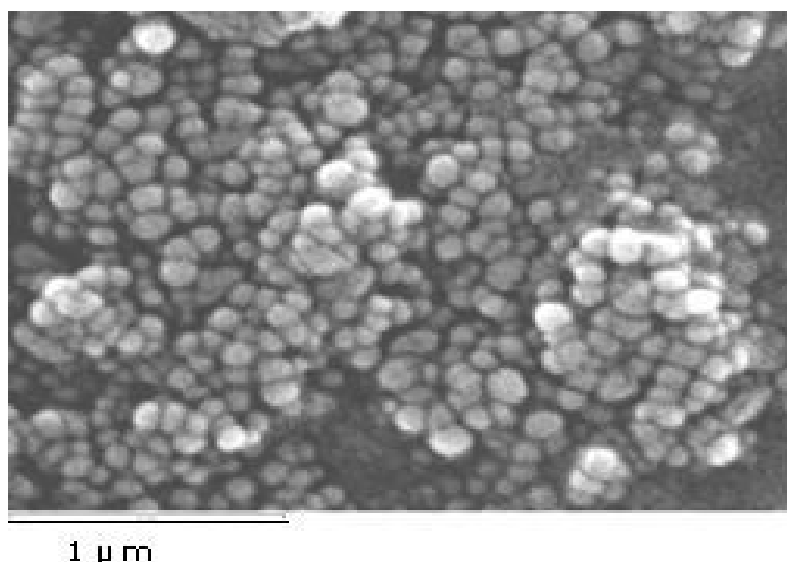


Figure 33: Electron micrograph of Sm- doped silica NPs as obtained by SEM. Particles were obtained after spinning at a low speed

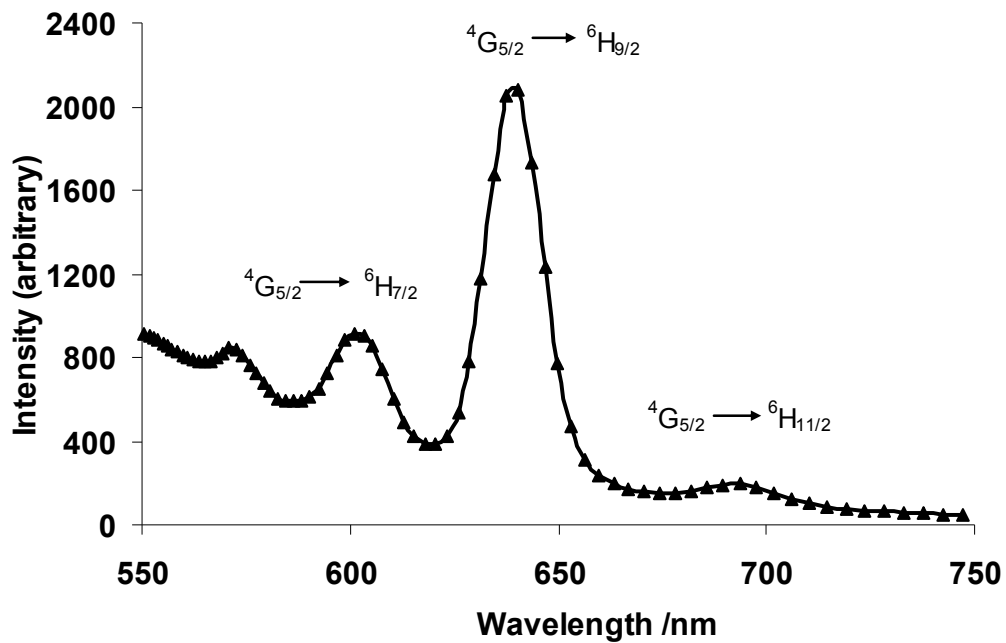


Figure 34: Luminescence spectrum of samarium-doped silica nanoparticles. The concentration of Sm is 735 μM .

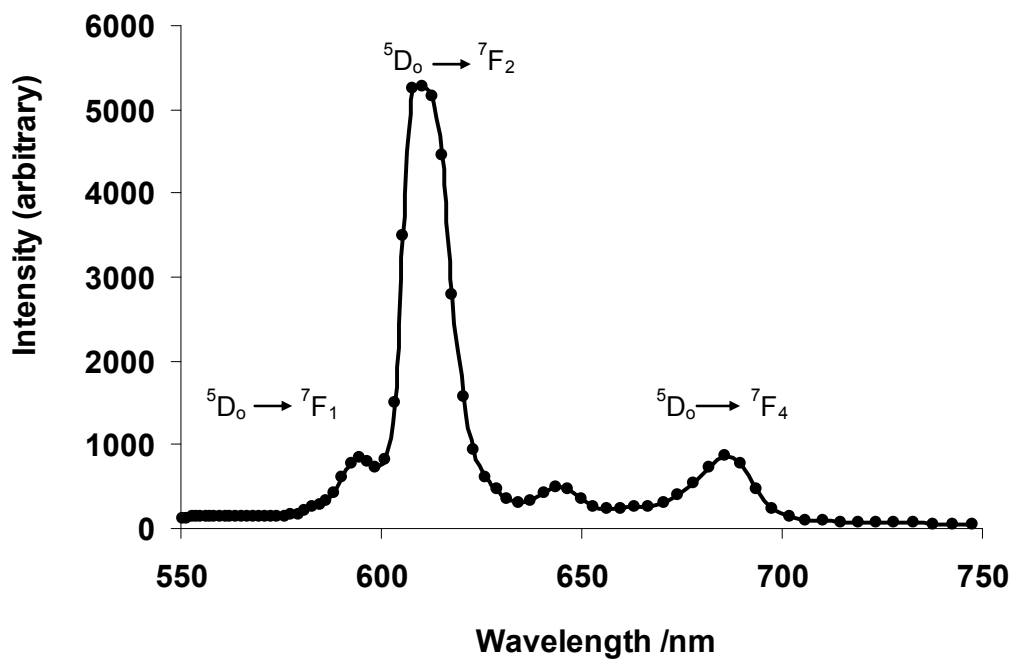


Figure 35: Luminescence spectrum of europium doped silica nanoparticles. The Eu concentration is 438 μM .

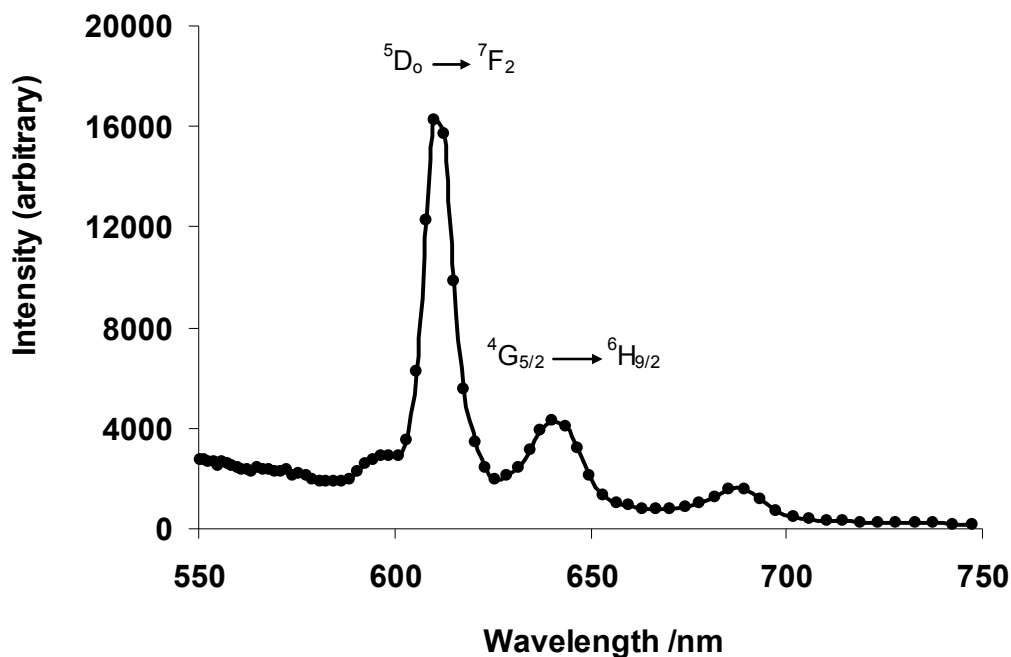


Figure 36: Luminescence spectrum of silica nanoparticles doped with europium and samarium. The Sm concentration is 409 μM while that of Eu is 270 μM .

The luminescence spectrum for Sm-doped NPs is shown in Figure 34. Four bands were obtained for the Sm NPs synthesised, are visible, with the most intense emission peak at 640 nm corresponding to $^4\text{G}_{5/2} \rightarrow ^6\text{H}_{9/2}$ and the others at 570 nm, 600 nm, and 694 nm, corresponding to the $^4\text{G}_{5/2} \rightarrow ^6\text{H}_{5/2}$, $^4\text{G}_{5/2} \rightarrow ^6\text{H}_{7/2}$ and $^4\text{G}_{5/2} \rightarrow ^6\text{H}_{11/2}$ transitions respectively.¹² A fifth band was also seen at 532 nm, and this broad band was attributed to the BTBCT ligand emission. This was not seen in the emission spectrum from the Eu NP. A similar pattern of strong ligand emission and weak Sm emission has been reported for a Sm complex and attributed to deactivation of the Sm complex through solvent O-H vibrations and inefficient energy transfer from the ligand to the metal. The first factor would not apply in this case unless there is water present in the coordination sphere. The Sm complex is encapsulated in the silica matrix and is therefore protected from solvent effects. Inefficient energy transfer between the ligand and the lanthanide however, seems

likely. When the ligand is irradiated with UV light, one pathway to deactivation of the excited state is through transfer of energy to the lanthanide.³² Ligand luminescence and transfer of energy to the lanthanide excited state are competitive processes. Compared to the Eu complex, the transfer is less efficient for the Sm complex, resulting in higher fluorescence intensity for the ligand.

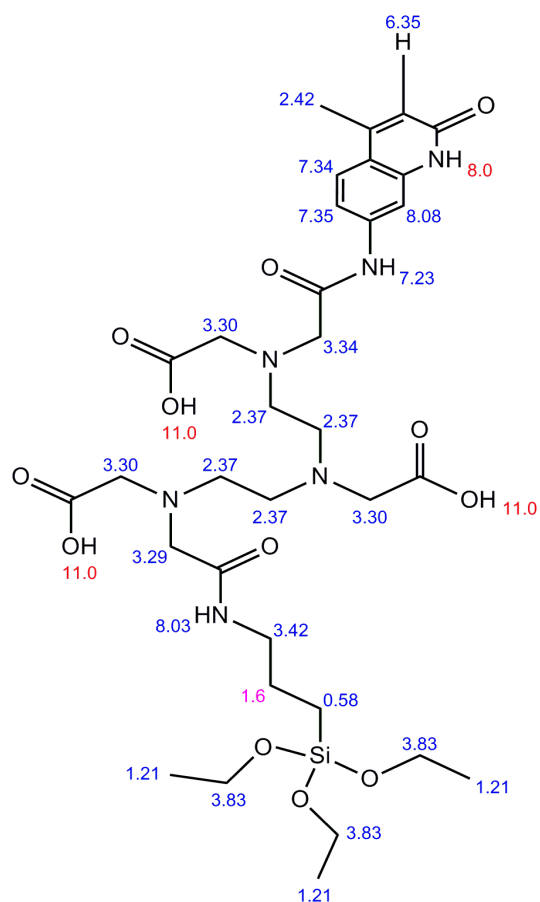
The Eu-doped NPs were found to have bands at 594 nm, corresponding to the $^5D_0 \rightarrow ^7F_1$ transition; 613 nm corresponding to the $^5D_0 \rightarrow ^7F_2$ transition and 689 nm, corresponding to the $^5D_0 \rightarrow ^7F_4$ transition, with the band at 613 nm having the most intense emission (Figure 35).³³

Synthesis of these particles allowed the creation of a particle which had all the peaks of both Eu and Sm. This particle was synthesised, also using the microemulsion method with Eu and Sm individually chelated to BTBCT, but encapsulated in the same silica matrix (Figure 36). This particle has fluorescence maxima corresponding to those of both Eu and Sm. Although added in a 1:1 molar ratio, the peak corresponding to Eu has fluorescence intensity 4 times that of Sm. Additionally, the intensity of the peak at 613 nm is almost 3 times greater in the mixed NP than it is in the particle doped with Eu alone. This has been described in a previous study²⁵ as energy transfer from the $^4F_{3/2}$ level of Sm^{3+} to the 5D_1 level Eu^{3+} , which lie close to each other, thereby leading to fluorescence enhancement of Eu. No peaks for Sm were observed in that study.²² All peaks for both chelated lanthanides were seen in the emission spectrum of our mixed NP, suggesting multiple energy transfer through orbital overlap from the ligand to Eu, ligand to Sm and the Sm complex to the Eu complex. The enhanced luminescence of Eu, coupled with visible luminescence from Sm makes this NP useful, and provides an advantage over the use of individually doped Eu and Sm particles. Its characterisation also differs from what has been previously published. This particle has a unique spectrum, making it

applicable to multiplexed measurements. Additionally, for assays where the analyte is of a low concentration, it is hypothesised that the enhanced luminescence of Eu would allow for low limits of detection. By carefully controlling the ratio between Eu and Sm, further particles with their own unique signatures can be developed, thereby allowing for sensitive assays. That, however, was not attempted during this project, as the main focus was to use probes with unique spectra in multiplexed assays. The probe with enhanced luminescence of Eu would be better suited to single analyte detection studies and could find utility in future work focussed on that area.

The spectrum of Tb-doped silica NPs is shown in Figure 41. The ligand used was DTPAA with cs 124 as the antenna, and APS used to bind the complex to the silica wall. The structure of a similar ligand has been described in literature¹⁴ and the peaks of interest for this ligand were not clearly seen using ¹HNMR (DMSO-D6). The shifts observed were not definitive due to the presence of solvent peaks obscuring the product peaks. Those looked for were δ 7.4 (d, CONH between DTPAA and cs 124); δ 10.55 (-COOH); δ 8.28 (CONH between APS and DTPAA). As a comparison, the presumed structure of the chelate was generated in ChemBioDraw (CambridgeSoft). ¹HNMR shifts were assigned theoretically and a comparison was made to the experimental NMR. This comparison is shown in Figures 37 and 38. From these figures, it can be seen that the expected peaks are indeed present, but are somewhat obscured by the presence of DMF and water peaks. Nevertheless, the roughly predicted position of the COOH shift (δ 11.00) appears at δ 10.27, the predicted position of the secondary amide formed between APS and DTPAA (δ 8.03) appears at 8.14 and the secondary amide between cs 124 and DTPAA (δ 7.33) is shown at 7.33 in the experimental spectra. These

correlations indicate that with more time, further attempts could be made to clean the product and make it more suitable for characterisation. Future work could also explore using solvents other than water and DMF, as these two were hard to remove after synthesis. For the purposes of the NMR, a D₂O shake would help clear the region between δ 2.0 and 3.0 of OH peaks, allowing better analysis and more in depth peak assignments. The shake would do little else for interpretation however, due to its removal of all OH and NH peaks. The product of the synthetic reaction should contain both starting materials DTPAA and cs124, with the addition of other peaks corresponding to APS and the amide bonds formed. Comparisons can be drawn between their respective NMR spectra and the spectrum of the chelate. These spectra are shown in Figures 39 and 40.



Estimation quality is indicated by color: good, medium, rough

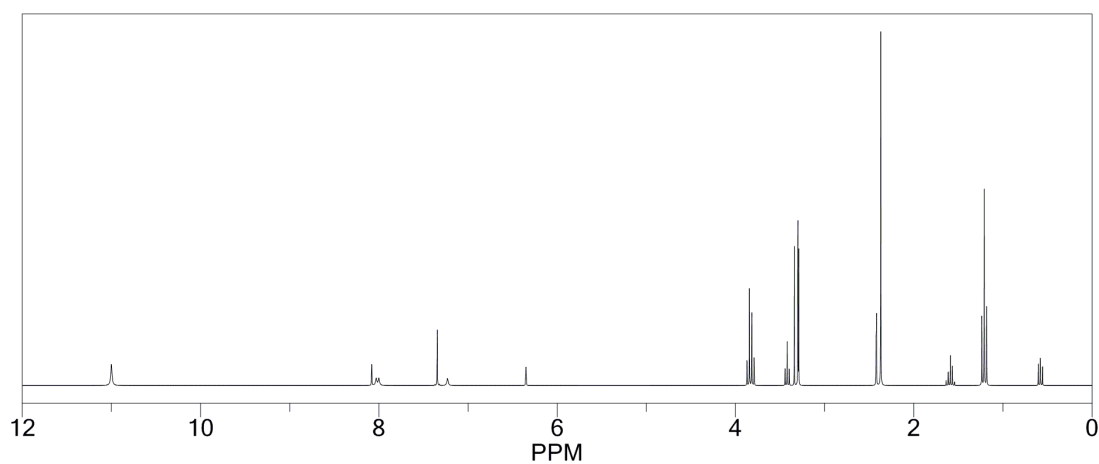


Figure 38: Predicted ^1H NMR spectrum of lanthanide chelate. Spectrum was generated using ChemBioDraw (CambridgeSoft)

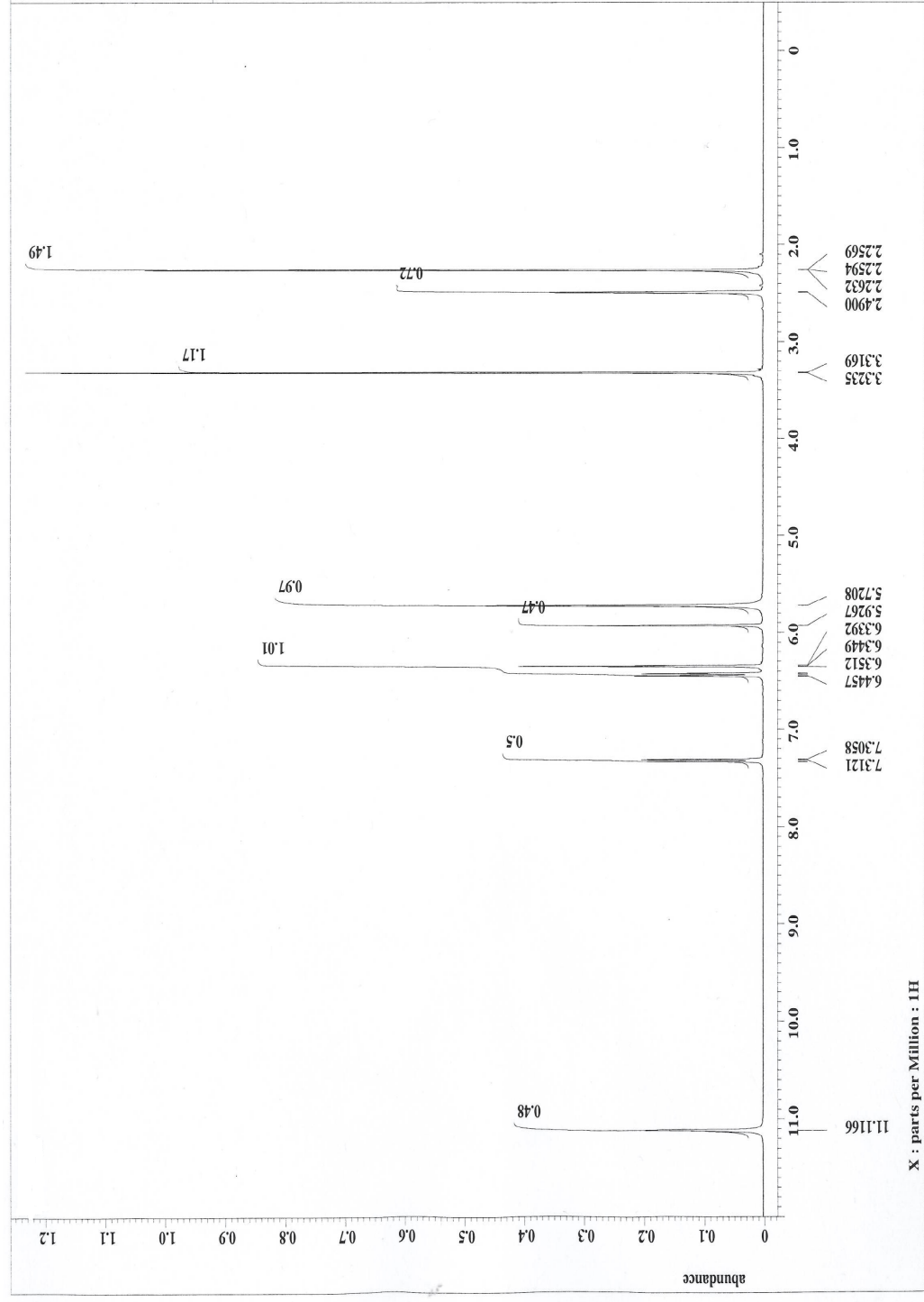


Figure 39: ¹H NMR spectrum of cs124 in DMSO-D6. Most of these peaks can also be seen in Figure 38

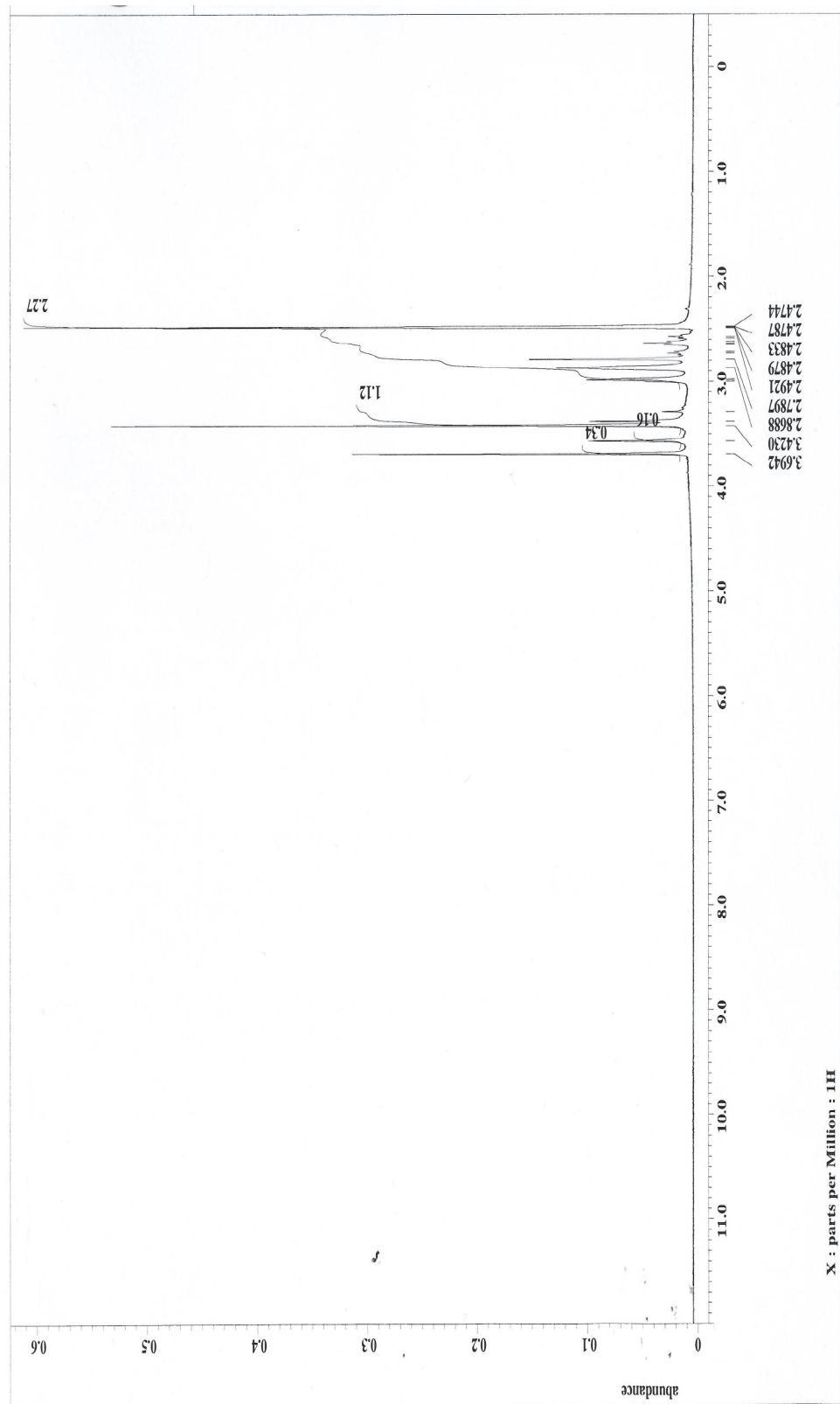


Figure 40: ^1H NMR spectrum of DTPAA in DMSO- D_6 . Some of these peaks can also be seen in Figure 38, but are obscured somewhat by water

Figures 39 and 40 compare well with their theoretical spectra (not shown here), and when compared to Figure 37 suggest that the amide bonds have been formed between Cs124, DTPAA and APS. This conclusion is drawn based on the absence of peaks in the region of δ 8.0 and 7.4 (Figures 39 and 40). The presence of water and the comparatively lower concentration of the chelate solution measured (based on the abundance) make further comparisons in the region of δ 2.0 to 4.0 difficult.

Further confirmation of the structure was obtained through the formation of a luminescent Tb-doped silica NP. This meant that cs 124 was bound to DTPAA and acted as an antenna, and APS was bound to both DTPAA and the inner wall of the silica particle. As the particles were washed extensively after synthesis, any chelated Tb that is not bound to the wall of the NP is washed away and would not contribute to the luminescence seen. To ensure that unbound Tb was being washed away, the fluorescence of wash solutions were checked until they were no longer luminescent. The maximum excitation wavelength of the complex was 316 nm. Emission occurring from the 5D_4 was seen, with peaks at 613 nm, 582 nm, 543 nm and 488 nm, corresponding to emission from the 5D_4 level to 7F_J levels ($J=3, 4, 5, 6$ respectively) (Figure 41).

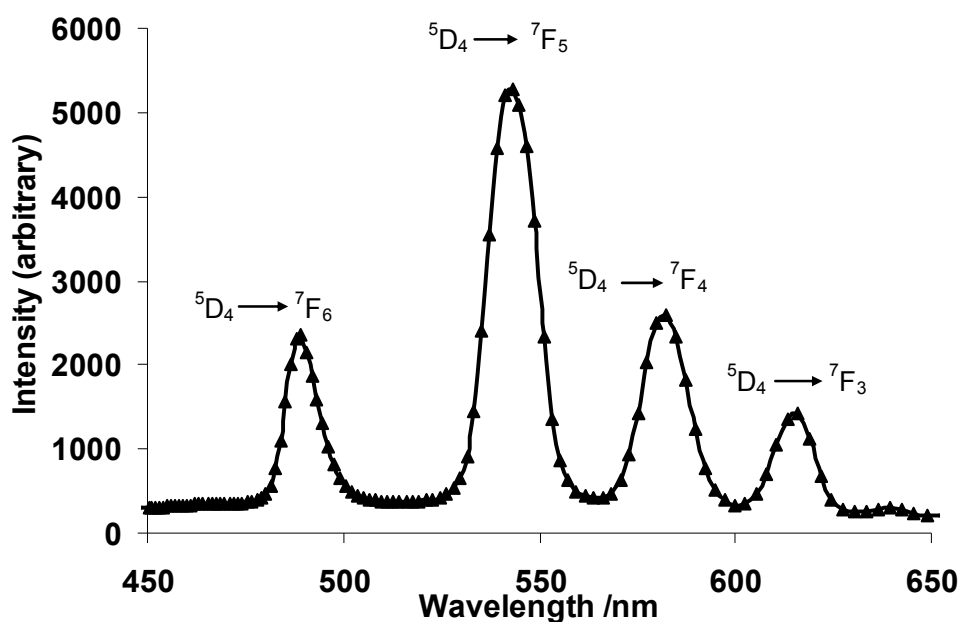


Figure 41: Fluorescence spectrum of terbium-doped silica nanoparticles. The concentration of Tb is 430 μ M.

Figures 34 through 36 and 41 show spectra of the chelated lanthanides and the width of the emission peaks are wider than the line-like emission bands mentioned previously. The dispersion and resolution of the peaks would be captured with a perfect imaging system. In an imperfect instrument however, the spectrum of a line is recorded with a finite width, which is known as the instrumental line profile.³⁴ The width of the measured spectrum is a result of the resolution of the spectrograph; characterised by the linear dispersion (Equation 2-7), the slit size and the 'real' peak width. At small slit widths, the width of the image is larger than the width of the slit as the spectrum is now controlled by dispersion, aberrations and diffraction. The image seen is no longer a slit image but is a diffraction pattern. This measured width can be determined quantitatively as the full width at half of the maximum intensity (FWHM) and is 18 nm for the Sm peak at 640 nm, 15 nm for the Eu peak at 613 nm, and 14 nm for the Tb peak at 543 nm (Figures 34, 35 and 41 respectively). This explanation is best visualised using an illustration (Figure 42).

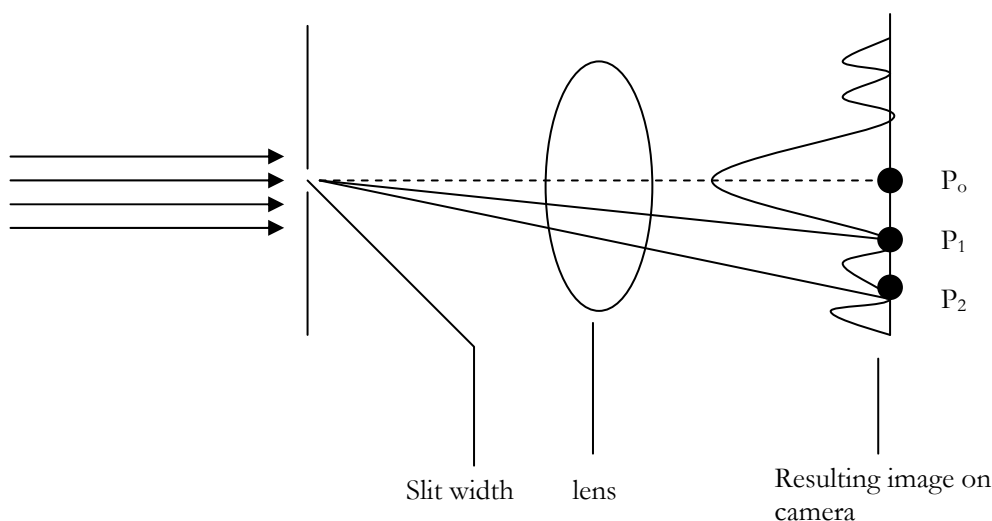


Figure 42: Diagram showing diffraction that occurs at a single slit of width W . Rays reaching P_0 have a central maximum of irradiance. The beams falling on P_1 and P_2 create minima when $W \sin \theta = \lambda$ and $W \sin \theta = 2\lambda$. For an exhaustive description see Spectrochemical Analysis³⁵

The spectrograph used has a manufacturer defined reciprocal linear dispersion of 54 nm mm^{-1} and a reported spectral resolution of 1 nm at 436 nm . These values are further limited by the size of the pixels of the camera used.³⁴ The camera used had pixels of size $7.4 \text{ } \mu\text{m}^2$, which means that an emission line from a monochromatic source, having FWHM of 1 nm theoretically occupies an area of 2.5 pixels ($54^{-1} / 0.0074$) at 405 nm . To determine if this stands true for our system, the spectrograph was calibrated using the lines of the mercury spectrum (calibration shown in Appendix 2, page 195). The sharpest lines in the calibration spectrum had an FWHM of 2 pixels. A plot of wavelength against pixel number showed a 3rd degree polynomial relationship between the number of pixels and wavelength. Using this relationship for Eu, an FWHM of 15 nm occupied 6 pixels, representing a dispersion of 338 nm mm^{-1} . These calculations show that the resolution of the

spectrograph used was poor in this region of the spectrum. This is expected with a prism spectrograph, due to the lower refractive index of glass in the red region relative to the blue. As a result, the resolution decreases as wavelength increases. Other factors such as the presence of an image intensifier would serve to further increase the FWHM of atomic line spectra.

4.3.2 Spectral unmixing of NPs

The concentration of lanthanide within a set volume of nanoparticle solution was measured using inductively coupled plasma (ICP) and defined as the concentration of the NPs. Eu-doped and Sm-doped NPs were mixed (Figure 43) and separated using chemometrics. Since Eu and Sm have distinct non-overlapping peaks, mixtures of the two nanoparticles can be easily separated using the same excitation and emission filter sets. Their presence is easily established qualitatively.

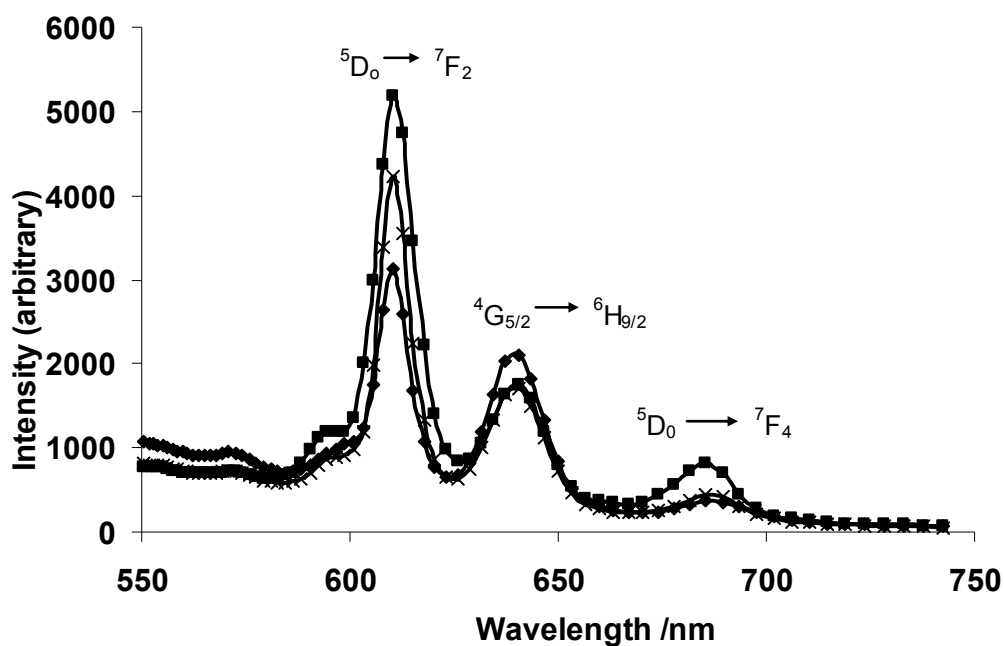


Figure 43: Luminescence spectra of mixtures of europium and samarium doped silica nanoparticles in the ratios Eu: Sm 2:3 ■, 3:7 ×, and 1:4 ♦

[Actual]/mM	[Predicted]/mM	[Actual]/mM	[Predicted]/mM
Eu	Eu	Sm	Sm
0.000	0.002 ± 0.06	0.735	0.736 ± 0.1
0.131	0.132 ± 0.02	0.513	0.513 ± 0.03
0.219	0.220 ± 0.08	0.368	0.368 ± 0.1
0.175	0.174 ± 0.02	0.439	0.438 ± 0.03
0.088	0.089 ± 0.006	0.585	0.586 ± 0.01
0.438	0.439 ± 0.09	0.000	0.001 ± 0.1

Table 4: Relationship between actual concentration and concentration predicted by the model for mixtures of Eu and Sm-doped SiO₂ NPs. The error between the actual and predicted concentrations is < 1 % for both Sm and Eu while the error in each simulation as calculated by Solver is tabulated.

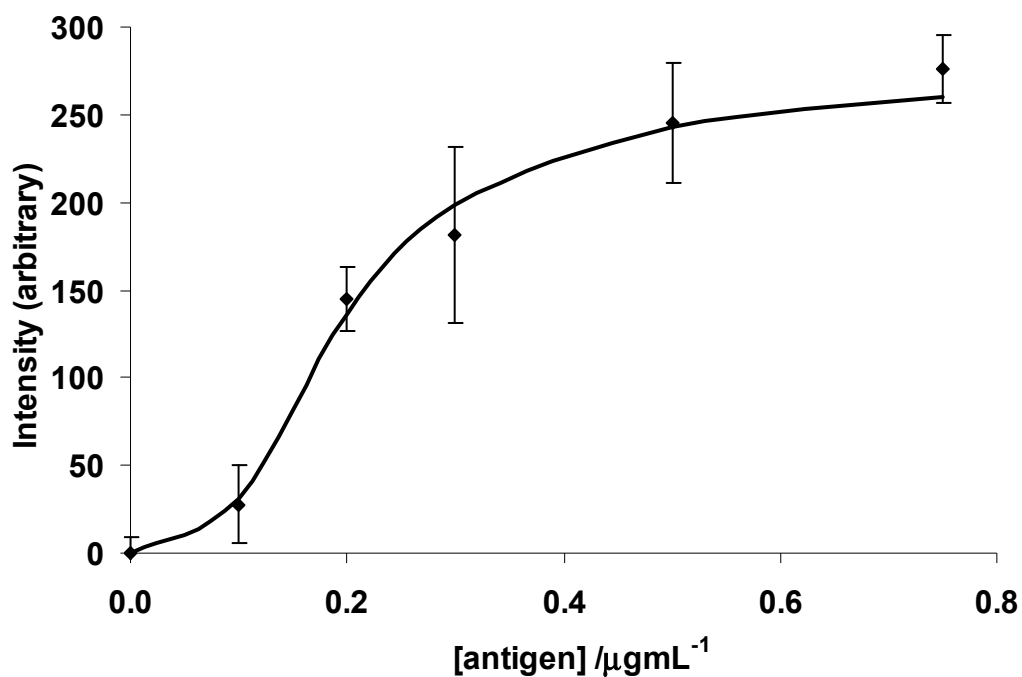
Table 4 shows the values obtained for the predicted concentration of lanthanide NP in the mixture after the spectral unmixing algorithm is applied to a series of mixtures of Eu and Sm-doped nanoparticles. The table illustrates that quantitative separation is also possible, as least squares analysis of the samples using Equations 3-3 and 3-4 gave a good linear relationship between actual and predicted concentrations for both Eu and Sm, with a relative standard deviation (RSD) <1%. When this value is compared to that obtained for prediction of rhodamine B and fluorescein concentrations (8 % and 0.5 % respectively, shown in Chapter 3), it is clearly visible that the use of the lanthanides reduces the error in estimating the concentration of the analyte, making them well suited to quantitative multiplexed immunosorbent assays. In addition to reduced error, the lanthanides offer a further advantage over conventional organic dyes, as they do not require pH control.

4.3.3 Bioconjugation of Nanoparticles

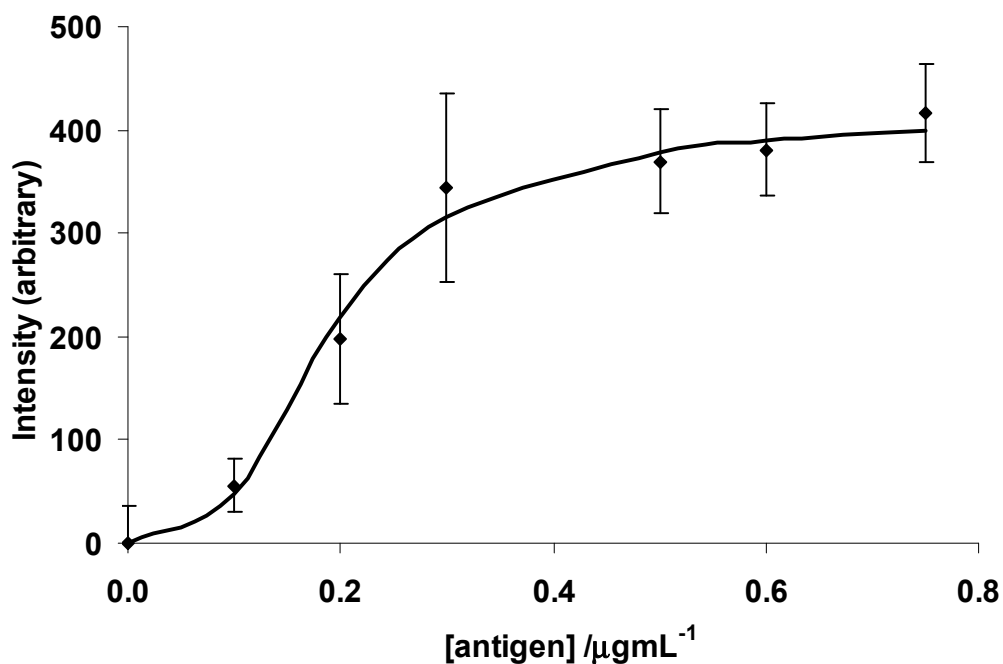
Of the methods attempted (listed in Chapter 2), bioconjugation using glutaraldehyde to conjugate first BSA to the NP and then avidin to BSA was the only one giving a result when an immunoassay with biotinylated secondary antibody was carried out. As a result, this method for conjugating NPs to proteins was adopted for this research. The protocol is outlined in Chapter 2 and was adopted because of the reduction of steric hindrance between the solid glass surface and the large NP.

4.4 Spectral analysis of multiplexed immunoassay

Multiplexed immunoassays employing the lanthanide doped SiO_2 NPs were implemented on species specific IgGs.

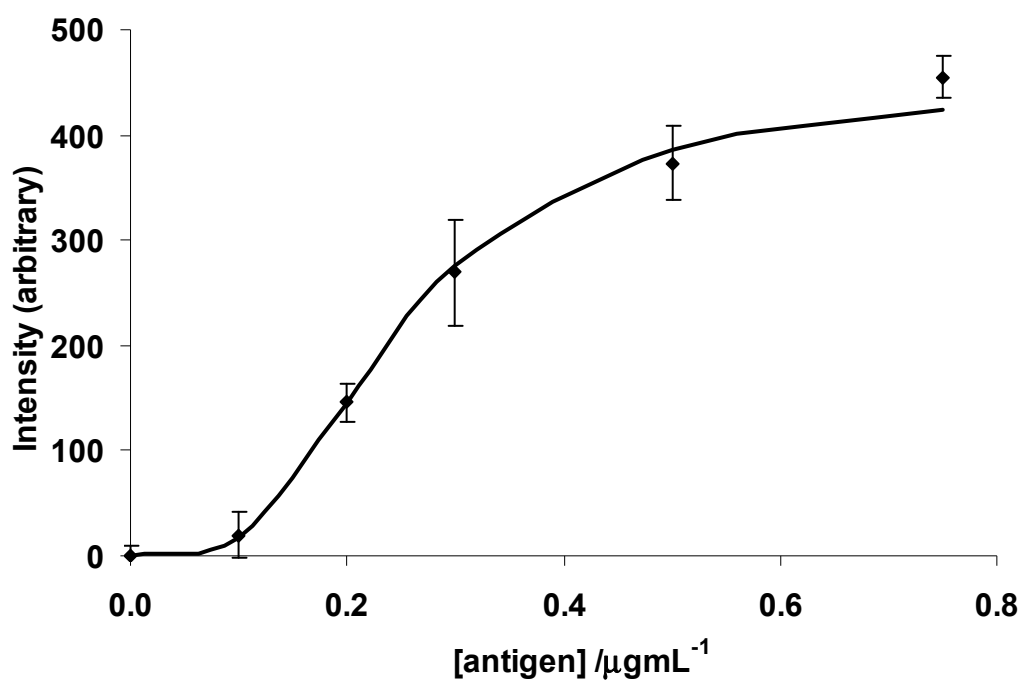


(a)

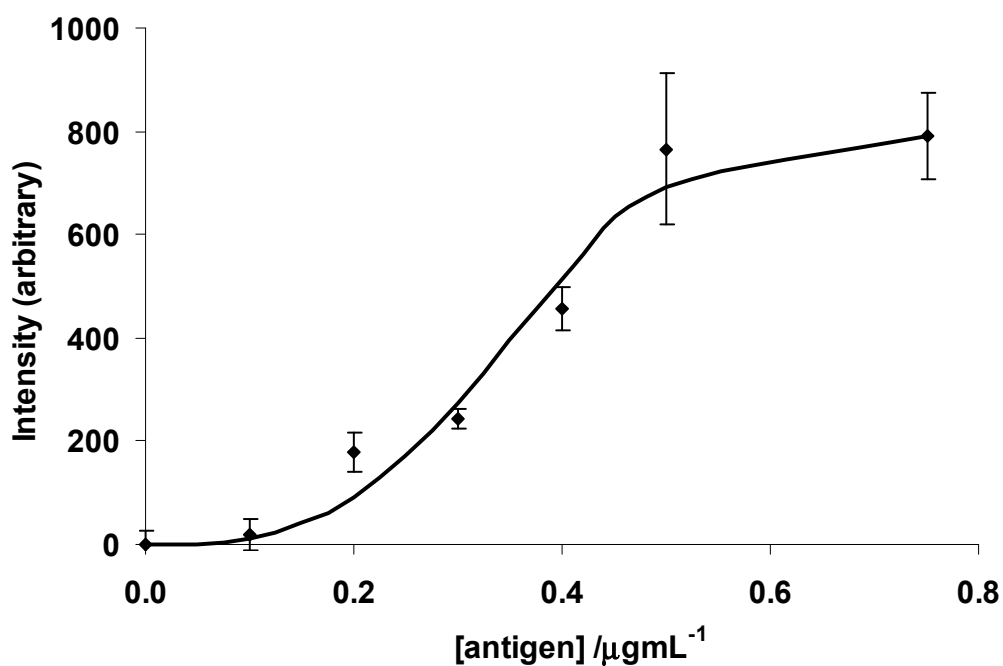


(b)

Figure 44: (a) Concentration response of human IgG on anti-human IgG, assayed with an Eu-doped SiO_2 NP, (b) Concentration response for human IgG assayed with mouse IgG on anti-human and anti-mouse IgGs. The line is a sigmoidal fit to the data, described in Chapter 6, the error bars represent the RSD of 9 measurements.



(a)



(b)

Figure 45: (a) Concentration response of mouse IgG, on anti-mouse IgG, assayed with a Sm-doped SiO_2 NP, (b) Concentration response for mouse IgG assayed with human IgG on anti-human and anti-mouse IgGs. The line is a sigmoidal fit to the data, the error bars represent the RSD of 9 measurements.

The individual IgGs were first assayed on their respective antibodies, followed by assay on a mixture of antibodies to assess the contributions from cross reactivity and non-specific binding. Finally, mixtures of the two IgGs were assayed on a mixture of the two antibodies. The assay was a human and mouse IgG model, and it has been observed that human IgG reacts with anti-mouse IgGs, but mouse IgG has limited reactivity with anti-human IgGs.

Figure 44 shows the dose response curves for human IgG assayed on anti-human IgG (a) and a mixture of anti-human and anti-mouse IgGs (b), while Figure 45 shows dose responses for mouse IgG on anti-mouse IgG (a) and a mixture of anti-mouse and anti-human IgGs (b). The data in Figures 44b and 45b were obtained after a series of mixtures of the two IgGs at different concentrations were assayed. The data shown have the blank intensities subtracted from the intensities of the samples. The intensity at the maximum emission wavelength of Eu and Sm was noted for each well and used to construct the graphs. The graphs show the typical sigmoidal shape of immunoassays, even in the presence of a second analyte, and this indicates that the presence of multiple analytes does not inhibit detection of individual IgGs. The main difference between the individual dose responses and the dose response in the mixture is that the signal from the mixture analysis (Figures 44b and 45b) is higher than obtained for individual analyses. This is a result of the binding of anti-mouse IgG to human IgG, and anti-human IgG to mouse IgG. In separate assays (not shown here) where mouse IgG was assayed on anti-human IgG and human IgG on anti-mouse IgG, it was determined that the binding was largely non-specific, a result of what we believe to be a measure of cross reactivity between

human and mouse IgGs. Although there is some cross reactivity, the assays clearly demonstrate that multiple analytes can be quantified simultaneously. Here, the advantage of the lanthanide doped NPs is realised because of their unique properties: narrow emission bands and the fact that there is no interaction between NPs in a mixture. As all results were obtained without time resolved measurements, these multiplexed assays further demonstrate the ability to produce a luminescence assay without specialised time resolved equipment.

A spectral unmixing algorithm described by Equations 3-3 and 3-4 was applied to the multiplexed assay. Table 5 shows the relationship between the measured and predicted intensities for both Eu and Sm in the multiplexed assay. There is an error less than 5% for both probes. These data therefore establish a method for quantifying analytes simultaneously in a single-welled immunoassay.

[human IgG]	Eu measured	Eu predicted	[mouse IgG]	Sm measured	Sm predicted
/μg mL⁻¹	Intensity	Intensity	/ μg mL⁻¹	Intensity	Intensity
0.10	295	295	0.50	908	908
0.20	436	436	0.75	723	723
0.50	542	542	0.10	240	240
0.00	239	253	1.00	978	978
0.00	265	253	0.00	221	200

Table 5: Comparison of measured and predicted intensities of lanthanide-doped SiO₂ NPs used as probes in a multiplexed immunoassay for human and mouse IgGs

There is a great deal of discussion that can be derived when Table 5 is examined. The first of these is that in spite of the excellent correlation between measured and predicted intensities of the NP probes, there are discrepancies between the results for the intensity of the $0 \mu\text{g mL}^{-1}$ sample of both human and mouse IgGs. The comparatively high values for these blank readings also evoke further discussion. The high blank readings are most likely a result of non-specific binding of the secondary antibody to the well of the assay plate. This is a widely recognized problem for which several solutions have been offered. In these assays, 1 % casein was used to reduce non-specific binding. This worked by providing a coating over the surface of the plate to prevent adsorption by unwanted antibodies, and was selected as a suitable blocking agent following research carried out in the laboratory (unpublished data). Other methods include anti-sera adsorption to the plate before adding the test sera, and the use of detergents such as Tween and Triton X-100. The effect of non-specific binding was accounted for in the model. However, as the values for the blank intensities form the basis of the intercept β_{oj} for the regression line, these are calculated by the model during the fitting procedures. This value is unlikely to be changed during simulations, leading to the difference between measured and calculated intensities of the $0 \mu\text{g mL}^{-1}$ sample. In spite of this, fluorescence readings of unknowns that are comparable; even though not identical, to the intensity of the $0 \mu\text{g mL}^{-1}$ standard are identified as $0 \mu\text{g mL}^{-1}$ during the fitting procedures. A second observation from Table 5 is that the intensity of $0.5 \mu\text{g mL}^{-1}$ mouse IgG has a higher intensity than $0.75 \mu\text{g mL}^{-1}$. The value for $1 \mu\text{g mL}^{-1}$ seems acceptable, making the intensity for $0.75 \mu\text{g mL}^{-1}$ an outlier, having an error of 40%. Low precision was encountered when these probes were used, as evidenced in Figures 44 and 45. This may be a result of aggregation due to the high avidity of

biotin and avidin. Aggregation would result in non-uniform binding throughout the well and is something that needs to be addressed in future work.

From Table 5, the lowest concentration of IgG detected was $0.1 \mu\text{g mL}^{-1}$. This value gives an idea of how effective this method would be for serological detection of infection such as dengue, both during and after infections. Dengue NS-1 has been detected at $15 \mu\text{g mL}^{-1}$ during secondary infection using ELISA.³⁶ The limit of detection for that assay was 4 ng mL^{-1} and NS-1 could not be detected in the sera of patients with a primary infection. In another study, NS-1 was detected by ELISA down to 600 ng mL^{-1} in patients with secondary infection.³⁷ In another report, primary sera were found to contain NS-1 levels between 0.04 and $2 \mu\text{g mL}^{-1}$, while those of secondary sera were between 0.01 and $2 \mu\text{g mL}^{-1}$ as determined by ELISA.³⁸ Protein concentrations post infection were undetectable. These values show that while the concentration of NS-1 in secondary sera would be detected using lanthanide doped silica nanoparticles (provided the affinity of anti-NS-1 antibodies used were the same as that of our anti-IgG antibody), more work has to be done in optimizing the present method for sensitive serological detection of dengue infection. This could be done through a time resolved assay, where the long lifetimes of the lanthanides allow them to be applied to sensitive work with low detection limits.

SiO_2 NPs doped with complexes of europium and samarium have been prepared, characterised and used as substitutes for conventional organic dyes in fluorescent mixtures. Despite reports of lanthanide complexes being used in multicolour detection schemes we are not aware of their application to spectral analysis of luminescent mixtures without time resolved measurements. The current work therefore provides a synthesis of lanthanide-doped SiO_2 NPs using existing methods

and demonstrates how they simplified problems that were encountered with conventional dyes and quantum dots. It is apparent that lanthanide doped SiO₂ NPs can be used for steady state measurements and can be applied in a simplified approach to multiplexing immunoassays. By tuning the relative amounts of lanthanide within the silica matrix, NPs with multiplexing capabilities can be synthesised, and this was demonstrated with the synthesis of the SiO₂ particle doped with both europium and samarium. This NP also exhibits what has been reported as energy transfer from Sm complex to the Eu complex, resulting in an Eu signal that is about 3 times greater than obtained when Eu³⁺ is the only dopant. Further applications would include use in sensitive immunoassays where the limit of detection could be lowered due to increased luminescence of Eu.

4.5 General discussion and conclusions

SiO₂ NPs doped with the lanthanides Eu, Sm and Tb have been synthesised and applied to spectral unmixing for diagnostic applications. They have also been used in novel single-welled multiplexed immunoassays. The ligands used were the commercially obtained BTBCT and a newly synthesised ligand, comprised of the popular ligand DTPA with cs 124 as the antenna, bonded to APS. APS was used to anchor the chelated lanthanide to the wall of the silica. The long term stability of the ligand in terms of leakage over time from the nanoparticles is currently unknown. However, it was observed that unconjugated particles were still brightly luminescent after a year. When conjugated to proteins and subsequently used as reporters in immunoassays, the luminescence was reduced in comparison to Eu-doped particles of the same age. Reduction in lanthanide luminescence is a result of nonradiative return to the ground state through quenching of luminescence. This is caused by the

presence of coordinated X-H molecules such as water ($X=OH$) and amine ($X=NH_2$) ligands. As the chelated lanthanide is encapsulated by silica it is not expected that these molecules could become coordinated to the lanthanide. This reflects some degree of leakage of the chelate from the NP. Very little is as yet known about these NPs, but it has been well established that with a suitable ligand they are useful probes for bioassays. This was evidenced in the results obtained for Sm and Eu doped probes which were chelated by the commercially obtained BTBCT.

Mixtures of the NPs were made and separated spectroscopically, thereby creating a new and simpler approach to unmixing of fluorescent dyes. As was mentioned in the previous chapter, subtle changes in the environment of fluorophores can lead to a change in the emission maximum. This is problematic in a mixture of fluorophores that may have similar emission maxima. Unlike organic fluorophores, the atomic line emission of the lanthanide doped NPs is not affected by changes in the environment, and allows these probes to be distinguished qualitatively, thereby simplifying the approach to unmixing.

Also made was an NP which contains two lanthanides in the same matrix of silica. The two lanthanides were Eu and Sm, and an enhanced luminescence of Eu was evidenced, in addition to emission from Sm. Although a similar type of particle has been previously synthesised, the difference here is that emission of Sm was evidenced, unlike what has been reported. This gives the particle a unique spectrum that could find applications in low limit of detection studies and multiplexed assays.

The NPs were made with amine groups on the surface and their presence confirmed by reaction with fluorescamine. The amine groups were used to

conjugate the NPs to antibodies. As mentioned, a number of methods were used to conjugate the NPs to proteins. A series of homo- and hetero-bifunctional cross linkers were employed, but all utilised the EDC/sulfo-NHS chemistry. It was determined that the large particle bound tightly to the secondary antibody introduced a degree of rigidity to the antibody, limiting attachment to the solid surface. This was determined when results of long flexible linkers were compared with those of short linkers. No signal was obtained when the latter were used. Another possibility could be that the large NP blocked the active site of the antibody and prevented antigen recognition. The method using BSA was adopted and the success of this method is a result of an increased surface area for attachment, as well as increased flexibility between the protein and NP.

Eu and Tb are generally the dopants of choice when SiO₂ NPs doped with lanthanide chelates are synthesised. This is readily understood because of the large energy gap between the lowest excited state and the highest ground state for both of their trivalent ions. Sm however, has a narrow band gap and is easily affected by solvents. In spite of this, a NP containing Sm chelated to BTBCT was successfully synthesised. This has not previously been reported. It was observed that when the particle was optimised such that high concentrations of lanthanide were incorporated, a highly luminescent particle was obtained which can be applied to immunoassays.

Lanthanides have found use in immunoassays, where the popular and sensitive dissociation-enhanced lanthanide fluorescent immunoassay (DELFA) allows multiplexed time resolved measurements of multiple luminescent molecules in a single well.³⁹⁻⁴¹ A lanthanide is conjugated to the secondary antibody and an enhancement solution is then added that allows luminescence of the lanthanide,

which is measured by a time resolved instrument. The existence of this method questions the need of the present work and the improvement over the DELFIA method. The following points highlight the novelty of this work, as well as the utility of the newly developed method. Firstly, the presence of free lanthanide in solution, as occurs with the DELFIA method, can bring about coordination to water or any amine containing molecules that can quench the luminescence of the particle, thereby giving inaccurate results. With the NPs, this is not an issue as the lanthanides are encapsulated by silica. Secondly, all lanthanides do not luminesce on sensitisation by the same ligand. As a result, for DELFIA multiplexed assays there is a need to add different enhancement solutions. When the lanthanides are encapsulated with silica, there is no need for addition of an enhancement solution which shortens the incubation time of the assays.

The assays performed using these NPs are the first of their kind. The NPs have been used in immunoassays previously, but there is no known report of their previous application to single-welled multiplexed assays. The ability to do this is a major advance, particularly for viruses that present themselves in multiple forms. That it can be done quantitatively with cheap probes without instruments such as Luminex, makes it more attractive.

In conclusion, silica nanoparticles doped with lanthanides provide a suitable alternative as probes for multiplexed immunoassays. When compared to the problems encountered with organic dyes and QDs as discussed in Chapter 3, these probes did not present with the same problems: there is no energy transfer occurring between particles in solution, and as the chelated lanthanide is encapsulated by silica, there is no interaction with the solution. This means that pH control is not necessary. Previous work with chelated Eu has shown that the pH

range at which these probes can be used effectively is > 3 .⁴² This allows a broad range that can be used without a change in the probe, unlike the fluorophores. The ability to excite the particles in the UV region means that all can be excited simultaneously, thereby simplifying measurement protocols.

4.6 References

- (1) Murray, K.; Cao, C. Y.; Ali, A.; Hanley, Q. Lanthanide doped silica nanoparticles applied to multiplexed immunoassays. *Analyst* **2010**, *135*, 2132-2138.
- (2) Yuan, J. L.; Wang, G. L. Lanthanide-based luminescence probes and time-resolved luminescence bioassays. *Trac-Trends Anal. Chem.* **2006**, *25*, 490-500.
- (3) Atkinson, P.; Findlay, K. S.; Kielar, F.; Pal, R.; Parker, D.; Poole, R. A.; Puschmann, H.; Richardson, S. L.; Stenson, P. A.; Thompson, A. L.; Yu, J. H. Azaxanthenes and azathioxanthenes are effective sensitizers for europium and terbium luminescence. *Org. Biomol. Chem.* **2006**, *4*, 1707-1722.
- (4) Li, M.; Selvin, P. R. Amine-reactive forms of a luminescent diethylenetriaminepentaacetic acid chelate of terbium and europium: Attachment to DNA and energy transfer measurements. *Bioconjug. Chem.* **1997**, *8*, 127-132.
- (5) Zhang, H.; Xu, Y.; Yang, W.; Li, Q. G. Dual-lanthanide-chelated silica nanoparticles as labels for highly sensitive time-resolved fluorometry. *Chem. Mat.* **2007**, *19*, 5875-5881.
- (6) Lakowicz, J. R. In *Principles of Fluorescence Spectroscopy*; Springer: New York, 2006; .
- (7) Turro, C.; Fu, P. K. L.; Bradley, P. M. Lanthanide ions as luminescent probes of proteins and nucleic acids. *Met. Ions Biol. Syst.* **2003**, *40*, 323-353.
- (8) Courrol, L. C.; de Oliveira Silva, F. R.; Gomes, L.; Vieira Júnior, N. D. Energy transfer study of europium–tetracycline complexes. *J Lumin* **2007**, *122-123*, 288-290.
- (9) Chrysochoos, J.; Beyene, K. Oxidative fluorescence quenching of zinc tetraphenylporphyrin (ZnTPP) by trivalent lanthanide ions in several solvents: Role of lanthanide-induced singlet–triplet crossing. *J Lumin* **1999**, *81*, 209-218.
- (10) Dossing, A. Luminescence from lanthanide(3+) ions in solution. *Eur. J. Inorg. Chem.* **2005**, 1425-1434.
- (11) Werts, M. H. V.; Nerambourg, N.; Pelegry, D.; Le Grand, Y.; Blanchard-Desce, M. Action cross sections of two-photon excited luminescence of some Eu(III) and Tb(III) complexes. *Photochem. Photobiol. Sci.* **2005**, *4*, 531-538.

- (12) An, B. L.; Gong, M. L.; Li, M. X.; Zhang, J. M. Synthesis, structure and luminescence properties of samarium (III) and dysprosium (III) complexes with a new tridentate organic ligand. *J. Mol. Struct.* **2004**, *687*, 1-6.
- (13) Escribano, P.; Julian-Lopez, B.; Planelles-Arago, J.; Cordoncillo, E.; Viana, B.; Sanchez, C. Photonic and nanobiophotonic properties of luminescent lanthanide-doped hybrid organic- inorganic materials. *J. Mater. Chem.* **2008**, *18*, 23-40.
- (14) Chen, J. Y.; Selvin, P. R. Thiol-reactive luminescent chelates of terbium and europium. *Bioconjug. Chem.* **1999**, *10*, 311-315.
- (15) Panigrahi, B. S.; Peter, S.; Viswanathan, K. S. Cofluorescence of Eu³⁺ in complexes of aromatic carboxylic acids. *Spectrosc. Acta Pt. A-Molec. Biomolec. Spectr.* **1997**, *53*, 2579-2585.
- (16) Harma, H.; Soukka, T.; Lovgren, T. Europium nanoparticles and time-resolved fluorescence for ultrasensitive detection of prostate-specific antigen. *Clin. Chem.* **2001**, *47*, 561-568.
- (17) Huhtinen, P.; Kivela, M.; Kuronen, O.; Hagren, V.; Takalo, H.; Tenhu, H.; Lovgren, T.; Harma, H. Synthesis, characterization, and application of Eu(III), Tb(III), Sm(III), and Dy(III) lanthanide chelate nanoparticle labels. *Anal. Chem.* **2005**, *77*, 2643-2648.
- (18) Hakala, H.; Mukkala, V. M.; Sutela, T.; Hovinen, J. Synthesis and properties of nanospheres copolymerised with luminescent europium(III) chelates. *Org. Biomol. Chem.* **2006**, *4*, 1383-1386.
- (19) Hai, X. D.; Tan, M. Q.; Wang, G.; Ye, Z. Q.; Yuan, J. L.; Matsumoto, K. Preparation and a time-resolved fluoroimmunoassay application of new europium fluorescent nanoparticles. *Anal. Sci.* **2004**, *20*, 245-246.
- (20) Tan, M. Q.; Wang, G. L.; Hai, X. D.; Ye, Z. Q.; Yuan, J. L. Development of functionalized fluorescent europium nanoparticles for biolabeling and time-resolved fluorometric applications. *J. Mater. Chem.* **2004**, *14*, 2896-2901.
- (21) Ye, Z. Q.; Tan, M. Q.; Wang, G. L.; Yuan, J. L. Novel fluorescent europium chelate-doped silica nanoparticles: preparation, characterization and time-resolved fluorometric application. *J. Mater. Chem.* **2004**, *14*, 851-856.
- (22) Lu, L. H.; Liu, F. Y.; Sun, G. Y.; Zhang, H. J.; Xi, S. Q.; Wang, H. S. In situ synthesis of monodisperse luminescent terbium complex-silica nanocomposites. *J. Mater. Chem.* **2004**, *14*, 2760-2762.
- (23) Xu, Y.; Li, Q. G. Multiple fluorescent labeling of silica nanoparticles with lanthanide chelates for highly sensitive time-resolved Immunofluorometric assays. *Clin. Chem.* **2007**, *53*, 1503-1510.
- (24) Liu, Z. Y.; Liu, M.; Song, W. L.; Pan, K.; Li, J. H.; Bai, Y. B.; Li, T. J. Multi-fluorescent dye-doped SiO₂. *Mater Lett* **2006**, *60*, 1629-1633.
- (25) Huang, C. Q.; Sun, T.; Tian, W. J.; Zhao, B. P. Multiple energy transfers in rare earth complex-doped SiO₂ spheres. *J. Rare Earths* **2006**, *24*, 134-137.

- (26) Li, M.; Selvin, P. R. Luminescent Polyaminocarboxylate Chelates of Terbium and Europium - the Effect of Chelate Structure. *J. Am. Chem. Soc.* **1995**, *117*, 8132-8138.
- (27) Bruni, A.; Fasulo, M. P.; Tosi, B.; Dallolio, G.; Vannini, G. L. Fluorogenic Detection of Primary Amines in Plant Histochemistry with Fluorescamine - Comparative-Study on Effects of Coagulant and Non-Coagulant Fixatives. *Histochemistry* **1976**, *48*, 269-281.
- (28) Udenfrie, S.; Stein, S.; Bohlen, P.; Dairman, W. Fluorescamine - Reagent for Assay of Amino-Acids, Peptides, Proteins, and Primary Amines in Picomole Range. *Science* **1972**, *178*, 871-&.
- (29) Hetherington, C. Aberration correction for TEM. *Materials Today* **2004**, *7*, 50-55.
- (30) He, J. H.; Wu, W. W.; Lee, S. W.; Chen, L. J.; Chueh, Y. L.; Chou, L. J. Synthesis of blue-light-emitting Si_{1-x}Gex oxide nanowires. *Appl. Phys. Lett.* **2005**, *86*, 263109.
- (31) Egerton, P. F. In *Physical Principles of Electron Microscopy: An Introduction to TEM, SEM and AEM*; Springer Science + Business Media, Inc.: New York, USA, 2005; , pp 202.
- (32) Binnemans, K. In Gschneidner, J., K, Bünzli, J. and Pecharsky, V., Eds.; *Handbook on the Physics and Chemistry of Rare Earths*; Elsevier B.V: The Netherlands, 2005; pp 163-164.
- (33) Cybinska, J.; Legendziewicz, J.; Trush, V.; Reisfeld, R.; Saraidarov, T. The orange emission of single crystals and sol gels based on SM³⁺ chelates. *J. Alloys Compounds* **2008**, *451*, 94-98.
- (34) Lerner, J. M. Imaging spectrometer fundamentals for researchers in the biosciences - A tutorial. *Cytom. Part A* **2006**, *69A*, 712-734.
- (35) Ingle, J. D.; Crouch, S. R. In *Spectrochemical Analysis*; Prentice-Hall Inc.: New Jersey, USA, 1988; , pp 590.
- (36) Young, P. R.; Hilditch, P. A.; Bletchly, C.; Halloran, W. An antigen capture enzyme-linked immunosorbent assay reveals high levels of the dengue virus protein NS1 in the sera of infected patients. *J. Clin. Microbiol.* **2000**, *38*, 1053-1057.
- (37) Libraty, D. H.; Young, P. R.; Pickering, D.; Endy, T. P.; Kalayanarooj, S.; Green, S.; Vaughn, D. W.; Nisalak, A.; Ennis, F. A.; Rothman, A. L. High circulating levels of the dengue virus nonstructural protein NS1 early in dengue illness correlate with the development of dengue hemorrhagic fever. *J. Infect. Dis.* **2002**, *186*, 1165-1168.
- (38) Alcon, S.; Talarmin, A.; Debruyne, M.; Falconar, A.; Deubel, V.; Flamand, M. Enzyme-Linked Immunosorbent Assay Specific to Dengue Virus Type 1 Nonstructural Protein NS1 Reveals Circulation of the Antigen in the Blood during the Acute Phase of Disease in Patients Experiencing Primary or Secondary Infections. *J. Clin. Microbiol.* **2002**, *40*, 376-381.

- (39) Samiotaki, M.; Kwiatkowski, M.; Ylitalo, N.; Landegren, U. Seven-color time-resolved fluorescence hybridization analysis of human papilloma virus types. *Anal. Biochem.* **1997**, *253*, 156-161.
- (40) Kimura, H.; Mukaida, M.; Wang, G. L.; Yuan, J. L.; Matsumoto, K. Dual-label time-resolved fluoroimmunoassay of psychopharmaceuticals and stimulants in serum. *Forensic Sci. Int.* **2000**, *113*, 345-351.
- (41) Chakravarty, A.; Hansen, T. S.; Horder, M.; Kristensen, S. R. A fast and robust dual-label nonradioactive oligonucleotide ligation assay for detection of factor V Leiden. *Thromb. Haemost.* **1997**, *78*, 1234-1236.
-
- (42) Song, B.; Wang, G. L.; Tan, M. Q.; Yuan, J. L. Synthesis and time-resolved fluorimetric application of a europium chelate-based phosphorescence probe specific for singlet oxygen. *New J. Chem.* **2005**, *29*, 1431-1438.

5 A model study: Dengue fever

5.1 Introduction

The single wellled multiplexed immunoassay was tested on a diagnostic model for anti-dengue antibodies. DF is a mosquito borne *Flavivirus* presenting itself in four serotypes. While it is not possible to be reinfected by the same serotype, infection by a second serotype leads to a secondary antibody response to the virus, characterised by differences in the ratio of IgM and IgG antibodies.¹ The ability to detect both of these in a single wellled format is presently not possible as multiplexed detection of dengue is normally a nucleic acid based method.²⁻⁴

Dengue is an interesting viral study because of the multiple serotypes and biomarkers exhibited during infection.⁵⁻⁸ This chapter describes the development of an immunoassay for the simultaneous detection of IgM and IgG in the same well of an assay plate, accomplished with organic fluorophores, CdSe quantum dots and lanthanide-doped silica nanoparticle probes. The methods used for separating differently coloured probes differ from the spectral unmixing methods discussed in Chapters 3 and 4. In this study, probes were separated by splitting detection channels. This change was a result of the inability to acquire dengue antibodies commercially. As a result, standard curves could not be obtained and quantitative statements on IgM and IgG concentration in sera, and their respective limits of detection could not be made. The change in methods of distinguishing differently coloured probes is further reflected in the choice of probes: Tb-doped NPs are now used with Eu-doped particles to effect greater separation of signal. Immunoassays were performed on sera collected over a three week period from mice immunised with recombinant dengue antigens. The immunoassays were similar to the popular

enzyme linked immunosorbent assay (ELISA), the main differences being the use of a fluorescently labelled probe, detection with an epi-fluorescence and confocal microscopes, and multiple analytes being detected in the same well. Balb/C mice were immunised with recombinant dengue antigens leading to the production of mouse anti-dengue IgG and IgM. The mouse anti-dengue IgM and IgG served as a basis for testing the hypothesis that multiple antibodies to a virus may be detected in the same well of an assay plate through the differentiation of fluorescent signals. It must be noted that due to reagent constraints, single well fluorescent assays were compared to multi-well ELISAs and multi-well fluorescence assays for mouse IgM and IgG. As a result, there are no data shown for multi-well fluorescent assays.

5.1.1 Methods and materials

Ten female Balb/C mice between the ages of two and four months (Harlan Olac, Oxon, UK) were bred in accordance with the Home Office Codes of Practice and the NTU Ethical Review Committee. Incomplete Freund's adjuvant (IFA) was obtained from Gibco UK (Gibco BRL., Paisley, Scotland) and PBS was obtained from Sigma Aldrich. Dengue antigens Types 3 and 4 and rabbit anti-dengue polyclonal antibody (Tebu-bio Ltd., Peterborough, UK), monoclonal dengue antibodies against dengue serotypes 3 and 4 (Santa Cruz Biotechnology, Santa Cruz, CA, USA), goat anti-mouse IgM-TRITC (Millipore UK Ltd., Watford, UK) and goat anti-mouse IgG-FITC (Invitrogen, Paisley, UK) were used as outlined in the protocol. Nunc 96-well glass bottomed plates (TKT-195-020V, Fisher scientific UK, Loughborough, Leicester, UK) were used as the solid phase. For assays with QDs, streptavidin-linked quantum dots (QDot® 525 streptavidin conjugate; Lot no. Q10141-MP, QDot® 655 streptavidin; Lot no. Q10121-MP, Invitrogen, Paisley, UK) were incubated with anti-mouse IgM-biotin (Lot no. B9265) and anti-mouse

IgG-biotin (Lot no. B0529), obtained from Sigma. These assays were performed on Porvair 384 well glass bottomed plates (Lot no. F324021, Flowgen Bioscience Ltd., Wilford, Nottingham). Assays for PAM readout used goat anti-mouse IgG-QD 565 nm (Lot no. Q-11031MP, Invitrogen, Paisley, UK) and rat anti-mouse IgM-NC 650 nm (eFluor® 650 NC anti-mouse IgM, Lot no. 95-5790, eBioscience Inc., San Diego, CA) as secondary antibodies. Assays were performed on 15 well chamber slides (μ -slide Angiogenesis, Lot no. IB81501, Ibidi GmbH, München, Germany).

5.1.2 Antigen preparation


Dengue antigen Types 3 and 4 were mixed with IFA and PBS in a concentration such that each mouse would be immunized with 100 μ g of antigen. Solutions were made under sterile conditions immediately before the mice were immunized.

5.1.3 Immunization and collection of sera

The mice were placed in two cages. The first contained control mice and those to be immunized with dengue antigen type 3. The second contained mice to be immunized with dengue antigen type 4. Mice were identified according to the method of immunization, but no record was kept of individual mice; that is, controls 1 and 2 were not differentiated, they were simply referred to as ‘the controls’. The mice immunised once were pierced on the right ear, while those immunised twice were pierced on the left ear. There was nothing done to distinguish between the two mice in each cage with similar ear piercings. For bleeding, mice were placed in an incubator set at 37°C. Antiseptic cream was applied to the tails after which a small slice was made with a scalpel blade. Approximately 200 μ L of blood were collected in eppendorf tubes and left to coagulate at room temperature for 30 minutes. Sera were collected by centrifugation of the blood at

13000 rpm for 5 minutes, and stored in eppendorf tubes at -20°C. Mice were immunized and bled according to Table 6. This table shows that they were 10 mice used for the study. Two were designated control mice and were not immunised throughout the study. Sera from these mice served as the blanks in the immunoassays performed. The remaining 8 mice were divided into two groups: one group was immunised with dengue type 3 antigen, the second with dengue type 4 antigen. There was further distinction made between the mice immunised with each type of antigen: in an attempt to produce a secondary response to the virus, two mice from each antigen group were immunised a second time after the first week. The remaining two mice from each antigen group were immunised only once and were used to determine the trend of a primary response to the antigens. The schedule for bleeding occurred over a period of four weeks, with all mice bled no more than 4 times in accordance with ethical requirements. Control mice were bled every week, as were mice immunised only once. The mice immunised twice were not bled on the first week as the intention was to bleed them a fourth time in the fifth week of the study. This was not followed through as there was no control sera available for comparison, and all 10 mice were sacrificed after the fourth week of the study.

Mouse	Dates of Immunisation and bleeding (I and B)							
	03/16		03/23		04/01		04/08	
	B	I	B	I	B	I	B	I
Control	√		√		√		√	
Control	√		√		√		√	
DEN 3	√	√	√		√		√	
DEN 3	√	√	√		√		√	
DEN 3		√	√	√	√		√	
DEN 3		√	√	√	√		√	
DEN 4	√	√	√		√		√	
DEN 4	√	√	√		√		√	
DEN 4		√	√	√	√		√	
DEN 4		√	√	√	√		√	

Table 6: Schedule for immunisation and bleeding of mice. Yes, √; no,


5.1.4 Dengue immunoassay

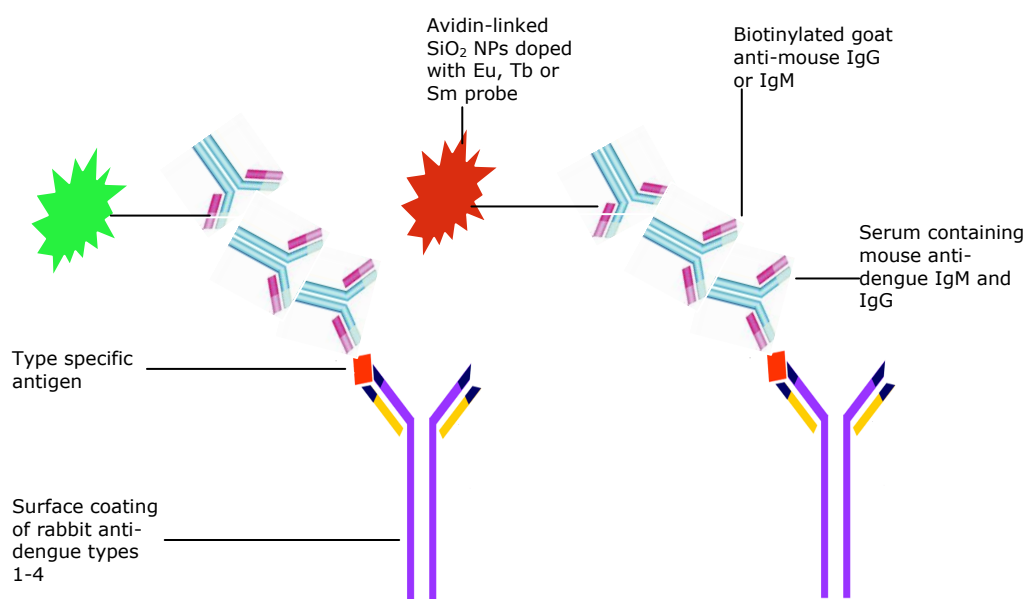


Figure 46: Format for the NP-based immunosorbant assay

Assays with confocal read out

Dengue immunoassays were performed in 96 well glass bottom plates. These plates had low fluorescence background and gave favourable results for the adsorption of antibodies. For confocal imaging using conventional fluorescent dyes, polyclonal rabbit anti-dengue type 1 - 4 antibody dissolved in carbonate/bicarbonate buffer (0.05 M, pH 9.2) at a concentration of $20 \mu\text{g mL}^{-1}$ was incubated overnight on the surface of the plate at 2 - 8°C. The experiment was structured to allow each sample to be analysed in triplicate (sample of raw data shown in Appendix 3, page 196). The plate was washed three times with PBS and tapped dry. Dengue antigen type 3 or 4 was then added for 2 hours at a concentration of $10 \mu\text{g mL}^{-1}$. The plate was washed three times, tapped dry and sera containing mouse anti-dengue IgG and IgM antibodies were added at a dilution of 1:500 in PBS for 2 hours. The plate was washed three times with PBS

and tapped dry, after which goat anti-mouse IgG labelled with FITC and goat anti-mouse IgM labelled with TRITC were added at an antibody concentration of $5 \mu\text{g mL}^{-1}$ and left for 1 hour. A final wash step was carried out and the sample was measured confocally. Confocal imaging was carried out with a confocal scanner head (TCS NT; Leica Microsystems, Germany) installed on an inverted microscope (DMIRIB, Leica Germany). The 488 nm line of an Ar ion laser was used for excitation of FITC and the intensity of fluorescence emitted was detected using a 530/30 nm bandpass filter. The 568 nm line of a Kr ion laser was used for excitation of TRITC and the intensity of fluorescence emitted was detected using a 570 nm long pass filter. The objective used was 40x NA 0.75 air objective. The thin film resulting from the immunoassays was measured in a 512×512 pixel area; which translates to $\sim 159 \mu\text{m}^2$. The scan speed was set at 400 Hz, corresponding to a dwell time of 4.9 μs . The axial response was measured in 0.4 μm intervals along the z-axis for a total of 50 images, using a 74 μm pinhole. The intensity as the sum of each x-y image was plotted against the z position, allowing the maximum intensity to be identified and used. Samples of the confocal images and resulting intensities are shown in Appendix 3 (page 196).

As a result of reagents constraints, the results from single well assays for dengue antibodies were compared to multi-welled assays performed using ELISA methods. The correlation with the ELISA method was used to determine the success of the multiplexed methods.

Assays using nanoparticles and QDs

For NP-based assays, (Figure 46), $100 \mu\text{g mL}^{-1}$ polyclonal rabbit anti-dengue type 1 - 4 antibody dissolved in carbonate/bicarbonate buffer (pH 9.5) was coated on the surface of 384-well glass bottom plates overnight at $2 - 8^\circ\text{C}$. The plate was washed three times with PBS and tapped dry. Dengue antigen type 3 or 4 was

then added for 2 hours at a concentration of $10 \mu\text{g mL}^{-1}$. The plate was washed three times, tapped dry and sera containing mouse anti-dengue IgG and IgM antibodies were added at a dilution of 1:500 in PBS for 2 hours. The plate was washed three times with PBS and tapped dry, after which each well was filled with a mixture of goat anti-mouse IgG biotin attached to an avidin conjugated Eu-doped NP and goat anti-mouse IgM biotin attached to an avidin conjugated Tb-doped NP. This mixture was left shaking overnight, after which the plate was washed with PBS and tapped dry in preparation for epi-fluorescence microscope measurement by a UV filter cube consisting of a 330 – 385 nm band pass excitation filter, 400 nm dichroic mirror and 420 nm long pass emission filter (U-MWU2; Olympus UK Ltd, Southall, UK). The biotinylated antibodies were mixed with the avidin conjugated NPs in PBS (pH 7.4) for more than 8 hours before their use. A 50-fold dilution of the antibody was dissolved in the required amount of avidin conjugated NP solution and left to shake. The mixture was then centrifuged at 8000 rpm for 10 minutes, after which it was washed twice with PBS. The pellet was redissolved in PBS and mixed with the second secondary antibody for use in multiplexed immunoassays.

Quantum dot-based assays were carried out in similar fashion to the NP-based assays. Streptavidin-linked quantum dots 655 nm and 525 nm were incubated with anti-mouse IgM-biotin and anti-mouse IgG-biotin respectively. Since these probes cannot be centrifuged, an excess of the QD was added to the antibodies to ensure that unlabelled anti-mouse IgG/M did not bind to mouse anti-dengue IgG/M. Excess streptavidin-QD label was established by observing the fluorescence of the tryptophan groups on streptavidin. When biotin is bound to streptavidin, the tryptophan fluorescence, observed at 333 nm, is quenched by 30 to 40 %. ⁹ A 10

nM solution of QD-streptavidin was prepared and the tryptophan fluorescence measured at 333 nm with 300 nm excitation with a fluorescence spectrophotometer (Carey Eclipse Fluorescence Spectrophotometer, Varian). Anti-mouse IgG-biotin was added in 2 μ L increments until the tryptophan fluorescence peak decreased by 40 %. The volume and concentration of biotinylated antibody added was used to determine optimal concentrations of antibody and streptavidin-linked QD. These optimal concentrations were 80 nM 655 nm QD incubated with a 1 in 10 000 dilution of anti-mouse IgM-biotin and 100 nM 525 nm QD incubated with a 1 in 100 000 dilution of anti-mouse IgG-biotin. For the assays utilising the biotin-avidin/streptavidin interaction, there is the possibility of exchange between the two labels as a result of their dissociation equilibrium. This equilibrium has been investigated previously¹⁰ using avidin, biotin and radioactively labelled biotin. The authors began with the statement that thermodynamically speaking, there must be a dissociation equilibrium between avidin and biotin, in spite of the avidity of the association. They determined that the formation and dissociation of the complex occurs simultaneously. The ramifications of this formation and dissociation with respect to the success of the multiplexed assays with NPs will be discussed.

Assays using the programmable array microscope

The solid phase for these assays was 15 well μ -slide Angiogenesis uncoated chamber for cell microscopy. The same assay protocol used for nanoparticles was carried out, but the secondary antibodies were goat anti-mouse IgG-QD 565 nm in a 1:10 dilution, and rat anti-mouse IgM-QD 650 nm (1:20 dilution). Each sample was analysed only once due to the size of the assay plate and time constraints.

Imaging spectroscopic measurements were carried out using a PAM installed on an inverted fluorescence microscope (IX 71 Olympus Germany Ltd., Hamburg, Germany). The 488 line of an argon ion laser (~ 200 mW, Coherent Innova 90, Spectra Physics 2000) was used for excitation and emitted light collected by D525/80 nm band pass filter and a 655/40 nm band pass filter (Chroma Technology GmbH, Fuerstenfeldbruck, Germany). The objective used was a water 40x NA 1.15. The camera (Ixon DV 897_BV) was cooled to -100 °C (Julabo Hc F30, Ultratemp 200). EM gain was set at 200 and the exposure time was 250 ms. Data for the two different dyes were not collected simultaneously; the instrument was set to perform a z-slice through the plate in two different channels. This allowed the signal of the 565 nm QD to be read first, followed by the signal from the 650 nm QD. Data were collected as TIFF files and converted to numerical data using Image J.

Conventional ELISAs

ELISAs were performed on the mouse serum where mouse anti-dengue IgG and IgM were detected in separate wells of the assay plate. Standard ELISA protocol was followed. The enzyme used was horse radish peroxidase and the plate was read at 415 nm on a TECAN SpectraFluor plate reader (MTX Lab Systems Inc. Virginia, USA).

5.2 Results

In this section, the results of assays done in ELISA and FLISA formats are presented. The data shown are intensity averages from sera of each group of mice obtained over the study. A comparison of the three different microscopic

methods of detection are presented, along with the advantages and disadvantages of the various probes used. The data demonstrates that the methods all go beyond what has been done before for detection of dengue, and demonstrate for the first time the ability to detect IgM and IgG in a single wellled assay. The results also demonstrate a clear comparison of three state of the art microscope systems.

5.2.1 Detection of IgM and IgG in a single assay well

5.2.2 Elisa Results

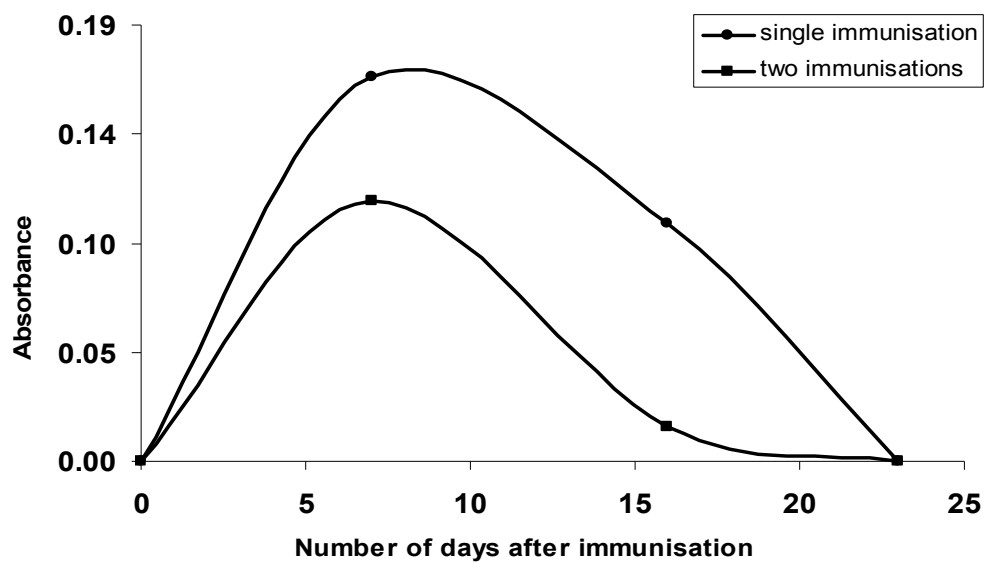


Figure 47: ELISA response of mouse anti-dengue IgM in mice immunised with dengue antigen type 3. Each data point represents the average from two serum samples each assayed twice. The RSDs are given in Table 7

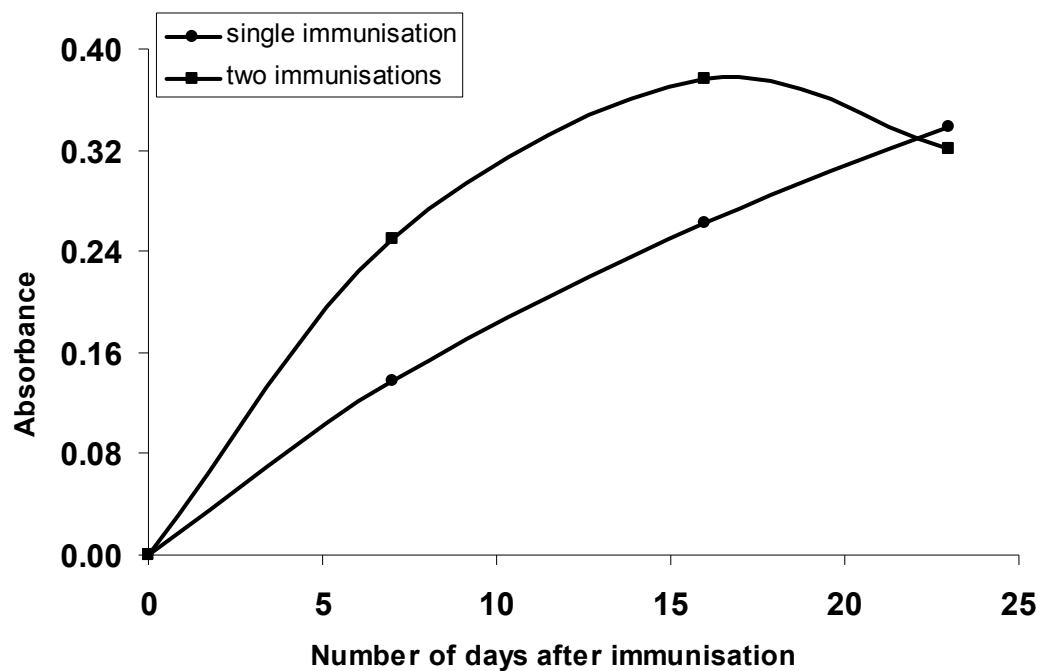


Figure 48: ELISA response of mouse anti-dengue IgG in mice immunised with dengue antigen type 3. Each data point represents the average from two serum samples each assayed twice. The RSDs are given in Table 7

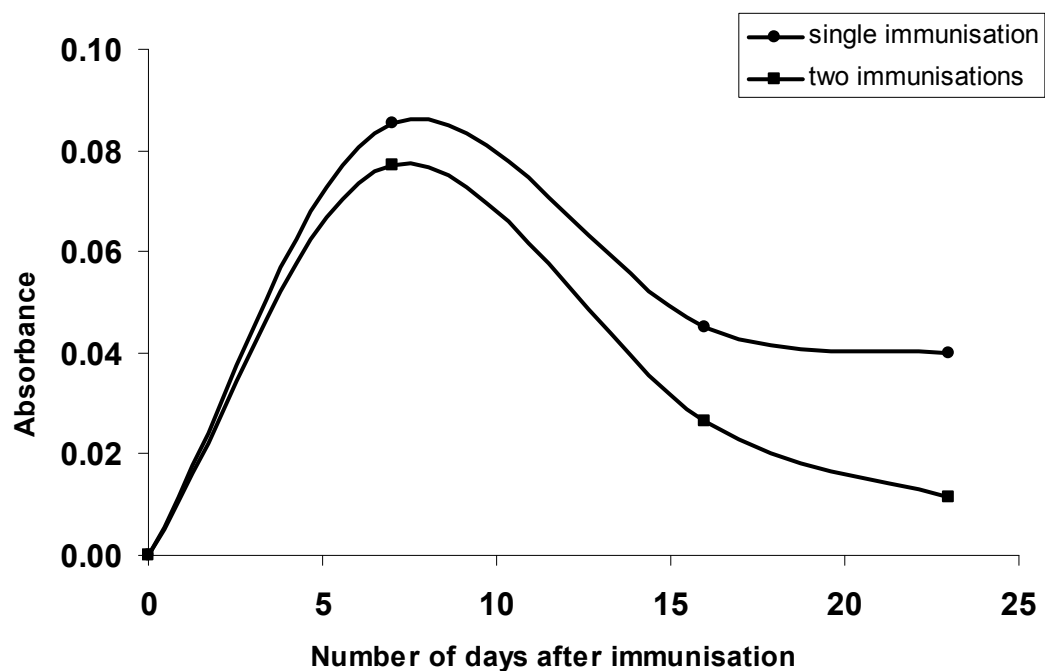


Figure 49: ELISA response of mouse anti-dengue IgM in mice immunised with dengue antigen type 4. Each data point represents the average from two serum samples each assayed twice. The RSDs are given in Table 7

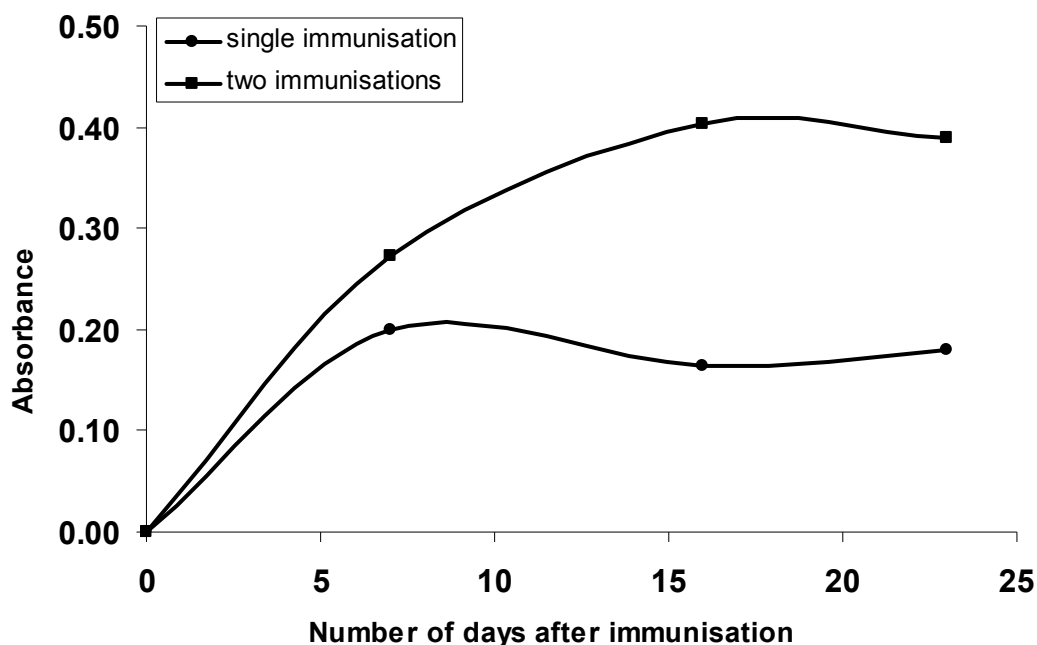


Figure 50: ELISA response of mouse anti-dengue IgG in mice immunised with dengue antigen type 4. Each data point represents the average from two serum samples each assayed twice. The RSDs are given in Table 7

Figures 47 through 50 show the results for ELISA performed on the mouse serum. The data represent an average of an assay carried out in duplicate. The graphs show the trend expected for production of anti-dengue IgM and IgG antibodies. IgM has a sharp rise and then falls sharply back to the level present before immunisation (Figures 47 and 49). IgG also has a sharp increase, but this persists without noticeable reduction in antibody concentration (Figures 48 and 50). There is no real evidence of a secondary response to the virus, with the graphs of primary and secondary antibodies having the same general trend. A secondary response would be evidenced with the IgG profile rising quickly and then returning to pre-immunisation levels, while the response of the IgM would follow the general trend for a primary IgG response. These assays were all performed in different wells of the multi-well assay plate, and were all done as the standard to which single well

assays could be compared. The relative standard errors are larger than the scale of the graphs and are not shown on the relevant graphs. These are shown in Table 7. There is a large spread of values, and IgM measurement shows generally a higher error than IgG. The values however, are all within acceptable for ELISA measurements.¹¹

% RSD								
	Primary type 3		Primary type 4		Secondary type 3		Secondary type 4	
Day	IgG	IgM	IgG	IgM	IgG	IgM	IgG	IgM
0	4	2	10	4	4	10	8	8
7	22	10	4	15	9	29	10	17
16	12	31	5	5	1	21	9	21
23	16	39	9	12	23	17	5	12

Table 7: RSD for ELISA experiments for 4 replicates. RSDs vary but are generally within acceptable values

5.2.3 Organic Dyes Measured Confocally

Assays were performed using secondary antibodies labelled with the organic dyes FITC and TRITC. The results are shown below. As the profiles for both types 3 and 4 anti-dengue antibodies are similar, only profiles from one serotype will be shown.

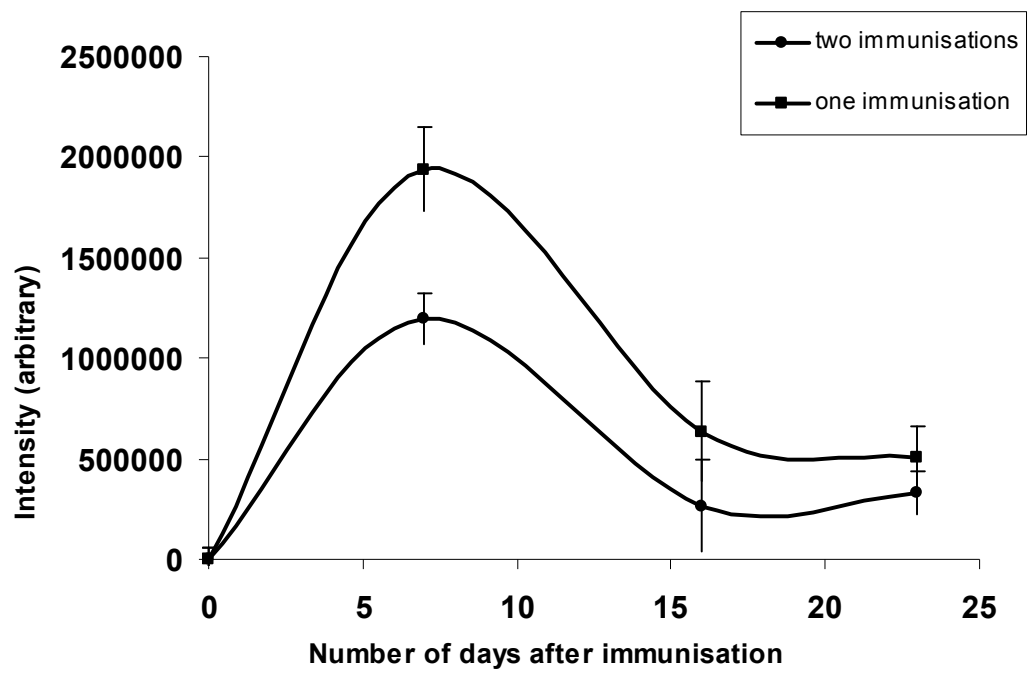


Figure 51: Confocally measured response of mouse anti-dengue IgM in mice immunised with dengue antigen type 4. Each data point represents the average from two serum samples each assayed three times (6 measurements). The error bar represents the standard deviation of the replicates.

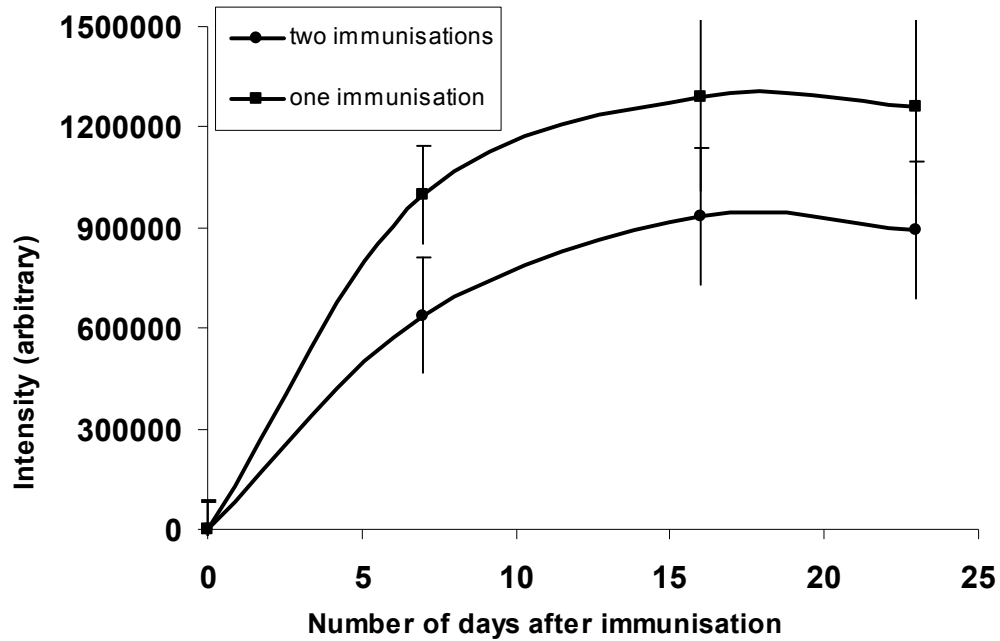


Figure 52: Confocally measured response of mouse anti-dengue IgG in mice immunised with dengue antigen type 4. Each data point represents the average from two serum samples each assayed three times (6 measurements). The error bars represent the standard deviation of the replicates

Figures 51 and 52 show the results of the FLISAs for mouse anti-dengue IgM and IgG. The fluorophores used were FITC and TRITC for IgG and IgM detection respectively. These data were obtained with a confocal microscope and IgG and IgM were assayed simultaneously in the same well of an assay plate. There was no evidence of cross reactivity between IgM and IgG antibodies, thereby simplifying the system and making it possible to easily detect whether a patient has a primary or secondary dengue infection. Additionally, there is no appearance of cross talk between the two dyes in the confocal. What is clearly demonstrated are the expected trends for both anti-dengue IgM and IgG production after infection by dengue. The mice are not infected by dengue but are simply showing an antibody response to

immunisation by the antigen, and this assay if repeated in human serum would be able to detect whether there is a primary or secondary response to the virus. The ratio of IgM to IgG would make this possible. When Figures 53 and 54 are compared to what was obtained for multi-well ELISA in Figures 47 through 50, some differences are noticed. The first of these is the increased response of the assay. The fluorophores are easily detected with the confocal microscope and their signals can be amplified through changing parameters such as increasing the power of the laser and increasing the gain of the microscope. These changes would allow the detection of low concentration of analytes, thereby creating an assay that can be used in the early stages of the immune response. With the ELISA method used, the method of visualisation did not allow for amplifying the enzyme signal, and as such low concentrations of antibodies produced could go undetected. While this was not a problem for this assay, it would be relevant in a clinical diagnostic setting. The ability to detect dengue in the early stages of the disease is of critical importance and as such the new confocal based fluorescent method would make this possible.

Another difference noted is the higher signal to background ratio obtained using the fluorescent method. Figures 47 through 52 are corrected by subtraction of the blanks intensity from the intensity of the samples; sera from mice that were not immunised. Figures 53 and 54 are constructed without subtraction of the blank intensity from the final intensity, and demonstrate that for the ELISA method, the blanks' signal is high relative to the samples. With the confocal method, the signals from the blanks are low with respect to the signals from the samples. Figure 54 illustrates what could be interpreted as one of the reasons why ELISAs return false positives: results indicate that the response for control mice is higher at day 16 than the response for mice immunised. ELISAs were found to be dependant on factors

such as the amount of time between addition of stop reagent and imaging, and the positioning of the well. It was observed that wells towards the edges of the 96 well plates gave higher absorbance values than those further towards the centre. This may simply be related to the fact that these wells are the first to be filled with solution, but for a sensitive assay, particularly in the early stages of infection this could lead to false negatives. This is not an issue when the new fluorescent method was carried out, as demonstrated in Figure 53. The background signal is due to non-specific binding; an issue that plagues immunosorbent assays, but can be minimised through the use of a suitable blocking reagent.

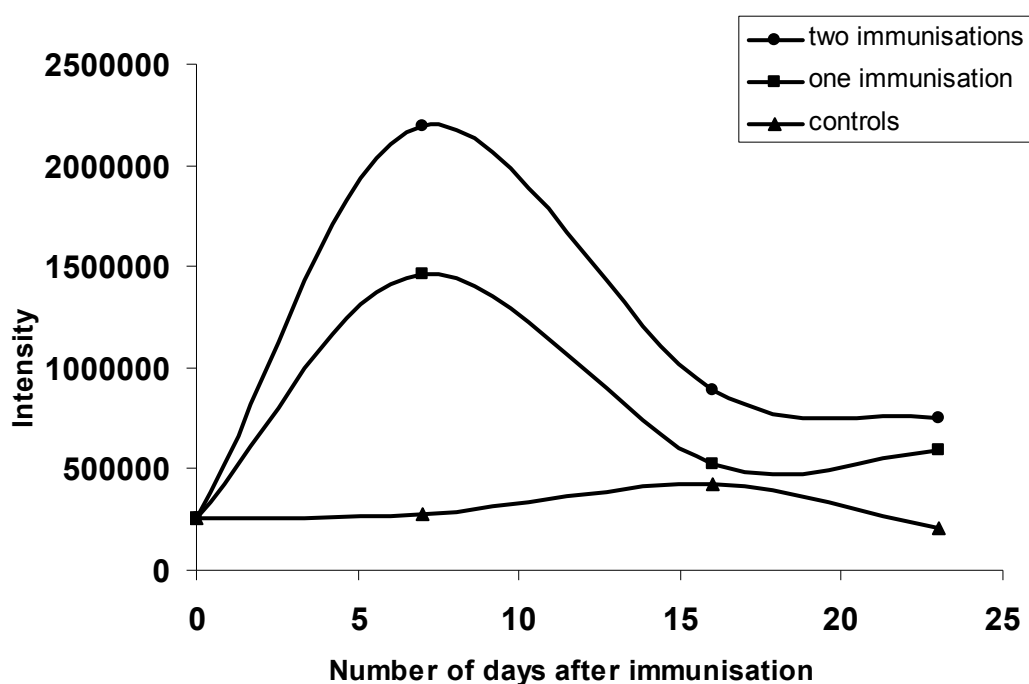


Figure 53: Graph demonstrating the high signal to background ratio of the confocal system

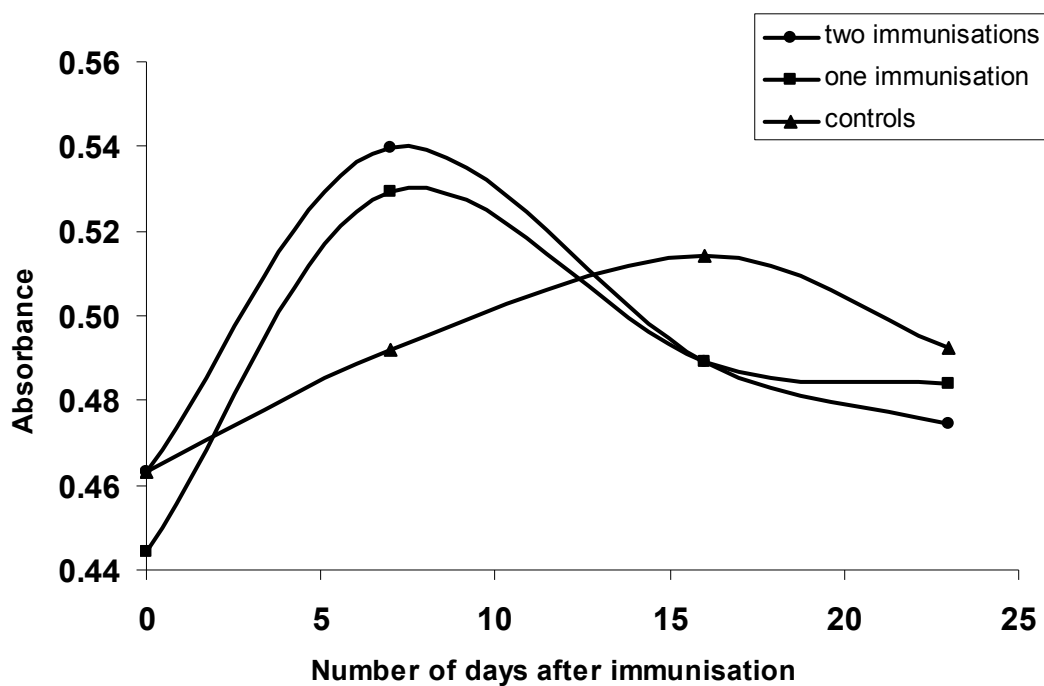


Figure 54: Graph demonstrating the low signal to background ratio using the ELISA method

The results obtained with conventional fluorophores show an improvement over ELISAs. Attempts will now be made to see if QDs and nanoparticles offer an improvement over conventional fluorophores.

5.2.4 Quantum Dots

The use of QDs is favoured over organic fluorophores.¹² The ability to excite QDs simultaneously makes them more attractive for use in multiplexed immunoassays. Assays for mouse anti-dengue IgM and IgG were performed using QD-labelled secondary antibodies. Anti-mouse IgM was labelled with a streptavidin linked 655 nm QD, and anti-mouse IgG was labelled with a 525 nm QD. The results of these assays are shown in Figures 55 and 56.

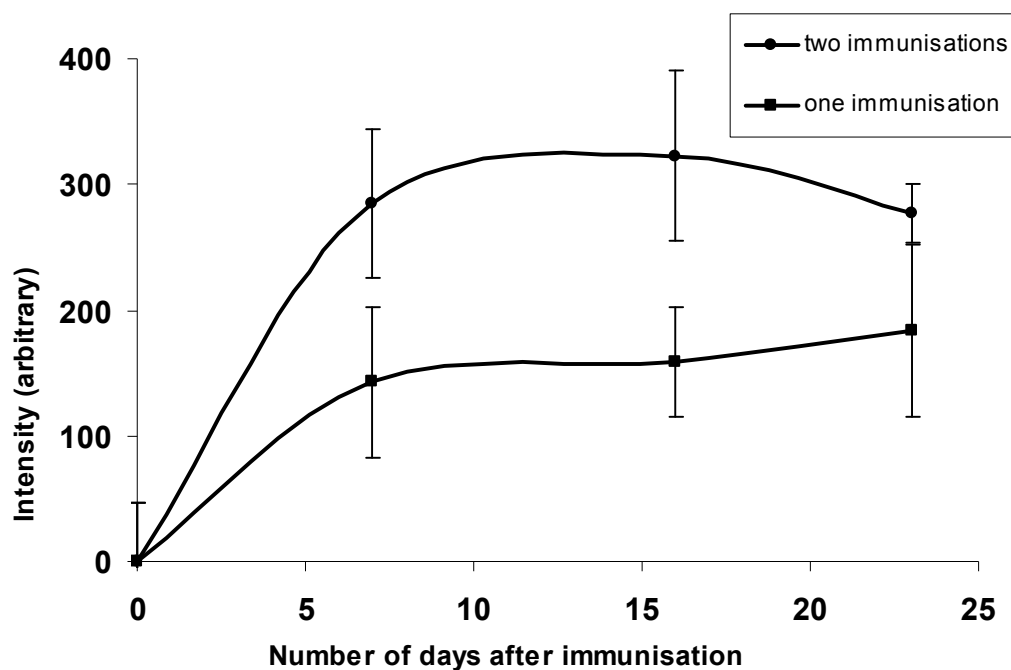


Figure 55: Anti-dengue IgG response in mice immunised with dengue antigen type 3. Each data point represents the average from two serum samples each assayed three times. Precision is poor, error bars are the RSD of 6 measurements

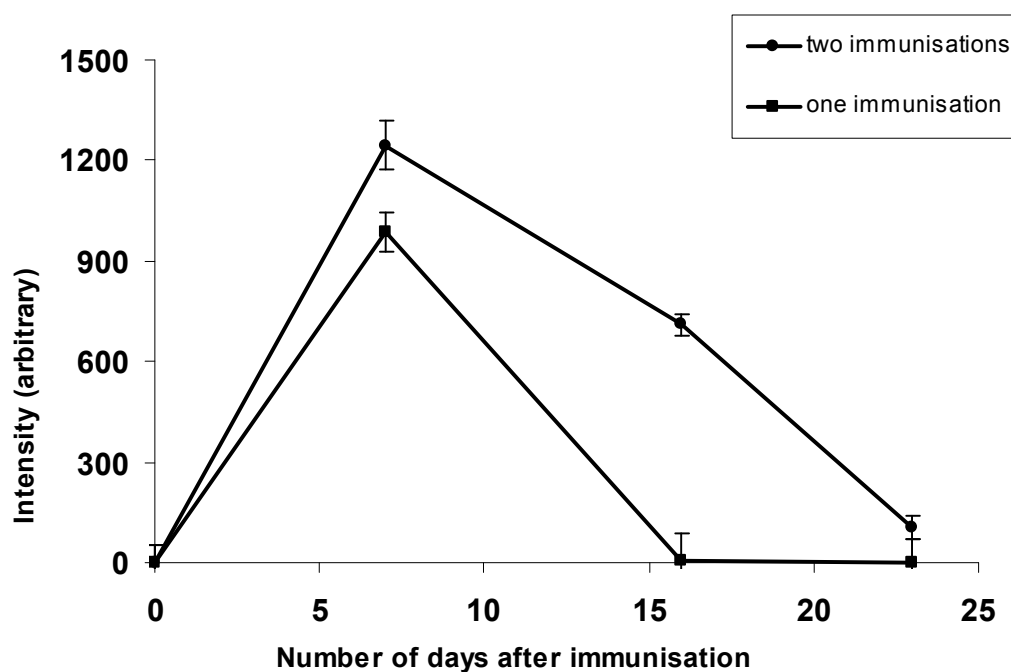


Figure 56: Anti-dengue IgM response in mice immunised with dengue antigen type 3. Each data point represents the average from two serum samples each assayed three times. Error bars are the RSD of 6 measurements

Figures 55 and 56 show the results of a QD-based single well immunoassay for anti-dengue IgM and IgG. An epi-fluorescence microscope using a band pass UV excitation filter and long pass emission filter were used for detection of the assay signal. The results for the two different antibodies are shown in two different graphs, due to the higher intensity of the IgM signal with respect to the IgG signal. Once again, the graphs show the expected trend for both anti-dengue IgM and IgG. There was low precision between the replicates, with RSD ranging between 24 and 68 % for both IgM and IgG. The binding was through the biotin/streptavidin interaction and as seen before with the assays using lanthanide doped silica NPs, the high avidity of streptavidin/avidin and biotin can lead to aggregation. This leads to variable binding within the wells and poor precision. The aggregation between these two entities had been previously documented.¹³

While this assay was simplified through the use of a single excitation and emission filter, there is a readily apparent disadvantage, which is the low signal of IgG relative to IgM. The 655 nm QD used to label anti-dengue IgM has a molar absorptivity of $9\,100\,000\text{ cm}^{-1}\text{M}^{-1}$, while the 525 nm QD has a molar absorptivity of $710\,000\text{ cm}^{-1}\text{M}^{-1}$ at 350 nm.¹⁴ These QDs were both excited at the same wavelength, and the 655 nm QD has a more intense signal than the 525 nm QD. This highlights the need for specially selected QDs with similar molar absorptivities when single well QD-based assays are performed and other methods of detecting QDs need to be explored. One such method employs the use of the programmable array microscope (PAM). With the PAM system, a series of multiple filters were used to excite the QDs sequentially in a multi-channel z-slice setting. In that mode the instrument detects the amount of fluorescence on the surface of the assay plate by imaging through the z axis.

5.2.5 Multiplexed Quantum Dot-based Immunoassays with PAM Readout

A PAM was applied to the single well multiplexed detection of anti-dengue IgM and IgG. The programme was set to take a series of images through the z-plane of the assay plate. The images were converted to intensity values using Image J. The QDs were anti-mouse IgM-QD 650 nm and anti-mouse IgG-QD 565 nm. The results of an assay performed for anti-dengue IgM and IgG is shown in Figure 57. The data indicate a ratio of approximately 1 for IgM/IgG, which is similar to the ratio obtained for multi-well ELISAs. This indicates that there is no energy transfer between the two QDs on the surface. There is also no evidence of the problem seen with the epi-fluorescence microscope, where the shorter wavelength QD had a lower intensity than the longer wavelength QD. This problem was solved through the use of band pass excitation and emission filters, which allowed the QDs to be optimally excited, while the use of well spaced band pass emission filters prevented any cross talk between the two labels. The decision to use emission filters of 525/50 nm and 655/40 nm was made after cross talk was evidenced with another set of filters, 585/20 nm and 655/40 nm. When the latter filters were used, the signal from the red QD spilled into the green channel and the intensities obtained for green QD (IgG) followed the same profile as the red QD (IgM) (data were not recorded). This indicated the importance of selecting QDs that are well spaced when using band pass filters. It also illustrated the benefits of hyperspectral imaging with subsequent unmixing. That way more colours can be used, allowing for the detection of more analytes.

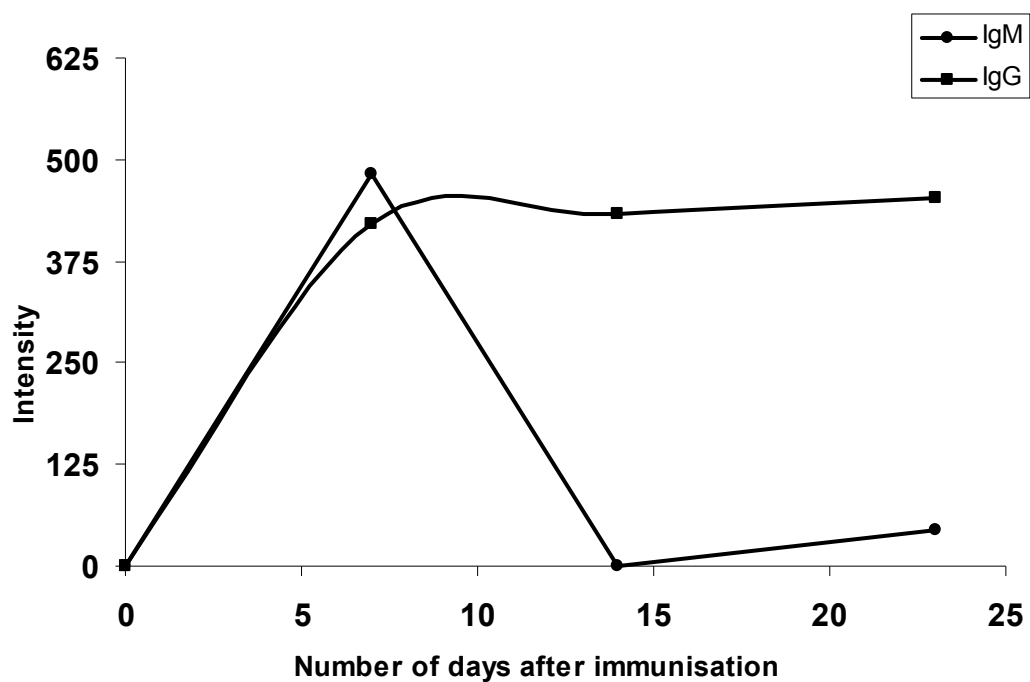


Figure 57: Response of mouse anti-dengue IgM and IgG in mice immunised twice with dengue antigen type 4. Data were collected with a PAM, and no replicate measurements were performed.

5.2.6 Lanthanide-doped Silica Nanoparticles

The lanthanide doped silica nanoparticles which were synthesised for use in multiplexed immunoassays were applied to detection of anti-dengue antibodies in mouse sera. Nanoparticles doped with Tb and Eu were conjugated to avidin, incubated with biotinylated secondary antibodies and added to the assay plate. The results are shown below in Figures 58 and 59.

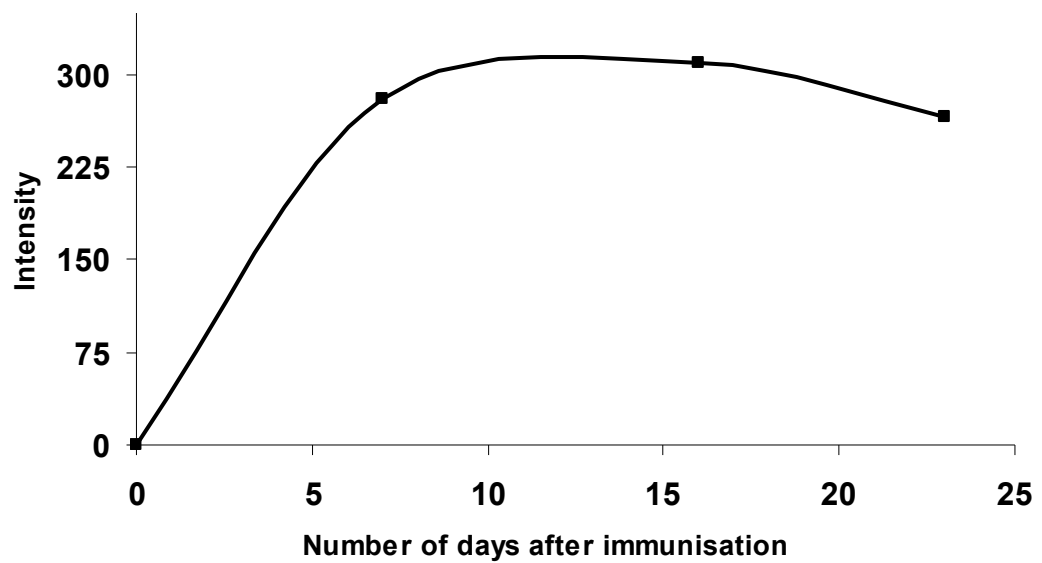


Figure 58: Response of mouse anti-dengue IgG in mice immunised with dengue antigen type 4. The probe was an Eu-doped silica NP. No replicates were performed.

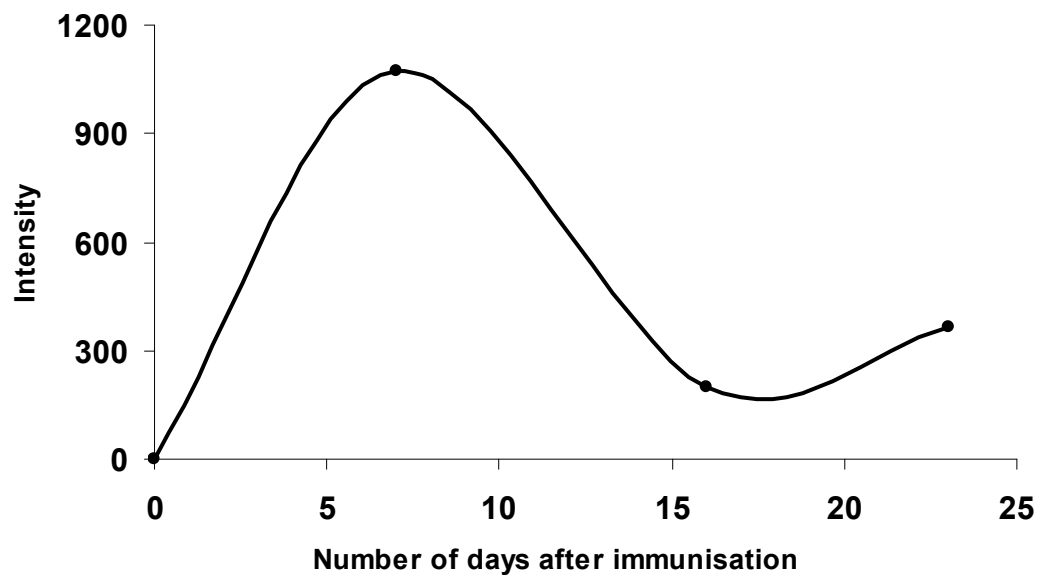


Figure 59: Response of mouse anti-dengue IgM in mice immunised with dengue antigen type 4. The probe was a Tb-doped silica NP. No replicates were performed.

Figures 58 and 59 are results obtained for multiplexed detection of mouse anti-dengue IgG and IgM respectively. The data shown were obtained from multiplexed assays, but were not collected from a single well and cannot be compared. Due to variable binding within the assay well, the nanoparticles proved to be difficult to work with in serum.

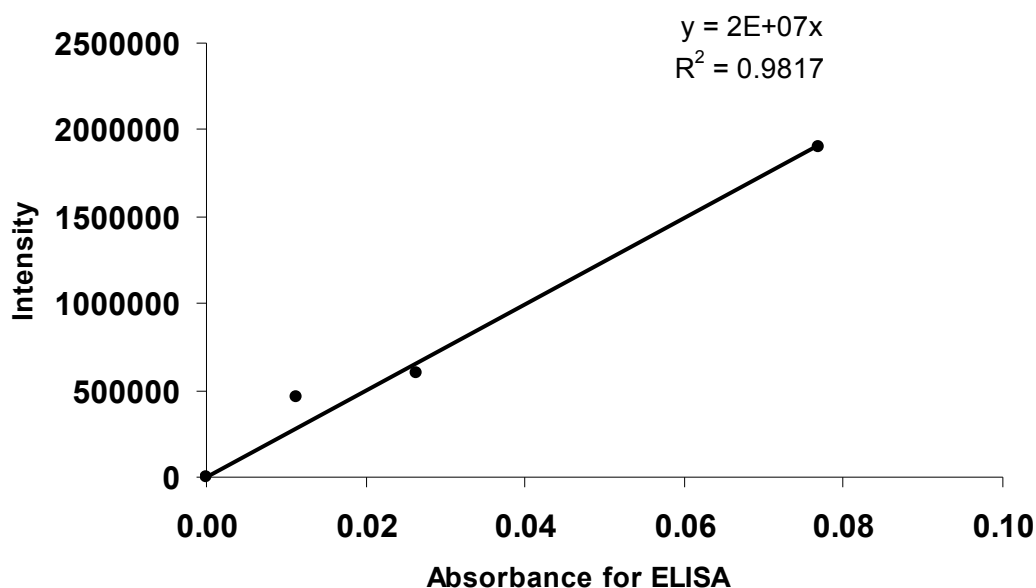
5.2.7 Comparison of the Four Fluorescent Immunoassays

Multiplexed immunosorbent assays for detection of anti-dengue IgM and IgG have been performed using fluorophores, quantum dots and lanthanide doped silica nanoparticles. These fluorescent and luminescent reporters were detected using confocal laser scanning microscopy (CLSM), epi-fluorescence microscopy and programmable array microscopy (PAM). While all methods and probes gave the same trend in results for the anti-dengue IgM and IgG response, each method has its advantages and disadvantages relative to the others and these will be discussed.

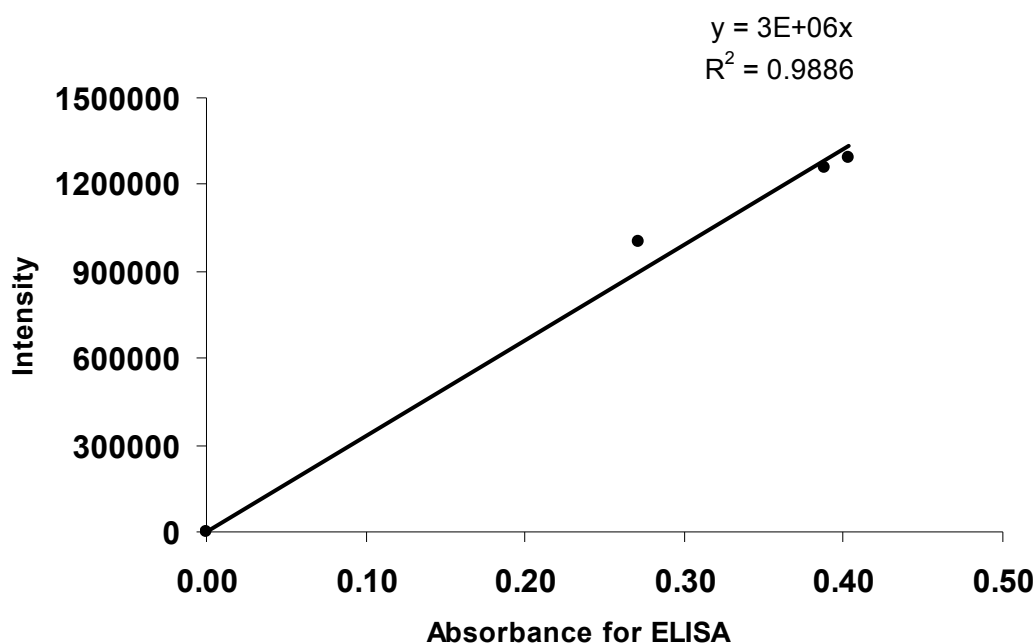
The first point that can be compared is the ability to simultaneously detect both analytes. This was possible with the epi-fluorescence system, which used a UV excitation filter and a spectral imager. These made it possible to excite both nanoparticles simultaneously, and collect the emission spectra in a hyperspectral image. The spectral imager was not present on any of the other microscopes, thereby making it necessary to use multiple excitation and emission filters. This makes data collection time consuming. The automation of the PAM meant that although data were not collected in a single hyperspectral image, the two channels were imaged quickly and this made that microscope attractive for use and preferred over the confocal method. The PAM was also preferred over the epi-fluorescence

microscope because the differing molar absorptivities of the two QDs were not an issue when specially suited excitation filters were used. Both were efficiently excited. While specially suited filters may have been used on the epi-fluorescence microscope, the lack of automation would prolong the imaging process.

A second point of comparison is the correlation of FLISA results with those of ELISA. ELISA has been adopted as the gold standard for serological diagnosis of dengue¹⁵ IgG and IgM with several kits having been developed for their detection. The success of the fluorescence and luminescence linked assays developed is therefore evaluated based on how well they compare to the results obtained for ELISAs done in separate wells. These will be compared below.



(a)



(b)

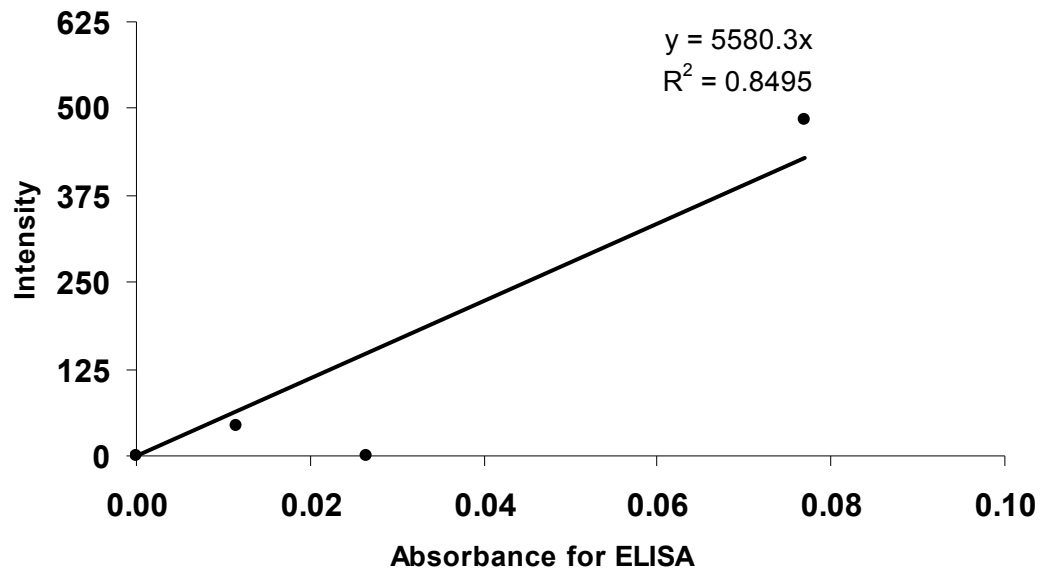
Figure 60: The relationship between values of intensity obtained with CLSM readout of organic fluorophores and ELISA methods for (a) an assay for anti-dengue IgM, (b) an assay for anti-dengue IgG

Figures 60 a and b show the correlation between the values obtained for single welled confocal detection of anti-dengue IgM and IgG with those obtained for multi well ELISAs. The graphs demonstrate a good correlation between the results of the two methods, indicating that despite the unfavourable properties of fluorophores (Chapter 3), they can still be used for single welled multiplexed analyses. The linear relationships suggest that assaying for the two different antibodies in the same well of an assay plate does not affect the detection of either antibody. This indicates that fluorophores can be used for multiplexed analyses, in spite of their previously mentioned disadvantages.

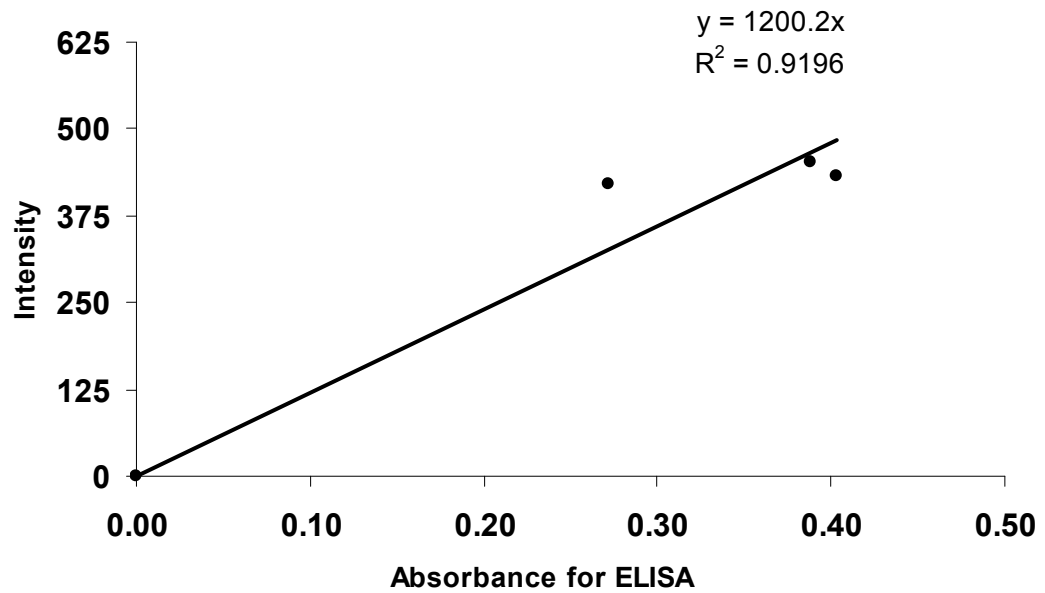
Based on the results, there is no cross reactivity between anti-dengue IgM and IgG. In practice, it would therefore be possible to detect dengue fever IgM and IgG in

the same well of an assay plate using fluorescent dyes. With a set of standards, the multiplexed assay can become quantitative, thereby giving the relative concentrations of IgM and IgG. This would allow an assessment of primary or secondary infection in a single assay well. The higher signal to background ratio of the confocal method relative to the ELISA method increases the sensitivity of detection, allowing low levels of antibody to be detected.

The comparisons between methods using QDs, NPs and ELISA methods will now be discussed.

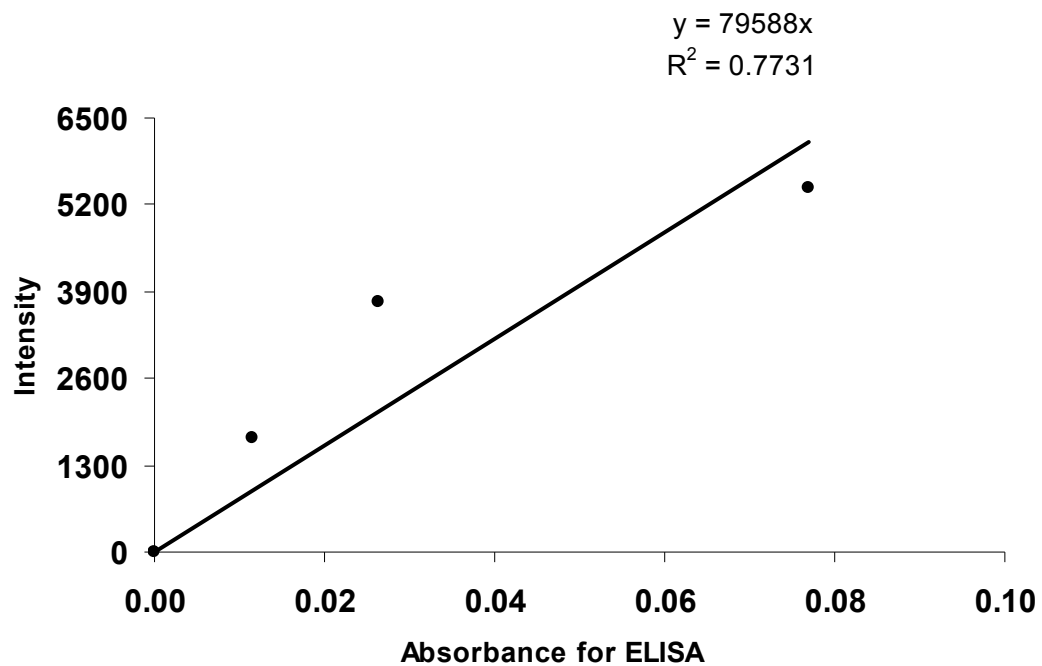


(a)

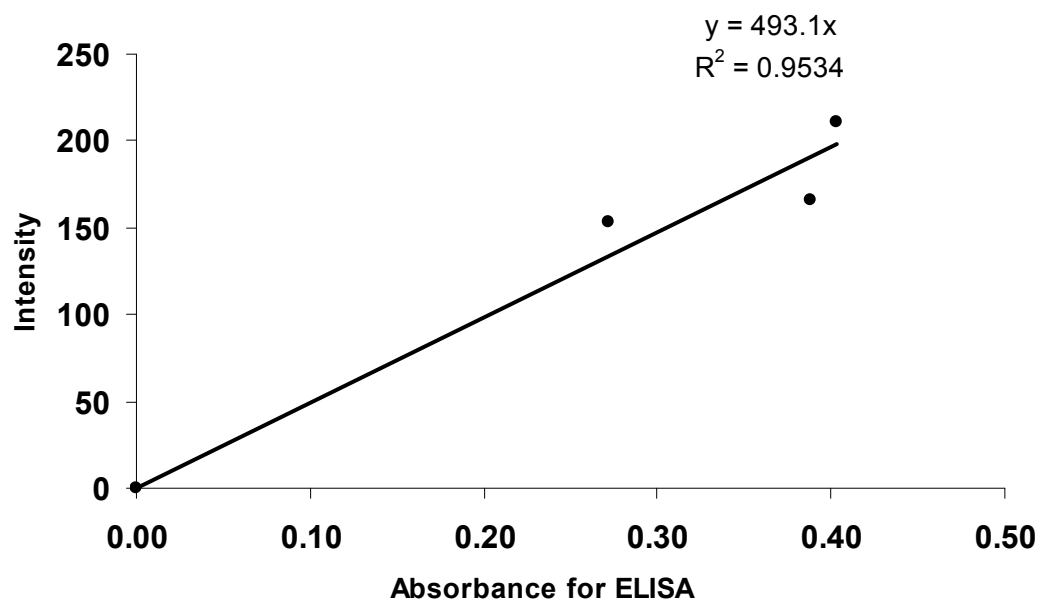


(b)

Figure 61: The relationship between values of intensity obtained with PAM and ELISA methods for (a) an assay for anti-dengue IgM, (b) an assay for anti-dengue IgG

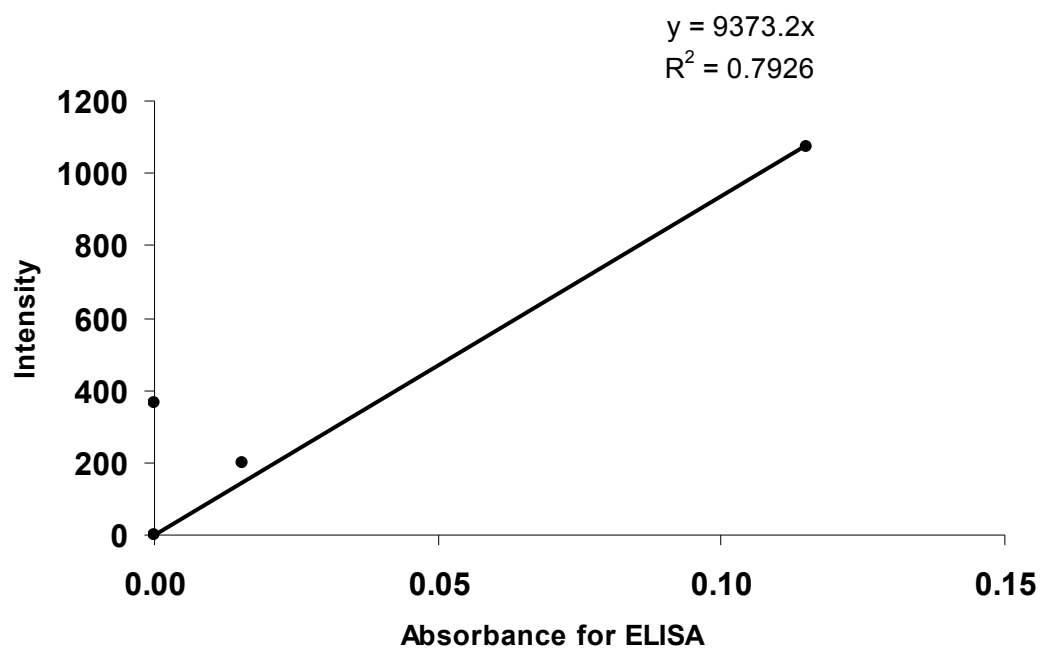


(a)

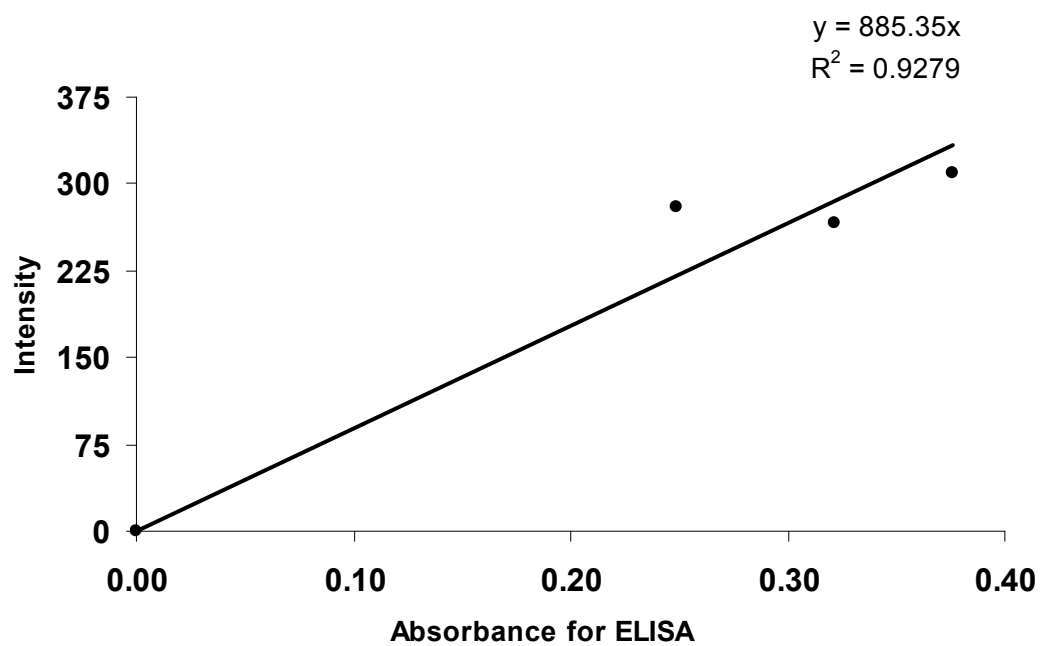


(b)

Figure 62: The relationship between values of intensity obtained with epi-illumination of QDs and ELISA methods for (a) an assay for anti-dengue IgM, (b) an assay for anti-dengue IgG



(a)



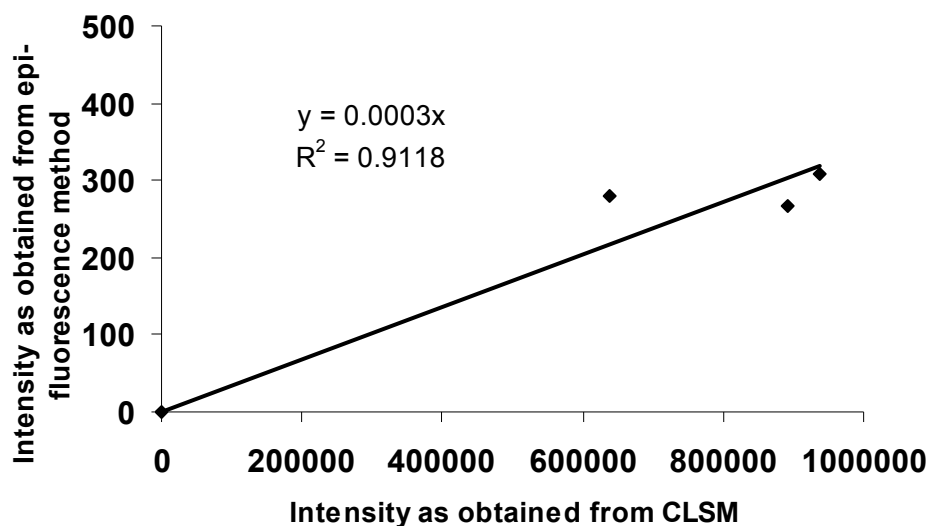
(b)

Figure 63: The relationship between values of intensity obtained with epi-illumination of lanthanide doped silica nanoparticles and ELISA methods for (a) an assay for anti-dengue IgM, (b) an assay for anti-dengue IgG

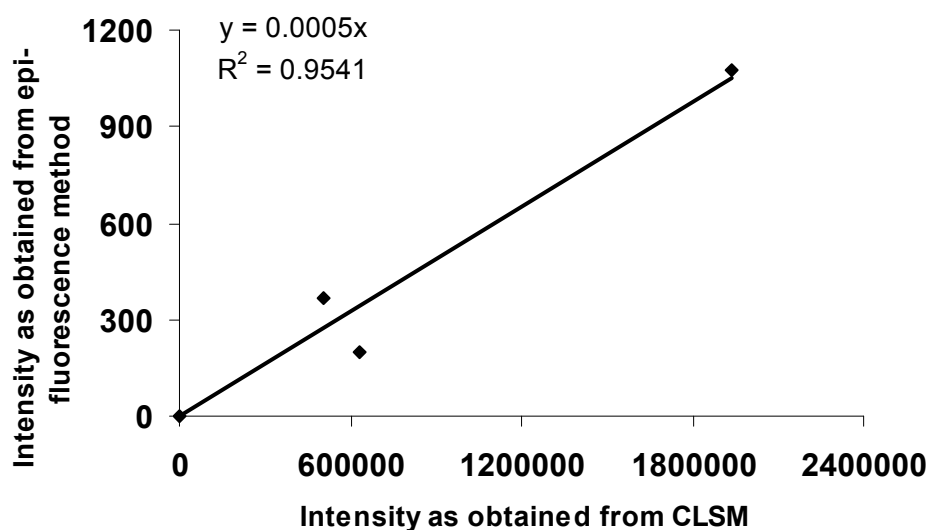
Figures 61 through 63 show the comparison between nanoparticle based methods and ELISA methods for antibody detection. There is a linear relationship between the two methods with the correlation coefficient between approximately 0.8 and 0.9 for most measurements. IgG detection results tend to be well correlated (Figures 61 (b), 62 (b) and 63 (b)), but the relationship for results of IgM detection is repeatedly less so (61 (a), 62 (a) and 63 (a)). A similar trend is seen in Figure 62 (a) and (b). In a multiplexed assay, there exists competition between the anti-dengue IgM and anti-dengue IgG in the assay well. This competition is influenced by some factors. One of these is the size of IgM relative to IgG; 950 kDa and 150 kDa respectively indicating that the rate of diffusion to the surface of the plate is somewhat slower, and attachment may be limited by IgG occupying the available sites preferentially. Another factor is that IgM also has a lower affinity for the antigen than IgG; that is, the strength of the interaction between the antigen and a single binding site of IgM is weaker than that between the antigen and a binding site of IgG. These two factors however, are contrasting with the higher avidity; the overall strength of the IgM-antigen interaction, due to the fact that it is a pentameric antibody. The result is IgG diffusing to the antigen faster but competing with a more effective overall interaction with IgM.¹⁶ These processes would eventually reach equilibrium. With this in mind, future work could be extended to look at the kinetics of binding of both IgM and IgG to the antigen in both single well and multi-well assay formats. This would allow for some improvements to the assay, such as optimising experimental times to ensure accurate concentration values. These are factors have all been put forward as explanations for the variability between single well and multi-well anti-dengue IgM assays, and now to be considered when a multiplexed assay is designed.

Based on the correlation with ELISAs, the conclusion is that fluorophores with CLSM readout give the best results for the multiplexed assays. There are however other factors that need to be considered. One of these relates specifically to the lanthanide doped silica nanoparticles and this is non-uniform attachment of the labelled secondary antibodies to the antibodies in serum. This is partly because of aggregation of the antibodies in the presence of the antigens. The aggregation results in clusters of particles at random points within the sample well, giving an uneven spread of luminescence throughout the well, evidenced when looking through the microscope eyepiece into the assay well. One benefit of the ELISA method is that the signal from the well is uniform and uneven sampling would not be a problem. The problem with NPs is common when dealing with sampling of particles; precision is generally limited by the homogeneity of the sample. One way to reduce aggregation would be to dilute the serum sample, thereby reducing the aggregation within the sample matrix.

In spite of these observations, however, there exists a good correlation between the results obtained using organic dyes with CLSM read-out and those obtained using the NPs with epi-fluorescence read-out (Figure 64). The results shown in Figure 64 are encouraging as they show that in spite of the difficulties encountered when using the lanthanide doped silica NPs, there exists a good correlation between results obtained using them and those using well established organic dyes as probes. What is also positive about this result is that the confocal microscope used was a commercially available instrument using a laser as the excitation source, while the epi-fluorescence microscope was assembled in-house and had a mercury lamp as the excitation source (this information is recorded in Chapter 2).



(a)

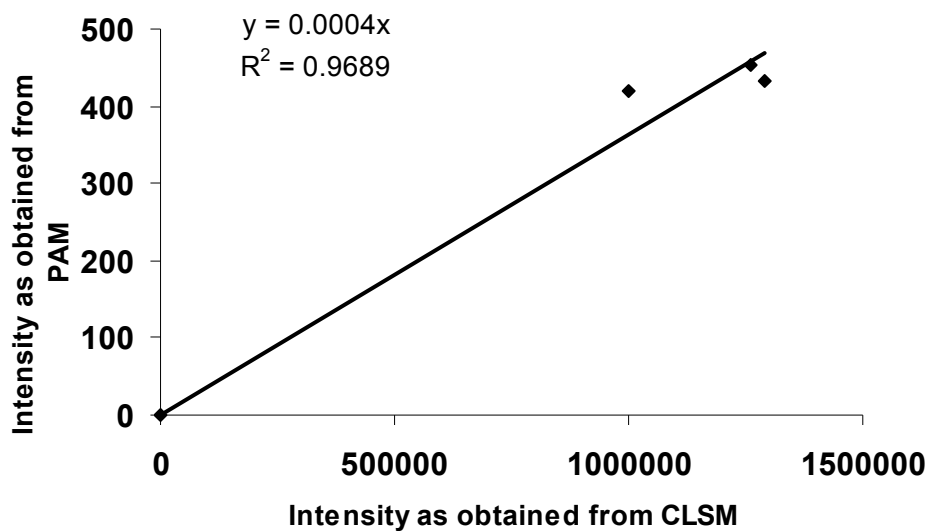


(b)

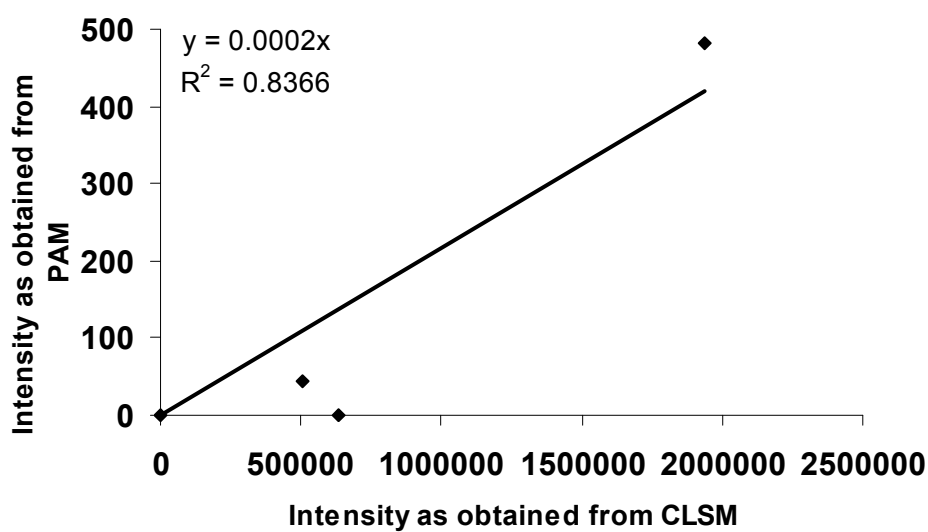
Figure 64: Comparison of results obtained from similar serum samples using NPs with epi-fluorescence read-out and organic dyes with CLSM read-out for (a) anti-dengue IgG and (b) IgM

These results show the success of the new microscopic method and provide a favourable framework for further development of both the probes and the microscope. It is also observed that in spite of the long incubation time of the NP assay coupled with the possible exchange of avidin linked probes with biotinylated

antibodies, there still remains a good correlation between the two methods. This indicates that the transfer was minimal in these experiments.



(a)



(b)

Figure 65 : Comparison of results obtained from similar serum samples using QDs with PAM read-out and organic dyes with CLSM read-out for (a) anti-dengue IgG and (b) IgM

As the PAM is a modified confocal instrument, it is of interest to compare results obtained from the CLSM and the PAM for the same serum samples and this comparison is shown in Figure 65. There is a linear relationship existing between the results from the PAM and CLSM methods, with the correlation coefficient as 0.97 for anti-dengue IgG and 0.84 for anti-dengue IgM. This result is also encouraging as once again the PAM; a recently developed and still presently a non-commercial instrument correlates reasonably well with the established confocal method. This also forms a good basis for future work on assay read-out with the PAM.

A more in depth investigation of the relative merits of both methods should take the form of a quantitative analysis. This should include a comparison of detection limits for anti-dengue IgM and IgG. No detection limits were carried out using the PAM. While no detection limits were obtained for dengue antibodies, mouse IgG detection limits were obtained using fluorophores imaged confocally and lanthanide-doped silica NPs imaged by epi-fluorescence microscopy. Using the confocal microscope and a FITC-labelled probe, mouse IgG had a detection limit of 8 ng mL⁻¹. The same analyte was detected down to 1 ng mL⁻¹ using a Sm-doped silica nanoparticle with epi-fluorescence read-out. This is a good indication of the relative superiority of the lanthanide-doped probes in single analyte detection systems. Future work should seek to better establish these comparisons, with limits of detection obtained by dilution of sera.

Another factor that can account for the varied results among the different methods of detecting anti-dengue IgM and IgG is the quality of the solid surface used, as this determines the attachment of the primary antibody to the surface of the plate. As ELISAs are widely performed, there are several plates available that are specially

suited to attachment of primary antibodies. The most suitable plate used for fluorescence was the Nunc glass bottom plate designed for tissue culture. In preliminary work carried out (will not be shown) it was ascertained that immunoassays performed on the Nunc glass bottom plates gave superior results to those performed on any other plate. This plate was only used for confocal applications, while other suitable but somewhat inferior plates had to be used for epi-fluorescence and PAM work. Different plates had to be used for the PAM as this microscope's stage could only accommodate chamber slides and 15-well plates. With epi-fluorescence work, smaller volumes were used to conserve samples, and as a result 384-well plates were the plates of choice. Attachment of the first antibody is of primary importance to the success of the assay and the results with FLISAs performed on the Nunc plate and imaged confocally seem to confirm this.

Finally, ELISAs and FLISAs with organic dyes were all performed within weeks of collection of sera. The other FLISAs were done some 8 to 12 months after collection, with the sera going through several freeze and thaw cycles. This has been shown to limit the accuracy of an assay and may be a reason for lower correlation between nanoparticle based methods and ELISAs.

5.3 General Discussion and Conclusions

A single-welled multiplexed immunoassay has been successfully developed and applied to a model virus system that presents itself in multiple forms. Mice were immunised with dengue antigens and the serum obtained was assayed. The assay was tested using three different types of fluorescent probes and these probes were applied with varied degrees of success. The results of the multiplexed immunoassay

compare favourably with those obtained with a multi-well ELISA, thereby offering several advantages over the adopted gold standard for serological diagnosis. The results show the reproducibility of the new method, with very similar results being obtained from a variety of methods over a period of 8 - 12 months (Figures 64 and 65). Each method of imaging was significantly different, with one method relying on absorbance measurements, another confocal readout, a third epi-fluorescence illumination and finally a modified confocal method. Differences with respect to attachment to the plate were noted and it was acknowledged that each method using a different type of plate could make a difference.

The presence of a primary and secondary response was not demonstrated by the assay results. The two sets of mice immunised once and twice show very similar profiles for the antibodies over the 4 week period. This pattern of antibody production was not expected in the mouse model, and is not expected in a human model, as double exposure to the virus should result in a secondary response. It is expected that if this experiment is performed on human sera, taking the ratio of IgM to IgG concentration would indicate whether the person has a primary or secondary infection. With this in mind, future similar experiments should be structured differently to ensure that a secondary response is obtained. Some reasons for the lack of a secondary response will now be explored. When referring to Table 6, it is observed that the mice were immunised a second time one week after the initial immunisation. Future work should explore allowing a greater period of time to pass between the first and second immunisations, thereby seeing the possibility of a secondary infection. In practice, the production of significant concentrations of antibody in mouse hybridoma production methods is a process spread over 6 to 8 weeks, with 2 additional immunisations at approximately equal intervals. The

animals are bled some 2 weeks after the third immunisation.¹⁷ The levels of antibodies produced in the present experiment are therefore substantially lower than could be obtained and are probably not representative of the true responses of the mice to immunisation. Additionally, a longer timing between primary and secondary 'infections' would better mimic a human model, as time periods between infections vary. With this in mind, future work could also seek to determine the effect of time between primary and secondary infection on the magnitude of the secondary response mounted. The lack of a defined secondary response can also be discussed in light of the persistence of the dengue antigens after immunisation. It was observed from a single experiment (data are shown in Appendix 4, page 199) that there was antigen present in the serum samples. This should not be the case. As long as the antigen persists, antibody production continues. This however is at a low and often undetectable concentration, and studies have shown¹⁸ that the antigen persists for a shorter period of time after a second immunisation. As stated in the introductory chapter, secondary dengue infections produce anamnestic reactions. Such a response is seen on re-injection with an antigen; antibody production is increased upon a second exposure to the antigen. As no anamnestic response was evidenced for this experiment, it may be acknowledged that in addition to the time between immunisations, the persistence of the antigen is a contributing factor to the unexpected results.

The method of taking the ratio of the IgM concentration to the IgG concentration for establishment of the type of infection has been described in the ELISA format, particularly in commercially produced kits, and involves separate tests in separate assay wells. This method, done in a single well for each serum sample, has some advantages. Firstly, the test is performed under the same environment and therefore variations cannot be due to the position in the plate. This can be a problem with

ELISA.¹⁸ Secondly; fewer materials, reagents and samples need to be used as the tests are not done individually, thereby saving money. Thirdly, when compared to ELISA, an advantage of the FLISAs is the greater flexibility of the assay; ELISA needs to be imaged very shortly after the addition of colour developer and stop solution. Here the assays can be imaged several hours after the assay has been completed, and in the case of QDs and lanthanide-doped NPs, can be imaged several days and multiple times after assay completion. A major disadvantage at present is the time the assay takes. With the confocal method, collection of data takes some 3 continuous hours and data analysis took a further 4 hours. With the lanthanide doped probes, data collection and analysis was just as quick as for ELISA, but the probes were not easily imaged on the same day of the assay; imaging was carried out after the plate was left shaking overnight. In light of the avidin-biotin dissociation equilibrium, other methods of conjugating the NPs to the antibodies need to be investigated. It is possible that the labels became interchanged and affected the result. When looking at the success of the multiplexed NP method compared with the multi-welled ELISA methods, it seems likely that some degree of interchange has occurred. QDs had a shorter incubation time than ELISA, with data collection and analysis taking a similar period of time.

Within the set of fluorescent and luminescent probes used, some probes have various benefits over others used. Organic fluorophores are the cheapest and most easily obtainable form of fluorescent probe. These probes are also very easily conjugated to antibodies using simple isothiocyanate and EDC/sulfo NHS chemistry. The QDs did not offer any great improvements over conventional fluorophores: in addition to their high cost, very high concentrations of the more blue shifted 525 nm QDs had to be used in order to get a signal that could be

detected with 365 nm excitation. This was in keeping with literature obtained from the company, which noted the very low molar absorptivity of the 525 nm probe with respect to that of the 655 and 605 nm probes. This problem was resolved with the use of a PAM, where both QDs were efficiently excited in their respective channels. The use of probes with well separated emission maxima ensured that there was no energy transfer between the labels.

The lanthanides provided bright, cheap alternatives to the QDs, but they also presented with some problems. Since they are in particulate form, there was non-uniform attachment to the plate as evidenced when looking through the microscope into the assay well. This resulted in low precision within and between the wells. What could improve this study is a time-resolved assay. This would image the entire well and the result would not be biased by the position at which a reading is obtained. Another disadvantage of using lanthanides is that they require specialised methods for attachment to antibodies. The previously published method using BSA as a flexible bridge between the particles and the antibodies was adopted. This method took 48 hours for completion, making them unattractive for clinical applications as a quick assay time is generally preferable. Other methods for attaching the silica nanoparticles to proteins could be explored in future work. The development of smaller probes presenting reduced steric hindrance with the solid surface of the assay could also be beneficial in the future.

The multiplexed method of analysis could not be applied to mixtures of cross reactive antibodies. As a result, virus serotyping was not achieved using the assay designed. A method for distinguishing cross reactive analytes is needed. Such a

method would find great utility, and the development of such a method will now be explored.

5.4 References

- (1) World Health Organisation In *Laboratory diagnosis*; World Health Organisation, Ed.; Dengue haemorrhagic fever: diagnosis, treatment, prevention and control; World Health Organisation: Geneva, Switzerland, 1997; pp 34-47.
- (2) Das, S.; Pingle, M. R.; Munoz-Jordan, J.; Rundell, M. S.; Rondini, S.; Granger, K.; Chang, G. -. J.; Kelly, E.; Spier, E. G.; Larone, D.; Spitzer, E.; Barany, F.; Golightly, L. M. Detection and serotyping of dengue virus in serum samples by multiplex reverse transcriptase PCR-ligase detection reaction assay. *J. Clin. Microbiol.* **2008**, *46*, 3276-3284.
- (3) Lo, C. L. H.; Yip, S. P.; Cheng, P. K. C.; To, T. S. S.; Lim, W. W. L.; Leung, P. H. M. One-step rapid reverse transcription-PCR assay for detecting and typing dengue viruses with GC tail and induced fluorescence resonance energy transfer techniques for melting temperature and color multiplexing. *Clin. Chem.* **2007**, *53*, 594-599.
- (4) Saxena, P.; Dash, P. K.; Santhosh, S. R.; Shrivastava, A.; Parida, M.; Rao, P. V. L. Development and evaluation of one step single tube multiplex RT-PCR for rapid detection and typing of dengue viruses. *Viro. J.* **2008**, *5*, 20.
- (5) Bozza, F. A.; Cruz, O. G.; Zagne, S. M.; Azeredo, E. L.; Nogueira, R. M. R.; Assis, E. F.; Bozza, P. T.; Kubelka, C. F. Multiplex cytokine profile from dengue patients: MIP-1beta and IFN-gamma as predictive factors for severity. *BMC Infect. Dis.* **2008**, *8*, 86.
- (6) Dussart, P.; Petit, L.; Labeau, B.; Bremand, L.; Leduc, A.; Moua, D.; Matheus, S.; Baril, L. Evaluation of Two New Commercial Tests for the Diagnosis of Acute Dengue Virus Infection Using NS1 Antigen Detection in Human Serum. *Plos Neglect. Trop. Dis.* **2008**, *2*, e280.
- (7) Vazquez, S.; Perez, A. B.; Ruiz, D.; Rodriguez, R.; Pupo, M.; Calzada, N.; Gonzalez, L.; Gonzalez, D.; Castro, O.; Serrano, T.; Guzman, M. G. Serological markers during dengue 3 primary and secondary infections. *J. Clin. Virol.* **2005**, *33*, 132-137.
- (8) Zainah, S.; Wahab, A. H. A.; Mariam, M.; Fauziah, M. K.; Khairul, A. H.; Roslina, I.; Sairulakhma, A.; Kadimon, S. S.; Jais, M. S. M.; Chua, K. B. Performance of a commercial rapid dengue NS1 antigen immunochromatography test with reference to dengue NS1 antigen-capture ELISA. *J. Virol. Methods* **2009**, *155*, 157-160.

- (9) Kurzban, G. P.; Gitlin, G.; Bayer, E. A.; Wilchek, M.; Horowitz, P. M. Biotin Binding Changes the Conformation and Decreases Tryptophan Accessibility of Streptavidin. *J. Protein Chem.* **1990**, *9*, 673-682.
- (10) Launer, H. F.; Fraenkel-Conrat, H. The avidin-biotin equilibrium. *J. Biol. Chem.* **1951**, *193*, 125-132.
- (11) Hoyashi, Y.; Matsuda, R.; Maitani, T. Precision, limit of detection and range of quantitation in competitive ELISA. *Anal. Chem.* **2004**, *76*, 1295-1301.
- (12) Lee, K. Quantum dots: A quantum jump for molecular imaging? *J. Nucl. Med.* **2007**, *48*, 1408-1410.
- (13) Meng, Q.; Li, Z.; Li, G.; Zhang, X.; An, Y.; Zhu, X. Aggregation of biotinylated polymeric microspheres induced by interaction with avidin. *Pure Appl. Chem.* **2007**, *79*, 1575-1582.
- (14) Full, S. **2009**, *Discussion thread*, 1.
- (15) Cuzzubbo, A. J.; Endy, T. P.; Nisalak, A.; Kalayanarooj, S.; Vaughn, D. W.; Ogata, S. A.; Clements, D. E.; Devine, P. L. Use of recombinant envelope proteins for serological diagnosis of dengue virus infection in an immunochromatographic assay. *Clin. Diagn. Lab. Immunol.* **2001**, *8*, 1150-1155. .
- (16) Kuby, J., Ed.; In *Immunology*; Goldsby, R. A., Kindt, T. J. and Osborne, B. A., Eds.; W. H. Freeman & Co Ltd: 2000;.
- (17) Nagata, S.; Salvatore, G.; Pastan, I. DNA immunization followed by a single boost with cells: a protein-free immunization protocol for production of monoclonal antibodies against the native form of membrane proteins. *J. Immunol. Methods* **2003**, *280*, 59-72
- (18) Campbell, D. H. Some speculations on the significance of formation and persistence of antigen fragments in tissues of immunized animals. *Blood* **1957**, *12*, 589-592.
- (19) Burrows, P. M.; Scott, S. W.; Barnett, O. W.; McLaughlin, M. R. Use of Experimental-Designs with Quantitative Elisa. *J. Virol. Methods* **1984**, *8*, 207-216.

6 Cross reactivity studies

This chapter deals with the development and use of a model for detecting the presence of cross reactive antibodies. The antibodies investigated are anti-dengue IgG types 3 and 4. A similar model has previously been used for the detection of cross reactive pesticides, but there are no reports of it being applied to dengue fever serotyping. The method presented in the preceding chapter was not a unique method for detecting anti-dengue IgM and IgG in a colocalised multiplexed method. It is a general method for multiplexed analyses applicable to anything with multiple serum biomarkers. One goal was to detect the various serotypes of a virus simultaneously, in the same well of an assay plate. It was proposed that serotype specific anti-dengue IgGs in serum would react selectively with the serotype specific antigen. These would be detected with secondary antibodies labelled with differently coloured fluorophores. What was found was that the polyclonal antibodies produced by the mice reacted non-selectively with all dengue antigens. Such a response would be seen when assaying for any mixtures of cross reactive antibodies. Therefore, the present method using different coloured secondary probes was of little utility for serotyping in the absence of a method for assessment of cross reactivity. Here, cross reactivity and its effect on diagnostics will be presented. This will be followed by discussion of a model commonly used for modelling and calibrating immunosorbent assays. Data are presented; first for a partially cross reactive system of human and mouse IgG, and finally for a fully cross reactive system of anti-dengue IgG types 3 and 4. Here, partially and fully cross reactive systems refer to one-way and two-way reactivity between the two species. In the one-way reactive system, anti-human IgG reacts with human IgG but has limited

reactivity with mouse IgG, while with the two-way reactive system anti-mouse IgG reacts with both mouse and human IgGs.

Simulations were initially carried out to test the robustness of this model for the present application and these data are shown in Appendix 5 (page 200).

6.1 Introduction

A cross reactant has typically been defined as an interferent causing a positive bias on an immunoassay result ¹ or an interferent causing a negative bias through the suppression of the signal. Positive bias results from the assay taking a longer time to reach equilibrium but giving a signal level similar to that obtained at equilibrium for the single analyte due to higher dissociation rates of the cross reactant-antibody complex.² Negative bias is a result of the cross reactant binding to the antibody and then being washed away after a short incubation time.

Cross reactivity is a form of analytical interference, which may be dependant upon or independent of the analyte.³ Analyte independent interference is a result of factors such as sample storage, while analyte dependent interference is brought about through interaction between the constituents of the sample with the reagent antibody. Structural similarities between the cross reactant and the analyte of interest lead to this type of interference, and can be problematic in diagnostic immunoassays, particularly where administration of drugs is concerned. What has been reported as one of the more severe cases of false positive results was the diagnosis of a 22 year old woman with human chorionic disease (hCG), which led to her unnecessarily undergoing chemotherapy, hysterectomy and segmental lungs resection.⁴ Eventually sixteen million US dollars were awarded in damages. ⁵ It is

believed that the reason for the false positive result was the presence of human anti-mouse IgGs, or some other heterophilic antibody.⁴

Antibodies used in immunoassay development may be placed into one of three groups: highly specific; where the antibody recognises only its specific antigen, cross reactive with other antigens of the same chemical class with similar binding affinities for all members of the group, and cross reactive with other antigens of the same chemical class, but having varied binding affinities for each member of the group.⁶ While the first and second groups of antibodies may be used for detection of specific antigens or a specific class of antigens respectively, the antibodies of the third group are difficult to use for quantitative analysis of an analyte in an unknown sample. Cross reactivity therefore poses challenges for epidemiology and serology when it comes to diagnosis of viruses with multiple antigenically related forms.

The arboviruses, belonging to the *Flaviviridae* genus, are a set of viruses for which serologic diagnosis is complicated. The viruses are commonly diagnosed using ELISA, but this method falls short due to the presence of common antigenic epitopes on the envelope protein of all flaviviruses, and a plaque reduction neutralisation test, which is costly and time consuming, must be used to confirm serology.⁷ The envelope protein contains the fusion peptide and this confers some degree of reactivity of all arbovirus antigens with virus specific antibodies, as a result of the amino acid sequence.⁸ One such example is a study performed in Columbia,⁹ where two arboviruses, dengue fever and yellow fever, co-circulate. ELISA for anti-dengue IgM performed on yellow fever patients showed that 46.2 % had reactivity for dengue fever, while 80 % of dengue fever patients were positive for the presence of yellow fever. The issue of cross reactivity with these viruses serves to decrease

the ability of public health services to respond efficiently and effectively to outbreaks.

Methods for overcoming the problem of cross reactivity include mutagenesis of the cross reactive epitope in order to ablate its effects.¹⁰ Other methods include the use of curve fitting procedures. One example is the herbicides triazines, which though easily separated through instrumental analytical methods can also be detected by immunoassays.¹¹ Differentiation between triazines was performed through mathematical modelling and curve fitting procedures.^{12, 13}

An equation frequently used to describe the shape of an immunoassay dose response curve is the five parameter logistic (5 PL) function.¹⁴ This function has parameters for the upper and lower asymptotes, the length of the transition region, the location of the transition and the degree of asymmetry present in the curve. This equation was applied to the cross reactive system.

6.2 Theory

The logistic law of growth assumes that systems grow exponentially until an upper limit is reached, at which point the growth rate slows and eventually saturates, thereby producing a characteristic S-shaped curve.¹⁵ Logistic models are empirical models which indicates that their parameters lack physical meaning, but can still be applied to data to obtain quantitative results.¹⁶ In an immunoassay, the concentration response curve is a result of the response y to the concentration of analyte present, x . These curves are characterised by 5 parameters: the response at infinite concentration, the response at zero concentration, the curve midpoint, the

slope of the curve and a factor modelling the asymmetric shape of the curve. If the curve is modelled in semi-logarithmic space; where the log of the concentration is used, the response at zero concentration is not considered and there are 4 parameters used to describe the curve. The 5 parameter logistic function is shown in Equation 6-1.¹⁴

$$y_i = d_i + \frac{a_i - d_i}{\left(1 + \left(\frac{x}{c_i}\right)^{b_i}\right)^{g_i}} \quad \text{Equation 6-1}$$

In Equation 6-1, y_i is the measured intensity, a_i is the intensity at zero concentration, b_i is the slope parameter, c_i is the midpoint concentration, d_i is the intensity at infinite concentration and g_i is the parameter that models asymmetry. The subscript 'i' refers to a given antibody. As these 5 parameters are all specific to each antibody, the identity of an unknown sample can be determined based on the deviation of measured y_i from y_i that is calculated using the 5 parameters. The deviation follows an approximate χ^2 distribution:

$$SSE = \sum_{j=1}^N w_j \left[y_j - \left(d + \frac{a - d}{\left(1 + \left(\frac{x_j}{c}\right)^b\right)^g} \right) \right]^2 \approx \chi^2 \quad \text{Equation 6-2}$$

In Equation 6-2, SSE represents the weighted sum of squared residuals, w_j is the weighting factor which is the inverse of the variance¹⁴ at the jth concentration. As

the value for x_i in an unknown sample is only approximate, the sum of squared errors (SSE) is minimised by changing x_i . The χ^2 distribution has $i-1$ degrees of freedom and the statistic is used to determine the identity of the unknown sample.

6.3 Methods and Materials

6.3.1 Materials

Reagents for the human IgG/mouse IgG cross reactivity model obtained from Sigma Aldrich were goat anti-mouse IgG (whole molecule) (Lot no. M8642), mouse IgG (Lot no. I5381), human IgG (Lot no. I4506), goat anti-human IgG (whole molecule) (Lot no. I1886), goat anti-human IgG-FITC (Lot no. F9512), technical grade casein from bovine milk (Lot no. C7078) and carbonate-bicarbonate buffer capsules (Lot no. C3041). Dengue antigens Types 3 and 4 and rabbit anti-dengue polyclonal antibody (Tebu-bio Ltd., Peterborough, UK), monoclonal dengue antibodies against dengue serotypes 3 and 4 (Santa Cruz Biotechnology, Santa Cruz, CA, USA) and goat anti-mouse IgG-FITC (Invitrogen, Paisley, UK) were used as outlined in the protocol. Nunc 96-well glass bottomed (Fisher scientific, UK, Loughborough, Leicester, UK) were used as the solid phase.

6.3.2 Assay Readout

Assays were imaged using an add-on to an inverted microscope (Figure 8) (IX71; Olympus UK Ltd, Southall, UK). Images were collected using an image intensifier (II118MD; Lambert Instruments, Leutingewolde, The Netherlands) attached to a CCD camera (PCO.1600; PCO Computer Optics GmbH, Kelheim, Germany). The intensified camera system was attached to an imaging spectrograph (PARISS;

Lightform Inc., Hillsborough, NJ) and then to the bottom port of the microscope. The microscope was illuminated using a mercury burner (Olympus USH-103OL; Olympus UK Ltd, Southall, UK) and light was filtered with a cube consisting of a 450 DF55 nm excitation filter, dichroic mirror of 485 nm and 500 nm long pass emission filter (XF77-2; Omega Optical Inc., Brattleboro VT).

6.3.3 Immunoassay

The immunoassays were performed by first immobilising separately anti-mouse IgG and anti-human IgG in carbonate/bicarbonate buffer (pH 9.65) at a concentration of $20 \mu\text{g mL}^{-1}$ each on the surface of a 96-well glass bottom plate. The plate was left to shake at room temperature overnight. The remaining sites for protein binding were blocked with a solution of 1% casein for 2 hours. After washing with PBS, a mixture of human IgG and mouse IgG was added and incubated at room temperature for 2 hours. Calibration samples for a dose response of the individual IgGs were also prepared and added to the wells for two hours. The plate was washed with PBS and the secondary FITC-labelled antibodies were added individually to their respective wells for two hours. A final wash step was performed before imaging microscopically.

6.3.4 Data Analysis

The data collected for the antigen/antibody dose response curves were fit to the 5 PL function and the values for a_i , b_i , c_i , d_i and g_i are obtained. The parameters b_i , c_i , d_i and g_i are optimised to give the best possible fit for the data. These parameters are then applied to a dose response of an unknown analyte on a known antibody. The SSE is minimised by changing x and comparing to a critical value for

χ^2 . The aim of the minimisation is to obtain an SSE that is as close to zero as possible; an ideal SSE is zero.

6.4 Results and Discussion

Anti-mouse and anti-human IgGs have some measure of cross reactivity with human and mouse IgGs respectively, based on the results presented in Chapter 4. They were therefore chosen as a partially cross reactive system to test the model. Human IgG was assayed on anti-human IgG and the 4 parameters were obtained. Mouse IgG was then assayed on anti-human IgG and the values for intensity were modelled using the parameters for assays on anti-human IgG.

Figure 66 shows the curve for the dose response of anti-human IgG with human IgG. The value of a_i is set to 0, and thus only 4 parameters are fit to the data. These data are shown below and are set as the standard for all assays on anti-human IgG.

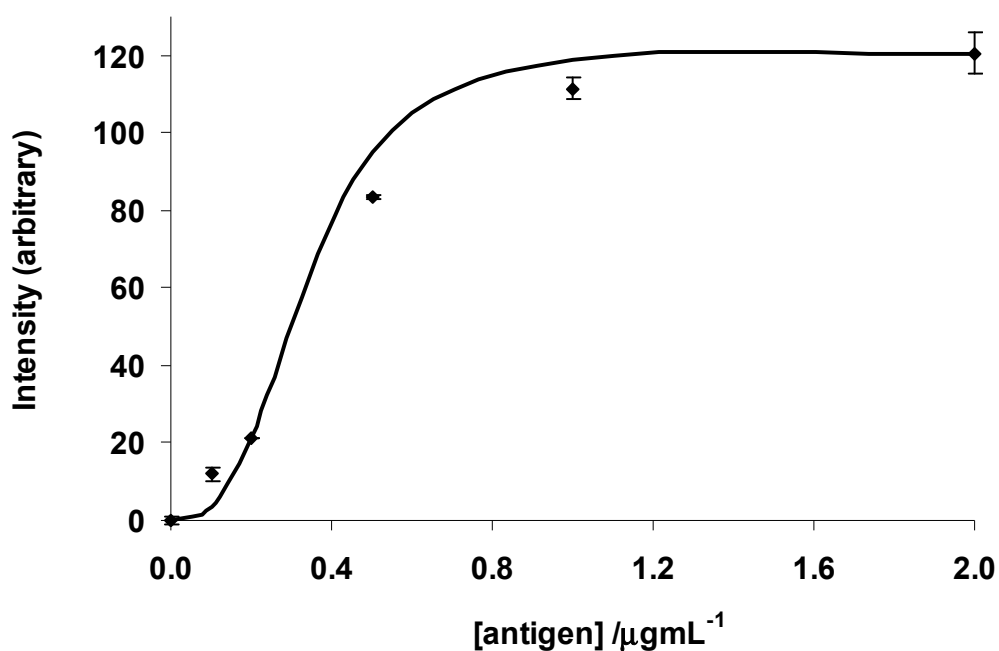


Figure 66: Dose response for human IgG. The line is a sigmoidal fit, modelled with 4 parameters. Each data point is an average of 3 replicate measurements and the error is % RSD.

Parameter	Modelled value
A	0
B	2.65
C	0.49
D	120.5
G	2.2

Table 8: The parameters obtained when the dose response of human IgG on anti-human IgG is modelled

The SSE of the fit of the parameters in Table 8 to human IgG data was 2.56. This value is used as the statistical basis of comparison for ‘unknown’ data fit to the

parameters for anti-human IgG. The parameters for anti-mouse IgG were also determined through a dose response for mouse IgG on anti-mouse IgG (Figure 67).

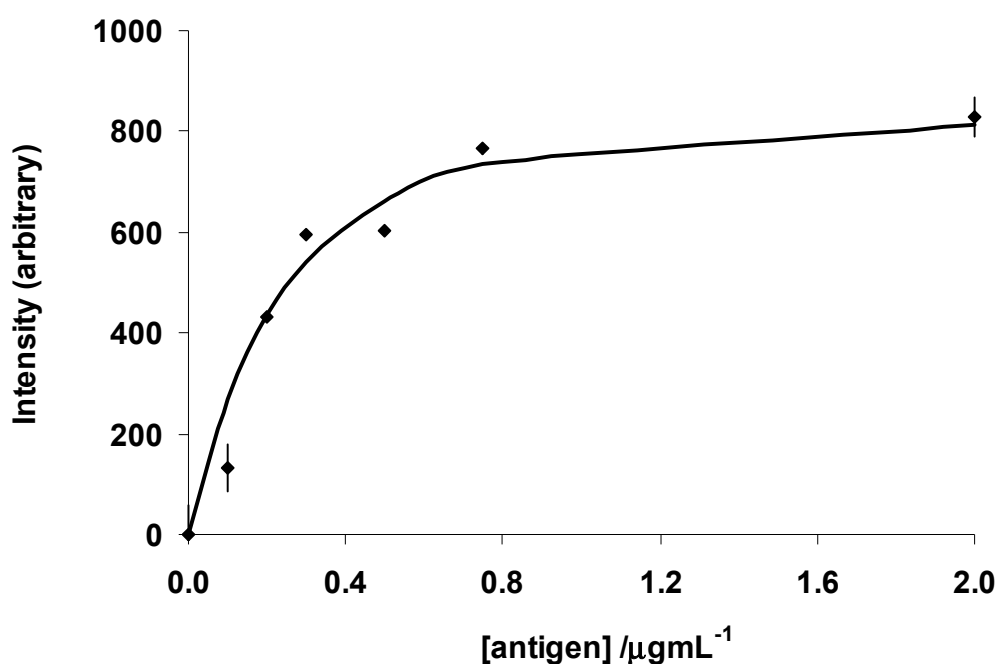


Figure 67: Dose response for mouse IgG. The line is a sigmoidal fit, modelled with 4 parameters. Each data point is an average of 3 replicate measurements and the error is % RSD.

Parameter	Modelled value
A	0
B	0.99
C	0.75
D	829.5
G	3.11

Table 9: The parameters obtained when the dose response of mouse IgG on anti-mouse IgG is modelled

Table 9 shows the parameters obtained from fitting 4 parameters to the dose response for mouse IgG. The SSE for this fit was 4.16. Using values from Tables 7 and 8, the identity of samples known to contain either mouse or human IgG could be determined and quantified.

Two samples known to contain $0.3 \mu\text{g mL}^{-1}$ and $0.75 \mu\text{g mL}^{-1}$ of mouse IgG were assayed on both anti-human and anti-mouse IgGs. The same was done for samples containing $0.3 \mu\text{g mL}^{-1}$ and $0.75 \mu\text{g mL}^{-1}$ of human IgG. Table 10 indicates that anti-human IgG does not react with mouse IgG, while the model is able to accurately quantify the amount of human IgG present in the sample, with $p > 0.2$ for the observation.

Analyte	[Predicted]/ $\mu\text{g mL}^{-1}$	[Actual]/ $\mu\text{g mL}^{-1}$
mouse IgG	0	0.3
human IgG	0.3	0.3
mouse IgG	0	0.75
human IgG	0.75	0.75

Table 10: Results of the cross reactivity model for mouse and human IgGs assayed individually on anti-human IgG.

Analyte	[Predicted]/ $\mu\text{g mL}^{-1}$	[Actual]/ $\mu\text{g mL}^{-1}$
mouse IgG	0.37	0.30
human IgG	0.09	0.30
mouse IgG	0.96	0.75
human IgG	0.09	0.75

Table 11: Results of the cross reactivity model for mouse and human IgGs assayed individually on anti-mouse IgG

Table 11 shows the results for two concentrations of analytes assayed on anti-mouse IgG. The model predicts the concentration of mouse IgG, but assumes that human IgG is mouse IgG at very low concentration. The predictions ($p > 0.95$) demonstrate the cross reactivity of anti-mouse IgG with human IgG, with no significant difference detected between the reaction of anti-mouse IgG with human IgG and anti-mouse IgG with mouse IgG. These results confirm what was noticed previously (Chapter 4) with the increased signal for mouse IgG when human and mouse IgGs were assayed together. Anti-mouse IgG reacts with human IgG, but the response is a fraction of what would be obtained if mouse IgG is the analyte. We recommend that the sample containing an unknown analyte is diluted by known factors to produce a concentration/response curve on the cross reactive antibody. The modelled curve that approximates closest to a dose response curve with a suitable error distance between the measured and calculated intensities reveals the identity of the unknown analyte.

The same curve fitting methods were then applied to a real viral system. The success with the partially cross reactive human IgG/mouse IgG model indicates that cross

reactants can be distinguished using the present method, and attempts were made to extend it to a fully cross reactive system of dengue antibodies.

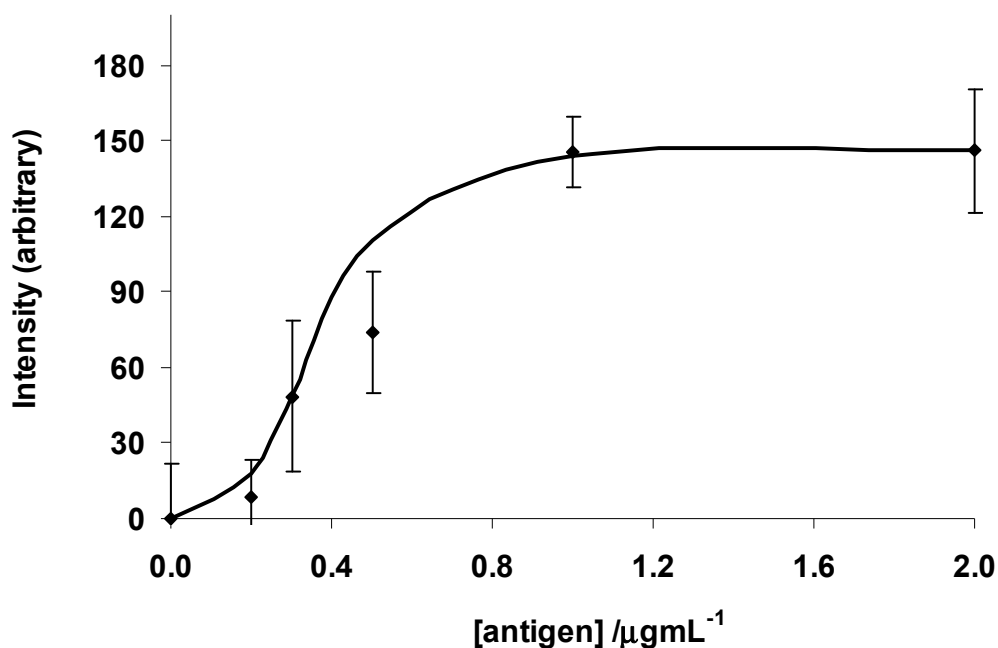


Figure 68: Dose response of anti-dengue IgG on dengue type 3 antigen. The line is a sigmoidal fit to 4 parameters. Each data point is an average of 3 replicate measurements and the error is % RSD.

Anti-dengue type 3 antibody was assayed on dengue type 3 antigen (Figure 68). The four parameters fit the data with a SSE of 0.15. These four parameters were then fit to data obtained from anti-dengue type 4 assayed on dengue type 3 antigen. The results of this fit indicate that there is reactivity of type 4 antibody with type 3 antigen, with the model assuming type 4 antibody to be type 3 antibody ($p > 0.95$) at very low concentrations. This same pattern was seen for the partially cross reactive system of human IgG with anti-mouse IgG, where the model assumed that human IgG was mouse IgG at a low concentration (Table 11).

Analyte	[Predicted]/ $\mu\text{g mL}^{-1}$	[Actual]/ $\mu\text{g mL}^{-1}$	SSE
dengue Ab 3	0.2	0.2	3.80E-23
dengue Ab 3	2	2	4.81E-12
dengue Ab 4	0.31	0.2	1.27E-14
dengue Ab 4	0.49	2	5.51E-29

Table 11: Assessment of a cross reactive assay, where type 3 and type 4 dengue antibodies are assayed individually on dengue type 3 antigen.

From Table 11, the sum of squared differences between the measured and calculated intensities is low, and the method of accepting the sample with the lowest χ^2 as the correct analyte cannot be performed with confidence.

6.5 General Discussion and Conclusions

A model for cross reactivity was developed and applied to a partially cross reactive system of human and mouse IgGs, and a fully cross reactive system of dengue types 3 and 4 antibodies. Standard dose response curves were measured and 4 parameters were obtained, which were then used to fit ‘unknown’ data. The sum of squared differences between the measured and calculated data was assumed to follow a χ^2 distribution and this value was optimised. While the components of the partially cross reactive system can be determined, results showed that the model cannot be applied to a fully cross reactive system.

Initially, simulations where noise was added to the system were performed to test the robustness of the model and these indicated that the error distance is large when the analyte is not assayed on its antibody, with $p < 0.005$. This value is statistically

significant and indicates that unrelated antibodies can be distinguished. A lower error distance is obtained when the correct analyte is assayed on its antibody, with $p > 0.1$. This value is not statistically significant. The simulations allowed use of the model as it works even in the presence of noise.

This method for distinguishing between cross reactive antibodies is similar to a previously described method¹⁷ for herbicides. The report also noted the difficulty of distinguishing between closely related analytes, and suggested developing more discriminatory antibodies for specialised detection. Indeed, this approach of developing discriminatory antibodies is frequently taken for detecting cross reactive viruses.¹⁸⁻²⁰ These methods are somewhat expensive, and therefore the combination of a multiplexed assay using specialist antibodies and quantified with the mathematical method described here would create a cheaper, sensitive method for specific detection of cross reactive viruses.

The method described for herbicides was an ELISA,¹⁷ and was modeled with the four parameter logistic function which fits three parameters to the data. This function did not always fit the immunoassay data, resulting in lack of fit error. The method used here employed the five parameter logistic function which adds a fourth fitting parameter that accounts for asymmetry in the dose response curve. The use of this parameter extends the utility of the method described here to several types of assays, as the shape of the curve varies for high and low binding assays, in the presence of cross reactants and with variation of incubation time.²¹

The method described in this chapter was applied with the intention to distinguish serotypes of dengue fever and other cross reactive viruses using a cheap and easily implemented technique. While this goal was not reached, the method provides a viable platform for future work when combined with multiplexed immunoassays using specialized antibodies.

6.6 References

- (1) Valdes, R.; Jortani, S. A. *Clin. Chem.* **2002**, *48*, 405-406.
- (2) Vining, R. F.; Compton, P.; McGinley, R. *Clin. Chem.* **1981**, *27*, 910-913.
- (3) Tate, J.; Ward, G. *Clin Biochem Rev* **2004**, *25*, 105-120.
- (4) Cole, L. A.; Rinne, K. M.; Shahabi, S.; Omrani, A. *Clin. Chem.* **1999**, *45*, 313-314.
- (5) Dodig, S. *Biochem. Medica.* **2009**, *19*, 50-62.
- (6) Nistor, C.; Christensen, J.; Ocio, N.; Norgaard, L.; Emneus, J. *Anal. Bioanal. Chem.* **2004**, *380*, 898-907.
- (7) Ocegueda, Leopoldo F., III; Patiris, P. J.; Chiles, R. E.; Busch, M. P.; Tobler, L. H.; Hanson, C. V. *Am. J. Trop. Med. Hyg.* **2007**, *77*, 159-163.
- (8) Chiou, S.; Crill, W. D.; Chen, L.; Chang, G. J. *Clin. Vaccine Immunol.* **2008**, *15*, 825-835.
- (9) Houghton-Trivino, N.; Montana, D.; Castellanos, J. *Rev Salud Publica (Bogota)* **2008**, *10*, 299-307.
- (10) Crill, W. D.; Trainor, N. B.; Chang, G. J. *J. Gen. Virol.* **2007**, *88*, 1169-1174.
- (11) Wortberg, M.; Jones, G.; Kreissig, S. B.; Rocke, D. M.; Gee, S. J.; Hammock, B. D. *Anal. Chim. Acta* **1996**, *319*, 291-303.
- (12) Wortberg, M.; Kreissig, S. B.; Jones, G.; Rocke, D. M.; Hammock, B. D. *Anal. Chim. Acta* **1995**, *304*, 339-352.
- (13) Reder, S.; Dieterle, F.; Jansen, H.; Alcock, S.; Gauglitz, G. *Biosens. Bioelectron.* **2003**, *19*, 447-455.
- (14) Gottschalk, P. G.; Dunn, J. R. *Anal. Biochem.* **2005**, *343*, 54-65.
- (15) Meyer, P. *Technol. Forecast. Soc. Chang.* **1994**, *47*, 89-102.
- (16) Giraldo, J.; Vivas, N. M.; Vila, E.; Badia, A. *Pharmacol. Ther.* **2002**, *95*, 21-45.
- (17) Jones, G.; Wortberg, M.; Hammock, B. D.; Rocke, D. M. *Anal. Chim. Acta* **1996**, *336*, 175-183.
- (18) Abhyankar, A. V.; Bhargava, R.; Jana, A. M.; Sahni, A. K.; Rao, P. V. L. *Hybridoma* **2008**, *27*, 191-198.
- (19) Roberson, J. A.; Crill, W. D.; Chang, G. J. *J. Clin. Microbiol.* **2007**, *45*, 3167-3174.
- (20) Ludolfs, D.; Schilling, S.; Altenschmidt, J.; Schmitz, H. *J. Clin. Microbiol.* **2002**, *40*, 4317-4320.
- (21) Wild, D., Ed.; In *The immunoassay handbook*; Elsevier Ltd.: Amsterdam, The Netherlands, 2005; pp 930.

7 General Discussion and Conclusions

This thesis explored the development of multiplexed immunosorbent assays through spectral unmixing of spectroscopic signals. Multiplexing is widely discussed, but implementing methods into viable immunoassays is difficult. The most easily implemented method is the microarray method, where the assays are performed in specific spots on a glass slide or in a glass plate. This, as mentioned previously, is done extensively and no attempts were made to multiplex in this manner. Another widely used but expensive method is through bead-based assay platforms such as Luminex® and other such technologies. The work presented in this thesis goes beyond what has been done before: multiplexed single well measurements have been performed in both solution and solid phase using organic fluorophores, quantum dots and lanthanide doped silica nanoparticles. The results were obtained through the use of spectroscopic techniques for detecting multiple spectra and subsequently separating these spectra into individual components. Additionally, a number of microscopic techniques are used, with a particularly novel application of an epi-fluorescence and programmable array microscope to the issue of multiplexing. In this chapter the work carried out is summarised, along with suggestions for further study.

7.1 Spectral Unmixing Of Conventional Fluorophores and Quantum Dots

In chapter 3 a method for separating mixtures of organic fluorophores was described where the fluorescence spectra of up to four co-localised dyes was unmixed. This concept was not straight forward, as conventional unmixing methods did not always give favourable results (Table 2). The problem was compounded by multiple forms of dyes (Figures 17 and Figure 18) and their intrinsic properties,

which have been discussed at length in chapter 3. The spectral unmixing algorithm assumes that the intensity of a mixture at a given wavelength is the sum of the intensities of all individual components of the mixture. The unmixing method is calibrated using standards of the individual mixture components. It was observed that this method does not allow for interactions of co-localised dyes, and the method presented in chapter 3 used standards that were comprised of mixtures of the dyes. That way, these behaviours were accounted for and any interactions would not hinder the unmixing process. Indeed, this method offers an improvement over existing methods, with the model better able to predict the concentration of each fluorophore in the mixture. These results were described in Figures 16 – 24 and Tables 2 and 3, with Figure 21 showing a comparison of the existing and new methods. Tables 2 and 3 show the improvement of the concentrations predicted by the new method over the old one. Attempts to unmix QDs using the same method were unsuccessful, indicating the need for alternative inorganic fluorophores. It was subsequently realised that the problems encountered with QDs were specific to the unmixing experiment and are not a generic issue.

Imaging of the samples was performed using spectral imaging microscopy with a single filter set for excitation and emission. This means all dyes in the mixture are not excited at their excitation maxima. The process of changing filter sets was not automated for this project. If this were done, multiple dyes could all be efficiently excited with band pass filters collecting the emission data. Doing this would increase the number of samples that can be imaged simultaneously and could be explored in future work.

7.2 Lanthanide-doped silica nanoparticles

The issues encountered with fluorophores and quantum dots indicated that although their use is possible, there is a need for probes that simplify multiplexed assays. The synthesis, characterisation and use of these probes were described in chapter 4. The probes used were silica nanoparticles doped with europium, terbium and samarium. While particles in this format have been described for terbium and europium, there was no record for samarium. These probes were chosen for their atomic line emission that removed the possibility of spectral overlap. Their encapsulation in silica meant that the particles could not interact with each other and thus there was no possibility of FRET. Silica also allowed for bioconjugation compatibility with biological molecules. All these factors made the particles suitable for multiplexed single wellled immunoassays. They were indeed suitable for these assays, with multiplexed assays for mouse and human IgGs demonstrating this (Figures 44 and 45). Figures 44 and 45 show a comparison between a dose response for the analytes human and mouse IgG assayed individually (Figures 44 (a) and 45 (a)) and in a mixture (Figures 44 (b) and 45 (b)). It is clearly observed that the detection of an analyte is not greatly affected by the presence of a second analyte, since the probes used for detection do not interact and their emission spectra do not overlap.

The results highlighted another factor that hinders wide-spread implementation of single wellled multiplexed immunoassays: cross reactivity. The partial cross reactivity of mouse and human IgGs is realised in the increased intensity of the response when the two analytes are assayed simultaneously (Figures 44 (b) and 45 (b)). The issue of cross reactivity was addressed subsequently (Chapter 6).

The studies with lanthanide doped silica nanoparticles were performed without time resolved measurements. Performing these (or similar) experiments in a time

resolved immunoassay format would extend the utility of the method to detection of low levels of analytes, and could be explored in further work.

Chapter 4 also discusses the synthesis of a ligand able to excited terbium in the UV region. The ligand BTBCT was also UV excited. The development of a ligand that can be excited by the 488 line of the Argon laser would allow these probes to be used with powerful microscopes such as the confocal laser scanning and programmable array microscopes. Visible-light excited probes are already in existence¹⁻³ and further work could optimise their development for use with instruments such as the confocal microscopes used in this project.

7.3 A Model Study: Dengue Fever

Chapter 5 presented the application of the multiplexed assay to simultaneous detection of anti-dengue IgM and IgG. The assays were performed with quantum dots, lanthanide doped silica nanoparticles and organic fluorophores, with epifluorescence, confocal laser scanning and programmable array microscopy used for assay readout. All results obtained were compared to multi-welled ELISAs. The results were discussed at length in chapter 5 and will not be discussed again here. However, the salient points are that conventional fluorophores with confocal readout gave the best results when compared to ELISA ($r^2 > 0.9$), while the PAM was the preferred instrument because of its speed and advanced capabilities.

The assays were performed on mouse sera and it would be of interest to extend the method to human samples. Here, the real utility of the differing ratios of IgM to IgG would be realised in patients suffering from secondary dengue infection. The antibodies were first detected 7 days after the first immunisation. Further work could investigate detection of antibodies in fewer days post infection.

7.4 Cross reactivity studies

Finally, chapter 6 presented a model for distinguishing cross reactive analytes. This model was designed and tested on a partially cross reactive system of mouse and human IgG, and a fully cross reactive system of anti-dengue IgG types 3 and 4. The model was able to distinguish between the partially cross reactive analytes, but there was no differentiation made between the fully cross reactive dengue antibodies. Future work could explore the use of engineered serotype specific antibodies twinned with the cross reactivity model. Combining the two methods in a multiplexed format would reduce the time and cost of the assay, making the technique suitable for use in poorer countries.

7.5 References

- (1) Jiang, L.; Wu, J.; Wang, G.; Ye, Z.; Zhang, W.; Jin, D.; Yuan, J.; Piper, J. *Anal. Chem.* **2010**, *82*, 2529-2535.
- (2) He, P.; Wang, H. H.; Liu, S. G.; Shi, J. X.; Wang, G.; Gong, M. L. *Inorg. Chem.* **2009**, *48*, 11382-11387.
- (3) Kadjane, P.; Charbonniere, L.; Camerel, F.; Laine, P. P.; Ziessel, R. *J. Fluoresc.* **2008**, *18*, 119-129.

Appendix 1: Linest data sets

This table shows the data that were put into the unmixing model. The first column contains the wavelengths used in the model. The top 4 rows contain the concentrations of the standards used and the body of the table contains the intensities of the solutions at the corresponding wavelength.

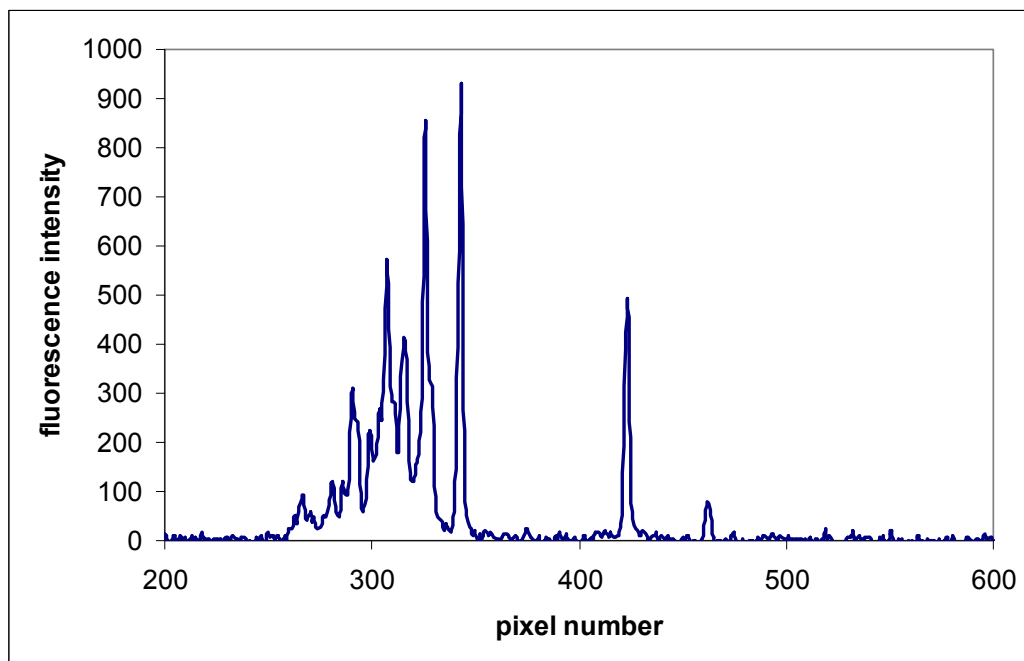
	concentration of standard solutions/ mol dm ⁻³						
R101	4.97E-06	9.94E-07	2.01E-06	7.93E-06	4.02E-06	2.96E-06	2.96E-06
RB	9.63E-07	2.03E-06	5.03E-06	5.99E-06	8.03E-06	3.00E-06	3.96E-06
F	4.67E-06	3.69E-06	1.85E-06	8.86E-07	7.38E-06	4.67E-06	5.54E-06
671.5488	1.933148	1.102128	1.087334	1.779374	2.951261	1.778882	1.952941
639.4831	3.168524	1.93617	1.78856	2.25395	4.956303	3.018634	3.220588
592.2238	6.369081	4.970213	2.448417	1.182993	7.921008	5.913043	6.567647
553.1066	11.47911	8.843617	4.368233	1.885665	15.1916	10.89938	12.275
524.437	0.261838	0.174468	0.105209	0.05688	0.270588	0.224845	0.266176
651.9106	2.986072	1.576596	1.555669	2.422292	4.383193	2.536646	2.819118
610.632	4.210306	3.842553	2.336057	1.383798	6.704202	4.554037	5.180882

The table below is the output from LINEST. The first column represents the wavelength of interest; the first row of columns 1 to 3 are values for β_j , the first value of column 3 is β_{0j} . The second row contains the standard errors in the values in row 1. Row 3 column 1 is the correlation coefficient, row 3 column 2 contains the standard error in calculated intensity values. Row 4 column 1 contains the F statistic and column 2 is the number of degrees of freedom. Row 5 column 1 contains the regression sum of squares, and column 2 contains the residual sum of squares.

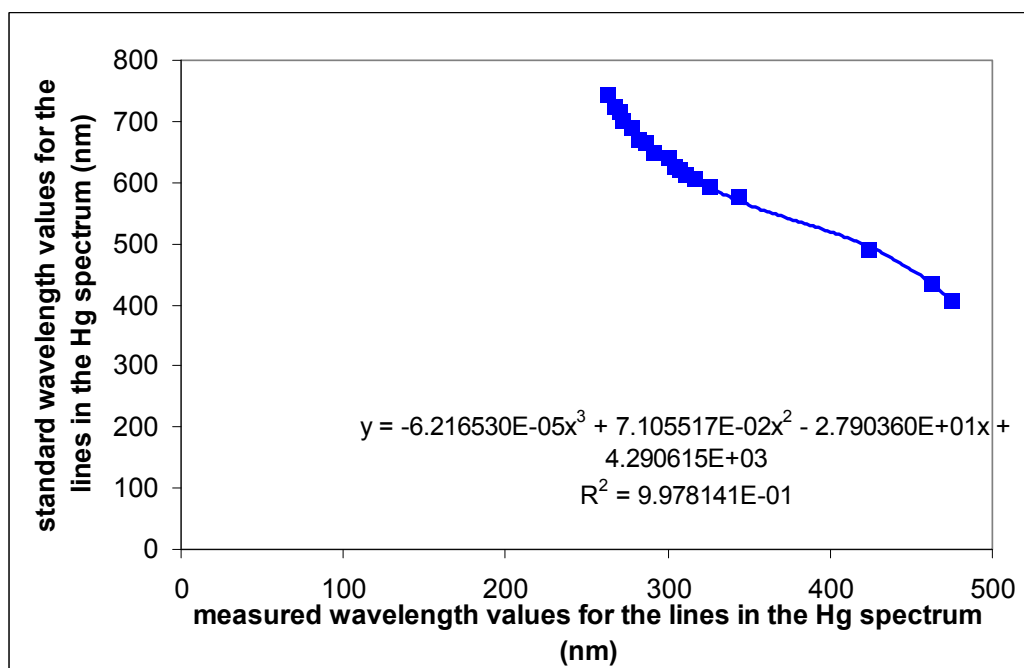
671.5488021	247799.3389	72856.37344	153461.6851	-0.077728137
	11213.3495	9982.859716	10834.54315	0.070976721
	0.99875209	0.053970633	#N/A	#N/A
	266.7798918	1	#N/A	#N/A
	2.331252774	0.002912829	#N/A	#N/A
	#N/A	#N/A	#N/A	#N/A
639.4831456	477007.3262	104466.8295	168857.8657	-0.075353524
	41227.09199	36703.06324	39834.36947	0.26095359
	0.994252549	0.198428867	#N/A	#N/A
	57.66338816	1	#N/A	#N/A
	6.811317399	0.039374015	#N/A	#N/A
592.2238109	1101796.58	-197498.3531	8451.973011	1.343995514
	15039.08784	13388.78309	14531.04143	0.095192355
	0.999828768	0.072384178	#N/A	#N/A
	1946.346069	1	#N/A	#N/A
	30.59346102	0.005239469	#N/A	#N/A

553.1065649	2130743.91	-277943.6071	5591.727864	1.683179418
	45971.94289	40927.24095	44418.9311	0.290986896
	0.999572355	0.221266165	#N/A	#N/A
	779.129188	1	#N/A	#N/A
	114.4354939	0.048958716	#N/A	#N/A
524.4369906	37504.79373	-11252.14403	3387.650137	0.071316253
	5056.567317	4501.688115	4885.747722	0.032006366
	0.983312168	0.024337611	#N/A	#N/A
	19.64130091	1	#N/A	#N/A
	0.034901765	0.000592319	#N/A	#N/A
651.9105764	404474.0765	84550.83675	227282.981	-0.188276061
	40152.46989	35746.36412	38796.04996	0.254151594
	0.993206013	0.193256636	#N/A	#N/A
	48.72966164	1	#N/A	#N/A
	5.459884842	0.037348127	#N/A	#N/A
	#N/A	#N/A	#N/A	#N/A
610.6320456	776108.1296	40703.33635	-58113.4642	0.879634291
	23802.80308	21190.81761	22998.70319	0.150663717
	0.999206034	0.11456455	#N/A	#N/A
	419.5001246	1	#N/A	#N/A
	16.51786295	0.013125036	#N/A	#N/A

Appendix 2-Calibration of the Spectrograph

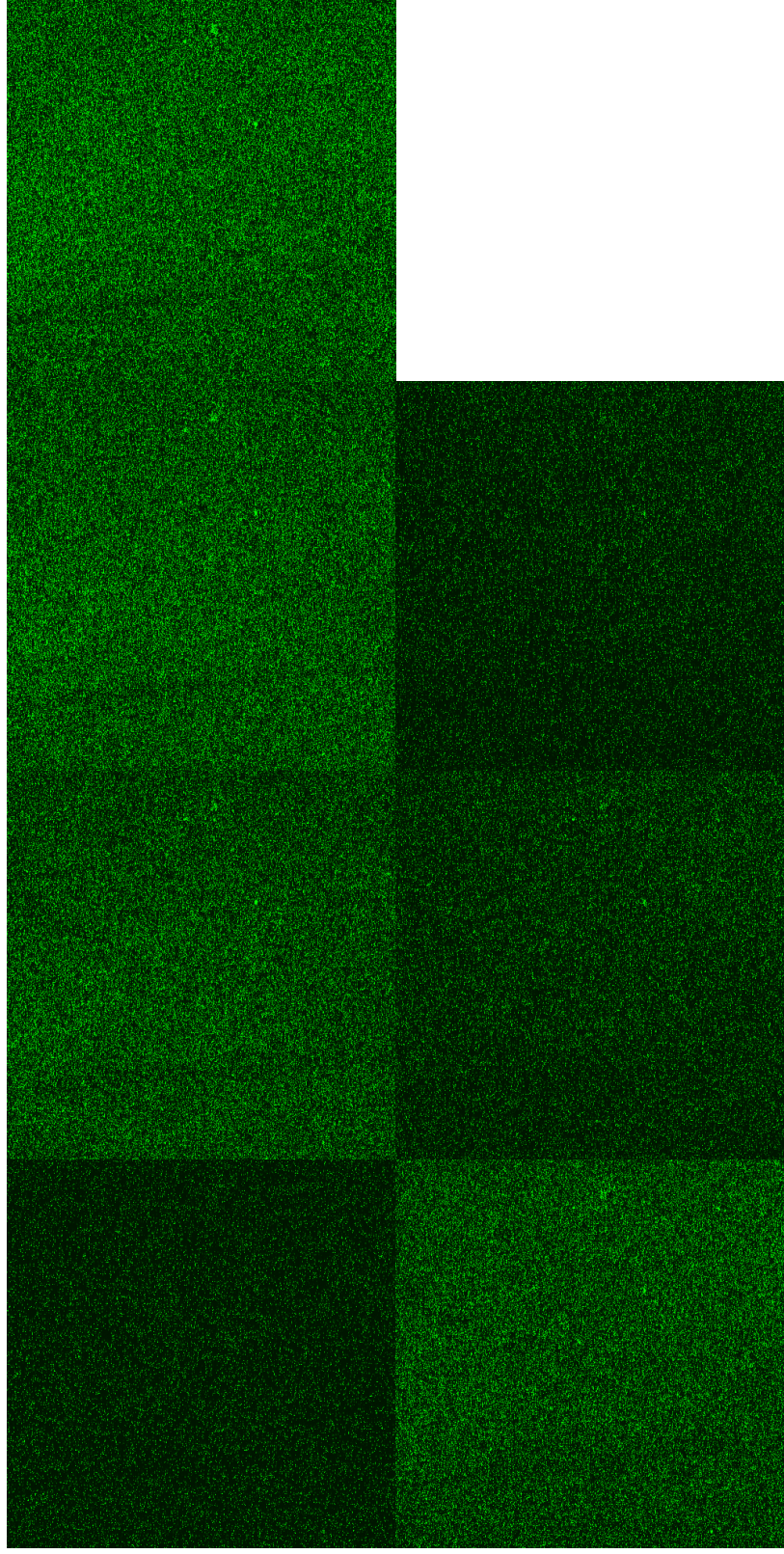


Spectrum of lines in the calibrating lamp, taken through the spectrograph



The 3rd degree polynomial line used to convert pixel number to wavelength

Appendix 3-Sample of raw data from confocal results for multiplexed dengue assays



x-y images through the z-axis of an assay plate. The stack shows from below the surface of the plate to the point of highest attachment and above.

Each x-y image (shown above) is summed and given an intensity value that can be plotted against z position. This table shows the data for 4 samples, each performed in triplicate.

Sample of raw intensity data from confocal microscope, samples assayed in triplicate															
z-position	1	1	1	2	2	2	2	3	3	3	3	4	4	4	4
0	142843	126430	114434	119455	106647	102495	86843	84885	67939	69215	67713	64374			
1	145686	128932	118636	117873	109117	101960	88379	87421	66722	71362	69948	63668			
2	147778	129293	119795	118054	111976	105485	89084	92411	67856	72423	68588	64552			
3	154440	130789	118526	117643	111058	109964	89921	96438	70030	72479	69409	62896			
4	156527	134506	120889	118256	113813	112576	91435	99771	69134	72776	68853	66323			
5	168396	135064	121198	116426	116001	114545	91461	102385	69175	75741	71484	66699			
6	173642	138410	123844	114756	117249	123381	92363	109462	68689	74552	75275	69243			
7	187817	141477	126644	117680	121476	134285	92176	119650	71447	77607	75466	72321			
8	207105	146353	128893	117870	130007	146019	94048	126077	73127	77105	77839	75542			
9	220150	151451	130653	117480	135195	156415	94199	141095	74545	83961	80210	76790			
10	238719	165300	135166	119328	143240	167623	95449	146721	75982	84738	84632	81672			
11	245900	169064	137694	125083	147545	179213	97226	171443	75820	93230	82591	87354			
12	260303	178103	140367	124283	164334	197732	94101	202739	81903	95950	87356	88607			
13	261241	190768	142936	126302	177661	211253	97086	212900	86584	104511	93884	98554			
14	254081	212953	149541	127415	193906	228096	98060	233392	91903	115939	97855	100302			
15	239004	219882	152314	132996	204024	228867	99893	252999	95401	123902	104034	106263			
16	226753	236274	164395	135132	233479	229399	103676	260996	100472	130956	119487	106995			
17	209149	258179	173836	149019	251463	221611	105544	257937	103671	150603	126250	106814			
18	192814	269167	185454	150299	263796	215283	108694	232707	108597	167815	141765	102647			
19	176011	287055	208004	162239	271164	202212	115144	232789	106028	180634	162512	96731			
20	166028	283988	226624	182651	288026	190155	119226	208206	110642	196995	189075	91206			
21	148633	288124	242999	196264	284251	164866	134995	186373	108544	216620	203895	85855			

22	142838	280719	270276	224416	281717	156133	139695	167104	104172	215332	231187	81491
23	135825	258775	289605	246956	262647	137310	148561	143924	104585	219260	263868	76314
24	133327	249122	309766	268907	250286	131494	169829	128174	93791	214594	286569	71024
25	129806	220182	310907	287099	222047	118351	184108	113255	89999	203835	301683	69273
26	127678	201407	330114	307042	199145	110235	204534	105873	84973	194328	316559	66754
27	127177	181532	323946	313226	174769	106997	223805	102821	80315	173765	309299	64183
28	125148	172594	316512	310859	156876	101453	232477	90769	79390	145550	298990	63813
29	121916	157842	304489	296302	143669	98414	243879	90882	72387	132767	283790	60164
30	123770	151350	286523	285684	132503	96271	254658	86012	73251	116716	253030	62130
31	120481	142048	263348	266757	125800	92959	253678	83810	70890	108622	224699	59533
32	120020	133184	237750	240663	115698	92379	253832	80820	69374	100681	199894	61021
33	118495	134746	207185	223693	108629	91117	233311	77689	68306	87833	162962	59882
34	118976	127340	195304	194728	108573	90512	214051	78883	67136	85396	141183	59171
35	116673	128466	176574	174300	105568	88077	201957	74724	64843	81528	125293	60924
36	115936	126537	159735	160510	101837	88383	184211	74154	64989	76885	114831	58740
37	116008	122198	148160	148258	97395	87225	160575	74315	63279	73683	105553	61087
38	114879	121387	137171	140230	97673	85724	142849	71991	65270	72408	90190	60962
39	115396	120572	129948	137089	97045	86075	135053	72360	63645	70575	85771	60858
40	114316	119219	128913	131717	94065	84270	122492	72050	63229	71089	83819	59070
41	114411	119382	124118	126910	98639	86499	109752	70251	63480	67276	76599	60700
42	114009	117667	120146	126408	93374	85574	107241	69509	64303	67308	77967	58577
43	111949	118018	117235	123362	93723	84652	98034	71737	63264	64174	72469	57128
44	112332	116139	117435	119651	91708	83584	96442	70656	61614	64999	69978	60067
45	112710	114912	113561	119785	92389	84054	92472	70453	63418	63377	69634	60343
46	113327	114885	111769	117490	90875	82787	91276	70967	61244	64450	67973	58725
47	113719	114106	113010	115390	89935	83083	87228	70265	61720	62990	65919	58067
48	112819	112920	109761	113313	88178	84643	86345	69066	61739	61619	66276	58850
49	111450	111474	111591	113263	88271	81395	83472	69233	61650	62526	65737	59498

Appendix 4-Persistence of dengue antigen in the serum of immunised mice

In these experiments mouse sera were assayed for the presence of persisting antigen. The assays were performed using a secondary probe labelled with europium doped silica nanoparticles. In this assay, particles were counted. As can be seen, there is antigen present in the samples.

sample	particles/well
blank	26
blank	188
blank	140
Ab3	276
Ab3	256
Ab3	268
Ab4	140
Ab4	247
Ab4	274
Ab3+Ab4	215
Ab3+Ab4	258
Ab3+Ab4	204
Sample	Average
blank	118
Ab3	266.666667
Ab4	220.333333
Ab3+Ab4	225.666667

Appendix 6 -Publications/ Conference Proceedings

- Murray, K., Cao, Y-C., Ali, S., Hanley, Q. *Analyst* **2010**, *135*, 2132-2138.
- Murray, K., Ali, S., Hanley, Q. Progress towards multiplexed nanoparticle based immunoassays for dengue fever. Presented at “Nanodots and Diagnostics” Symposium Spain 2009.
- Murray, K., Ali, S., Hanley, Q. The Use of Nanoparticles, Quantum Dots and Fluorophores in Confocally and Spectroscopically Detected Immunoassays presented at MICROSCIENCE 2010 London 2010.
- Murray, K., Ali, S., Hanley, Q. Multiplexed biochemical detection of the immunoresponse to dengue fever antigens presented *in absentia* at ACS 240th national meeting, Boston 2010.